3-20-2020

A Coupled Numerical Model of Vadose Zone Hydrology and Subsidence in the Everglades Wetlands

Anupama John
Florida International University, ajohn188@fiu.edu

FLORIDA INTERNATIONAL UNIVERSITY

Miami, Florida

A COUPLED NUMERICAL MODEL OF VADOSE ZONE HYDROLOGY AND SUBSIDENCE IN THE EVERGLADES WETLANDS

A dissertation submitted in partial fulfillment of the

requirements of the degree of

DOCTOR OF PHILOSOPHY

in

CIVIL ENGINEERING

by

Anupama John

2020

To: Dean John L. Volakis
College of Engineering

This dissertation written by Anupama John, and entitled A Coupled Numerical Model of Vadose Zone Hydrology and Subsidence in the Everglades Wetlands, having been approved in respect to style and intellectual content, is referred to you for judgement.

We have read this dissertation and recommend that it be approved.

_____
Arturo S. Leon

_____
Seung Jae Lee

_____
Florence George

_____
Hector R. Fuentes, Major Professor

Date of Defense: March 20, 2020

The dissertation of Anupama John is approved.

_____
Dean John L. Volakis
College of Engineering

_____
Andres G. Gil
Vice President for Research and Economic Development
and Dean of the University Graduate School

Florida International University, 2020

DEDICATION

To my wonderful family

ACKNOWLEDGMENTS

Completing this dissertation was a personal achievement but it was only possible because of the wonderful individuals who supported me through this process. My sincere gratitude to my advisor, Dr. Hector R. Fuentes for his constant guidance, encouragement, and support throughout my doctoral program. I thank my committee members, Dr. Arturo S. Leon, Dr. Seung Jae Lee, and Dr. Florence George for their valuable feedback, and encouragement. This study would not have been possible were it not for programs like the United States Environmental Protection Agency's Regional Environmental Monitoring and Assessment Program, which collected the soil samples used, and Dr. Jennifer Richards and Dr. Daniel Gann, who facilitated access to them. I thank Dr. Luis Perez for introducing me to vadose zone hydrology and training me in the laboratory procedures, and Maxhanry Silveira Lopes Coutinho, Juan Pablo Almagro and Fabian Rangel for their assistance with laboratory work. I'm grateful for the assistance I received from Himadri Biswas and Fabian Rangel with the challenging task of field work in the difficult Florida marshes. I thank the anonymous reviewers who provided insightful reviews to parts of this dissertation. My sincere gratitude to Carlton Nguyen and the office staff at the Department of Civil and Environmental Engineering. In addition, I would like to acknowledge the Department of Civil and Environmental Engineering and the University's Graduate School for providing me financial support through a graduate assistantship. Finally, my never-ending gratitude to my family and my husband for being a constant source of inspiration, support, and encouragement.

ABSTRACT OF THE DISSERTATION

A COUPLED NUMERICAL MODEL OF VADOSE ZONE HYDROLOGY AND SUBSIDENCE IN THE EVERGLADES WETLANDS

by

Anupama John

Florida International University, 2020

Miami, Florida

Professor Hector R. Fuentes, Major Professor

Peatlands, a type of wetlands, cover less than 3% of the earth's surface but are responsible for nearly 5% of global carbon emissions when drained. Alterations to the natural hydrology of the Everglades, one of the largest peatlands in the United States, have resulted in the presence of vadose zones and the consequent subsidence of peat. Everglades restoration efforts are guided by hydrological models that neglect unsaturated water flow, which limits their ability to quantify critical wetland processes. Large datasets of the spatially varying soil hydraulic parameters (SHPs) like the soil water retention curves (SWRCs) are necessary to develop distributed, deterministic models. Furthermore, conventional models of unsaturated flow parameterization and transport ignore the effect of volume-change (VC) commonly observed in peat.

The main objectives of this study were to characterize the SHPs of Everglades soil, investigate the effect of VC on the SWRC parameterization process, and develop and test

an improved finite-difference model, REVC (Richards Equation Volume Change), which incorporates subsidence in the Richards equation transport mode. Using laboratory methods, a large dataset of SWRC, shrinkage, organic content, fiber content, and saturated hydraulic conductivity from 53 sites across the Everglades was generated. Agglomerative clustering resulted in three clusters with distinct SWRCs - marl, mixed marl-peat and peat. Application of volume-correction to the van Genuchten Mualem (vGM) model resulted in deviations from typical SWRC behavior (attributed to the collapse of macropores).

Mesh convergence analysis was conducted to guide REVC spatial and temporal discretization. Sensitivity of REVC to vGM parameters with three parameter-transport model combinations for shallow vadose zones resulted in lower surficial pressure heads and volumetric water contents (VWCs) when VC was ignored in both parameterization and transport models. REVC simulated VWC and subsidence in a lysimeter experiment with constant boundary conditions (BCs) and a field subsidence study with variable BCs produced excellent to fair model fit. The practical application of the REVC model is demonstrated through the case scenarios of multiple accretion, reversible shrinkage models. Although the generated SWRCs with REVC can be implemented to model distributed flow, further testing at field-scale with site-specific calibration by practitioners is recommended.

TABLE OF CONTENTS

CHAPTER PAGE

LIST OF TABLES

TABLE PAGE

LIST OF FIGURES

FIGURE PAGE

ABBREVIATIONS AND ACRONYMS

ANOVA	Analysis of Variance
BD	Bulk Density
CERP	Comprehensive Everglades Restoration Program
EAA	Everglades Agricultural Area
EDEN	Everglades Depth Estimation Network
EM	Electro-magnetic
ENP	Everglades National Park
EPA	Everglades Protected Area
FC	Fiber Content
GHG	Green House Gas
GIS	Geographic Information Systems
GOES	Geostationary Operational Environmental Satellites
GWC	Gravimetric Water Content
HCR	Height Change Ratio
LiDAR	Light Detection and Ranging
NEXRAD	Next Generation Radar
NAVD	North American Vertical Datum
NGVD	National Geodetic Vertical Datum
NSRSM	Natural System Regional Simulation Model
OC	Organic Content

PTF	Pedotransfer Function
RADAR	Radio Detection and Ranging
RE	Richards Equation
RETC	Retention Curve
RMSE	Root Mean Squared Error
$RMSE_N$	Normalized Root Mean Squared Error
RSET	Rod Surface Elevation Table
RSM	Regional Simulation Model
SET	Surface Elevation Table
SOFIA	South Florida Information Access
SWAP	Soil Water Atmosphere Plant
SWRC	Soil Water Retention Curve
TDR	Time Domain Reflectometry
USEPA	United States Environmental Protection Agency
USGS	United States Geological Survey
VC	Volume Correction
vGM	van Genuchten Mualem
VWC	Volumetric Water Content
WCA	Water Conservation Area
WRDA	Water Resources and Development Act

SYMBOLS

a_i	Coefficient in the matrix notation solution of the Richards equation
α	Empirical shape fitting parameter of the van Genuchten model
b_i	Coefficient in the matrix notation solution of the Richards equation
c	Velocity of light in vacuum
c_i	Coefficient in the matrix notation solution of the Richards equation
CH_4	Methane
CO_2	Carbon di-oxide
$C_w(h)$	Capacity function
d_i	Coefficient in the matrix notation solution of the Richards equation
d_{jk}^2	Squared Euclidean distance with the *j*-th and *k*-th sample
$\sqrt{\varepsilon_{ra}}$	Apparent relative permittivity
E	Maximum potential evaporation or infiltration
F	Ratio of organic content to ash content
$F(t)$	Relative humidity of the air fraction with respect to time
H	Total head
h	Matric potential head
h_A	Minimum allowable pressure head
h_L	Prescribed pressure head at the lower boundary
h_S	Maximum allowable pressure head
h_U	Prescribed pressure head at the upper boundary

J_w	Volumetric flux across a cell
$K(h)$	Hydraulic conductivity as a function of matric potential
K_{sat}	Saturated Hydraulic Conductivity
l	Pore connectivity parameter
m	Empirical shape fitting parameter of the van Genuchten model
M	Molecular weight of water
M_w	Mass of water
M_{wet}	Mass of wet soil
M_{dry}	Mass of dry soil
n	Empirical shape fitting parameter of the van Genuchten model
N	Number of samples
N_i, N_j, N_k	Number of elements in clusters *i*, *j*, and *k*
Ψ_m	Soil matric potential
Ψ_t	Soil total potential
Ψ_z	Soil gravity potential
φ	Porosity
ρ_g	Bulk Density
ρ_p	Particle density
$q(t)$	Darcian flux density
R	Universal gas constant
S_a	New agglomerated cluster
$S(h)$	Source or sink in the vadose zone

S_i, S_j, S_k	Agglomerated clusters *i*, *j*, and *k*
θ	Volumetric water content
θ_r	Residual volumetric water content
θ_s	Saturated volumetric water content
V_a	Volume of air
V_w	Volume of water
V	Total volume of soil matrix
v	Velocity of EM wave
	Pore connectivity parameter
L	Length of wave guide
z	vertical spatial coordinate
Z_{ij}	Standardized value for the *i*-th parameter and the *j*-th sample

1. INTRODUCTION

1.1. Motivation

Peatlands Global Extent, Importance

Despite their low spatial coverage, peatlands are a very valuable ecosystem to the global carbon cycle. They cover less than 3% of the earth's surface however, they store two times the carbon stocks of all the forests in the world combined (Yu et al., 2011; Crump, 2017). A peatland is a type of wetland which forms over millennia in water logged conditions through the slow anaerobic decomposition of plant matter that accumulates as peat soil (Holden et al., 2011). They exist on every continent, although they are largely found in the northern hemisphere as boreal peatlands (Yu et al., 2011). About 10-12% of peatlands are tropical peatlands commonly found in Southeast Asia and Central America, but they are estimated to store greater than 30% of the global peatland carbon (Crump, 2017). However, largescale changes in peatlands in the last century, in pursuit of economic development, threaten to convert these ecosystems from net carbon sinks to net carbon sources.

Vulnerability of Peatlands

Peat and peatlands are valuable resources for people. Unsustainable exploitation has resulted in their degradation, decline of peatland extent, and loss of peat soil. Since the mid-twentieth century, peatlands have been drained for land reclamation, agricultural resource and fossil fuel extraction, commercial forestry, and infrastructure development (Crump, 2017). The long-term drainage of peat results in loss of soil through oxidation

releasing Green House Gases (GHGs) like carbon dioxide (CO_2) and methane (CH_4) into the atmosphere. Peatlands cover 0.4 percent globally but drained peatlands are responsible for nearly five percent of global Carbon emissions (Joosten, 2010). Drained peatlands are vulnerable to fires which occur visibly on the surface or invisibly on the subsurface observed only as smoke (Joosten, 2010). Furthermore, the high surface temperatures from global warming are expected to increase the rate of peat loss. The United States has 223,809 square kilometers of peatlands totaling 26,454 Mtonnes of C of which 91,819 square kilometers exist in the lower 48 states (excluding Alaska) (Joosten, 2010; Crump, 2017).

Everglades a Tropical Coastal Peatland and its Historical Drainage and Management

The Everglades in South Florida is one of the largest peatlands in the United States. It consists of 5,600 square kilometers of extensive communities of freshwater wetland vegetation, stretching from Lake Okeechobee south towards Florida Bay and the Gulf of Mexico (DeAngelis et al., 1998; United States Geological Survey, 2003). Practices in the early 20th Century like reclamation of land for agricultural purposes in the northern Everglades and the building of levees, canals, pumping stations and control structures in response to hurricanes and frequent flooding, resulted in compartmentalization of the single hydrologically integrated Everglades system (Davis and Ogden, 1994; DeAngelis et al., 1998; Ogden, 2005). Furthermore, additional stressors like urban expansion, industrial and agricultural practices, and human influences on species composition have led to reduced spatial extent, degraded water quality, reduced water storage capacity, and compartmentalization (Ogden, 2005). The net effect of these changes on hydrology has

been 1) a loss of uninterrupted sheet flow; 2) pronounced fluctuations in water levels; and 3) higher frequency of major dry downs (DeAngelis et al., 1998).

Challenges from Everglades Drainage – Loss of Soil Depth

Hydrological changes to the Everglades system have resulted in largescale subsidence of peat soil from the Everglades. Surveys conducted by Loveless, 1959 concluded that the Everglades once contained the largest single body of organic soil in the world. However, a century of land reclamation and mismanagement have resulted in its degradation and loss of spatial extent. Subsidence as a phenomenon has been recorded in the Everglades for the past half century. Snyder et al., 1978 reported average subsidence rates of 1 inch per year in the Everglades Agricultural Area (EAA) measured using subsidence posts and benchmarks. EAA Surveys in 1969, 1978, 1988, 1997 have all reported a trend of continued subsidence (Ingebritsen et al., 1999). Dreschel et al., 2018 used remote sensing with land surveys and pre-drainage maps to estimate peat loss from different areas within the Everglades. They concluded that 45% of peat has been lost over the last century. Subsidence rates were found to depend on the water table depth. In the EAAs, elevations once 20 feet above mean sea level is currently just 5 feet above sea level. For an area like South Florida, where land elevation is very close to sea level, subsidence poses additional challenges like increased salinity through salt water intrusion which is known to further exacerbate peat loss through peat collapse (Chambers et al., 2019). The net effect of which are compromised coastal aquifers and ecosystems through loss of freshwater storage and lack of freshwater head to combat saltwater intrusion.

Management of the Everglades and Restoration Efforts

The Comprehensive Everglades Restoration Program (CERP) is an USD 8-10 billion hydrologic project authorized by the U.S. Congress in 2000, as a part of the Water Resources and Development Act (WRDA) (Mclean et al., 2002). It is an ambitious undertaking involving multiple organizations with the goal of "restoration, preservation, and protection of the South Florida ecosystem while providing for other water–related needs of the region, including water supply and flood control" (National Research Council, 2014). Since hydrology is a major driver for landscape processes in the Everglades environment, the program focusses on restoring the hydrologic features of the undeveloped wetlands on the assumption that improvements in ecological conditions will follow (National Research Council, 2014). With regard to soil conservation, it is believed that increasing the quantity of water will prevent the oxidation of organic soil and encourage the accretion of new soil (Hohner and Dreschel, 2015). However, competing water demands makes the process of allocation and distribution of water throughout the entire system a challenge. Restoration of the Everglades, a priority for the region, is currently guided by hydrological models like the Regional Simulation Model (RSM) that are capable of simulating overland sheet-flow and subsurface flow in the limestone bedrock (SFWMD, 2005). However, the RSM does not account for transient, vertical, unsaturated soil water flow, a critical phenomenon observed in drained wetlands, which requires an extensive dataset of soil hydraulic parameters, not currently available for the Everglades soils. The lack of an unsaturated flow model for the Everglades wetlands limits the understanding and quantification of unsaturated flow processes like solute and nutrient transport, gaseous flux, plant water uptake, drought monitoring, and hydrological subsidence.

Unsaturated Zone Models and Subsidence Modeling

Hydrological models of the Everglades have generally focused on sheetflow over the soil surface or saturated groundwater flow with comprehensive hydrological models like the RSM combining the two processes and treating the unsaturated zone as a boundary condition. For wetland hydrology, unsaturated zone models can be used to investigate a wide range of processes associated with drainage. Unsaturated zone models typically use the Richards Equation (RE) with numerical methods to solve for non-steady flow. Compared to saturated flow models, unsaturated flow models are more complex in terms of model parameters and their determination, numerical stability of solutions, and computational resources for determining solutions. A common challenge with most unsaturated zone studies, particularly for organic soils of wetlands, is determination of soil parameters. RE model parameterization requires the soil water retention curve (SWRC) which is a relationship between the matric potential of the soil and its soil moisture content. The laboratory methods for determining the SWRC require expensive, specialized equipment; whereas indirect methods to estimate SWRC from field data requires large datasets derived from intensive field monitoring. For mineral soils, parameters are relatively well-defined hence, previous work may be used to parameterize vadose zone hydrology models of these soils. However, peatland parameters have been found to vary from region to region due to the dependence of hydraulic properties on contributing plant matter, organic content (OC), bulk density (BD), fiber content (FC) etc. The SWRC has been determined for other vulnerable peatlands though no such dataset exists for the Everglades peatland. Furthermore, the volume changing behavior of peat adds complexity in the definition of the SWRC and the application of the RE for unsaturated flow modeling

of peat. Although it is widely accepted that the accurate modeling of peat unsaturated behavior requires a dynamically changing peat matrix, very few peatland studies implemented these (Camporese et al., 2006). Studies like Camporese et al., 2006 have modeled the unsaturated flow of a dynamic matrix using RE using constitutive laws that link the volumetric water content to the void ratio to calculate volume change. This method works only with SWRCs that are not volume corrected; in addition, water content-based RE models are insensitive to the small changes in pressure head typically seen in very shallow groundwater tables like in the Everglades.

Knowledge Gaps

This work attempts to study the unsaturated zone hydrology of the Everglades environments using a comprehensive approach by determining zone by determining soil hydraulic model parameters and volume change parameters through laboratory work, developing a new coupled RE-based volume change model, and testing this model with laboratory soil cores and a field subsidence study. Through this work, the following limitations of previous Everglades unsaturated zone studies have been overcome: 1) well-defined parameters for Everglades peat, Loxahatchee peat and Everglades marl obtained through laboratory testing; 2) unsaturated flow hydrology model that couples the volume-change experienced by histosols with the capability of predicting soil moisture content and subsidence in the Everglades environments.

1.1 Literature Review

1.1.1. The Everglades and its Hydrology

Prior to drainage, the Everglades was a single hydrological system estimated to be about 11,000 square kilometers with freshwater from Lake Okeechobee flowing south and south west driven by a low elevation gradient (Dreschel et al., 2018). Efforts to drain the Everglades to reclaim land for agriculture began in the early 19th century. In 1917, major canals that conveyed water from the present-day EAA and into the Atlantic Ocean were constructed. From the 1950's to the 1960's, levees were built that impeded the flow south into the present-day Everglades National Park (ENP) and created the Water Conservation Areas (WCAs). These constructions resulted in both the lowering of the water levels in the wetland marshes and the compartmentalization of the previously integrated hydrological system causing in severe ecological degradation of the Everglades system through reduced spatial extent, degraded water quality, reduced water storage capacity, decline in fish, bird and plant species (Ogden, 2005).

The present-day Everglades is about 5,000 square kilometers consisting of the Everglades Protected Areas (EPAs) : WCA-1, WCA-2A, WCA-2B, WCA-3A, WCA-3B and the Everglades National Park (ENP) (Dreschel et al., 2018). The primary objective of the WCAs was to 1) store excess water from agricultural areas, 2) prevent floodwater from inundating the urban lands on the east, 3) recharge groundwater, 4) supply water for agriculture, 5) benefit fish and wildlife, and 6) release water to ENP (USACE, 1996). Lake Okeechobee provides the headwater for flow into the Everglades. It is the largest lake in the South Eastern US although, it is quite shallow with an average depth of 8.9 ft (Abtew

et al., 2013). Water flow is controlled by the South Florida Water Management District (SFWMD) through a network of water control structures like canals, levees, and pump stations. High levels of nutrients like nitrogen and phosphorous in the water (due to run off from agricultural lands) delivered to the ENP led to building of constructed wetlands for water purification prior to delivery in the ENP. This has reduced the water delivery times to the southern part of the Everglades. Currently, water delivery is guided by flood control, upstream agricultural needs, and needs of the Everglades ecosystems (fish, wildlife, ecology).

The natural hydrology of the Everglades was modified to an excessively managed system marked by extreme variations in hydrology between wet and dry seasons. The wet season of the current system is from May to November. Wet season is characterized by high rainfall, increase in water levels, and high temperatures. The dry season is from December to April and is characterized by limited rainfall, decrease in water levels, and low temperatures. The water levels in the Everglades are monitored by a network of gages operated by the SFWMD, the USGS, and the ENP called the he Everglades Depth Estimation Network (EDEN). This dataset includes daily water levels, potential evapotranspiration, and rainfall. It is available through the South Florida Information Access (SOFIA) program of the USGS. Water levels obtained through EDEN show that the unsaturated zone thickness can vary between 0 to 3 feet and these unsaturated zones can occur for a few days to months during the dry season from December to April, when rainfall is limited.

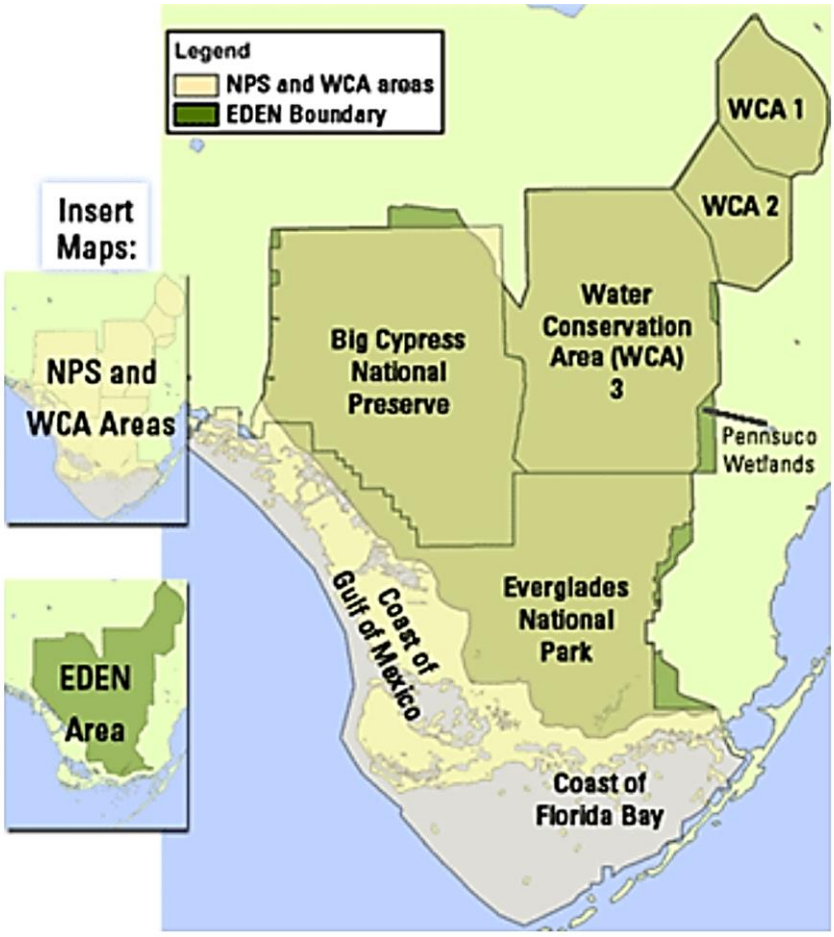

Figure 1-1. Map of National Park Service (NPS) and Water Conservation Areas (WCAs) along with the areas covered by the Everglades Depth Estimation Network (EDEN) as part of the South Florida Information Access (SOFIA). (Source: *https://sofia.usgs.gov/eden*)

1.1.2. Soils of the Everglades

Soils of the Everglades are broadly classified as histosols and consist of two main types: 1) peat which is formed by the anaerobic decomposition of plant matter; and 2) marl which consists of silt and fine grained calcite formed by changes in pH mediated by photosynthesis with the periphyton mat communities (Fling et al., 2012). These soils

overlie a permeable limestone bedrock with its elevation varying from 12 ft NGVD at the northern parts of the system (EAA) to 1 foot NGVD in Shark River Slough (Dreschel et al., 2018). The EPA and the EAA overly multiple geological formations: 1) Pamlico Sand, 2) Miami Limestone, 3) Anastasia Formation, 4) Fort Thompson Formation, and 5) Tamiami Formation (Jarosewich and Wagner, 1985).

The organic rich peat soil is formed by the anaerobic decomposition of wetland vegetation in the Everglades. Peat types in the Everglades vary based on the contributing plant matter. In the protected areas, the two main types of peat are 1) Everglades peat – formed from the partially decomposed sawgrass leaves and root and 2) Loxahatchee peat – formed from aquatic plants like water lilies. Everglades peat is found in the ridges while Loxahatchee peat is found in the sloughs (Dreschel et al., 2018). Hydrology may also influence differences in these two peats as sloughs tend to be wet most of the year compared to ridges which are periodically subject to dry-down. The peat in the EAA is primarily Everglades peat which was classified as a typic fibrist in the 1940's; however, post drainage subsidence over the past decades have resulted in its classification to saprists, a more decomposed suborder (Dreschel et al., 2018). Marl and peat require opposite hydrological regimes for their formation. While peat formation requires the soil surface to be submerged to provide for anaerobic conditions, marl is formed during periods of prolonged dry-down (Sklar et al., 2000; Ross et al., 2003). Hence, their presence on the landscape is often an indicator of the hydrological regimes observed over time in an area. The prevalence of peat soil in the Everglades landscape decreases from north to south whereas the prevalence of marl increases.

1.1.3. Subsidence in the Everglades

The term ‘Subsidence’ is used in this study to denote a vertical downward displacement of the soil surface resulting in a lowering of the soil elevation. For peatlands, the term ‘mire-breathing’ refers to the rising and sinking of soil surface in response to changes in water content (Camporese et al., 2006). In the Everglades, subsidence over large spatial scales have been quantified through transect surveys and remote sensing methods, while local, small scale subsidence studies have also been conducted using Surface Elevation Tables (SETs) (Jones, 1948; Stephens and Johnson, 1951; Stephens et al., 1984; Glaz, 1995; USEPA, 1997; Whelan et al., 2005; Dreschel et al., 2018). Peat thickness was estimated to be about 12 feet deep in the EAA reducing to about 5 feet in the south prior to drainage (Hohner and Dreschel, 2015). The phenomenon of subsidence in the Everglades was observed as early as the 1940s in the EAA. Comparisons of present-day conditions with land surveys conducted by Glaz, 1995; Jones, 1948; Stephens et al., 1984; Stephens and Johnson, 1951; USEPA, 1997; Whelan et al., 2005 estimate a loss of ranging from 3 to 9 feet in cultivated areas and 3 feet in uncultivated areas (Ingebritsen et al., 1999). The loss of soil in the EAA is greater than the ENP due to 1) deeper peat soils in the EAA pre-drainage, 2) intense drainage effort resulting in a drier system, and 3) agricultural practices causing the compaction of the land.

Initial subsidence surveys were conducted with the goal of aiding agriculture; hence, they are not as prevalent in non-cultivated parts the system i.e., areas other than the EAA like the EPA. The earliest surveys of the WCAs and the ENP were conducted by Davis, 1946 and Jones, 1948. Subsequent surveying was done by the USEPA in 1995-1996

at 459 points across the EPA using a metal rod with a maximum depth of 12 feet which was inserted into the ground. It was found that the deepest peats were in the areas with the longest hydroperiods. WCA-1 had the highest soil thickness with mean depth of 8.1 (±2.6) feet, followed by WCA-2, WCA-3, and ENP with means depths of 4.3 (±1.5), 2.4 (±1.4), and 1.3 (±1.0) feet respectively (USEPA, 1997). Compared to the initial survey, critical areas of peat loss were identified as southeastern part of WCA-3B (42% volume loss) and Northeast Shark Slough (53% volume loss) (USEPA, 1997).

A more recent effort to quantify soil loss was conducted by Dreschel et al., 2018 combining GIS data with land surveys. Datasets were collected in the form of Regional Environmental Monitoring and Assessment Program (REMAP) surveys, LIDAR topography, RADAR from Shuttle Radar Topographic Mission, bathymetric surveys, photogrammetry, and measured spot elevations. Using kriging, surface elevation maps were created, and peat volumes calculated. The pre-drainage Everglades surface was obtained from the Natural System Regional Simulation Model (NSRSM). From the post-drainage and pre-drainage maps, peat volume loss was calculated for different areas within the EPA and for the EAA. Maximum average subsidence and maximum volume loss were observed in the EAA with 1.7 m and 4.9 x 10^9 m^3. Peat loss in the EPA was lower with maximum volume loss seen in WCA-3A experiencing a peat loss of 1.3 x 10^9 m^3.

1.1.4. Mechanisms of Subsidence in Peatlands

Subsidence in peatlands occurs through different mechanisms which may be physical, biological or biochemical and can occur either through the direct loss of peat soil or through changes to the soil structure and composition (Camporese et al., 2006; Crump,

2017; Wang et al., 2017; Chambers et al., 2019). All mechanisms of subsidence mentioned in this section are irreversible except the subsidence through the draining of soil pores which may be reversible to an extent.

Peat loss can occur through the compaction of voids in the highly porous soil due to drainage. This is an example of a physical mechanism with no loss of soil mass which is reversible to an extent. Initial subsidence in the peat matrix occurs due to compaction of the soil matrix from draining of the water filled pores. Peat is a highly porous, highly compressible soil. With the loss of buoyant force, the drained pores collapse resulting in a shrinking of the soil matrix. It can be described with three phases: 1) near-normal shrinkage, which occurs when the soil volume decreases at approximately the same rate as moisture content and the peat matrix remains close to saturation; 2) subnormal shrinkage, which occurs when the soil becomes unsaturated, and the moisture loss exceeds the change in volume with air entering the larger pores while the smaller pores remain saturated; and 3) supernormal shrinkage, which occurs when the small pores dry and the matrix collapses to its minimum volume (Camporese et al., 2006). Rewetting of the peat soil results in swelling of the matrix. The swelling, however, shows hysteretic behavior, which is attributed to the formation of water repelling films (hydrophobia), effects of pore geometry (ink-bottle-effect), and alterations of spatial structure of pores during shrinkage (Schwarzel et al., 2002). Part of this shrinking may be reversible; that is, upon rewetting, the peat matrix can return to its original volume. However, it could be partly irreversible due to structural changes of the soil matrix that occur during shrinkage, A reduced water holding capacity is witnessed upon rewetting to saturation, that is the peat matrix does not regain its initial volume (Szajdak and Szatylowicz, 2002; Camporese et al., 2006).

Mechanisms where subsidence occurs due to mass-loss are always irreversible. Mass loss can occur through mechanisms like oxidation. Oxidation maybe biological like the in the case of microorganisms breaking down the peat soil or it could take place through the combustion of peat soil. Bio-oxidation of the soil matrix occurs over a longer time scale than through compaction of the voids. When the previously anaerobic peat matrix is exposed to air, aerobic microorganisms break down the cellulose and lignin releasing CO_2 as a by-product (Chambers et al., 2019). The rate of bio-oxidation is influenced by the temperature and humidity with micro-organisms preferring warmer and more humid conditions. Oxidation can also occur through peat fires, a common problem facing drained peatlands. These fires may be visible as above-ground fires or invisible as below-ground fires observed only as smoke on the surface (Crump, 2017). The combustible nature of peat makes it prone to peat fires when the soil is too dry and surface temperature is high (Davies et al., 2013; Marlier et al., 2015). This mechanism of peat loss is also an environmental hazard with dangerous particulates like trace metals, polycyclic aromatic hydrocarbons (PAHs) and nitrated PAHs that are linked to cardiovascular diseases, respiratory conditions and cancer (Betha et al., 2012; Haikerwal et al., 2015).

Saltwater intrusion is another phenomenon resulting in peat loss. There is some debate on the direct loss of peat through increased salinity. Studies that directly measure subsidence due to the salinity were not found. However, laboratory-based studies found increase in salinity for freshwater or oligohaline wetlands causes an increase in CO_2 flux which could result in greater soil loss (Chambers et al., 2011, 2013; Wang et al., 2017). Field experiments at freshwater, tidal sites did not see any increase in CO_2 flux (Neubauer, 2013; Neubauer et al., 2013). Salinity was found to have no effect in CO_2 flux for wetlands

which are already brackish (Chambers et al., 2014). However, it is known to cause indirect loss of peat surface elevation through the collapse of the plant root network. Increased salinity can cause salinity-intolerant plant species to die resulting in the collapse of the root network which holds the soil together. This phenomenon is observed as pockets of peat collapse around vegetation in the field. Most experimental works that recorded soil loss as a result of root collapse chose to treat soil cores obtained from wetland environments with herbicide (DeLaune et al., 1994; Lane et al., 2016). Experimental work by Portnoy and Giblin, 1997 found that root collapse could result in 6-8 cm of soil loss for freshwater wetlands treated with artificial sea-water. A similar effect can be caused due to water stress experienced by wetlands plants in drained wetlands or during periods of drought when water stressed plants die. In peatlands with limestone bedrocks, like the Everglades, subsidence can occur through the dissolution of carbonates due to changes in the soil pH (Chambers et al., 2019).

1.1.5. Unsaturated Zone Flow and Its Modeling

The unsaturated zone of the soil is defined from the surface to the water table; it is bounded by the atmosphere and the aquifer. Desert environments can have unsaturated zones that are hundreds of meters deep however, in the case or wetlands, the unsaturated zone is seasonal appearing during their dry seasons when the water table is below the soil surface. Despite the short temporal and vertical-spatial extent, crucial processes for wetland health like solute and nutrient transport, gaseous flux and plant water uptake take place in the vadose zone and are governed by soil hydrology. The efforts to restore, recover, and

manage drained wetlands need to be aided by a strong foundation of the soil principles that govern flow and transport in the soil medium.

With increased awareness of the effects of drained wetlands on the global cycle, there has been renewed interest in understanding the processes resulting from aeration of the wetland soil matrix. While initial efforts have focused their investigations on the mechanisms of these critical processes – an important component of the restoration process, meaningful actions require the use of simulation models to evaluate scenarios and develop optimal restoration strategies. It has been established that most critical processes in the wetland unsaturated zone are dependent on the hydrology of the soil matrix. In fact, one of the major assumptions of the Everglades restoration is that a restoration in hydrology will enable ecological restoration (National Research Council, 2014). Hence, there is a need for physically based, deterministic models of hydrology in the unsaturated zone particularly for wetland restoration.

1.1.5.1. Principles of Soil Physics

Before looking into specific deterministic models of unsaturated hydrology, it is first important to understand the principles of soil physics that govern flow in the vadose zone. The two factors that drive flow in the soil matrix, soil water content (also known as moisture content) and soil water potential are discussed below. Sections 1.1.5.1.1 and 1.1.5.1.2 have been summarized from Radcliffe and Simunek, 2010.

1.1.5.1.1 Soil Water Content

The water content of the soil is an important variable in both the calculation of unsaturated flow as well as, an indicator of the state of the soil matrix for phenomenon like

drought. One of the challenges in the field of soil science is the lack of unifying terms between disciplines and regions that apply its principles. The soil water content is one such term which is often the source of confusion as it may either be expressed either as a gravimetric water content (GWC),

$$GWC = \frac{M_w}{M_{dry}} \quad [1.1]$$

Or a volumetric water content (VWC),

$$VWC = \frac{V_w}{V} \quad [1.2]$$

Where, M_w is the mass of the water, M_{dry} is the mass of the dry soil, V_w is the volume of the water, and V is the total volume of the soil matrix (sum of the volume of air, V_a, the volume of water, V_w, and the volume of soil, V_s)

In this study, the soil water content is always expressed as a VWC as the results are easily translatable to the physical understanding of soil water content when it is expressed as a fraction of the total volume of the soil. The porosity of the soil (φ) is the total volume of water and air and is given by,

$$\varphi = \frac{V_w + V_a}{V_s} \quad [1.3]$$

At complete saturation, the VWC of the soil is equal to its porosity.

Soil water content can be measured either in the lab with a soil core obtained from the field. This method involves weighing a soil core of known volume before oven drying

it (usually at a temperature of 105°C for 24 hours) and weighing the dried core. This method may be used to calculate the GWC of the sample. The GWC can be converted to VWC using the following equation:

$$VWC = GWC\ \frac{BD}{\rho_g} \quad [1.4]$$

Where, ρ_g is the density of water ~ 1 g cm^{-3}, and BD is the bulk density of the soil, calculated by,

$$BD = \frac{Mass\ of\ dry\ soil}{Volume\ of\ sample} \quad [1.5]$$

For the measurement of soil water content in-situ in the field, time domain reflectometry (TDR) probes are widely employed. TDR probes have two- or three- rod wave guides which are inserted into the soil surface. The travel time, t, of a voltage step of electromagnetic (EM) radiation transmitted from the wave guide is measured and used to calculate the velocity of the EM wave using,

$$v = \frac{2L}{t} \quad [1.6]$$

Where, L is the length of the waveguide.

The EM wave is easily carried by the water in the soil and depends on the dielectric permittivity of the soil which is the measure of the displacement of constrained charges when exposed to an electric field. The apparent relative permittivity of the soil ($\sqrt{\varepsilon_{ra}}$), measured by the TDR probe, is inversely related to the wave velocity in the soil,

$$v = \frac{c}{\sqrt{\varepsilon_{ra}}} \quad [1.7]$$

Where, c is the velocity of light in vacuum (3 x 10^8 m s^{-1}).

The apparent dielectric constant is calculated as,

$$\varepsilon_{ra} = \left(\frac{ct}{2L}\right)^2 \quad [1.8]$$

Topp et al. (1980) empirically developed the following calibration equation for TDR probes after considering the effect of soil texture, BD, temperature and soluble salt content on the apparent di-electric permittivity measured by the probe,

$$\theta = (-5.3 \times 10^{-2}) + (2.92 \times 10^{-2}\varepsilon_{ra}) - (5.5 \times 10^{-4}{\varepsilon_{ra}}^2) + (4.3 \times 10^{-6}{\varepsilon_{ra}}^3) \quad [1.9]$$

Where, θ is the VWC.

While the above equation is applicable to a wide range of mineral soils, its ability to predict VWC of low-density soils with high organic and high clay content is poor; hence, such soils require a soil specific calibration.

1.1.5.1.2 Soil Water Potential

The soil water potential approach is widely used in many fields by hydrologists, soil scientists, plant physiologists and climatologists. It is based on the concept that water flows in the direction of high energy to low energy. The kinetic energy, in the case of soil water, is difficult to quantify, and in most applications, can be reasonably ignored. The potential energy, as a result of the position of the water is influenced by forces like gravity,

capillarity, surface tension etc. By determining the energy state and gradient of the soil water at different points within the soil matrix, the direction and rate of flow can be calculated. Soil water potential is the difference in potential energy between per unit volume, mass or weight of water compared to the standard state of water, that is, water without solutes or external forces other than gravity at atmospheric temperature and pressure. The total soil potential is divided into four main components: 1) gravitational – difference in energy per unit volume or weight between standard water and soil water due to gravity, 2) hydrostatic – difference in energy per unit volume or weight between standard water and soil water pressure due to overlying free water, 3) matric – difference in energy per unit volume or weight between standard water and soil water due to capillarity and adsorption, 4) solute – difference in energy per unit volume or weight between standard water and soil water due to the effect of soil air pressure, and 5) air pressure component – difference in energy per unit volume or weight between standard water and soil air pressure. For saturated conditions (below the water table), the three components that exist are gravity, hydrostatic, and solute, whereas for the vadose zone with unsaturated conditions, they are gravity, matric, solute and air pressure. Generally, for freshwater applications, the solute component of the total potential in the vadose zone is very low and can be neglected. In addition, the soil air potential is difficult to measure and rarely used. Hence, the total potential of the soil can be expressed as,

$$\Psi_t = \Psi_m + \Psi_z \qquad [1.10]$$

WhereΨ_t is the total soil potential, Ψ_m is the matric potential, and Ψ_z is the gravity potential. Since,

$$\Psi_m = \rho_w g h \qquad [1.11]$$

And,

$$\Psi_m = \rho_w g (z_{soil} - z_0) \qquad [1.12]$$

Where, g is the acceleration due to gravity, h is the matric potential head, and z_{soil} and z_0 are the elevation of the soil water and standard water. Using the above equations, the total head, H, can be expressed as,

$$H = h + z \qquad [1.13]$$

The matric potential head is expressed as a negative value. The above equation is also applicable to the saturated zone; however, in that case, h is positive and is called the hydrostatic head.

There are many methods to measure the soil water potential like 1) tensiometers, 2) thermocouple psychrometers, 3) heat dissipation sensors, 4) electrical resistance sensors, and 5) piezometers. Tensiometers are the most widely used method for determining the matric potential of the soil both in the laboratory and in the field, while piezometers are commonly used to measure the hydrostatic potential of the soil.

1.1.5.1.3 Soil Water Retention Curve (SWRC)

The SWRC, which relates the soil water content to the matric pressure head of the soil, is used to derive the parameters of the transport model and calculate the unsaturated hydraulic conductivity of the soil. The SWRC may be obtained through laboratory work using oedometer tests or inverse methods from field data. For the oedometer method, soil samples collected from the field are placed on a ceramic plate which are connected to outflow tubes. The ceramic plate with the samples is subject to multiple pressure settings in a closed chamber and the VWCs of the samples are measured.

Inverse determination of the SWRC may be conducted using evaporation tests, in-situ field data or using lysimetry. This method requires the measurement of VWC (using TDR probes) and matric pressure head (tensiometers). The boundary conditions are specified to solve a deterministic model from which the SWRC parameters are calculated. Schwärzel et al., 2006 employed three methods of estimating SWRCs using field lysimeter, transient evaporation, and oedometer hanging column for fen peat from Rhinluch, Germany. They found the results with the three methods were comparable. The oedometer method is quicker, more cost-effective and allows a greater range of measurements compared to the field lysimeter or the evaporation method. In addition, field lysimeters are limited by the precision of the sensors (tensiometers or TDR probes) and the range of conditions experienced in the field.

There exist many models to define the parameters for the soil water retention curve like Brooks and Corey, 1964; Fredlund and Xing, 2008; GARDNER, 1958; van Genuchten, 1980; Williams et al., 1982. The van Genuchten Mualem (vGM) model is the

most popular method due versatility and applicability. It is versatile as it uses a single equation to define the entire SWRC, and its applicability has been successfully tested for a wide range of mineral and organic soils (Schwarzel et al., 2002; Gnatowski et al., 2010; Kechavarzi et al., 2010; Hallema et al., 2015; Wallor et al., 2018b). Hallema et al., 2015 tested the applicability of three soil hydraulic property models – vGM, Groenevelt–Grant model, and a modified vGM model for 85 cultivated histosols from Quebec. SWRCs were determined using laboratory oedometer method at applied pressure heads of 20, 50, 100, 200, and 300 cm. The vGM model was found to provide the best fit for the datapoints. Although other works have observed volume changing behavior of the soil with the oedometer method, Hallema et al., 2015 did not mention any such observation with their dataset and hence a volume correction was not performed.

Studies that have investigated the unsaturated behavior of organic soils have found a variability in its unsaturated zone parameters from region to region. For soils like peat whose composition is strongly influenced by its contributing plant matter and hydrology, this regional variability is expected. Furthermore, peat is a dynamic soil in terms of its composition. Studies like Oleszczuk et al., 2008; Rezanezhad et al., 2009; Wallor et al., 2018 have found that peat physical properties transform temporally due to wetting and drying cycles. Peat transformation also changes the hydraulic properties of the soil (Rezanezhad et al., 2016). Spatial variations in hydrology within the ecosystems can result in spatial variability of hydraulic properties within the peatland.

Due to its temporal and spatial variability, it is important to characterize these properties for vulnerable peatlands. Schwärzel et al., 2002 studied the water retention

properties of earthified to strongly earthified peat from Rhinluch, Germany. They used laboratory methods to determine the SWRC with pressure heads up to 300 hPa using the hanging water column and its consequent shrinkage was measured using a Vernier caliper. They found that decomposition decreased the hydraulic conductivity of the soil samples and the consideration of shrinkage of the samples resulted in higher VWCs.

Gnatowski et al., 2010 studied the hydraulic properties of 87 fen peat soils in low fen soils in Poland. A multistep outflow chamber was used to determine the VWC at pressure heads of 10 kPa, 30 kPa, and 50 kPa. These pressure heads were selected to avoid the volume change in the soil samples. The vGM parameters were determined and agglomerative clustering was used to determine clusters within the data. They found that the vGM parameters were influenced by the botanical origin of the peat and its degree of decomposition (measured using the von Post scale).

Wallor et al., 2018 investigated the unsaturated hydraulic properties of fen peat from 12 sites at different moorsh-forming process in Germany. They obtained SWRC using the laboratory oedometer method. The vGM model was found to be applicable with high R-squared values reported. However, there was a tendency of the model to over-estimate the VWC at higher pressure heads. Wallor et al., 2018 did not consider the volume changing behavior of the soil but the authors do acknowledge that assuming no volume change results in inaccurate VWCs, particularly for the higher pressure heads tested (Wallor et al., 2018). They also tested the ability of bulk density (BD) to predict vGM parameters however, they found that only bulk density and saturated VWC were corelated with VWC decreasing with bulk density.

The volume change behavior of peat adds complexity to the parameter estimation process. Conventional laboratory methods like the oedometer method measures the VWC of the soil sample at the select pressure settings. Generally, the VWC is expressed as a ratio of the volume of water over the saturated volume however, the volume change behavior of the soil requires the need for a volume correction which involves adjusting to the volume of the sample at each pressure setting. This method has been applied to volume changing soils like clay and has been adapted to some peat studies also (Schwarzel et al., 2002; Schwärzel et al., 2006). Some studies of peatland hydraulic behavior which tested at lower pressures did not use this correction however, they have stated that no volume change was observed at their tested pressure heads (Gnatowski et al., 2010). Other peat studies that have tested at higher pressure heads where volume change was expected have acknowledged that peat volume change could result in discrepancies with the actual VWC (Wallor et al., 2018). Since peat is a highly porous soil with a large water holding capacity, its drying and wetting results in volume changes to the peat matrix (Price and Schlotzhauer, 1999; Camporese et al., 2006; Rezanezhad et al., 2016). Simulation models of unsaturated hydrology should also consider a volume changing peat matrix rather than a rigid matrix.

1.1.5.2. Water Flow Models for the Vadose Zone

Currently, both steady flow and transient flow models of unsaturated flow exist. Reliable analytical models of steady unsaturated flow have been developed for specific cases; however, transient flow models require the use of numerical methods with the RE. The RE continues to be the most popular deterministic method for water flow while the convection dispersion equation is used to model solute transport (Vereecken et al., 2016).

The RE is derived and discussed in detail in section 3.2.1. A common drawback of this RE model is that it is highly non-linear; hence, a limited number of analytical solutions exist. In addition, These solutions are generally simplistic in nature (Radcliffe and Simunek, 2010). A non-steady state solution of the RE is computationally heavy; it requires the use of numerical methods like the finite-difference, finite-volume, or finite-element methods. Developed and verified numerical codes, with and without Guided User Interfaces (GUIs) exist to solve unsaturated flow using RE for a variety of applications. Convergence is also complex and it is highly influenced by the time-step, node heights, and boundary condition. Instabilities in the numerical code are often observed for cases like sharp wetting fronts, where there is a large change in the state variables. The hydraulic parameters can also cause instabilities in the code. For example, the steepness unsaturated hydraulic conductivity curve which drives the flow in the numerical model can cause issues in the convergence of the model. (Oh et al., 2015). Non-convergence can sometimes be solved by varying the timesteps during iteration however, the solution then becomes computationally intensive. Established and verified codes like Hydrus implement a dynamic temporal and geometrical stepping to allow for a wider range of solutions (Šimůnek et al., 2013)

The model parametrization of the RE is also challenging as it requires a larger number of parameters than saturated flow models. Parameterization is used to determine the unsaturated hydraulic conductivity and soil water capacity function both of which vary with soil composition and structure. The unsaturated hydraulic conductivity tends to be lower than saturated hydraulic conductivity due to the presence of air-filled voids. Water, in such cases, moves along the surface of the soil particle, avoiding the air pockets (Chaberneau, 2006). Unsaturated hydraulic conductivity is dynamic with the VWC of the

soil matrix and is expressed as a function of the state variable in the RE which may be VWC or matric pressure head. RE may also be expressed in a mixed form using both VWC and matric pressure head as dependent variables. Mixed form equations like the one defined by Celia et al., 1990(used in Hydrus) popular since they are more stable with lower mass balance errors.

Numerical models have been successfully implemented to study wetland and peatland unsaturated behavior. These applications are characterized by high water tables and a soil matrix with generally low hydraulic conductivity. In such cases, the state variable is affected by evaporation and transpiration on the soil surface and the depth of the water table on the bottom surface (McCarter and Price, 2013, 2014; Goetz and Price, 2016; Dixon et al., 2017; Wallor et al., 2018a). However, most of the studies have not considered a volume change soil matrix despite acknowledgement from the peat hydrology community of its importance. A possible reason for this could be the unavailability of volume change modeling in established computer codes like Hydrus and SWAP (Soil Water Atmosphere Plant) which are commonly used in these studies.

Volume change models to predict subsidence have previously been applied, particularly for applications in clay soil (Briaud et al., 2003; Vu and Fredlund, 2004; Wray et al., 2005; Oh et al., 2009; Adem and Vanapalli, 2013). Volume change models in the unsaturated zone should describe the time dependent fluctuations in VWC or soil matric pressure head and include a relationship between the volume change to the state variables which may be soil moisture, matric pressure or mechanical stress (Adem and Vanapalli, 2015). Based on the type of state variables, Adem and Vanapalli, 2015 classify these

models as 1) consolidation theory-based (Zhang, 2004; Vu and Fredlund, 2004), 2) water content-based (Briaud et al., 2003; Overton et al., 2006) and 3) pressure head-based (Wray et al., 2005; Adem and Vanapalli, 2013).

Peat soils have different volume change behavior compared to mineral soils hence, they require different constitutive relationships to define the volume-change model. One of the earliest attempts to model peat shrinkage behavior was by Pyatt and John, 1989 to understand volume change under conifer plantations. They based their model on a similar model by McGarry and Malafant (1987) who described the shrinkage of clay on a graph of specific volume (bulk volume divided by mass of solids) and gravimetric water content as having three phases: structural, normal and residual shrinkage. Pyatt and John, 1989 used empirically derived data to determine the shrinkage of peat using a similar graph and concluded that peat shrinkage can be modeled as a two-stage process with an initial shrinkage caused by vertical subsidence followed by an equidimensional shrinkage at lower water contents. The equidimensional shrinkage explains the presence of cracks in the soil matrix.

Price, 2003 applied the Pyatt and John, 1989 model to study seasonal peat soil deformation in an undisturbed and disturbed cutover peatland. Price developed a model of deformation based on the VWC using the constitutive relationship by Pyatt and John, 1989 and Terzhagi's consolidation theory; however, the model was not able to accurately model deformation with the predicted deformation grossly overestimating the actual deformation. Kennedy and Price, 2005 presented a conceptual model using soil shrinkage characteristics curves, developed from laboratory data, that relates the void ratio to the moisture ratio

along with Terzhagi's consolidation equation to determine soil shrinkage and compression. They also estimated the oxidation from carbon flux. In addition, their conceptual model can simulate the coupled subsidence of both the saturated and the unsaturated zone. A major drawback of this model is the requirement of multiple physical and empirical parameters that need to be determined through laboratory and field work. In addition, extending the use of effective intergranular stress to the unsaturated zone is not valid without the use of a corrective coefficient (Bishop and Blight, 1963; Camporese et al., 2006).

Camporese et al., 2006 proposed a model of subsidence based on the Richards' equation for which a storage term was used to vary the porosity with saturation. A two-parameter constitutive relationship was defined which uses empirical data in the form of void ratio to gravimetric moisture content to determine the parameters. Porosity and saturation were related using the void ratio to develop a constitutive model, and this model when compared to experimental data from Oleszczuk et al., 2003 showed a good fit (Camporese et al., 2006). The RE model was solved using a finite-element solution for 1-D and 2-D applications to a site in Zennare Basin in Venice, Italy where temporal field data were collected from piezometers, extensometers, tensiometers and TDR probes. It was observed that the calibrated model presented a good fit to the soil surface elevation change. It is worth noting that the elevation change at this site was strongly correlated to the water table depth and this was not the case for Price, 2003.

Parameterizing the Camporese et al., 2005 model still requires two separate tests – one to determine soil water retention curve from which the relationship between matric

pressure and the VWC is defined and a second to determine the shrinkage curve. In addition, this method which links the VWC to the peat deformation may provide good results in the case of peatlands with larger vadose zones since a wide range of VWCs are observed across the peat profile. However, in applications with a very small vadose zone and smaller fluctuations in VWC, using a method that links the matric pressure head to the volume change would produce a more sensitive model.

It is also important in these models to understand the irreversible shrinkage of peat soil. Oleszczuk et al., 2008 studied the shrinking and swelling behavior of peat-moorsh soils from Poland. They used the saran-resin method to measure the changes in the VWC of the soil for three drying and wetting cycles. Based on these laboratory tests, they defined the reversible and irreversible shrinkage coefficients. It was found that most of the shrinkage experienced is reversible however, reversible shrinkage decreased with multiple drying cycles. On the other hand, irreversible shrinkage increased with multiple drying cycles with lower ranges of irreversible shrinkage coefficients for more decomposed peat from the catotelm (Oleszczuk et al., 2008). Reversible and irreversible shrinkage coefficients when implemented into numerical models could allow for understanding of the long-term hydrology induced subsidence observed in peatlands.

1.1.6. Knowledge Gaps

Restoration of the Everglades, a priority for the region, is currently guided by hydrological models like the RSM that are capable of simulating overland sheet-flow and subsurface flow in the limestone bedrock (SFWMD, 2005). However, this model does not account for transient, vertical, unsaturated soil water flow, a critical phenomenon observed

in drained wetlands, which requires an extensive dataset of soil hydraulic parameters not currently available for the Everglades soils. The RSM module assumes that the water table does not fall below the soil surface, that is, the unsaturated zone does not exist (SFWMD, 2005). The RSM uses a module for unsaturated flow; however, it uses sa boundary condition to calculate recharge into saturated groundwater zone. One of the challenges in implementing unsaturated flow in regional-scale models like RSM is a lack of unsaturated flow model parameters for the Everglades system.

Investigations of unsaturated hydrology have been limited in extent, method, and applicability. The saturated hydraulic parameters have been widely investigated for the Everglades system but very few studies have attempted to characterize the unsaturated flow parameters in the Everglades (Pumo et al., 2010). Pumo et al. (2010) applied an inverse solution method to estimate hydraulic parameters from water table fluctuations at three different sites. This method assumes the soil column to be homogenous and isotropic; however, substrates in systems like the Everglades are mostly layered due to interruptions in soil forming processes (Corstanje et al., 2006). Furthermore, the parameters determined were not verified with soil testing. Perez, 2014 characterized the unsaturated parameters of a 100 m by 100 m field in the northern part of Shark River Slough with the aim of simulating vadose zone hydrology using SWAP and investigating the application of RADARSAT derived soil moisture readings; however, parts of the site were modified by construction resulting in few samples of peat and none of marl. Due to the spatial and temporal variability of wetland properties, there is a need for comprehensive sampling with laboratory-based methods to accurately define soil hydraulic parameters for numerical modeling.

Modeling of the unsaturated zone requires the quantification of the volume-change behavior of the system to parameterize the model and its inclusion in the solution of the deterministic RE. Models using consolidation-based methods, VWC-based methods and pressure head-based methods exist and have been applied for mineral soil. Peat unsaturated hydrology has been modeled using a constitutive relationship which relates the soil VWC to the shrinking of the soil. However, the use of the conventional parameterization process like the vGM model requires the VWC and pressure head relationship. Furthermore, the VWC-based models that exist for peatlands have been applied to peatlands with deeper vadose zones than typical Everglades wetlands, and they are not sensitive enough to model the small variations in pressure head seen in wetlands with shallow groundwater.

1.2 Research Objectives

This research uses a comprehensive approach to investigate unsaturated zone hydrology and hydrological subsidence in the Everglades. The overall objective of this research is to develop a numerical model capable of predicting VWCs and the hydrological subsidence in the soil profile of the unsaturated zone. Such a model is crucial not only to hydrological resource allocation programs and subsidence modeling but can also serve as the foundational numerical model for understanding other unsaturated processes like critical unsaturated zone process like nutrient and solute transport, gaseous flux, plant water uptake etc.; such applications would require ancillary data. The general objectives of this work, as presented in each chapter are:

1. Characterize the hydraulic parameters of Everglades soil derived from laboratory work and investigate the effect of volume change on the SWRC parameterization

process, in support of future efforts to build numerical models that can best simulate fluxes in the soil matrix.

2. Propose, develop, and test a new volume changing numerical model that accurately predicts the VWC and hydrological subsidence of the unsaturated zone in the Everglades.

3. Identify critical parameters of the model for wetland applications using a sensitivity analysis.

4. Apply the model to study field subsidence observations in the Everglades.

5. Apply the model to investigate hydrological subsidence in a site with ridge and slough landscape in WCA-3B for different case scenarios of accretion and reversible shrinkage.

1.3 Approach

The approach used to obtain the research objectives through the specific chapters is outlined below:

Chapter 2

The general objective of characterizing the unsaturated properties and volume change behavior of the Everglades soils is achieved through the following approach:

1. Determine, through laboratory work, the OC, FC, BD, K_{sat}, SWRC and shrinkage of 53 soil samples collected from across the Everglades system

2. Characterize the soil water retention and shrinkage data soil using an unsupervised clustering algorithm to detect patterns in the data.
3. Investigate the properties of the clusters using the OC, FC, and BD.
4. Using the Retention Curve (RETC) code, estimate the volume-corrected vGM (vGM VC) parameters and non-volume-corrected vGM (vGM NonVC) parameters and assess their applicability in modeling the SWRCs of Everglades soils.
5. Investigate the effects of volume-correction on the SWRC and in turn, the vGM parameters.
6. Using analysis of variance (ANOVA) and linear regression, investigate the differences in peat properties as a result of hydrology and vegetation.

Chapter 3

The general objective of simulating unsaturated zone flow in a volume-changing matrix for a shallow water table is achieved through the following approach:

1. Present the current finite-difference pressure-head based formulation of the RE and propose a model which incorporates volume-change of the matrix using a look-up table.
2. Create R-scripts solving the one-dimensional RE with and without volume change (RE and REVC) using the finite difference method and verify the script using four examples: 1) downward infiltration, 2) upward infiltration, 3) system-dependent atmospheric boundary condition, and 4) system-dependent atmospheric boundary condition with bottom tension.

3. Perform a sensitivity analysis of model parameters to time to equilibrium surficial pressure head for a shallow-water table with constant evaporation from the surface using three models: 1) vGM NonVC RE, 2) vGM NonVC RE, and vGM VC REVC and compare differences.

4. Test the model using data collected from three lysimeter cores and perform the necessary TDR sensor calibrations for marl and peat.

Chapter 4

The general objective of applying the proposed model to a site in Shark River Slough, Everglades where subsidence of the root zone was measured for non-steady boundary conditions is achieved through the following approach:

1. Use meteorological data (evapotranspiration) and river stages available from the Everglades Depth Estimation Network (EDEN) to calculate top and bottom boundary conditions for the soil profile.

2. Apply the time-varying boundary conditions to the soil profile determined by Whelan et al., 2005 at the site.

3. Calibrate the height-change look-up tables and compare to the soil subsidence measurements obtained through the Surface Elevation Tables (SETs).

Chapter 5

The general objective of demonstrating the practical application of the newly developed REVC model in research, development and ecosystem management focuses on a case within the Everglades National Park, for which some basic data was available,

where hydrologic subsidence for different case scenarios of the ridge and slough accretion and reversible shrinkage was simulated as described next:

1. Use vegetation maps derived from spectral data to conduct the ridge and slough classification of the study site.
2. Apply a random normal distribution (mean = 30 cm and standard deviation = 5cm) to assign cell heights.
3. Simulate case scenarios with 1) low accretion, no reversible shrinkage, 2) high accretion, moderate reversible shrinkage, and 3) moderate accretion, moderate reversible shrinkage for a 10-year time-period.

References

Abtew, W., D. Cadavid, and V. Ciuca. 2013. Chapter 2: South Florida Hydrology and Management. *In* 2013 South Florida Environmental Report.

Adem, H.H., and S.K. Vanapalli. 2013. Constitutive modeling approach for estimating *1-D* heave with respect to time for expansive soils. Int. J. Geotech. Eng. 7(2): 199–204Available at http://www.tandfonline.com/doi/full/10.1179/1938636213Z.00000000024 (verified 18 June 2019).

Adem, H.H., and S.K. Vanapalli. 2015. Review of methods for predicting in situ volume change movement of expansive soil over time. J. Rock Mech. Geotech. Eng. 7: 73–86Available at http://dx.doi.org/10.1016/j.jrmge.2014.11.002 (verified 24 October 2018).

Betha, R., M. Pradani, P. Lestari, U.M. Joshi, J.S. Reid, and R. Balasubramanian. 2012. Chemical speciation of trace metals emitted from Indonesian peat fires for health risk assessment. Atmos. Res. 122: 571–578.

Bishop, A.W., and G.E. Blight. 1963. Some Aspects of Effective Stress in Saturated and Partly Saturated Soils. Géotechnique 13: 287–295.

Briaud, J.-L., X. Zhang, and S. Moon. 2003. Shrink Test–Water Content Method for Shrink and Swell Predictions. J. Geotech. Geoenvironmental Eng. 129(7): 590–600Available at http://ascelibrary.org/doi/10.1061/%28ASCE%291090-0241%282003%29129%3A7%28590%29 (verified 18 June 2019).

Brooks, R.H., and A.T. Corey. 1964. Hydraulic Properties of Porous Media. Color. State Univ. Hydrol. Pap. No 3: 27.

Camporese, M., S. Ferraris, M. Putti, P. Salandin, and P. Teatini. 2006. Hydrological modeling in swelling/shrinking peat soils. Water Resour. Res. 42(6): 1–15.

Celia, M.A., E.T. Bouloutas, and R.L. Zarba. 1990. A general mass-conservative numerical solution for the unsaturated flow equation. Water Resour. Res. 26: 1483–1496.

Chaberneau, R.J. 2006. Groundwater Hydraulics and Pollutant Transport. Waveland Press, Long Grove, IL.

Chambers, L.G., S.E. Davis, T. Troxler, J.N. Boyer, A. Downey-Wall, and L.J. Scinto. 2014. Biogeochemical effects of simulated sea level rise on carbon loss in an Everglades mangrove peat soil. Hydrobiologia 726: 195–211.

Chambers, L.G., T.Z. Osborne, and K.R. Reddy. 2013. Effect of salinity-altering pulsing events on soil organic carbon loss along an intertidal wetland gradient: a laboratory experiment. Biogeochemistry 115: 363–383Available at https://sciences.ucf.edu/biology/abl/wp-content/uploads/sites/109/2015/08/chambers_et_al._2013.pdf (verified 18 June 2019).

Chambers, L.G., K.R. Reddy, and T.Z. Osborne. 2011. Short-Term Response of Carbon Cycling to Salinity Pulses in a Freshwater Wetland. Wetl. Soils 75(5): 2000–2007Available at https://soils.ifas.ufl.edu/wetlands/publications/PDF-articles/355.Short-Term Response of Carbon Cycling to.pdf (verified 18 June 2019).

Chambers, L.G., H.E. Steinmuller, and J.L. Breithaupt. 2019. Toward a mechanistic understanding of "peat collapse" and its potential contribution to coastal wetland loss. Ecology: e02720Available at https://onlinelibrary.wiley.com/doi/abs/10.1002/ecy.2720 (verified 24 May 2019).

Corstanje, R., S. Grunwald, K.R. Reddy, T.Z. Osborne, and S. Newman. 2006. Assessment of the spatial distribution of soil properties in a northern Everglades marsh. J. Environ. Qual. 35: 938–949.

Crump, J. 2017. Smoke on Water - Countering Global Threats From Peatland Loss and Degradation. A UNEP Rapid Response Assessment. Nairobi.

Davies, G.M., A. Gray, G. Rein, and C.J. Legg. 2013. Peat consumption and carbon loss due to smouldering wildfire in a temperate peatland. For. Ecol. Manage. 308: 169–177.

Davis, J.R. 1946. The peat deposits of Florida. Florida Geol. Surv. Bull. 30: 247.

Davis, S., and J.C. Ogden. 1994. Everglades: The Ecosystem and Its Restoration. CRC Press.

DeAngelis, D.L., L.J. Gross, M. a. Huston, W.F. Wolff, D.M. Fleming, E.J. Comiskey, and S.M. Sylvester. 1998. Landscape Modeling for Everglades Ecosystem Restoration. Ecosystems 1(1): 64–75.

DeLaune, R.D., J.A. Nyman, and W.H.P. Jr. 1994. Peat Collapse, Ponding and Wetland Loss in a Rapidly Submerging Coastal Marsh. J. Coast. Res. 10: 1021–1030Available at https://www.jstor.org/stable/4298293 (verified 18 June 2019).

Dixon, S.J., N. Kettridge, P.A. Moore, K.J. Devito, A.S. Tilak, R.M. Petrone, C.A. Mendoza, and J.M. Waddington. 2017. Peat depth as a control on moss water availability under evaporative stress. Hydrol. Process. 31(23): 4107–4121.

Dreschel, T.W., S. Hohner, S. Aich, and C.W. McVoy. 2018. Peat Soils of the Everglades of Florida, USA. *In* Peat. InTech.

Fling, H., N. Aumen, T. Armentano, and F. Mazzotti. 2012. The Role of Flow in the Everglades Landscape.

Fredlund, D.G., and A. Xing. 2008. Erratum : Equations for the soil-water characteristic curve . Can. Geotech. J.

Gardner, W.R. 1958. Some Steady-State Solutions of the Unsaturated Moisture Flow Equation with Application to Evaporation from a Water Table. Soil Sci.

van Genuchten, M.T. 1980. A closed form equation for predicting the Hydraulic Conductivity of Unsaturated Soils. Soil Sci. Soc. Am. J. 44(5): 892–898.

Glaz, B. 1995. Research seeking agricultural and ecological benefits in the Everglades: J. Soil Water Conserv. 50: 609–612.

Gnatowski, T., J. Szatyłowicz, T. Brandyk, and C. Kechavarzi. 2010. Hydraulic properties of fen peat soils in Poland. Geoderma 154(3–4): 188–195.

Goetz, J.D., and J.S. Price. 2016. Ecohydrological controls on water distribution and productivity of moss communities in western boreal peatlands, Canada. Ecohydrology 9(1): 138–152Available at http://doi.wiley.com/10.1002/eco.1620 (verified 20 September 2018).

Haikerwal, A., M. Akram, A. Del Monaco, K. Smith, M.R. Sim, M. Meyer, T.A. M., M.J. Abramson, and M. Dennekamp. 2015. Impact of Fine Particulate Matter (PM2.5) Exposure During Wildfires on Cardiovascular Health Outcomes. J. Am. Heart Assoc. 4.

Hallema, D.W., Y. Périard, J. a. Lafond, S.J. Gumiere, and J. Caron. 2015. Characterization of Water Retention Curves for a Series of Cultivated Histosols. Vadose Zo. J. 14(6): 0.

Hohner, S.M., and T.W. Dreschel. 2015. Everglades peats : using historical and recent data to estimate predrainage and current volumes , masses and carbon contents. Int. Mire Conserv. Gr. Int. Peat Soc. 16: 1–15.

Holden, J., Z.E. Wallage, S.N. Lane, and A.T. McDonald. 2011. Water table dynamics in undisturbed, drained and restored blanket peat. J. Hydrol. 402(1–2): 103–114Available at http://dx.doi.org/10.1016/j.jhydrol.2011.03.010.

Ingebritsen, S.., C.W. Mcvoy, B. Glaz, and W. Park. 1999. Florida Everglades. p. 95–106. *In* Galloway, D., Jones, D.R., Ingebritsen, S.E. (eds.), Land Subsidence in the United States. U.S. geological Survey Circular; 1182.

Jarosewich, M., and J. Wagner. 1985. Geologic Structure of the Surificial Aquifer System underlying Everglades National Park and Big Cypress National Park.

Jones, L.A. 1948. Soils, geology, and water control in the Everglades region: University of Florida Agricultural Experiment Station Bulletin 442.

Joosten, H. 2010. The Global Peatland CO2 Picture. Peatland status and drainage related emissions in all countries of the world. Ede.

Kechavarzi, C., Q. Dawson, and P.B. Leeds-Harrison. 2010. Physical properties of low-lying agricultural peat soils in England. Geoderma 154(3–4): 196–202Available at http://dx.doi.org/10.1016/j.geoderma.2009.08.018.

Kennedy, G.W., and J.S. Price. 2005. A conceptual model of volume-change controls on the hydrology of cutover peats. J. Hydrol. 302(1–4): 13–27.

Lane, R.R., S.K. Mack, J.W. Day, R.D. DeLaune, M.J. Madison, and P.R. Precht. 2016. Fate of Soil Organic Carbon During Wetland Loss. Wetlands 36(6): 1167–1181Available at http://link.springer.com/10.1007/s13157-016-0834-8 (verified 18 June 2019).

Loveless, C.M. 1959. A Study of the Vegetation in the Florida Everglades. Ecol. Soc. Am. 40(1): 1–9.

Marlier, M.E., R.S. DeFries, P.S. Kim, D.L. Gaveau, S.N. Koplitz, D.J. Jacob, L.J. Mickley, B. Margono, and S.S. Myers. 2015. Regional air quality impacts of future fire emissions in Sumatra and Kalimantan. Environ. Res. Lett. 10(54010).

McCarter, C.P.R., and J.S. Price. 2013. The hydrology of the Bois-des-Bel bog peatland restoration: 10 years post-restoration. Ecol. Eng. 55.

McCarter, C.P.R., and J.S. Price. 2014. Ecohydrology of *Sphagnum* moss hummocks: mechanisms of capitula water supply and simulated effects of evaporation. Ecohydrology 7(1): 33–44Available at http://doi.wiley.com/10.1002/eco.1313 (verified 9 November 2018).

Mclean, A.R., J.C. Ogden, and E.E. Williams. 2002. Chapter 7 : Comprehensive Everglades Restoration Plan. East: 1–16.

National Research Council. 2014. Progress Toward Restoring the Everglades : The Fifth Biennial Review.

Neubauer, S.C. 2013. Ecosystem Responses of a Tidal Freshwater Marsh Experiencing Saltwater Intrusion and Altered Hydrology. Estuaries and Coasts 36(3): 491–507Available at http://link.springer.com/10.1007/s12237-011-9455-x (verified 18 June 2019).

Neubauer, S.C., R.B. Franklin, and D.J. Berrier. 2013. Saltwater intrusion into tidal freshwater marshes alters the biogeochemical processing of organic carbon. Biogeosciences 10(12): 8171–8183Available at https://www.biogeosciences.net/10/8171/2013/ (verified 18 June 2019).

Ogden, J.C. 2005. Everglades ridge and slough conceptual ecological model. Wetlands 25(4): 810–820.

Oh, S., Y.K. Kim, and J.W. Kim. 2015. A modified van Genuchten-Mualem model of hydraulic conductivity in Korean residual soils. Water (Switzerland) 7(10): 5487–5502.

Oh, W.T., S.K. Vanapalli, and A.J. Puppala. 2009. Semi-empirical model for the prediction of modulus of elasticity for unsaturated soils. Can. Geotech. J. 46(8): 903–914Available at http://www.nrcresearchpress.com/doi/10.1139/T09-030 (verified 18 June 2019).

Oleszczuk, R., K. Bohne, J. Szatylowicz, T. Brandyk, and T. Gnatowski. 2003. Influence of load on shrinkage behavior of peat soils. J. Plant Nutr. Soil Sci. 166(2): 220–224.

Oleszczuk, R., T. Brandyk, T. Gnatowski, J. Szaty, and J. Kami. 2008. The comparison of soil moisture content changes in the moorsh layer under shrubs and grass vegetation. 6(1): 141–148.

Overton, D.D., K.-C. Chao, and J.D. Nelson. 2006. Time Rate of Heave Prediction for Expansive Soils. p. 1–6. *In* GeoCongress 2006. American Society of Civil Engineers, Reston, VA.

Portnoy, J.W., and A.E. Giblin. 1997. Biogeochemical Effects of Seawater Restoration to Diked Salt Marshes. Ecol. Appl. 7(3): 1054–1063Available at https://esajournals.onlinelibrary.wiley.com/doi/abs/10.1890/1051-0761%281997%29007%5B1054%3ABEOSRT%5D2.0.CO%3B2 (verified 18 June 2019).

Price, J.S. 2003. Role and character of seasonal peat soil deformation on the hydrology of undisturbed and cutover peatlands. Water Resour. Res. 39(9)Available at http://doi.wiley.com/10.1029/2002WR001302 (verified 1 June 2019).

Price, J.S., and S.M. Schlotzhauer. 1999. Importance of shrinkage and compression in determining water storage changes in peat: The case of a mined peatland. Hydrol. Process. 13(16 SPEC. ISS.): 2591–2601.

Pumo, D., S. Tamea, L.V. Noto, F. Miralles-Wilhem, and I. Rodriguez-Iturbe. 2010. Modeling belowground water table fluctuations in the Everglades. Water Resour. Res. 46(11).

Pyatt, D.G., and A.L. John. 1989. Modelling volume changes in peat under conifer plantations. Soil Sci. 40: 695–706.

Radcliffe, D.E., and J. Simunek. 2010. Soil Physics with HYDRUS: Modeling and Applications [Hardcover]. CRC Press.

Rezanezhad, F., J.S. Price, W.L. Quinton, B. Lennartz, T. Milojevic, and P. Van Cappellen. 2016. Structure of peat soils and implications for water storage, flow and solute transport: A review update for geochemists. Chem. Geol. 429: 75–84.

Rezanezhad, F., W.L. Quinton, J.S. Price, D. Elrick, T.R. Elliot, and R.J. Heck. 2009. Examining the effect of pore size distribution and shape on flow through unsaturated peat using 3-D computed tomography. Hydrol. Earth Syst. Sci. Discuss. 6(3): 3835–3862.

Ross, M.S., D.L. Reed, J.P. Sah, P.L. Ruiz, and M.T. Lewin. 2003. Vegetation:environment relationships and water management in Shark Slough, Everglades National Park. Wetl. Ecol. Manag. 11(5): 291–303.

Schwarzel, K., M. Renger, R. Sauerbrey, and G. Wessolek. 2002. Soil physical characteristics of peat soils. Plant Nutr. Soil (165): 479–486.

Schwärzel, K., J. Šimůnek, H. Stoffregen, G. Wessolek, and M.T. van Genuchten. 2006. Estimation of the Unsaturated Hydraulic Conductivity of Peat Soils. Vadose Zo. J. 5(2): 628.

SFWMD. 2005. Theory Manual Regional Simulation Model. West Palm Beach, FL.

Šimůnek, J., M. Šejna, H. Saito, M. Sakai, and M.T. van Genuchten. 2013. The Hydrus-1D Software Package for Simulating the Movement of Water, Heat, and Multiple Solutes in Variably Saturated Media. : 342.

Sklar, F., C. Mcvoy, R. Van Zee, D. Gawlik, W. Park, C. Fitz, Y. Wu, D. Rudnick, S. Miao, A. Ferriter, S. Krupa, T. Armentano, K. Tarboton, K. Rutchey, Q. Dong, and S. Newman. 2000. Everglades Consolidated Report Chapter 2 : Hydrologic Needs : The Effects of Altered Hydrology on the Everglades. : 2:1–68.

Snyder, G.H., H.W. Burdine, J.R. Crockett, G.J. Gascho, D.S. Harrison, G. Kidder, J.W. Mishoe, D.L. Myhre, F.M. Pate, and S.F. Shih. 1978. Water Table Management For Organic Soil Conservation and Crop Production in the Florida Everglades. Gainesville.

Stephens, J.C., A.L. H., and E. Chen. 1984. Organic soil subsidence, in Holzer, T.L., ed., Man-induced land subsidence. Geol. Soc. Am. Rev. Eng. Geol. 6: 107–112.

Stephens, J.C., and L. Johnson. 1951. Subsidence of organic Soils in the upper Everglades region of Florida. Soil Sci. Soc. Florida Proc. XI: 191–237.

Szajdak, L., and J. Szatylowicz. 2002. Impact of Drainage on Hydrophobicity of Fen Peat-Moorsh Soils. Mires Peat: 158–174.

United States Geological Survey. 2003. Measuring and Mapping the Topography of the Florida Everglades for Ecosystem Restoration.

USACE. 1996. Master Water Control Manual for the Water Conservation Areas, Everglades National Park and ENP-South Dade Conveyanve System. Jacksonville, Florida.

USEPA. 1997. South Florida Ecosystem Assessment: Monitoring for Adaptive Management: Implications for Ecosystem Restoration: Final Technical Report - Phase I.

USGS. Everglades Depth Estimation Network (EDEN). Available at https://sofia.usgs.gov/eden/ (verified 18 June 2019).

Vereecken, H., A. Schnepf, J.W. Hopmans, M. Javaux, D. Or, T. Roose, J. Vanderborght, M. Young, W. Amelung, M. Aitkenhead, S.D. Allison, S. Assouline, P. Baveye, M. Berli, N. Brüggemann, P. Finke, M. Flury, T. Gaiser, G. Govers, T. Ghezzehei, P. Hallett, and K. Lamorski. 2016. Modeling Soil Processes: Review, Key challenges and New Perspectives. Vadose Zo. J. 15Available at file:///G:/CAOS (2)/Citavi Attachments/Vereecken - Modeling Soil Processes.pdf.

Vu, H.Q., and D.G. Fredlund. 2004. The prediction of one-, two-, and three-dimensional heave in expansive soils. Can. Geotech. J. 41(4): 713–737Available at http://www.nrcresearchpress.com/doi/10.1139/t04-023 (verified 18 June 2019).

Wallor, E., A. Herrmann, and J. Zeitz. 2018a. Hydraulic properties of drained and cultivated fen soils part II — Model-based evaluation of generated van Genuchten parameters using experimental field data. Geoderma 319: 208–218.

Wallor, E., N. Rosskopf, and J. Zeitz. 2018b. Hydraulic properties of drained and cultivated fen soils part I -Horizon- based evaluation of van Genuchten parameters considering the state of moorsh-forming process.

Wang, C., C. Tong, L.G. Chambers, and X. Liu. 2017. Identifying the Salinity Thresholds that Impact Greenhouse Gas Production in Subtropical Tidal Freshwater Marsh Soils. Wetlands 37(3): 559–571Available at http://link.springer.com/10.1007/s13157-017-0890-8 (verified 18 June 2019).

Whelan, K.R.T., T.J. Smith, D.R. Cahoon, J.C. Lynch, and G.H. Anderson. 2005. Groundwater control of mangrove surface elevation: Shrink and swell varies with soil depth. Estuaries 28(6): 833–843Available at http://link.springer.com/10.1007/BF02696013 (verified 25 October 2018).

Williams, J., R.E. Prebble, W.T. Williams, and C.T. Hignett. 1982. The influence of texture, structure and clay mineralogy on the soil moisture characteristic. Aust. J. Soil Res.

Wray, W.K., B.M. El-Garhy, and A.A. Youssef. 2005. Three-Dimensional Model for Moisture and Volume Changes Prediction in Expansive Soils. J. Geotech. Geoenvironmental Eng.

Yu, Z., D.W. Beilman, S. Frokling, G.M. MacDonald, N.T. Roulet, P. Camill, and D.J. Charman. 2011. Peatlands and Their Role in the Global Carbon Cycle. Eos (Washington. DC). 92(12): 97–108Available at https://agupubs.onlinelibrary.wiley.com/doi/pdf/10.1029/2011EO120001 (verified 13 September 2018).

Zhang, X. 2004. Consolidation theories for saturated-unsaturated soils and numerical simulation of residential buildings on expansive soils. Elements.

2. CHARACTERIZATION OF UNSATURATED HYDRAULIC PROPERTIES OF EVERGLADES WETLAND SOILS

2.1 Introduction

The Everglades in South Florida, an intensely managed, subtropical, freshwater wetland system, is threatened by devastating shifts in landscape patterns caused by changes in the quantity and quality of water distributed in the system (Harvey et al., 2017; M.S. Ross et al., 2003; Scheidt et al., 2007; SCT, 2003). Interruptions to the historic sheetflow in the Everglades have resulted in pronounced fluctuations in water levels causing higher frequency and longer duration dry-downs (water level dropping below the soil surface) leading to the presence of seasonal unsaturated zones in typically inundated environments (DeAngelis et al., 1998; SCT, 2003). Water level gages as part of the Everglades Depth Estimation Network (EDEN) show that the unsaturated zone thickness can vary between 0 to 3 feet and these unsaturated zones can occur for a few days to months during the dry season from December to April when rainfall is limited. Gages in the northern Water Conservation Areas (WCAs, compartmentalized units created through the construction of water control structures that have similar hydrology within the unit) record shallower and shorter-duration unsaturated zones while gages in the southern Everglades National Park (ENP) record deeper and longer-duration unsaturated zones. Even within hydrologically similar areas, microtopographic features (1 m horizontal scale) in the form of topographically elevated sawgrass ridges could mean the presence of the unsaturated zone may be more prevalent than anticipated.

Dry-down of organic wetland soils are known to be a major contributor of green-house gases and their regulation is a topic of international interest (Joosten, 2010). Dry-down also results in the loss of organic soil through oxidation thereby reducing the storage of the surficial aquifer; for coastal wetlands like the Everglades which are already vulnerable to sea-level rise and saline intrusion, this could be catastrophic (Dreschel et al., 2018; Hohner and Dreschel, 2015). Distributed numerical models of unsaturated hydrology, with accurately derived parameters, can define soil water storage and flux, and serve as valuable tools in the conservation, restoration, and management of altered, ecologically sensitive systems like wetlands. However, models of this kind require an extensive dataset of unsaturated soil hydraulic parameters (SHPs), which are not currently available for the Everglades soils.

The Everglades system consists of two principal soils – marl and peat, which overlay a highly permeable limestone bedrock. Marl is a light-colored soil consisting of silt and fine-grained calcite. It is formed during dry-downs through the weathering of limestone or the oxidization of periphyton – an assemblage of benthic algae, cyanobacteria and micro-fauna (Clark and Reddy, 2005; Gaiser et al., 2011). Whereas peat, formed by the slow anaerobic decomposition of plant matter, can be further classified as Everglades peat and Loxahatchee peat based on its botanical origin. Everglades peat is formed from the decomposition of sawgrass sedges, while Loxahatchee peat is formed from aquatic plants like water lilies (Dreschel et al., 2018). Due to the contrasting hydroperiod (number of days of per year the soil surface is wet) requirements for soil formation, peat is prevalent in marshes of the Northern Everglades region, which are wetter (hydroperiods greater than

330 days), whereas marl is prevalent in marshes of Southern Everglades (hydroperiods greater than 120 days) (M. S. Ross et al., 2003; Sklar et al., 2000).

Hydric soils like peat, which are composed of organic matter in various states of decomposition, have been gaining recognition for their role in biodiversity, water dynamics and carbon sequestration (Rocha Campos et al., 2011). However, as their physical properties are influenced by local vegetation, and hydrology, spatial variability of soil hydraulic properties may be observed (Boelter, 1964; Crockett et al., 2015; Rezanezhad et al., 2016). Differences in peat characteristics may also be observed within the same patterned landscape, where differences in vegetation and flow patterns are seen, and over time, as these patterns shift. The accurate modeling of peatland soil hydrology requires understanding of both its spatial and temporal soil hydraulic properties (Wallor et al., 2018).

Unsaturated soil hydraulic properties are parameterized in the Richards equation-based, transient, unsaturated flow models using soil water retention curves (SWRCs). Due to the continuous nature of the curve function, the van Genuchten Mualem (vGM) model is widely applied in modelling water retention of peat soil (Goetz and Price, 2016; Hallema et al., 2015; Kettridge et al., 2016; Oleszczuk et al., 2008; Schwarzel et al., 2002; Schwärzel et al., 2006; van Genuchten, 1980; Wallor et al., 2018). More recently, new SWRC models capable of modeling water retention for peats with bi-modal and tri-modal pore-size distributions have been developed and tested (Dettmann et al., 2014; Weber et al., 2017); however, the popularity of the vGM model has not waned. Parameters of the vGM model (or other SWRCs) are obtained either directly – by fitting SWRC models to water retention

data obtained from oedometer or evaporation experiments or indirectly – from field data or pedotransfer functions (PTFs). Due to their limitations, fewer studies have used the indirect methods for hydric soils (Liu and Lennartz, 2019). Indirect methods like inverse modeling from field data are limited to point-based observational data collection and to the narrow range of moisture conditions experienced in-situ whereas PTFs are limited to the database of prior studies from which unsaturated parameters are estimated (Schwärzel et al., 2006). Furthermore, variability in unsaturated hydraulic parameters across landscapes have been observed for hydric soils like peat whose hydraulic properties are influenced by vegetation, hydrology and climate (Crockett et al., 2015; Gnatowski et al., 2010); hence, PTFs may be inaccurate if not generated from a regional database.

SHPs of peat are influenced by its degree of decomposition (quantified by fiber content (FC)), contributing plant matter, and organic content (OC) (Rezanezhad et al., 2016). Due to its high porosity, peat has a very high water holding capacity at saturation which decreases with increase in degree of decomposition and its bulk density (BD) (Rezanezhad et al., 2016). The modeling of peat is challenging due to its volume changing behavior. The desaturation of peat is accompanied by its shrinking which is described in three phases: 1) near-normal - the decrease in soil volume is proportional to moisture content, 2) subnormal - moisture loss exceeds volume change, and 3) super normal – drying of the smallest pores causing collapse of the matrix (Camporese et al., 2006). Rewetting of the peat soil results in swelling of the matrix. The swelling however shows hysteretic behavior, which is attributed to the formation of water repelling films (hydrophobia), effects of pore geometry (ink-bottle-effect), and alterations of spatial structure of pores during shrinkage (Schwarzel et al., 2002). In addition, due to structural changes of the soil

matrix that occur during shrinkage and bio-oxidation of the organic matter during drying, the peat matrix loses volume, and a reduced water holding capacity is witnessed upon rewetting to saturation (Camporese et al., 2006; Szajdak and Szatylowicz, 2002). This results in irreversible subsidence causing a loss of soil elevation – a common issue observed in drained peatlands.

Previous efforts to study soil hydrology of Everglades soils have mainly focused on determining saturated hydraulic conductivity (K_{sat}). Myers (1999) used an unsaturated column water balance test to estimate unsaturated hydraulic conductivity of undisturbed soil cores collected from two isolated South Florida wetlands; however, the soil cores consisted of mixed soil layers (peat and sand). Subsequent works like Pumo et al. (2010) have used Myers (1999) data to model water-table fluctuations in three sites with peat, marly-peat, and marl assuming, based on the limited Myers (1999) data, that hydrology in soils are similar. No efforts to compare the unsaturated SHPs of Everglades soils using soil testing are available in literature. Perez (2014) studied unsaturated hydraulic conductivity for two plots in Shark River Slough Everglades. However, their sampling was limited to small plots whose soil profile had been altered by construction and no SHPs for Everglades marl were reported. The overall objective of this work is to characterize the SHPs of Everglades soil derived from soil testing and investigate the effect of VC on the SWRC parameterization process, in support of future efforts to build numerical models that can best simulate fluxes in a volume-changing soil matrix during the dry season. Laboratory methods were used to determine the hydraulic properties like the SWRCs (from which vGM parameters were obtained) and K_{sat}, and soil physical properties like OC, FC, and

BD. These properties were then used to achieve the following specific objectives of this work :

(1) Characterize the water retention during desaturation and resulting volume-change of hydromorphic histosols collected from relatively hydrologically compartmentalized areas in the Everglades using an unsupervised clustering algorithm, and define the clusters using soil properties like OC, FC, and BD.
(2) Evaluate the differences in water retention, shrinkage, and vGM parameters of the defined clusters using ANOVA and post-hoc Tukey's HSD,
(3) Investigate the effect of shrinkage on the Everglades soils and assess the applicability of the widely used van Genuchten-Mualem (vGM) model for defining the retention curve of volume-changing samples, and
(4) Study the differences in peat properties as a result of hydrology (between WCAs) and vegetation (between dominant vegetation types) using ANOVA and linear regression.

2.2 Methodology

2.2.1. Sites and Sampling

A subset of 53 sites sampled as a part of the Environmental Protection Agency's 2013-2014 Everglades Ecosystem Monitoring and Assessment Program (EMAP) (Figure 2-1) was used to determine soil properties like OC, FC, BD, K_{sat} and SWRC. Soil cores were collected from freshwater marshes in the Everglades using a statistical probability-based sampling approach (Scheidt et al., 2007). The cores were collected in a clear acrylic tube inserted into the top 10 cm of the ground. It is important to note that the samples were

disturbed, that is, they were not preserved as intact cores in the acrylic tube post sampling. Instead, they were placed in a sealed plastic container and preserved in a refrigeration unit to minimize loss in soil moisture and minimize decomposition until lab testing. Prior to testing, three retaining rings (1500F Pressure Plate Extractor by SoilMoisture Corp) of height 1 cm and diameter 5.15 cm were inserted into the collected soil to extract samples for OC, BD, and SWRC testing. SWRC and BD were calculated from the same test while the samples were reused for OC testing. For the FC tests used 100 g of moist soil was used while the hydraulic conductivity tests were performed with repacked samples of diameter 77 cm and approximately similar heights (minimum height and maximum height). The re-packing done using a three-layer compaction procedure similar to one described in Klute, 1986 and was kept consistent for all the sites.

2.2.2. Soil Organic Content (OC)

The OC of three replicates for each site was measured using the loss of ignition (ASTM D2974, 2000). Dried soil samples were placed in pre-weighed ceramic containers. The mass of the containers with dried soil were recorded, and the containers were placed in a muffle furnace and incinerated at 440^{o}C until no change in weight is observed (approximately 4 hours). At this point, the organic matter is burned off leaving only the ash. The weight of the containers with the ash were recorded, and the weight of the organic matter burned off was calculated. The OC of the soil was calculated as a percentage of initial soil weight. The raw data and calculations are presented in Appendix A Table A1.

2.2.3. Fiber Content (FC)

FC of organic soils (OC greater than 80%) was determined using the wet sieving method (ASTM D1997, 2001). First, the moisture content of each soil sample was determined by oven drying a representative sample of undried soil of known mass for 24 hours in pre-weighed containers. The moisture content of the sample is calculated as a percentage of its initial mass. Undried soil with a known moisture content weighing approximately 100 g was paced in 500 mL of 5% sodium hexametaphosphate for 15 hours and stirred at 240 r/min for 10 minutes. The mixture was poured into a 100-mesh stainless steel sieve and washed with a jet of water at low pressure. The sieve was placed in a pan containing 2% solution of hydrochloric acid for 10 minutes to dissolve the carbonates. The sieve was washed a second time to remove residual hydrochloric acid. Any large piece of stone or plant material like roots or wood were removed from the sieve before inverting the screen over a large, pre-weighed #4 filter paper placed in a funnel. The back of the screen was washed into the filter paper to remove any remaining fibers on the screen. The filter paper with the fibers were dried in an oven at 105^{o}C for 24 hours and weighed. The FC was calculated as a percentage of the dry mass of soil. Photographs of the methodology are presented in Figure 2-2. The raw data and calculations are presented in Appendix A Table A2.

2.2.4. Dry Bulk Density

The dry bulk density was measured by oven drying triplicates of known volume (cylindrical samples of height 1 cm, diameter of 5.15 cm and volume of 20.820 cm^3) from

each site for 24 hours at 105°C. The weight of the dried samples was used to calculate bulk density using the following equation:

$$BD = \frac{Mass\ of\ dry\ soil}{Volume\ of\ sample} \quad [2.1]$$

2.2.5. Saturated Hydraulic Conductivity

The K_{sat} of the soil samples was estimated using Darcy's Law for flow through porous media (ASTM D4511, 2011). For this test, a cylindrical soil sample (minimum diameter to height ratio 1:1) was saturated for 3 days and placed at the bottom of a 310 mm high clear acrylic tube with diameter of 77 mm. A No. 40 mesh was placed above and beneath the sample. A reservoir tank, into which a water source was connected, was used to maintain the hydraulic head in the clear tube with the sample. For different hydraulic heads, outflow at the base of the tube was measured. Water column heights were kept below 100 mm to reduce the effects of peat compression for organic soil. Readings were taken in sets of three. Using Darcy's Law, the K_{sat} (cm d^{-1}) was calculated. The raw data and calculations are presented in Table A3.

2.2.6. Soil Water Retention Curves

2.2.6.1. Saturated Volumetric Water Content

The porosity of the soil samples is assumed to be equal to its saturated VWC since during saturation all the pores of the soil and filled with water (Chaberneau, 2006). The porosity of the soil samples were calculated from the bulk density and the particle density

using the method described in Hallema et al., 2015. The particle density (ρ_p) at each site is calculated using the method by Paquet et al., 1993:

$$\rho_p = \frac{1 + F}{\left(\frac{F}{1.55}\right) + \left(\frac{1}{2.65}\right)} \quad [2.2]$$

Where F is the ratio of OC to ash content, and the particle density of peat and marl were assumed to be 1.55 g cm^{-3} and 2.65 g cm^{-3}, respectively

The porosity is then calculated from particle density and BD as:

$$\varphi = 1 - \frac{BD}{\rho_p} \quad [2.3]$$

2.2.6.2. Drying Curve

Unsaturated soil parameters were estimated using the drying SWRCs at suctions of 6 kPa (61 cmH_2O), 10 kPa (102 cmH_2O), 50 kPa (510 cmH_2O), and 1500 kPa (15296 cmH_2O), which provide the relationship between matric potential and water content. The drying curve of the SWRC was obtained through laboratory testing using the 1500 F Pressure Plate Extractor (Soilmoisture, 2009). Triplicates from each site contained in retaining rings of 1 cm height and 5.15 cm diameter were placed on ceramic pressure plate cells and saturated in water bath for 24 hours allowing the bottom-up saturation of the soil samples. The saturated samples and plates are then placed in a pressurized chamber until outflow from the chamber ceases. This can take anywhere from 5-14 days with peat

samples being on the higher end of the range (Waters, 1980). Once outflow ceases, the samples were removed from the chamber. Photographs of some soil samples post applied pressures of 10 kPa, 50 kPa and 1500 kPa are presented in Figure 2-3. The volume of the samples was determined by measuring the diameter and height of each sample with a digital caliper. Three measurements of diameter and height were made at 120^{o} angles to ensure representativeness. The samples were then placed in pre-weighed containers and oven dried at 105^{o}C for 24 hours to calculate their VWC. Two sets of VWCs were calculated with and without VC - VC VWC and NonVC VWC. The raw data and calculations are presented in tables A4, A5, A6, and A7.

2.2.6.3. The van Genuchten Mualem (vGM) Unsaturated Model

The van Genuchten equation is commonly applied to model the relationship between VWC and the matric potential of unsaturated soils. Unlike the Brooks and Corey (1964) model, the van Genuchten model provides a continuous soil characteristic curve over the range of matric potential and is given by:

$$\theta(h) = \frac{\theta_s - \theta_r}{[1 + (-\alpha h)^n]^{(m)}} + \theta_r \qquad [2.4]$$

Where h is the matric potential (cm), θ_r is the residual VWC (cm^3 cm^{-3}), θ_s is the VWC at saturation (cm^3 cm^{-3}), and α and n are empirical parameters. The van Genuchten model when combined with Mualem's pore-size distribution model gives the fixed relationship between parameters m and n (Mualem, 1976):

$$m = 1 - \frac{1}{n} \qquad [2.5]$$

The vGM unsaturated model was fit to the SWRC and optimized vGM parameters were determined using the RETC code (van Genuchten, 1980). For each site, the retention curve data consisted of porosity (calculated in 2.2.6.1) and triplicates of VWCs at pressures of 6 kPa (), 10 kPa, 50 kPa and 1500 kPa. Two sets of vGM parameters – NonVC vGM and VC vGM were generated using NonVC VWCs and VC VWCs. Although quite robust, the code does require initial estimates for parameters θ_s, θ_r, α, and n. For parameter θ_s, the maximum porosity at the site was used as the initial estimate whereas for parameter θ_r, the minimum VWC at 1500 kPa was assigned. Based on the vGM estimates by Gnatowski et al., 2010, peat was assigned initial estimates of 0.0231 cm^{-1} and 1.292 for α, and n, while marl was assigned 0.002 cm^{-1} and 1.2 based on preliminary testing. RETC uses a least-squared optimization procedure to calculate the best fitting vGM parameters. The resulting values are presented in an output file along with the R-squared of the curve fit. Values that were outside two times the interquartile range for each cluster were removed as outliers from the analysis.

2.2.7. Statistical Analysis

Exploratory data analysis of the water retention and shrinkage of the samples was performed with agglomerative clustering using porosity (assumed to be equal to the saturated VWC) of the sample, and the volume of water in the sample at the end of each pressure setting and its corresponding total sample volume as observations. Due to the lack of previous studies on the soil hydraulic properties of Everglades soil, this study preferred

to use an unsupervised clustering algorithm like agglomerative clustering which can recognize subtle patterns in the data. Four agglomerative clustering methods – Average, Single, Complete and Ward were evaluated using the clustering coefficient. The Ward method of clustering was chosen as it had the highest clustering coefficient of 0.925. Agglomerative clustering is advantageous for identifying small clusters within the data. Cluster analysis can be performed with multiple parameters; however, all parameters must be standardized for a mean of zero and a standard deviation of one. The clusterability of the data can be measured using a clustering coefficient. This approach considers each sample to be a cluster of its own – or a leaf. Samples with the smallest Euclidean distance (Equation 2.5) to each other are combined to form a new cluster called a node (Gnatowski et al., 2010). Euclidean distance is given by,

$$d_{jk}^2 = \sum_{i=1}^{i=N} (Z_{ij} - Z_{ik})^2 \qquad [2.6]$$

Where, d_{jk}^2 is the squared Euclidean distance with the *j*-th and *k*-th sample, Z_{ij} is the standardized value for the *i*-th parameter and the *j*-th sample, Z_{ik} is the standardized value of the *i*-th parameter and the *k*-th sample, and N is the number of samples.

The nodes with the minimum within-cluster variance are merged together to form a larger cluster node using Ward's hierarchical clustering method (Equation 2.6) (Ward, 1963). The process is repeated until all nodes are combined to form one large cluster called a root comprising of all samples. The distance between clusters is calculated using Ward's clustering method is given by,

$$d(S_a, S_k) = \frac{((N_i + N_k)d(S_i, S_k) + (N_j + N)d(S_j, S_k) - N_k d(S_i, S_j))}{N_i + N_j + N_k} \quad [2.7]$$

Where, d is the distance between two clusters, S_i, S_j, S_k are the agglomerated clusters *i, j,* and *k*, S_a is the new cluster by joining clusters S_i and S_j, and N_i, N_j, N_k are the number of elements in clusters *i, j,* and *k* (Ward, 1963).

There are no definite rules used to select the number of clusters; it is often conducted through a combination of methods for optimal cluster selection (which may each produce different results) and the interpretation of clustered data. This work uses three methods to determine the optimal number of clusters: (1) elbow method – calculates the total within intra-cluster variation, reported as total with sum of squares (WSS) and a plot of WSS with corresponding number of clusters is used to select the optimal number (Kodinariya and Makwana, 2013; Thorndike, 1953); (2) silhouette method – uses both the intra-cluster variation and the inter-cluster variation to calculate a mean coefficient with high values indicating good clustering (Kodinariya and Makwana, 2013; Rousseeuw, 1987); and (3) gap-statistic method – compares the log of the intra-cluster variation with their expected values with a null reference distribution (random distribution with no obvious clustering) and selects the optimal number of clusters where the gap-statistic is maximum (Tibshirani et al., 2001).

R-Statistical software was used to conduct the cluster analysis (R Core Team, 2014). The data was first standardized, and the package 'cluster' was used to perform the agglomerative clustering. The clustering coefficient which measures the clusterability of

the data was computed. The R-package ‘factoextra’ was used to determine the optimal number of clusters with the elbow, silhouette, and gap statistic methods (Kassambara and Mundt, 2016). The clusters were then plotted using ‘factoextra’. The cluster tree was cut into the optimal number of clusters using the ‘dendextend’ package and the cluster dendrogram with the optimal clusters were plotted (Galili, 2015).

One-way ANOVA was used to test for statistically significant differences in means of hydraulic properties (K_{sat}, water retention, shrinkage and vGM parameters) between clusters, to test the effect of VC in vGM parameterization (between models NonVC vGM and VC vGM) and study differences in peat properties between hydrological units (WCAs) and dominant vegetation types (SG- sawgrass, SR-spikerush, WL-water lily, CT-cattail). One site was dropped from the analysis as it had an unusually high VC vGM n (Site x_221, n = 11.850). Prior to ANOVA testing, outliers were removed from the data. Outliers were identified as values outside 1.5 times the interquartile range (calculated from the first and third quartile). When deviations from normality were observed in a Q-Q plot of the residuals, the data was log-transformed. Where statistically significant differences were identified by ANOVA, Tukey’s HSD test was used to identify differences at a significance level of 0.05. ANOVA tests were also conducted with outliers and the results and conclusions were similar. Linear regression was to study the relationship between FC and BD on the VWCs. The scripts created to perform all the statistical analysis are presented in Appendix B.

2.3 Results

Clustering of water retention data

Figure 2-4 presents the optimal number of clusters calculated by three methods applied. The elbow method (Figure 2-4a) shows that the elbow in the graph occurs at three optimal clusters; the gap statistic method (Figure 2-4c) also calculates three optimal number of clusters. The silhouette method (Figure 2-4b), which is superior to the elbow method as it considers both the inter-cluster and intra-cluster variation, has a maximum mean silhouette width at two clusters. However, silhouette width is high with three clusters and four clusters; hence, three optimal clusters are selected. Figure 2-5 presents the dendrogram with the Euclidean distance between the cluster nodes and the selected clusters. Cluster 1 and Cluster 2 are more similar and fuse together at a Euclidean distance of approximately 12 while the combination of Cluster 1 and Cluster 2 joins with Cluster 3 at a distance of 18 indicating dissimilarity of Cluster 3 from the other two clusters.

The three clusters have a mean OC of 21.7% (Cluster 1), 66.7% (Cluster 2), and 90.0% (Cluster 3) (Table 2-1). As expected, a pattern of increase in BD with decrease in OC is observed in Table 2-1 with mean BDs of 0.503 g cm^{-3} (Cluster 1), 0.183 g cm^{-3} (Cluster 2), and 0.104 g cm^{-3} (Cluster 3) (Walczak and Rovdan, 2002). Henceforth, based on the OC and BD, the clusters will be called marl (Cluster 1), mixed marl-peat (Cluster 2), and peat (Cluster 3). Marl (Cluster 1) had OCs ranging from 11.8% to 37.0% The peat cluster (Cluster 3) consists entirely of peat samples with OCs ranging from 84.3% to 95.2% while the marl-peat cluster consists of higher OC marl and lower OC peat with an OC range of 28.0% to 89%. The marl-peat cluster contains two samples with OC < 37%, nine mixed

samples with OC between 37% and 80%, and nine peat samples with OC between 80% and 89%. Since, FC testing was performed only on samples with OC > 80%, no FC values are reported for Cluster 1. Mean FC of Cluster 2 (FC=29.7%) and Cluster 3 (FC=29.9%) are similar (Table 2-1); however, the FC test was conducted on only five out of 11 samples with OC > 80% in Cluster 2 (mixed marl-peat) and 18 out of 21 samples in Cluster 3 (peat) due to a lack of soil material for testing.

The clusters are grouped based on the porosity, the volume of water retained after each applied incremental pressure and its consequent reduced sample volume (Figure 4). As expected, significant differences in means of the cluster observations between clusters are observed (Table 2-2). At each applied pressure head, marl (Cluster 1) has a higher mean V_w than peat (Cluster 3) at each applied pressure head and marl was less prone to volume-change as observed with the higher mean V_s. However, at lower pressure heads of 6 kPa and 10 kPa, the mean V_w of marl (Cluster 1) and peat (Cluster 2) are not statistically different (Table 2-2). At 6 kPa and 10 kPa, the V_w of mixed marl-peat (Cluster 3) is significantly greater than marl ($p=0.0003$ and $p=0.0318$) by 12.6% and 7.5%, and peat ($p=0.0004$ and $p<0.0001$) by 10.7 and 12% respectively (Table 2-1 and Table 2-2). Tukey's HSD results presented in Table 2-2 shows that, at 50 kPa, the mean V_w of all three clusters at 50 kPa are statistically different. From Figure 2-6 and Table 2-1, it is observed that marl (Cluster 1) retains the highest mean V_w followed by marl- peat (Cluster 2), and peat (Cluster 3). At 1500 kPa, the mean V_w of peat (Cluster3) is significantly lower than marl ($p<0.0001$) and marl-peat ($p<0.0001$) by 86% and 115%, respectively (Table 2-2). With incremental pressure, the rate of desaturation and the rate of volume-change of the peat cluster is much higher than marl (Cluster 1) or marl-peat (Cluster 2) (Figure 2-6). Peat

(Cluster 3) is most susceptible to volume-change compared to the marl (Cluster 1) or the marl-peat (Cluster 2) at all applied pressure heads. From applied pressure of 10 kPa onwards, noticeable volume-change is observed for all clusters. At applied pressures of 10 kPa, 50 kPa, and 1500 kPa, the mean V_s of the peat cluster decreases to 76%, 55% and 37% of its initial volume, while for marl, (Cluster 1) decrease to 93%, 78% and 64%. For the marl-peat (Cluster 2) with the same applied pressure heads, sample volumes decrease to 93%, 65%, and 47%. Significant differences in means between all clusters at all pressure heads are observed except between marl (Cluster 1) and marl-peat (Cluster 2) at 10 kPa (Table 2-2).

The effect of VC on VWC

Calculating VWC without shrinkage can result in underestimating the VWC of the samples and hence, result in an entirely different water retention curve. Figure 2-7 presents the VWC's calculated for each cluster with and without shrinkage. The largest differences in the calculations are observed for the peat cluster as it more prone to shrinkage than the marl (Cluster 1) or marl-peat (Cluster 2). The main effect of including shrinkage is a decrease in the steepness of the curve progression with increasing pressure. Neglecting the change in volume can result in underestimating of the peat VWCs, on average, by 23%, 45% and 64% at pressure heads of 10 kPa, 50 kPa and 1500 kPa. Despite not being as susceptible to shrinkage as peat, the marl (Cluster 1) too exhibited the similar behavior with the mean VWC without shrinkage being 7%, 20% and 37% lower than the mean VWC with shrinkage at the same pressures. For some samples, VC causes the VWC at 10 kPa to be higher than the VWC at 6 kPa. This behavior is observed in some peat samples analyzed.

Although the average V_w from the peat cluster reduces by 19% from 6 kPa to 10 kPa, the V_s decreases by 24%. Since the VWC is inversely related to the volume of the sample, a higher VWC is observed at 10 kPa.

Parameterizing the water retention curves

The relationship between the measured and estimated VWCs for the two sets of model parameters generated (NonVC vGM and VC vGM) for a total sample size of 780 samples (five VWCs from triplicates at 52 sites) is presented in Figure 2-8 . The NonVC vGM model tends to underestimate the VWC at 6 kPa and overestimate the VWC at 10 kPa but the overall fit of the NonVC vGM model (R-squared of 0.9797) is better than the VC vGM model (R-squared 0.9147). For the VC vGM models, maximum dispersion is observed for pressures of 6 kPa, 10 kPa and 1500 kPa indicating a decrease in model accuracy at these pressures. In addition, a noticeable upward shift in the scatter is observed for pressure heads at 10 kPa, 50 kPa and 1500 kPa compared to the NonVC vGM model as result of the higher calculated VWCs due to VC. Model estimates of θ_s for the VC vGM models were found to be lower than the NonVC models; however, no significant difference in θ_s is seen between the two model types (Table 2-3). As θ_r approaches zero for most of the sites, significant difference in θ_r is not observed either. ANOVA testing revealed significant differences in means of model parameters α ($F(1,90)=7.716$, $p=0.0066$) and n (($F(1,102)=124.9$, $p<0.0000$) between VC vGM and NonVC vGM Table 2-2 (Table 2-3). Parameter α, which affects the air-entry value of the soil, is on average observed to be 30.3% higher when volume-corrected (Table 2-4). On the other hand, a statistically significant decrease in parameter n of 20.5% shows that, on average, volume-correction

reduces the steepness of the vGM curve (Table 2-3 and Table 2-4). Between clusters, significant differences are observed in all NonVC vGM parameters indicating that the curves are distinctly different for marl (Cluster 1), marl-peat (Cluster 2) and peat (Cluster 3) when they are not volume-corrected (Table 2-2). However, with the inclusion VC, significant differences between clusters are seen only for vGM parameter θ_s ($F(2,45) = 118.7$, $p<0.0001$). But significant difference in θ_s is to be expected as porosity was found to be significantly different. Figure 2-9 presents the vGM curves by cluster for all three clusters, as well as the mean vGM curves for each cluster. Mean curves show that the mean curve progression of peat (Cluster 3) is steeper than marl-peat (Cluster 2). Marl (Cluster 1) and marl-peat (Cluster 2) have similar mean curve progression; however, marl-peat has a higher mean θ_s and θ_r when compared marl.

Deviations from the vGM model

Observations of some of the VC vGM models deviated from the vGM model curve for some of the sampled sites. These deviations are observed for sites from all three clusters (marl, marl-peat and peat) with the maximum number of deviations in the peat cluster (Cluster 3). Figure 2-10 presents examples of typical deviations of the VC vGM models observed for each cluster. Deviations appeared in the form of higher VWCs at incremental pressures occurring due to a greater loss of samples volume than water volume. For peat samples with recorded deviations, the VC VWC at 10 kPa is higher than the VWC at 6 kPa (Example: site x_300 in Figure 2-10). No volume-change occurs at 6 kPa. Marl experiences shrinkage at high pressure heads; hence, deviations from the vGM curves for marl typically occur at higher pressure levels like 50 kPa (Example: site x_300 in Figure 2-10). The curves

were fit with RETC which uses a least squares optimization to obtain the best curve fit. For the deviations, RETC tends to fit a model which underestimates the VWC at the pressure head with the deviation and overestimates the VWC at the preceding pressure to keep the overall R-squared of the model low. The NonVC vGM models at all sites have better R-squared than the VC vGM models. There is no evidence of bi-modality in the NonVC vGM models with the data points at the pressures tested by current study.

Influence of Hydrology, Fiber Content and Bulk Density on Peat Water Retention

Peat properties like BD and the FC may be influenced by the hydrological regimes in their location which evolve under different water management scenarios. Assuming that the peat (Cluster 3) collected from the same hydrological units (Eg: WCAs) experience similar hydrological regimes, a one-way ANOVA, used to test difference in FC due to location, found significant difference in mean FC ($F(2,15)= 8.81$, $p=0.003$) and BD ($F(2,17)=5.13$, $p<0.018$) between locations (Table 2-5). As only one site is present in ENP, this data point was dropped from the ANOVA. Tukey's HSD test showed a significant difference in FC ($p=0.0021$) between WCA-3 and WCA-1 and a significant difference in BD between WCA-3 and WCA-1 ($p=0.0137$). The mean FC of WCA-1 (41.0%) was 96.9% greater than the FC of WCA-3 (20.8%), while the mean BD of WCA-1 (0.092 g cm^{-3}) was 25.5% lower than WCA-3 (0.116 g cm^{-3}).

Regression models are used to quantify the influence of FC and BD on the VWCs of the soil are presented in Table 2-6. FC has a greater number of significant VWC linear regression models than BD suggesting that it is a better linear predictor of peat VWC than BD. For BD, the only significant models are VWC at 0 kPa (porosity) and VWC at 1500

kPa. BD is expected to be inversely related to porosity as it is one of the variables used to calculate porosity. A positive slope is observed for FC with VWC of 0 kPa indicating that an increase in FC results in increase in VWC of the sample. The slope becomes more negative at higher pressures as seen at 50 kPa and 1500 kPa, indicating a reduced VWC with increasing FC. Regression models with BD as the independent variable show the opposite effect as BD is inversely related to FC. Since FC correlates with the VWCs at the applied pressures, it is expected to be a better predictor of vGM parameters than BD. No significant linear relationship exists between FC and VWCs at low pressure heads (6 kPa and 10 kPa).

The difference between VC vGM parameters between locations were tested. Since only one site from ENP was available, it was dropped from the analysis resulting in locations WCA-1, WCA-2 and WCA-3 in the analysis. No significant difference in parameters θ_s (F(2,17)=0.050, p=0.9490), θ_r (F(2,17)=1.293, p=0.3000), and α (F(2,17)=1.29, p=0.0570) are found. However, vGM parameter *n* is found to be significantly different between the locations (F(2,14)=9.21, p=0.0020). Tukey's HSD test showed significant difference in *n* between WCA-3 and WCA-1 (p=0.0014). The mean of vGM parameter *n* for WCA-1 (1.299) is 12.4% is higher than WCA-3 (1.137). ANOVA testing between vegetation types (SG, CT, SR, WL) for FC, BD, and VC vGM parameters (not presented in tabular format) shows only statistically significant differences in mean BD (F(3,17)=3.675, p=0.0331) with significant differences between SR and WL (p=0.0261). The mean BD of WL peat is 38% higher than that of SR. Figure 2-11 presents the VC vGM curves by location and vegetation types; there is insufficient data to run a

two-way ANOVA which could be used to ascertain the influence of both vegetation and location on the physical and hydraulic properties.

Table 2-1. Summary of the statistics calculated for the measured properties like organic content (OC), fiber content (FC), bulk density (BD), saturated hydraulic conductivity (K_{sat}), and the cluster observations like porosity, volume of water and volume of sample at tested pressures.

		Soil Properties				Cluster Observations								
							Volume of Water (V_w) at				Volume of Sample (V_s) at			
	Statistic	OC [%]	FC [%]	BD [g cm^{-3}]	K_{sat} [cm d^{-1}]	Porosity [cm^3/cm^{-3}]	6 kPa [cm^3]	10 kPa [cm^3]	50 kPa [cm^3]	1500 kPa [cm^3]	6 kPa [cm^3]	10 kPa [cm^3]	50 kPa [cm^3]	1500 kPa [cm^3]
Cluster 1	Mean	21.7	-	0.503	5.4	0.781	15.390	13.232	10.004	5.361	20.820	19.364	16.237	13.225
	Median	19.0	-	0.509	1.9	0.776	15.180	13.250	9.895	4.988	20.820	20.219	15.800	12.456
	Min	11.8	-	0.370	0.5	0.715	13.740	11.089	7.979	3.131	20.820	16.519	14.461	10.891
	Max	37.0	-	0.641	18.7	0.833	16.980	15.253	11.908	8.670	20.820	20.820	18.936	17.471
	Sites	12	0	12	8	12	12	12	12	12	12	12	12	12
Cluster 2	Mean	66.7	29.7	0.183	15.3	0.902	17.329	14.225	9.218	4.657	20.820	19.257	13.59	9.731
	Median	72.6	24.2	0.161	8.0	0.907	17.489	13.953	9.389	4.497	20.820	19.314	13.824	9.999
	Min	28.0	21.2	0.121	2.0	0.822	14.803	13.314	7.565	3.010	20.820	17.178	10.522	6.404
	Max	89.0	44.5	0.394	124.2	0.928	19.417	16.170	10.830	7.441	20.820	20.820	16.545	13.492
	Sites	20	5	20	16	20	20	20	20	20	20	20	20	20
Cluster 3	Mean	90.0	29.9	0.104	17.1	0.936	15.642	12.689	6.992	2.492	20.820	15.914	11.486	7.666
	Median	89.1	28.9	0.104	7.7	0.936	15.390	12.792	6.931	2.338	20.820	15.914	11.422	7.407
	Min	84.3	9	0.073	2.1	0.919	13.877	11.305	6.100	1.653	20.820	12.663	10.185	4.871
	Max	95.2	57.6	0.134	114.2	0.954	17.418	14.043	8.267	4.061	20.820	18.081	14.184	12.516
	Sites	21	18	21	18	21	21	21	21	21	21	21	21	21

Table 2-2. ANOVA testing for differences in cluster observations (Porosity, V_w 6 kPa, V_w 10 kPa, V_w 50 kPa, V_w 1500 kPa, V_s 10 kPa, V_s 50 kPa, and V_s 1500 kPa), saturated hydraulic conductivity (K_{sat}), and parameters of both VC vGM and NonVC vGM (θ_s, θ_r, α, n) with significant p-values in italics. Tukey's HSD test is presented for clusters with significant differences.

		ANOVA between Clusters				Tukey's HSD p-value		
		F	**Df**	**Df(Residuals)**	**p-value**	**Cluster 1 - 2**	**Cluster 2 - 3**	**Cluster 3 - 1**
Observations	**log(Porosity)**	158.80	2	49	*<0.0001*	*<0.0001*	*0.0001*	*<0.0001*
	V_w 6 kPa	11.77	2	47	*<0.0001*	*0.0003*	*0.0004*	0.7666
	V_w 10 kPa	9.02	2	48	*<0.0001*	*0.0318*	*<0.0001*	0.1861
	V_w 50 kPa	58.66	2	50	*<0.0001*	*0.0387*	*<0.0001*	*<0.0001*
	V_w 1500 kPa	42.96	2	47	*<0.0001*	0.6980	*<0.0001*	*<0.0001*
	V_s 10 kPa	43.68	2	50	*<0.0001*	0.9720	*<0.0001*	*<0.0001*
	V_s 50 kPa	50.24	2	49	*<0.0001*	*<0.0001*	*<0.0001*	*<0.0001*
	V_s 1500 kPa	26.59	2	48	*<0.0001*	*0.0006*	*0.0009*	*<0.0001*
log(K_{sat})		2.77	2	36	*0.0413*	0.0570	0.0523	0.9999
VC vGM	**θ_s**	118.70	2	45	*<0.0001*	*<0.0001*	*0.0481*	*<0.0001*
	θ_r	0.74	2	45	0.4830	-	-	-
	α	0.54	2	40	0.5350	-	-	-
	log(n)	0.45	2	46	0.6410	-	-	-
NonVC vGM	**log(θ_s)**	103.80	2	46	*<0.0001*	*<0.0001*	*0.0010*	*<0.0001*
	θ_r	8.70	2	47	*0.0006*	0.2359	*0.0004*	0.1944
	α	12.17	2	48	*<0.0001*	0.7791	*0.0004*	*0.0004*
	n	4.30	2	47	*0.0193*	*0.0156*	0.7430	0.0668

Table 2-3. ANOVA testing for significant differences in mean vGM parameters between VC and NonVC vGM models with significant p-values in italics.

	ANOVA between vGM Model Types			
vGM Parameters	**F**	**Df**	**Df(Residuals)**	**p-value**
$\log(\theta_s)$	0.03	1	92	0.8640
θ_r	1.736	1	97	0.1910
α	7.716	1	90	*0.0066*
n	124.9	1	102	*<0.0000*

Table 2-4. Summary of statistics calculated for VC vGM and NonVC vGM models.

		vGM VC				vGM NonVC			
	Statistic	**θ_s [$cm^3\ cm^{-3}$]**	**θ_r [$cm^3\ cm^{-3}$]**	**α [cm^{-1}]**	**n [-]**	**θ_s [$cm^3\ cm^{-3}$]**	**θ_r [$cm^3\ cm^{-3}$]**	**α [cm^{-1}]**	**n [-]**
Cluster 1	Average	0.783	0.159	0.025	1.262	0.787	0.155	0.012	1.426
	Median	0.780	0.000	0.019	1.243	0.797	0.178	0.012	1.418
	Min	0.772	0.000	0.002	1.050	0.723	0.000	0.003	1.135
	Max	0.835	0.558	0.099	1.579	0.837	0.379	0.019	1.726
	Sites	11	11	11	11	11	11	11	11
Cluster 2	Average	0.904	0.214	0.062	1.230	0.912	0.184	0.013	1.598
	Median	0.915	0.158	0.023	1.172	0.915	0.182	0.012	1.621
	Min	0.772	0.000	0.004	1.055	0.822	0.000	0.007	1.239
	Max	0.942	0.683	0.417	1.544	0.953	0.337	0.02	1.845
	Sites	20	20	20	20	20	20	20	20
Cluster 3	Average	0.927	0.085	0.038	1.227	0.940	0.087	0.018	1.583
	Median	0.933	0.000	0.027	1.204	0.938	0.080	0.017	1.562
	Min	0.867	0.000	0.002	1.074	0.921	0.000	0.013	1.415
	Max	0.948	0.404	0.187	1.401	0.959	0.186	0.027	1.871
	Sites	21	21	21	21	21	21	21	21

Table 2-5. ANOVA testing for significant differences in mean FC, BD, VC vGM , and VC vGM with significant p-values in italics

		ANOVA between locations - peat				Tukey's HSD p-value		
		F	Df	Df(Residuals)	p-value	WCA2-WCA1	WCA3-WCA1	WCA3-WCA2
Soil Properties	**FC**	8.81	2	15	*0.0030*	0.0935	*0.0021*	0.2572
	BD	5.13	2	17	*0.0181*	0.4187	*0.0137*	0.2837
VC vGM	**$\log(\theta_s)$**	0.05	2	17	0.9490	-	-	-
	θ_r	1.29	2	17	0.3000	-	-	-
	$\log(\alpha)$	3.41	2	17	0.0570	-	-	-
	n	9.21	2	17	*0.0020*	0.0996	*0.0014*	0.2605

Table 2-6. Results of the regression analysis of volumetric water content (VWC) and shrinkage as a function of fiber content and bulk density (BD) with significant p-values in italics.

	Dependent Variable		Regression Model		
Independent Variable	**Variable**	**Pressure (kPa)**	**Slope**	**R-Squared**	**p-value**
Fiber Content	Volumetric Water Content	0	*0.0004*	*0.232*	*0.0430*
		6	0.0002	0.181	0.8590
		10	-0.0020	0.168	0.0911
		50	*-0.0033*	*0.357*	*0.0089*
		1500	*-0.0059*	*0.512*	*0.0008*
Bulk Density	Volumetric Water Content	0	*-0.5900*	*0.998*	*<0.0001*
		6	-0.9825	0.126	0.1140
		10	0.6267	0.030	0.4540
		50	0.3587	0.359	0.6860
		1500	*2.9778*	*0.275*	*0.0146*

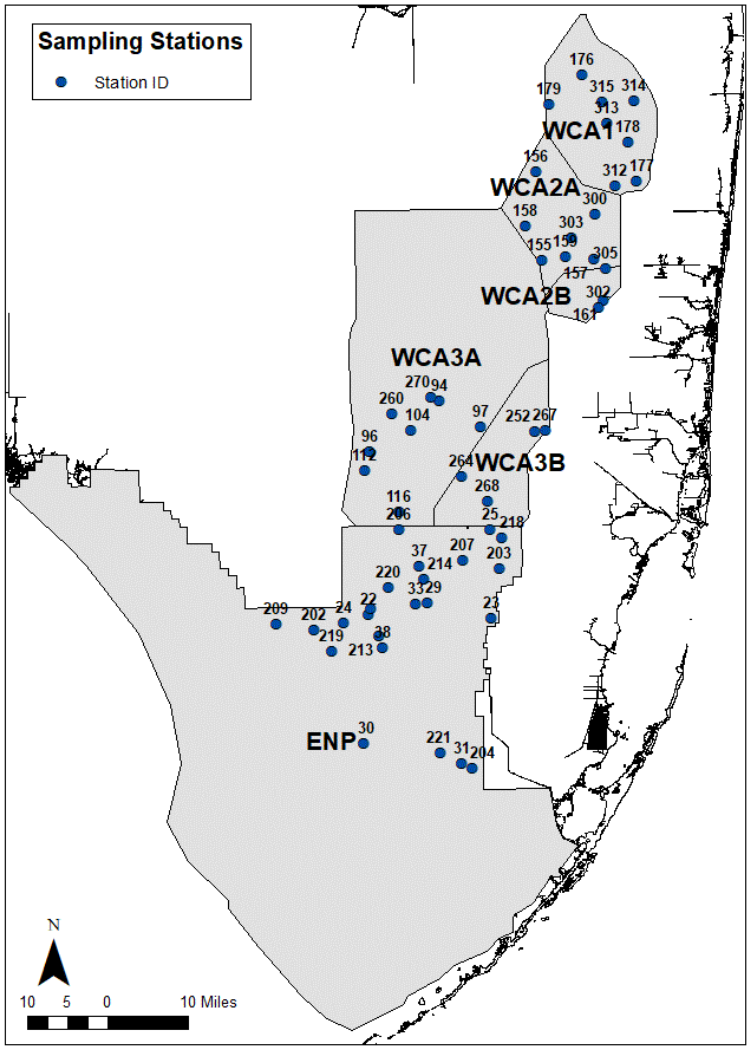

Figure 2-1. Map of South Florida showing the locations of the stations were soil for this study were collected. Peat and marl samples were collected from Water Conservations Areas (WCAs) 1, 2A, 2B, 3A, and 3B, and the Everglades National Park (ENP) at 53 sampling sites.

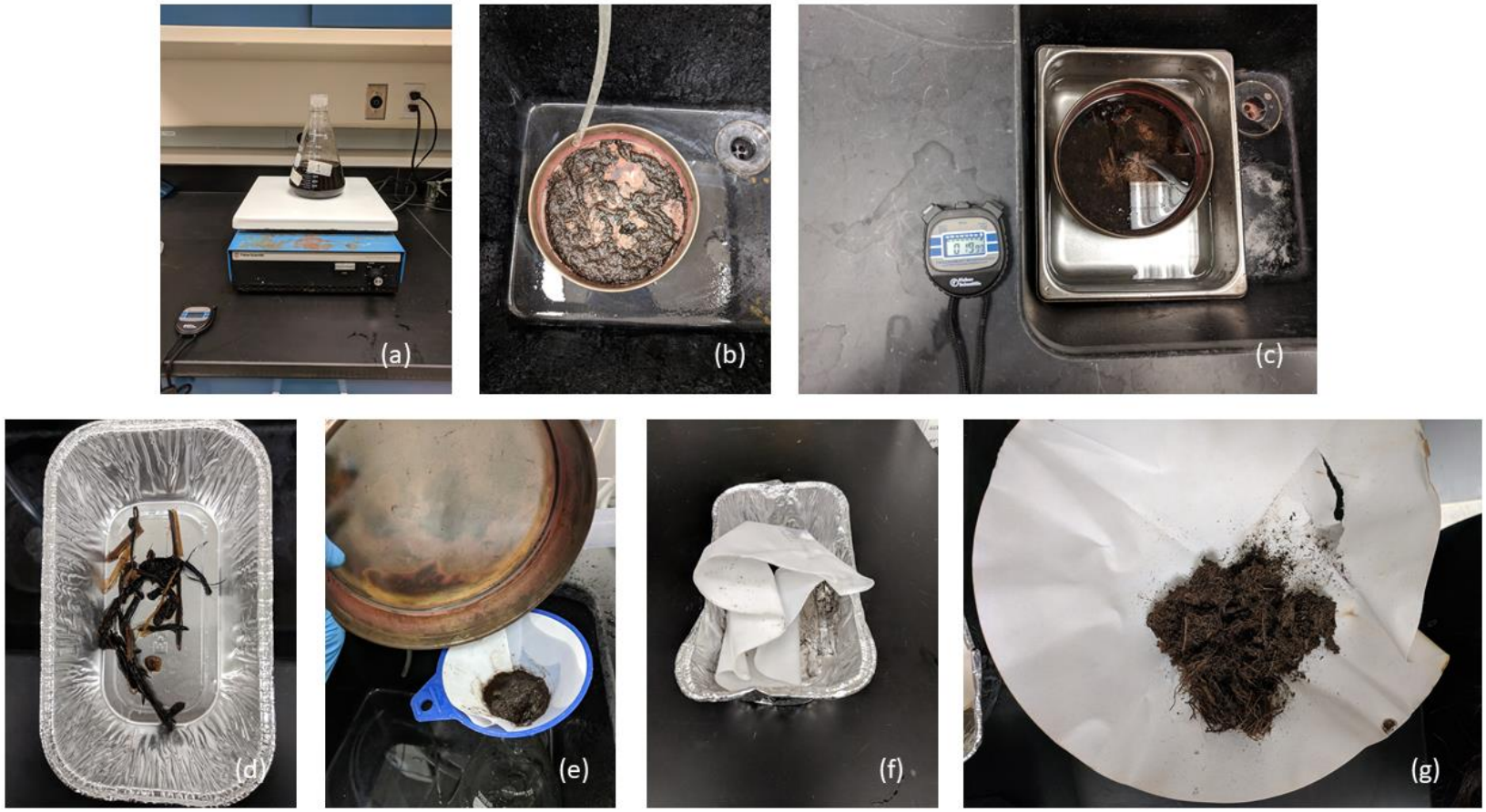

Figure 2-2. Methodology for dermining the fiber content (FC) of the samples using ASTM D-1997.

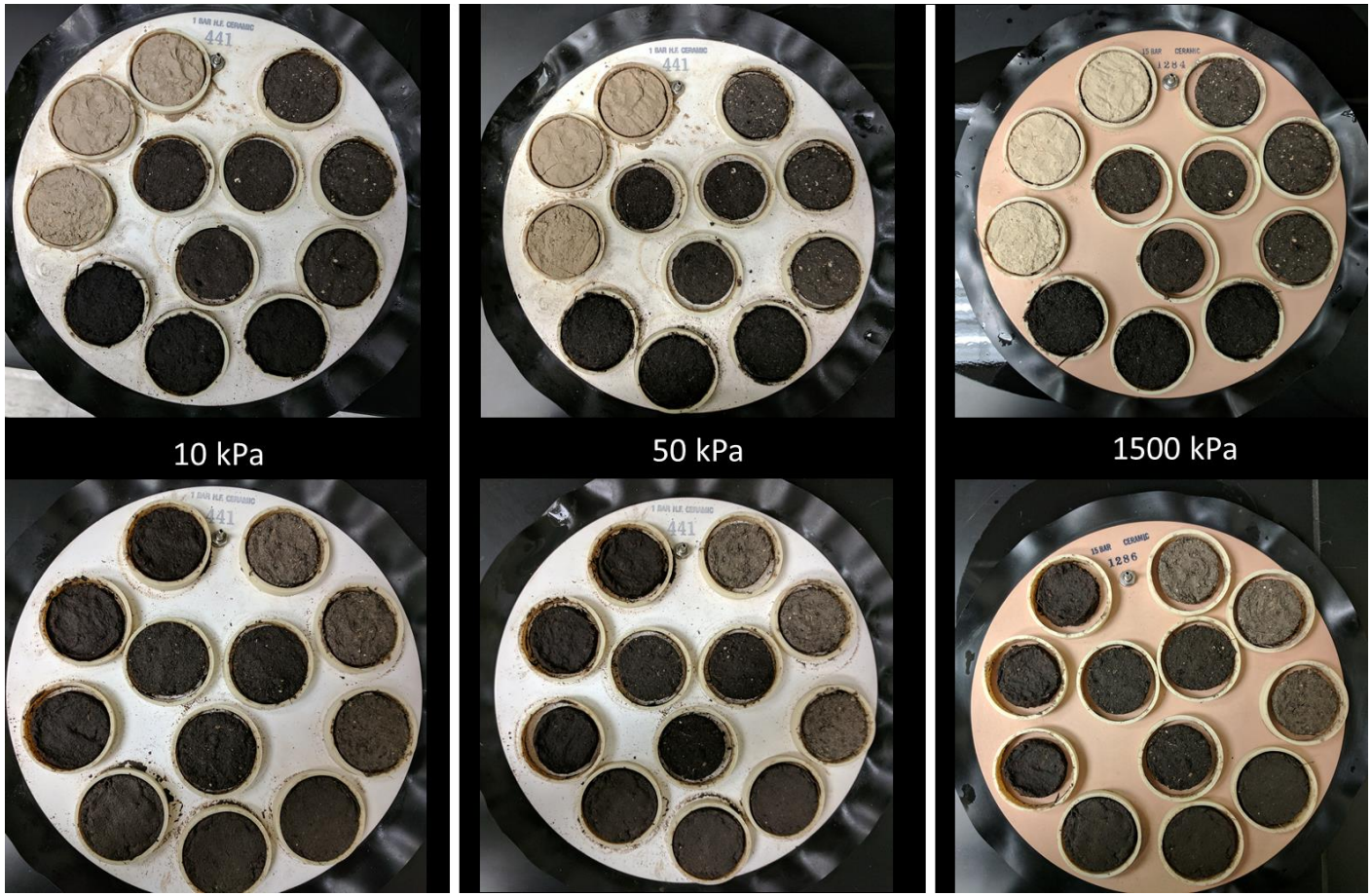

Figure 2-3. Soil samples from the 1500 Pressure Plate Extractor after applied pressures of 10 kPa, 50 kPa and 1500 kPa.

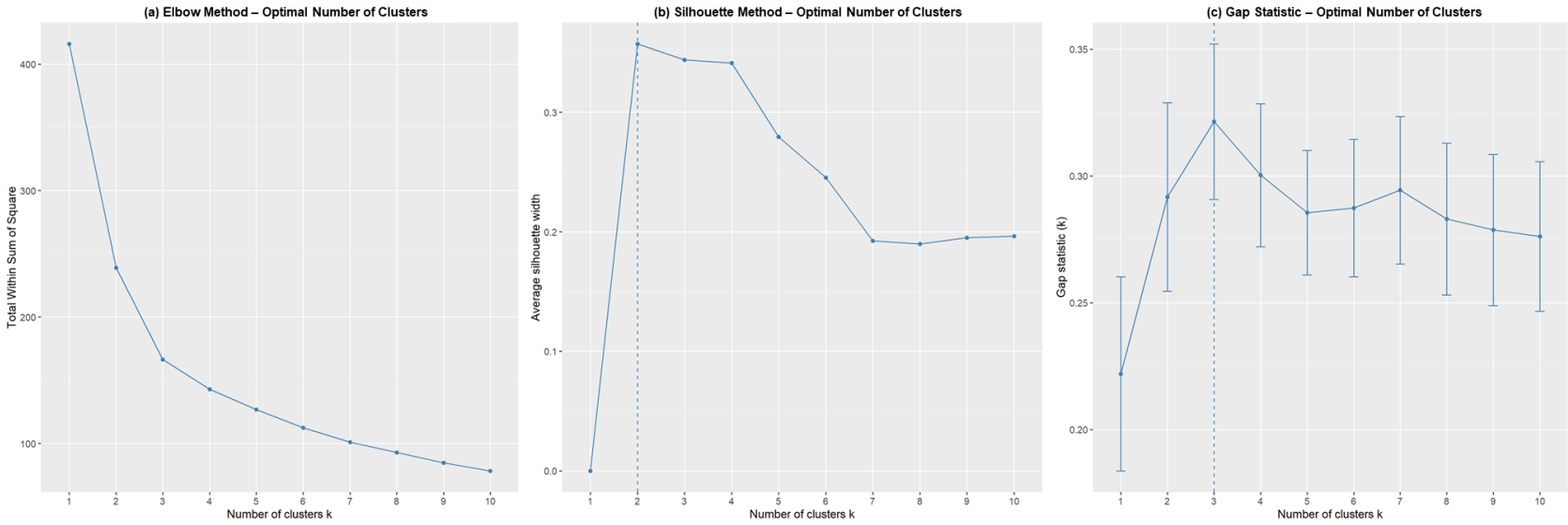

Figure 2-4. Evaluation for the selection of optimal number of clusters using (a) Elbow method, (b) Silhouette method, and (c) Gap-statistic method

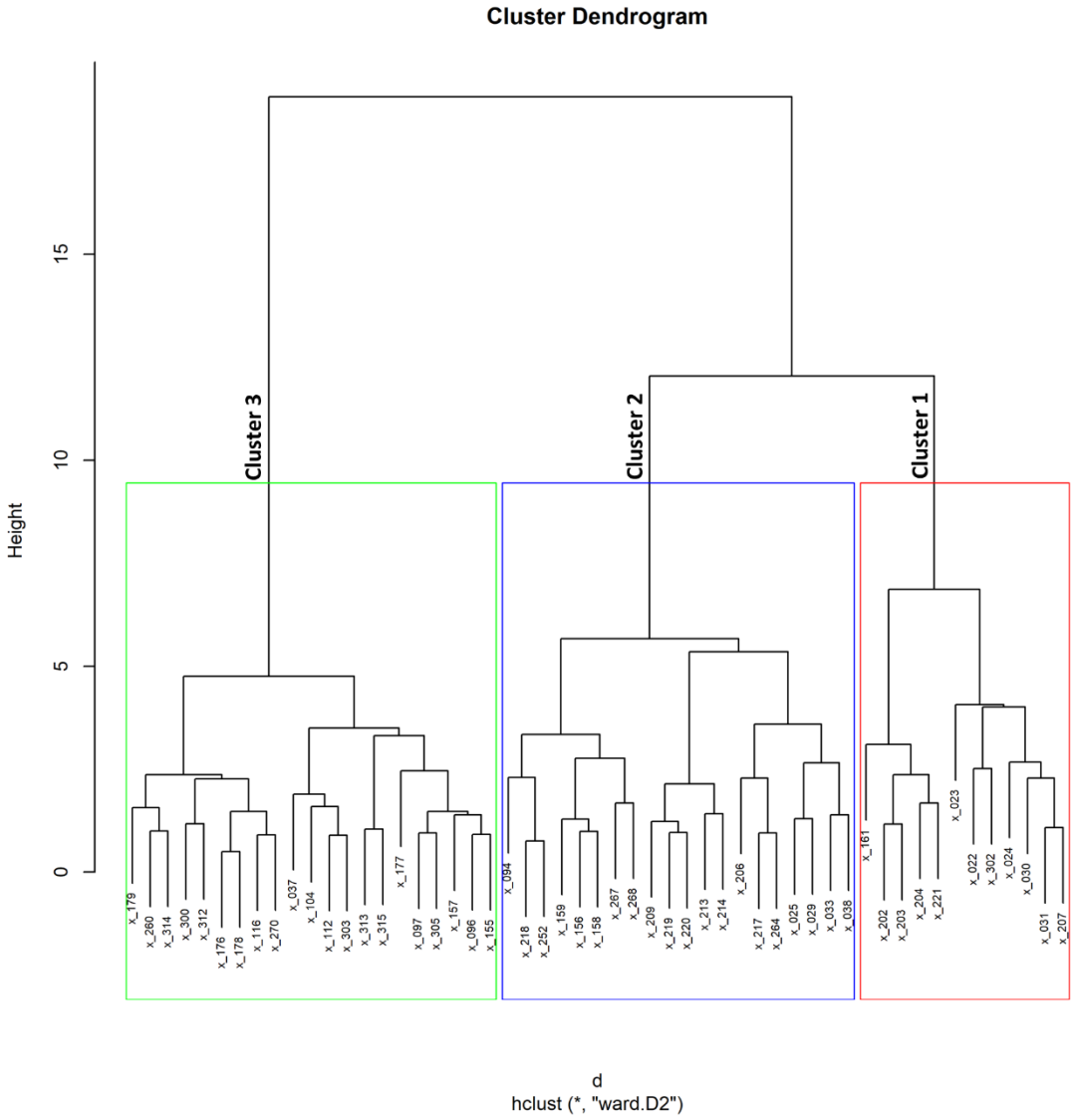

Figure 2-5. Cluster dendrogram of the agglomerative cluster analysis of 53 R-EMAP soil samples with the Euclidean distance between clusters the y-axes and the samples codes in the x-axis. The rectangular boxes representing the clusters are drawn around each cluster – Cluster 1 (red), Cluster 2 (green), and Cluster 3 (blue).

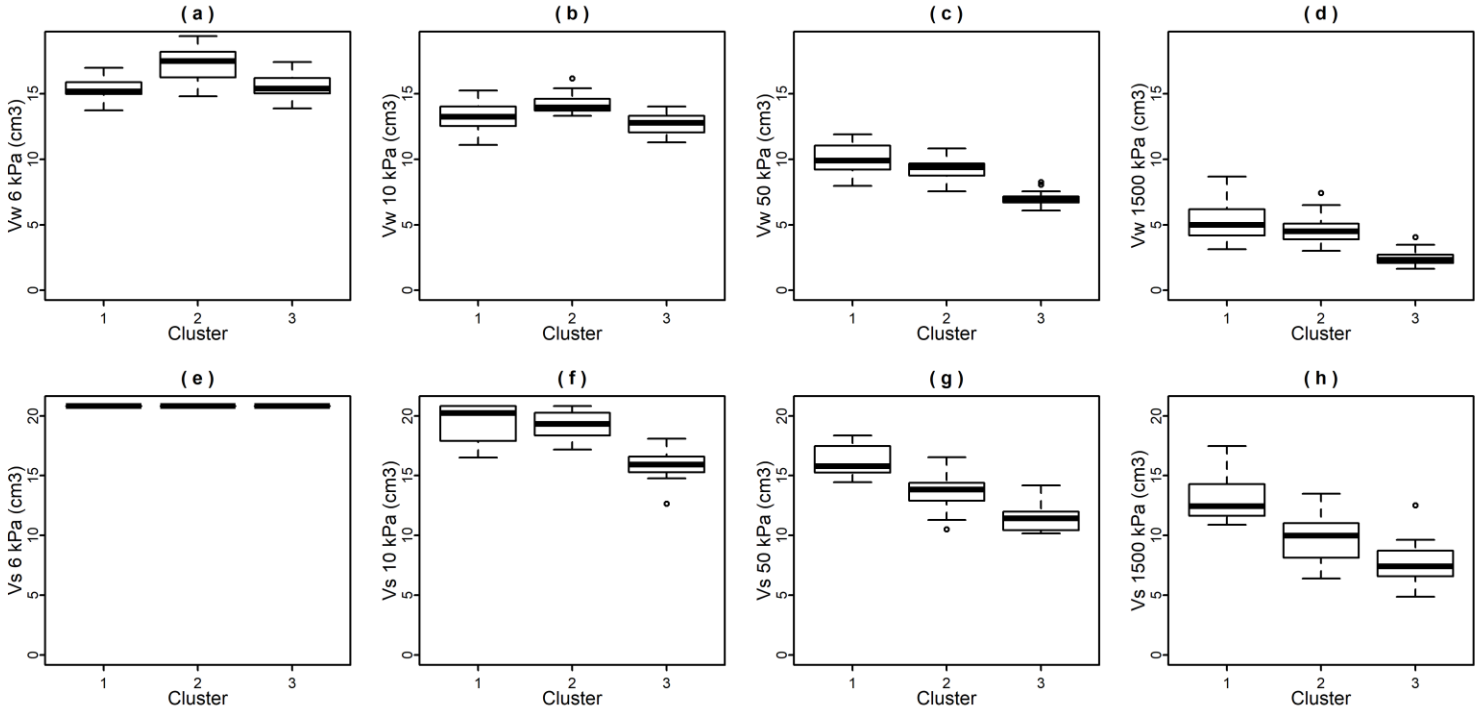

Figure 2-6. Boxplots of the volume of water (V_w) and volume of the sample (V_s) used as observations in the agglomerative clustering algorithm.

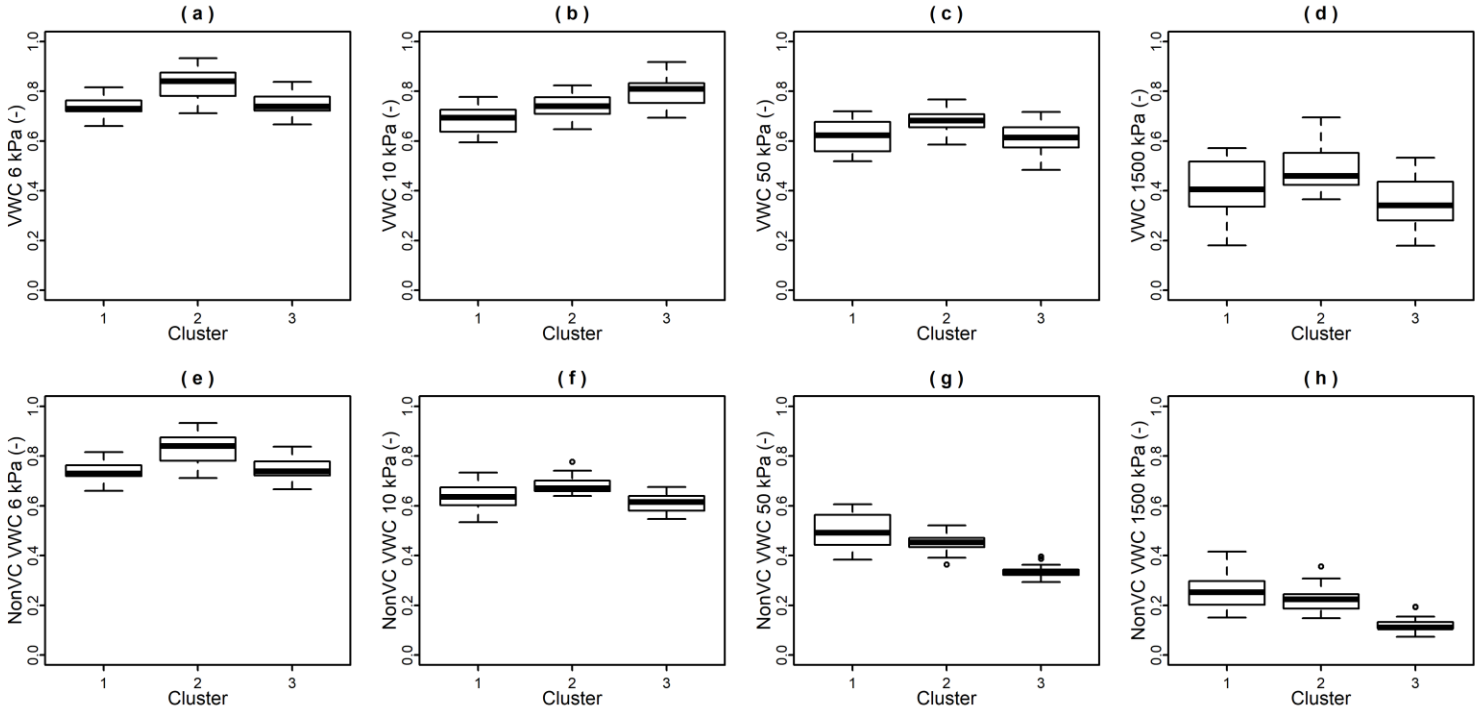

Figure 2-7. Volumetric water contents (VWCs) calculated with and without volume-correction (VC).

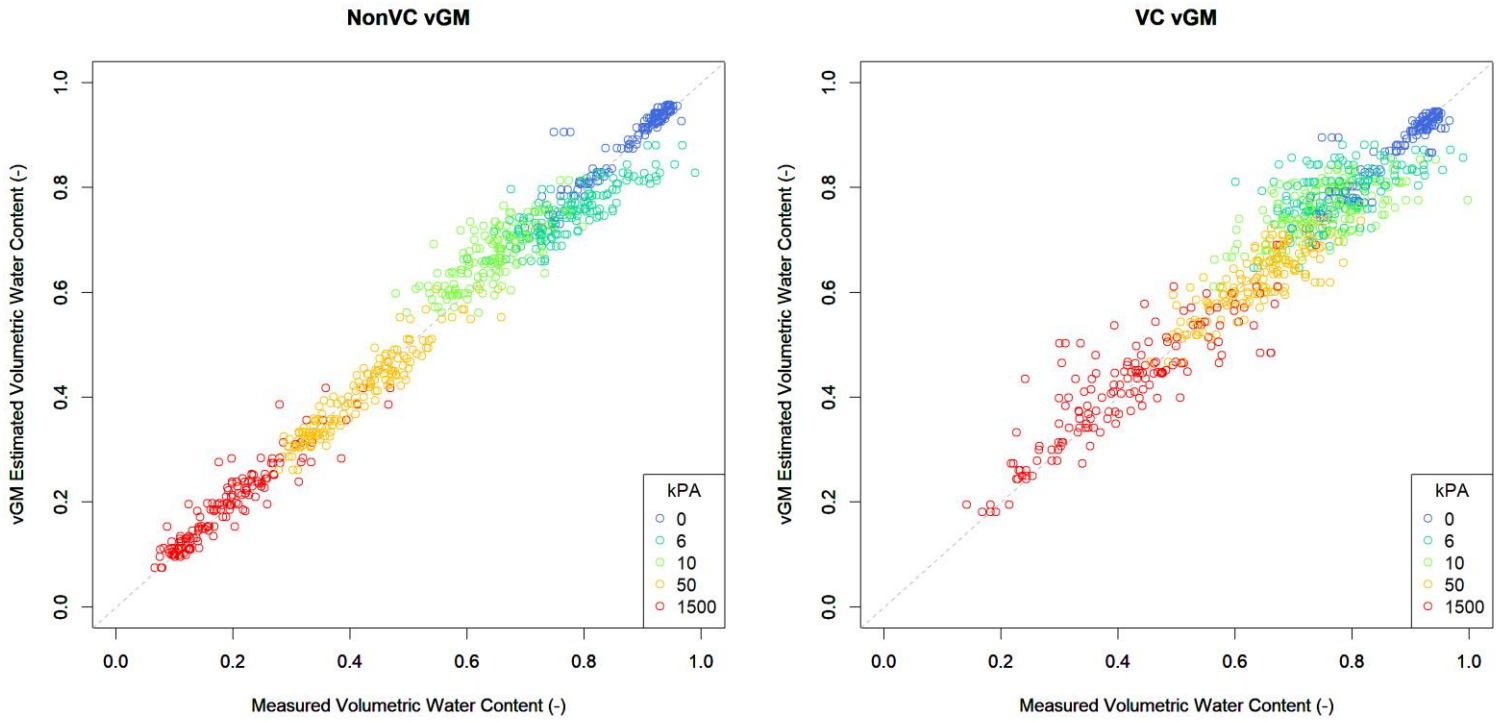

Figure 2-8. The relationship between volumetric water contents (VWCs) estimated with the vGM model versus the observed VWCs for the model with and without volume-correction – VC vGM and NonVC vGM.

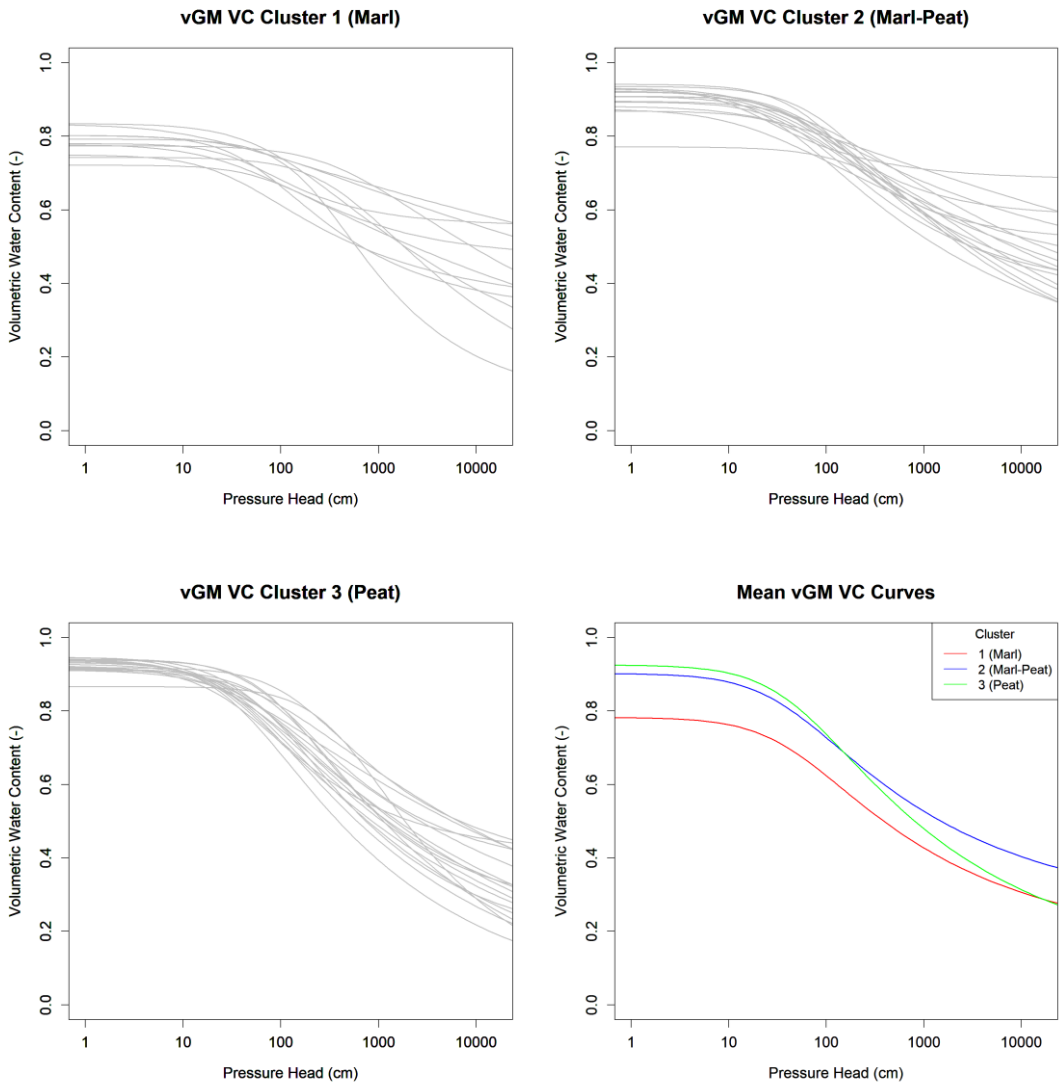

Figure 2-9. vGM curves generated for all sites by cluster and mean vGM curves of each cluster.

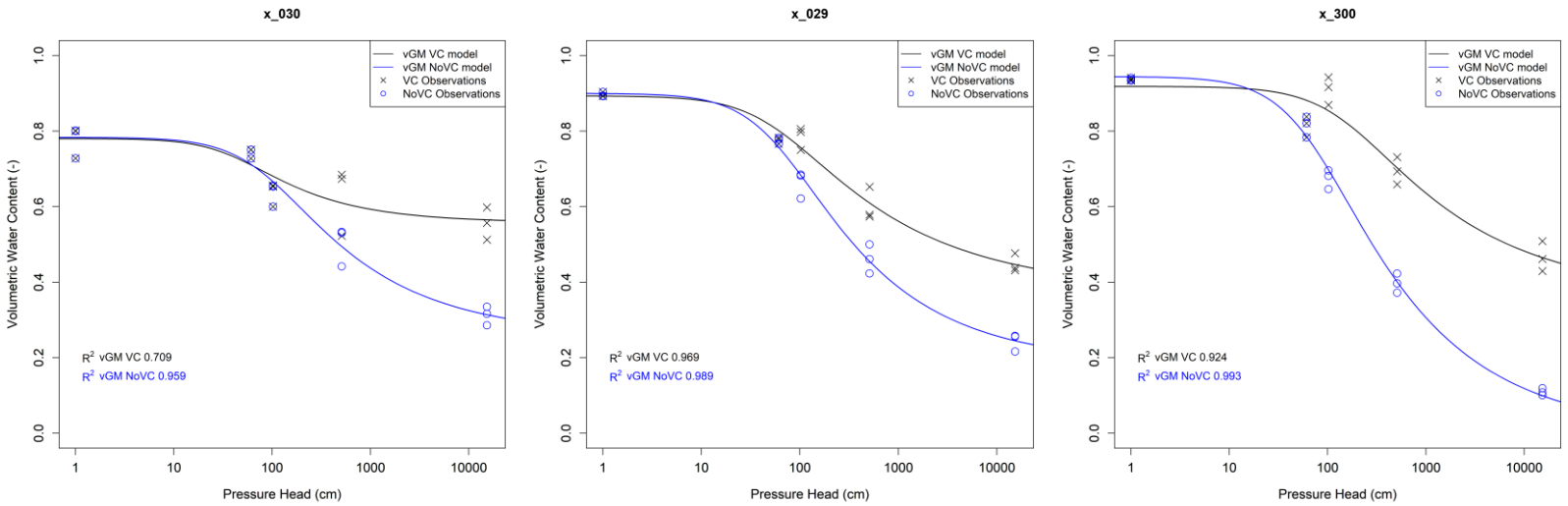

Figure 2-10. Examples of sites with deviations from the vGM model from each cluster: x_030 (Cluster 1 - marl), x_029 (Cluster 2 - marl-peat), and x_300 (Cluster 3 - peat).

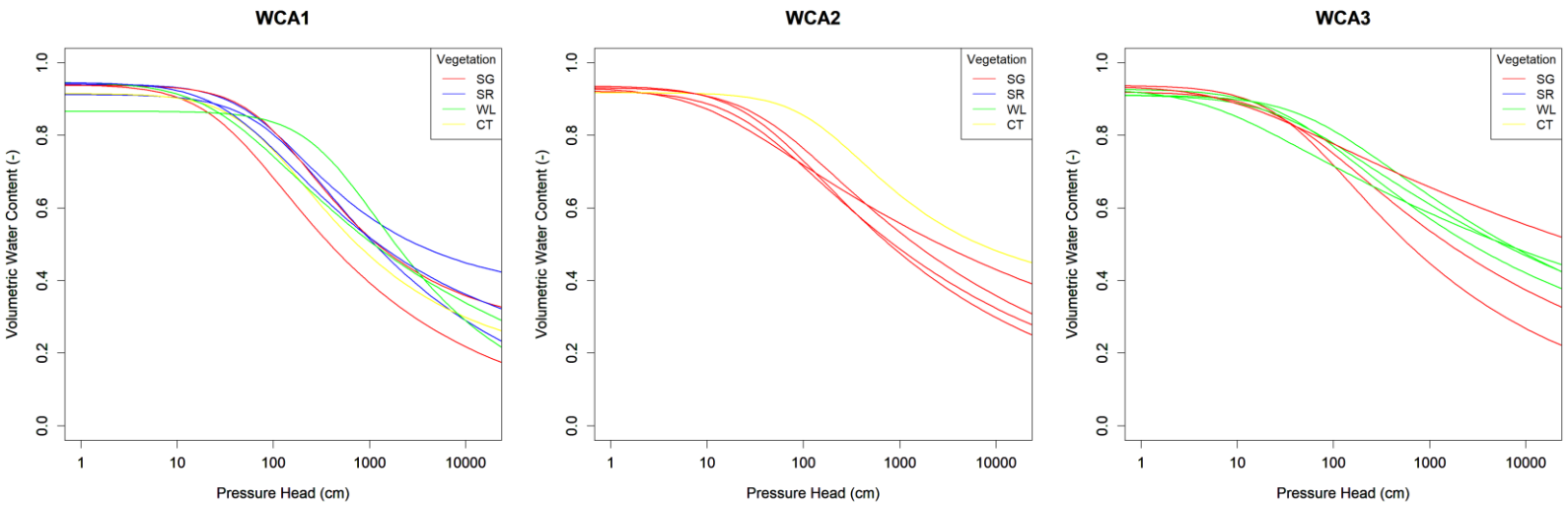

Figure 2-11. VC vGM curves for peat sites by location (WCA-1, WCA- 2, and WCA-3) and vegetation type (SG-sawgrass, SR-spikerush, WL-water lily, CT-cattail).

2.4 Discussion

Previous studies have indicated that the Everglades wetland soils may be hydrologically similar (Myers, 1999; Pumo et al., 2010); however, this study found the two predominant soils of the Everglades (marl and peat) were hydraulically different. Marl is prevalent in the southern marshes of the Everglades which are subject to longer periods of dry-down (Corstanje et al., 2005). Compared to most low OC soils, marl has a fine -pore size distribution which makes it hydraulically restrictive (low K_{sat}) but also more retentive. Marl has a higher bulk density and lower porosity than peat. In terms of their ability to retain water (measured by V_w), marl and peat are comparable at low pressure heads; however, at higher pressure heads, the ability of peat to retain water is significantly compromised due to shrinkage. The very low BD and high porosity of peat can cause shrinkage as early as 10 kPa. Marl-peat has better water retention than either parent substrate at low-pressure heads. Overall, the retention of marl-peat is better than peat and at high pressure heads like 1500 kPa, its retention is like marl indicating that marl component in mixed marl-peat may increase retention through smaller pore sizes.

The volume-change of peat has been widely recorded (Camporese et al., 2006; Kennedy and Price, 2005; Price and Schlotzhauer, 1999; Rezanezhad et al., 2016, 2009; Schwarzel et al., 2002). In some peatlands, a term known as ‘mire-breathing’ describes the seasonal change in surface elevation of the peatland with water levels (Camporese et al., 2006). Due to its high porosity, the desaturation of peat causes shrinkage. Highly decomposed peat in earthified layers (drained layers) have low porosity and low BD, and they experience less shrinkage (Schwarzel et al., 2002). Studies of water retention in

inorganic soils like clay that are susceptible to volume-change have used VC for calculating VWCs; however, most studies of peat water retention data have either ignored VC in calculating VWCs (Hallema et al., 2015; Wallor et al., 2018) or collected data only at lower pressure settings where shrinkage is not observed (Gnatowski et al., 2010; Oleszczuk et al., 2008). Schwarzel et al., 2002 studied water retention and shrinkage of reed-sedge peats in a fen in Germany. They found that shrinkage occurred as early as 6 kPa for a deep, permanently inundated horizon with a 37% volume loss at 500 kPa. In comparison, the shrinkage of Everglades peat was observed starting at 10 kPa; however, a mean volume loss of 45% is observed at 50 kPa indicating that the Everglades soil is more vulnerable than the reed-sedge fen peat to shrinkage at higher pressure settings. The shrinkage reported by Schwarzel et al., 2002 is for peat from a deep horizon (on average 120 cm deep) whereas, the Everglades samples were collected from the shallow horizons (maximum of 10 cm deep) which have lower BDs and are therefore more susceptible to shrinkage. It is possible that the effect of shrinkage measured using laboratory tests may be exacerbated due to the inevitable disturbance to the soil caused during extraction. In the case of this study, the lack of intact cores could compound that. Despite this, the results presented herewith offer insight into the VWCs during desaturation of soils with extreme shrinkage (which may be observed in the case of peatlands that have been disturbed).

Soil shrinkage has implications on the parameter estimation of unsaturated flow models. Typically, this is observed through underestimating the VWC of the sample with larger differences (between VC and NonVC VWCs) observed at higher pressure levels (Schwarzel et al., 2002; Wallor et al., 2018). Since parameterization models use the VWCs as raw data to which water retention curve parameters are fitted, the VC SWRCs have less

steep and more gradual curve progression than the NonVC SWRCs. The steepness of the vGM curve is described by vGM parameter *n*, which was significantly lower for the VC vGM model. Soil shrinkage causes a reduction in the air-filled or water filled pores of the soil matrix; hence, a narrower pore-size distribution as evidenced through lower vGM *n* should be expected for shrinking soils. The vGM parameter α is significantly higher in the VC models compared to the NonVC models indicating that air-entry zone may be narrower for models that consider shrinkage (Radcliffe and Simunek, 2010). However, inferring the air-entry from the vGM shape fitting parameter α is debatable (Quirijn and Everton Alves Rodrigues, 2018). Often, using the VWCs at selected pressure heads, the macro-, meso- and micro-pore distribution is estimated; however, for volume-changing soils like peat, such estimates will be flawed unless the volume-changing behavior is considered (Schwarzel et al., 2002). A decrease in vGM parameter, *n* through VC could also result in differences in calculated unsaturated hydraulic conductivity between VC and NonVC models, with larger differences at higher pressure heads. Golubev and Whittington, 2018 measured unsaturated hydraulic conductivity for peat at various states of compression and found that initial compression increased the unsaturated hydraulic conductivity but at high levels of compression, unsaturated hydraulic conductivity decreased. On the other hand, while shrinkage does cause a reduction in the pore-size within the matrix making the soil matrix hydraulically restrictive, it may also create large cracks (soil-root interfaces), where water can flow preferentially, resulting in higher hydraulic conductivity (Radcliffe and Simunek, 2010).

When volume-correction is not included in the vGM parameterization process, the mean vGM parameters are significantly different between soil types (or clusters). However, with the inclusion of volume-correction, excepting θ_s, no statistically significant differences exist between vGM parameters. Despite this Figure 2-9 shows that differences do exist in the shape of the mean vGM VC curve. The highly organic peat (Cluster 3) has a high porosity, and, as a result, a high θ_s, compared to marl-peat or marl; however, its VWC decreases at a steeper rate then either marl-peat or peat. The inclusion of VC results in the overall decrease in model fitness of the vGM model due to deviations from the vGM model in the form of higher measured VWCs at incremental pressure heads than the preceding pressure head; this phenomenon, observed at 10 kPa and 50 kPa for Everglades soil, occurs when the soil matrix substantially decreases in sample volume but not water volume as is to be expected in the case of collapsing macropores within the soil matrix. Macropores are known to cause bi-modal and tri-modal pore-size distributions in peat and parametrization models have been developed to account for this (Dettmann et al., 2014; Weber et al., 2017). Although the empirical studies of multimodality of peat reported observing shrinkage of the soil, it was not measured and the VWCs were not VC. Depending on the tension at which the draining and possible collapse of the macropores occurs, it is possible that some of those studies would have observed similar deviations of higher VWCs at higher pressure settings had they accounted for shrinkage. The current parameterization models, both unimodal and multimodal are both developed from empirical data of soils that are non-deforming or where the deformation has been ignored.

The intrinsic properties of peat like FC are influenced by hydrology and contributing plant matter (Rezanezhad et al., 2009). Differences in peat properties were observed between WCAs and vegetation types. Peat from the northern marshes of the Everglades, like WCA-1, which experience higher water levels and lower dry-downs, are significantly more fibric and have lower bulk densities than the southern marshes, like WCA-1. Anoxic conditions from high water levels lower the rate of decomposition of peat. Fibric peats of the northern mashes also have a steeper vGM curve compared the southern marshes, as observed through a significantly higher VC vGM parameter *n*. Linear regression analysis found that FC has a significant linear relationship with VWCs at higher pressure heads (50kPa and 1500 kPa). Peats with higher FCs results have lower VWCs at 50 kPa and 1500 kPa resulting in steeper SWRC curves, and in turn higher *n*, for fibric peat. Gnatowski et al., 2010 investigated fen peats in Poland and found that vGM parameter n, was lower for the amorphous, herbaceous peat from a decomposed layer compared to the fibric moss peat with a low degree of decomposition. Contrary to this study, they did not report a significant difference in n, possibly because their data was limited to low pressure heads. Wallor et al., 2018 generated vGM parameters from a wider range of pressure heads (0 to 1500 kPa) and found that, for drained and cultivated fen soils, vGM parameter α varied strongly compared to n for the moorsh-forming process; however, shrinkage was not accounted for in their VWC data, and accounting for shrinkage will significantly increase α as found in this study. Hence, with volume-correction, the strong negative linear correlation between vGM parameter α and decomposition recorded by Wallor et al., 2018, may not be observed.

Differences in the peat properties as a result of the contributing vegetation type is observed across the entire system. Peat from marshes where spike-rush was the dominant vegetation have a significantly lower mean BD than marshes with WL. As spike-rush is a sedge, it is possible that the contributing plant matter consists of longer fibers, resulting in a more fibrous soil matrix compared to WL. It is possible to argue that differences between SR and WL could also be attributed to the differences in hydrology between these communities. SR and SG communities are known to dry out for several months compared to WL marshes, which are at lower elevations, and typically stay inundated most of the year (Olmsted and Armentano, 1997); however, aeration of the soil should result in an increase in BD through decomposition, which was not observed here (Rezanezhad et al., 2016; Wallor et al., 2018). Due to limited number of peat samples obtained from each dominant vegetation type within a hydrological unit, it was not possible to conduct a two-factor ANOVA test controlling for both vegetation and location.

2.5 Conclusions

It is widely accepted that SHPs which are crucial to simulate water distribution and flow in the vadose zone, are strongly influenced by the intrinsic properties of the soil matrix. Vadose zone simulations of the Everglades have been limited by the lack of SHPs of Everglades marl and peat which have often led to the incorrect assumption of similarity in their hydraulic behavior (Myers, 1999; Perez, 2014; Pumo et al., 2010). This research characterized the laboratory tested soil water retention and shrinkage data at 53 sites in the Everglades using agglomerative clustering technique and found that the three distinct clusters comprised of marl (Cluster 1), mixed marl-peat (Cluster 2) and peat (Cluster 3).

The investigations established marl as the hydraulically restrictive layer for unsaturated flow. For layered substrates of peat and marl, marl, which is predominant in the Southern marshes, would serve as the restrictive layer with higher water residence time that peat, which is predominant in the northern marshes (Clark and Reddy, 2005). Peat from the northern marshes were found to be more fibric with steeper vGM curves compared to the southern marshes. The calculation of exact residence times can be conducted using from surveys of soil depth; this information would be beneficial for water budget analysis, as well as the nutrient and contaminant transport analysis. Mixed marl-peat was found to have better water retention than peat, while also being less affected by shrinkage.

Previous studies have indicated that the shrinkage observed in wetland soils is a self-preservation mechanism to reduce the loss of moisture from the surface. This work found that including shrinkage in the SWRC parameterization process results in significant differences in the vGM parameters α and n. Volume-correction resulting in higher α and lower n, and could, ultimately, result in lower calculated unsaturated hydraulic conductivity. In addition, the vGM parameters and VWCs (at low pressure heads) of marl and peat were not significantly different with volume-correction; however, they were found to have significantly different V_w and V_s; volume-correction is required both at the SWRC parameterization level and at the transport model level for highly organic wetland soils.

Volume-correction was also found to result in deviations from the typical SWRC behavior. Although, the overall vGM model had high R-squared with the inclusion of VC, deviations from the SWRC were observed at individual pressure levels. Some of these deviations are assumed to be due to collapsing macropores and the consequent substantial

soil volume loss. These deviations require thorough investigation as they are evidence of the inapplicability of conventional SWRC models like the Brooks and Corey and the vGM models, which were developed using empirical data from non-deforming soils. Defining the water retention behavior of highly deforming soils may require the development of a new parameterization model.

Acknowledgments

The authors thank Florida International University (Soil Water Laboratory) for the resources to conduct this study, and the United States Environmental Protection Agency's Everglades Ecosystem Monitoring and Assessment Program for the collection of and access to the soil samples used in this study. The first author expresses gratitude to the Department of Civil and Environmental Engineering at FIU for the Graduate Assistantship which supported her during this research work. Beyond the above, this research did not receive any specific grant from funding agencies in the public, commercial, or not-for-profit sectors.

References

ASTM D1997, 2001. Standard Test Methods for the Laboratory Determination of Fiber Content of Peat Samples by Dry Mass.

ASTM D2974, 2000. Standard Test Methods for Moisture, Ash, and Organic Matter of Peat and Other Organic Soils.

ASTM D4511, 2011. Standard Test Method for Hydraulic Conductivity of Essentially Saturated Peat. ASTM International, West Conshohocken, PA.

Boelter, D.H., 1964. Water Storage Characteristics of Several Peats in situ. Soil Sci. Soc. Proc. 443–435.

Camporese, M., Ferraris, S., Putti, M., Salandin, P., Teatini, P., 2006. Hydrological modeling in swelling/shrinking peat soils. Water Resour. Res. 42, 1–15. https://doi.org/10.1029/2005WR004495

Chaberneau, R.J., 2006. Groundwater Hydraulics and Pollutant Transport. Waveland Press, Long Grove, IL.

Clark, M.W., Reddy, K.R., 2005. Spatial Variability and Modeling of Soil Accretion in Shark River Slough 2004 Annual Report December 2005 U . S . Department of Interior National Park Service Everglades National Park.

Corstanje, R., Grunwald, S., Reddy, K.R., Osborne, T.Z., Newman, S., 2005. Assessment of the spatial distribution of soil properties in a northern Everglades marsh. J. Environ. Qual. 35, 938–949. https://doi.org/10.2134/jeq2005.0255

Crockett, A.C., Ronayne, M.J., Cooper, D.J., 2015. Relationships between vegetation type, peat hydraulic conductivity, and water table dynamics in mountain fens. Ecohydrology. https://doi.org/10.1002/eco.1706

DeAngelis, D.L., Gross, L.J., Huston, M. a., Wolff, W.F., Fleming, D.M., Comiskey, E.J., Sylvester, S.M., 1998. Landscape Modeling for Everglades Ecosystem Restoration. Ecosystems 1, 64–75. https://doi.org/10.1007/s100219900006

Dettmann, U., Bechtold, M., Frahm, E., Tiemeyer, B., 2014. On the applicability of unimodal and bimodal van Genuchten-Mualem based models to peat and other organic soils under evaporation conditions. J. Hydrol. 515, 103–115. https://doi.org/10.1016/j.jhydrol.2014.04.047

Dreschel, T.W., Hohner, S., Aich, S., McVoy, C.W., 2018. Peat Soils of the Everglades of Florida, USA, in: Peat. InTech. https://doi.org/10.5772/intechopen.72925

Gaiser, E.E., McCormick, P. V., Hagerthey, S.E., Gottlieb, A.D., 2011. Landscape Patterns of Periphyton in the Florida Everglades. Crit. Rev. Environ. Sci. Technol. 41, 92–120. https://doi.org/10.1080/10643389.2010.531192

Galili, T., 2015. dendextend: an R package for visualizing, adjusting, and comparing trees of hierarchical clustering. Bioinformatics. https://doi.org/10.1093/bioinformatics/btv428

Gnatowski, T., Szatyłowicz, J., Brandyk, T., Kechavarzi, C., 2010. Hydraulic properties of fen peat soils in Poland. Geoderma 154, 188–195. https://doi.org/10.1016/j.geoderma.2009.02.021

Goetz, J.D., Price, J.S., 2016. Ecohydrological controls on water distribution and productivity of moss communities in western boreal peatlands, Canada. Ecohydrology 9, 138–152. https://doi.org/10.1002/eco.1620

Golubev, V., Whittington, P., 2018. Effects of volume change on the unsaturated hydraulic conductivity of Sphagnum moss. J. Hydrol. https://doi.org/10.1016/j.jhydrol.2018.02.083

Hallema, D.W., Périard, Y., Lafond, J. a., Gumiere, S.J., Caron, J., 2015. Characterization of Water Retention Curves for a Series of Cultivated Histosols. Vadose Zo. J. 14, 0. https://doi.org/10.2136/vzj2014.10.0148

Harvey, J.W., Wetzel, P.R., Lodge, T.E., Engel, V.C., Ross, M.S., 2017. Role of a naturally varying flow regime in Everglades restoration. Restor. Ecol. 25, S27–S38. https://doi.org/10.1111/rec.12558

Hohner, S.M., Dreschel, T.W., 2015. Everglades peats : using historical and recent data to estimate predrainage and current volumes , masses and carbon contents. Int. Mire Conserv. Gr. Int. Peat Soc. 16, 1–15.

Joosten, H., 2010. The Global Peatland CO2 Picture. Peatland status and drainage related emissions in all countries of the world. Ede.

Kassambara, A., Mundt, F., 2016. factoextra: Extract and Visualize the results of PCA, CA and MCA. R package version 1.0.2.

Kennedy, G.W., Price, J.S., 2005. A conceptual model of volume-change controls on the hydrology of cutover peats. J. Hydrol. 302, 13–27. https://doi.org/10.1016/j.jhydrol.2004.06.024

Kettridge, N., Tilak, A.S., Devito, K.J., Petrone, R.M., Mendoza, C.A., Waddington, J.M., 2016. Moss and peat hydraulic properties are optimized to maximize peatland water use efficiency. Ecohydrology 9, 1039–1051. https://doi.org/10.1002/eco.1708

Klute, A., 1986. Water Retention: Laboratory Methods, in: Method of Soil Analysis, Part 1. Physical and Mineralogical Methods. Madison, WI, pp. 635–662.

Kodinariya, T.M., Makwana, P.R., 2013. Review on determining number of Cluster in K-Means Clustering. Int. J. Adv. Res. Comput. Sci. Manag. Stud. 1, 2321–7782.

Liu, H., Lennartz, B., 2019. Hydraulic properties of peat soils along a bulk density gradient-A meta study. Hydrol. Process. 33, 101–114. https://doi.org/10.1002/hyp.13314

Mualem, Y., 1976. A New Model for Predicting the Hydraulic Conductivity of Unsaturated Porous Media. Water Resour. Res. 12.

Myers, R.D., 1999. Hydraulic Properties of South Florida Peatlands. University of Florida.

Oleszczuk, R., Brandyk, T., Gnatowski, T., Szaty, J., Kami, J., 2008. The comparison of soil moisture content changes in the moorsh layer under shrubs and grass vegetation 6, 141–148.

Olmsted, I., Armentano, T. V, 1997. Vegetation Of Shark Slough , Everglades National Park SFNRC Technical Report 97-001.

Paquet, J.M., Caron, J., Banton, O., 1993. In situ determination of the water desorption characteristics of peat substrates. Can. J. Soil Sci. https://doi.org/10.4141/cjss93-035

Perez, L.G., 2014. Develeopment Of a Methodology that Couples Satellite Remote Sensing Measurements To Spatial-Temporal Distribution Of Soil Moisture In The Vadose Zone Of The Everglades National Park. Florida International University.

Price, J.S., Schlotzhauer, S.M., 1999. Importance of shrinkage and compression in determining water storage changes in peat: The case of a mined peatland. Hydrol. Process. 13, 2591–2601. https://doi.org/10.1002/(SICI)1099-1085(199911)13:16<2591::AID-HYP933>3.0.CO;2-E

Pumo, D., Tamea, S., Noto, L.V., Miralles-Wilhem, F., Rodriguez-Iturbe, I., 2010. Modeling belowground water table fluctuations in the Everglades. Water Resour. Res. 46. https://doi.org/10.1029/2009WR008911

Quirijn, D.J.V.L., Everton Alves Rodrigues, P., 2018. An alert regarding a common misinterpretation of the van genuchten α parameter. Rev. Bras. Cienc. do Solo. https://doi.org/10.1590/18069657rbcs20170343

R Core Team, 2014. R: A language and environment for statistical computing.

Radcliffe, D.E., Simunek, J., 2010. Soil Physics with HYDRUS: Modeling and Applications [Hardcover]. CRC Press.

Rezanezhad, F., Price, J.S., Quinton, W.L., Lennartz, B., Milojevic, T., Van Cappellen, P., 2016. Structure of peat soils and implications for water storage, flow and solute transport: A review update for geochemists. Chem. Geol. 429, 75–84. https://doi.org/10.1016/j.chemgeo.2016.03.010

Rezanezhad, F., Quinton, W.L., Price, J.S., Elrick, D., Elliot, T.R., Heck, R.J., 2009. Examining the effect of pore size distribution and shape on flow through unsaturated peat using 3-D computed tomography. Hydrol. Earth Syst. Sci. Discuss. 6, 3835–3862. https://doi.org/10.5194/hessd-6-3835-2009

Rocha Campos, J.R. Da, Silva, A.C., Fernandes, J.S.C., Ferreira, M.M., Silva, D.V., 2011. Water retention in a peatland with organic matter in different decomposition stages. Rev. Bras. Ciência do Solo 35, 1217–1227. https://doi.org/10.1590/S0100-06832011000400015

Ross, M.S., Reed, D.L., Sah, J.P., Ruiz, P.L., Lewin, M.T., 2003. Vegetation:environment relationships and water management in Shark Slough, Everglades National Park. Wetl. Ecol. Manag. 11, 291–303.

Ross, M. S., Reed, D.L., Sah, J.P., Ruiz, P.L., Lewin, M.T., 2003. Vegetation:environment relationships and water management in Shark Slough, Everglades National Park. Wetl. Ecol. Manag. 11, 291–303. https://doi.org/10.1023/B:WETL.0000005541.30283.11

Rousseeuw, P.J., 1987. Silhouettes: A graphical aid to the interpretation and validation of cluster analysis. J. Comput. Appl. Math. https://doi.org/10.1016/0377-0427(87)90125-7

Scheidt, D.J., Kalla, P.I., Usepa, 2007. Everglades ecosystem assessment: water management and quality, eutrophication, mercury contamination, soils and habitat: monitoring for adaptive management: a R-EMAP status report. 98.

Schwarzel, K., Renger, M., Sauerbrey, R., Wessolek, G., 2002. Soil physical characteristics of peat soils. Plant Nutr. Soil 479–486.

Schwärzel, K., Šimůnek, J., Stoffregen, H., Wessolek, G., van Genuchten, M.T., 2006. Estimation of the Unsaturated Hydraulic Conductivity of Peat Soils. Vadose Zo. J. 5, 628. https://doi.org/10.2136/vzj2005.0061

SCT, 2003. The Rolse of Flow in the Everglades Ridge and Slough Pattern.

Sklar, F., Mcvoy, C., Zee, R. Van, Gawlik, D., Park, W., Fitz, C., Wu, Y., Rudnick, D., Miao, S., Ferriter, A., Krupa, S., Armentano, T., Tarboton, K., Rutchey, K., Dong, Q., Newman, S., 2000. Everglades Consolidated Report Chapter 2 : Hydrologic Needs : The Effects of Altered Hydrology on the Everglades 2:1–68.

Soilmoisture, 2009. 1500F1 Operating Instructions. Santa Barbara.

Szajdak, L., Szatylowicz, J., 2002. Impact of Drainage on Hydrophobicity of Fen Peat-Moorsh Soils. Mires Peat 158–174.

Thorndike, R.L., 1953. Who belongs in the family? Psychometrika. https://doi.org/10.1007/BF02289263

Tibshirani, R., Walther, G., Hastie, T., 2001. Estimating the number of clusters in a data set via the gap statistic. J. R. Stat. Soc. Ser. B Stat. Methodol. https://doi.org/10.1111/1467-9868.00293

van Genuchten, M.T., 1980. A closed form equation for predicting the Hydraulic Conductivity of Unsaturated Soils. Soil Sci. Soc. Am. J. 44, 892–898.

Walczak, R., Rovdan, E., 2002. Water retention characteristics of peat and sand mixtures. Int. Agrophysics 161–165.

Wallor, E., Rosskopf, N., Zeitz, J., 2018. Hydraulic properties of drained and cultivated fen soils part I -Horizon- based evaluation of van Genuchten parameters considering the state of moorsh-forming process. https://doi.org/10.1016/j.geoderma.2017.10.026

Ward, J.H., 1963. Hierarchical Grouping to Optimize an Objective Function. J. Am. Stat. Assoc. 58, 236–244. https://doi.org/10.1080/01621459.1963.10500845

Waters, P., 1980. Comparison of the Ceramic Plate and the Pressure Membrane to Determine the 15 BAR Water Content of Soils. J. Soil Sci. 31, 443–446.

Weber, T.K.D., Iden, S.C., Durner, W., 2017. Unsaturated hydraulic properties of Sphagnum moss and peat reveal trimodal pore-size distributions. Water Resour. Res. 53. https://doi.org/10.1002/2016WR019707

3. DEVELOPMENT AND TESTING OF A COUPLED ONE-DIMENSIONAL MODEL OF VADOSE ZONE HYDROLOGY AND SUBSIDENCE

3.1 Introduction

Numerical solutions to the Richards governing equation continue to be the most widely used method of modeling transient flow in the unsaturated zone (Chen and Ren, 2008; He and Ren, 2009; Cumming et al., 2011; Caviedes-Voullième et al., 2013; List and Radu, 2016). These models have been applied to simulate water, nutrient, contaminant and gaseous transport in wetlands and peatlands (McCarter and Price, 2013, 2014a; Kettridge et al., 2016; Dixon et al., 2017; Wallor et al., 2018a). Information on water availability and distribution in the vadose zone in support of monitoring and restoration rely on numerically simulated data of vadose zone hydrology models. However, most simulations using the RE assume a rigid soil matrix that is non-deformable with desaturation (Kroes and Dam, 2003; Šimůnek et al., 2013; Kettridge et al., 2016; Dixon et al., 2017; Wallor et al., 2018a). While such assumptions may be valid for most mineral soils, its extension to volume changing soils like clay or organic soils like peat is problematic (Kennedy and Price, 2005; Camporese et al., 2006; Adem and Vanapalli, 2015). The volume changing behavior of the soil can result in inaccuracies in both the soil hydraulic parameterization model and the RE solution (Schwärzel et al., 2006; Wallor et al., 2018b). These inaccuracies may be very large for soils like peat which have porosities greater than 80%.

As discussed in section 1.1.5.2, coupled models of hydrology and volume change in the unsaturated zone are implemented through (1) defining the shrinkage through shrinkage curves, and (2) incorporating shrinkage parameters in the transport model. The

application of volume-change models to study subsidence in clay is prevalent (Briaud et al., 2003; Vu and Fredlund, 2004; Wray et al., 2005; Oh et al., 2009; Adem and Vanapalli, 2013). In the case of peat, many studies have attempted to define the shrinkage characteristic of different types of peat (Pyatt and John, 1989; McCarter and Price, 2014b); however, the incorporation of volume change from shrinkage in the RE transport model has been limited (Camporese et al., 2006). In this chapter, a coupled hydrology-subsidence model that incorporates shrinkage in model parametrization and the governing Richards transport equation is developed and tested for the shallow water tables observed in Everglades wetlands. The specific objectives of this chapter are:

1. Present the current finite-difference pressure-head based formulation of the RE, propose a model which incorporates volume-change of the matrix using a look-up table, and develop the R-script of the model, REVC.
2. Perform a sensitivity analysis of model parameters to equilibrium surficial pressure head for a shallow-water table with constant evapotranspiration from the surface using three models: 1) vGM NonVC RE, 2) vGM VC RE, and vGM VC REVC and compare differences.
3. Test the model using data collected from three lysimeter cores and perform the necessary sensor calibrations for marl and peat.

3.2 Model Development

3.2.1. Richards Equation (RE)

Buckingham (1907) formulated the earliest functional relationship for water flow in the vadose zone. Assuming the unsaturated hydraulic conductivity would be much less

than saturated hydraulic and that it will be a function of the matric potential of the soil, Buckingham modified Darcy's equation as follows,

$$J_w = -K(h)\frac{\partial H}{\partial z} = -K(h)\frac{\partial (h+z)}{\partial z} = -K(h)\left(\frac{\partial h}{\partial z} + \frac{\partial z}{\partial z}\right) \quad [3.1]$$

$$= -K(h)\left(\frac{\partial h}{\partial z} + 1\right)$$

Where J_w is the volumetric flux across a cell, $K(h)$ is the hydraulic conductivity as a function of matric potential, h, z is the vertical spatial coordinate.

Models like Gardner (1958), Campbell (1974), Haverkamp (1977), Burdine (1953), and Mualem (1976) have been developed to calculate the unsaturated hydraulic conductivity as a function of the matric pressure head. The vGM function coupled with the Mualem (1976) model is the most widely applied; it is given by,

$$K_s(h) = K_{sat}\left[\frac{1}{(1+(-\alpha h)^n)^{\left(1-\frac{1}{n}\right)}}\right]^l \left[1-\left(1-\frac{1}{(1+(-\alpha h)^n)}\right)^{\left(1-\frac{1}{n}\right)}\right]^2 \quad [3.2]$$

Richards (1931) produced a mass conservation equation by considering an elementary unit where the water flux in should be equal to the sum of the water flux out, change in storage within the volume, and any sources or sinks during a time interval (Radcliffe and Simunek, 2010). This equation is given by,

$$\frac{\partial \theta}{\partial t} = -\frac{\partial J_w}{\partial z} - S(h) \quad [3.3]$$

Where θ is the VWC, t is the time, and $S(h)$ is the sink (negative for source).

The mixed-form solution of the Richards' equation, developed by substituting the Buckingham-Darcy equation [3.1] into [3.3]; it is given by

$$\frac{\partial \theta(h)}{\partial t} = -\frac{\partial}{\partial z}\left(K(h)\frac{\partial h}{\partial z}\right) + \frac{\partial K(h)}{\partial z} - S(h) \qquad [3.4]$$

The Richards' equation can be expanded into two and three dimensions to model variably saturated flow in unsaturated zone. It may be solved with θ or h as the dependent variable, mixed form solutions also exist. The pressure head formulation is given by,

$$C_w(h)\frac{\partial h}{\partial t} = -\frac{\partial}{\partial z}\left(K(h)\frac{\partial h}{\partial z}\right) + \frac{\partial K(h)}{\partial z} - S(h) \qquad [3.5]$$

Where $C_w(h)$ is the capacity function. The capacity function is the slope of the water retention function, it is calculated by the following equation for the vGM model:

$$C_w(h) = \frac{\alpha^n(\theta_s - \theta_r)(n-1)(-h)^{n-1}}{[1 + (-\alpha h)^n]^{2-(\frac{1}{n})}} \qquad [3.6]$$

3.2.1.1. Numerical Model

Applications of the Richards' equation require a numerical solution because it is a strongly nonlinear partial differential equation with very few derived analytical solutions. Non-steady solutions to the RE may be developed using the finite difference method or the finite element method. This work uses a finite-difference scheme with a fully implicit time discretization.

3.2.1.2. Finite Difference Solution

Equation [3.6] may be expanded using the finite difference method in space and time. Presented below is the pressure head-based formulation with the source/sink term neglected (Radcliffe and Simunek, 2010):

$$C_w\left(h_i^{j+\frac{1}{2}}\right)\left(\frac{h_i^{j+1}-h_i^{j}}{\Delta t}\right)=\frac{\left[K(h)\left(\frac{\partial h}{\partial z}+1\right)\right]\Big|_{i+1/2}-\left[K(h)\left(\frac{\partial h}{\partial z}+1\right)\right]\Big|_{i-1/2}}{\Delta z}$$

$$=\frac{K\left(\frac{h_i+h_{i+1}}{2}\right)\left(\frac{h_{i+1}-h_i}{\Delta z}+1\right)-K\left(\frac{h_{i-1}+h_i}{2}\right)\left(\frac{h_i-h_{i-1}}{\Delta z}+1\right)}{\Delta z}$$

$$=\frac{K\left(\frac{h_i+h_{i+1}}{2}\right)}{(\Delta z)^2}(h_{i+1}-h_i+\Delta z)-\frac{K\left(\frac{h_{i-1}+h_i}{2}\right)}{(\Delta z)^2}(h_i-h_{i-1}+\Delta z) \qquad [3.7]$$

Where the spatial discretization is given by $z = i\Delta z$ and the time discretization is given by $t = j\Delta t$. Subscripts i-1, i, and i+1 represent the position in the finite difference mesh and superscripts j and j+1 represent the previous and current time levels. The RE may be solved explicitly by specifying all the terms on the right-side of the equation at the j-th time step and solving for the $j+1$-th, it may be solved implicitly by specifying all the terms on the right-side of the equation at the $j+1$-th, or it may be solved using the Crank-Nicolson method by taking an average of the j-th and the $j+1$-th timestep (Radcliffe and Simunek, 2010). The fully implicit method and the Crank Nicolson method are preferred since the fully explicit method is only stable for small time steps. This work uses the fully

implicit method. Following are the coefficients generated for an unknown time-step of $(j+1)$:

$$a_i h_{i-1}^{j+1} + b_i h_i^{j+1} + c_i h_{i+1}^{j+1} = d_i \qquad [3.8]$$

The coefficients in the above equation are given by,

$$\begin{aligned} a_i &= -r\frac{K_{i-1/2}}{C_{wi}} \\ c_i &= -r\frac{K_{i+1/2}}{C_{wi}} \\ b_i &= 1 - a_i - c_i \\ d_i &= h_j^i + \Delta z(a_i - c_i) \end{aligned} \qquad [3.9]$$

And,

$$a_i = -r\frac{K_{i-1/2}}{C_{wi}} \qquad [3.10]$$

$$c_i = -r\frac{K_{i+1/2}}{C_{wi}} \qquad [3.11]$$

$$b_i = 1 - a_i - c_i \qquad [3.12]$$

$$d_i = h_j^i + \Delta z(a_i - c_i) \qquad [\ 3.13]$$

The model can be expressed in matrix notation as:

$$\begin{bmatrix} 1 & 0 & 0 & & & & 0 \\ a_1 & b_1 & c_1 & & & & 0 \\ 0 & a_2 & b_2 & c_2 & & & 0 \\ & . & & . & & . & \\ 0 & & & a_{N-2} & b_{N-2} & c_{N-2} & 0 \\ 0 & & & & a_{N-1} & b_{N-1} & c_{N-1} \\ 0 & & & & 0 & 0 & 1 \end{bmatrix} \begin{bmatrix} h_0^{j+1} \\ h_1^{j+1} \\ h_2^{j+1} \\ . \\ h_{N-2}^{j+1} \\ h_{N-1}^{j+1} \\ h_N^{j+1} \end{bmatrix} = \begin{bmatrix} h_0^j \\ h_1^j + \Delta z(a_1 - c_1) \\ h_2^j + \Delta z(a_2 - c_2) \\ . \\ h_{N-2}^j + \Delta z(a_{N-2} - c_{N-2}) \\ h_{N-1}^j + \Delta z(a_{N-1} - c_{N-1)} \\ h_N^j \end{bmatrix} \qquad [\ 3.14]$$

This model is solved with fully-implicit time discretization using the Picard iteration. The Picard iteration sequentially estimates the unknown h_i^{j+1} using the latest estimates of $K_{i\pm1/2}$ and C_{wi} (Paniconi et al., 1991).

3.2.1.3. Proposed Volume Change Model

Based on evidence in section 1.1.5.2 and the literature review, this model assumes that the volume change observed in unsaturated soil is a function of VWC and in turn, the pressure head. Since the pressure head in an unsaturated soil column varies with depth and time, the proposed model uses a variable node height Δz with time for each cell. Equation [3.14] becomes:

$$\begin{bmatrix} 1 & 0 & 0 & & & & 0 \\ a_1 & b_1 & c_1 & & & & 0 \\ 0 & a_2 & b_2 & c_2 & & & 0 \\ & . & & . & & . & \\ 0 & & & a_{N-2} & b_{N-2} & c_{N-2} & 0 \\ 0 & & & & a_{N-1} & b_{N-1} & c_{N-1} \\ 0 & & & & 0 & 0 & 1 \end{bmatrix} \begin{bmatrix} h_0^{j+1} \\ h_1^{j+1} \\ h_2^{j+1} \\ . \\ h_{N-2}^{j+1} \\ h_{N-1}^{j+1} \\ h_N^{j+1} \end{bmatrix}$$

$$= \begin{bmatrix} h_0^j \\ h_1^j + \Delta z_1(a_1 - c_1) \\ h_2^j + \Delta z_2(a_2 - c_2) \\ . \\ h_{N-2}^j + \Delta z_{N-2}(a_{N-2} - c_{N-2}) \\ h_{N-1}^j + \Delta z_{N-1}(a_{N-1} - c_{N-1)} \\ h_N^j \end{bmatrix} \quad [3.15]$$

And,

$$r_i = \frac{\Delta t}{\Delta z_i{}^2} \quad [3.16]$$

At each time-step, the coefficients, $a_i, b_i,$ and c_i are calculated at each time step using the updated r_i. An R-script with the proposed model was developed. Figure 3-1 presents the flow chart of the scripted model. The parameterization of the model is discussed in the next section.

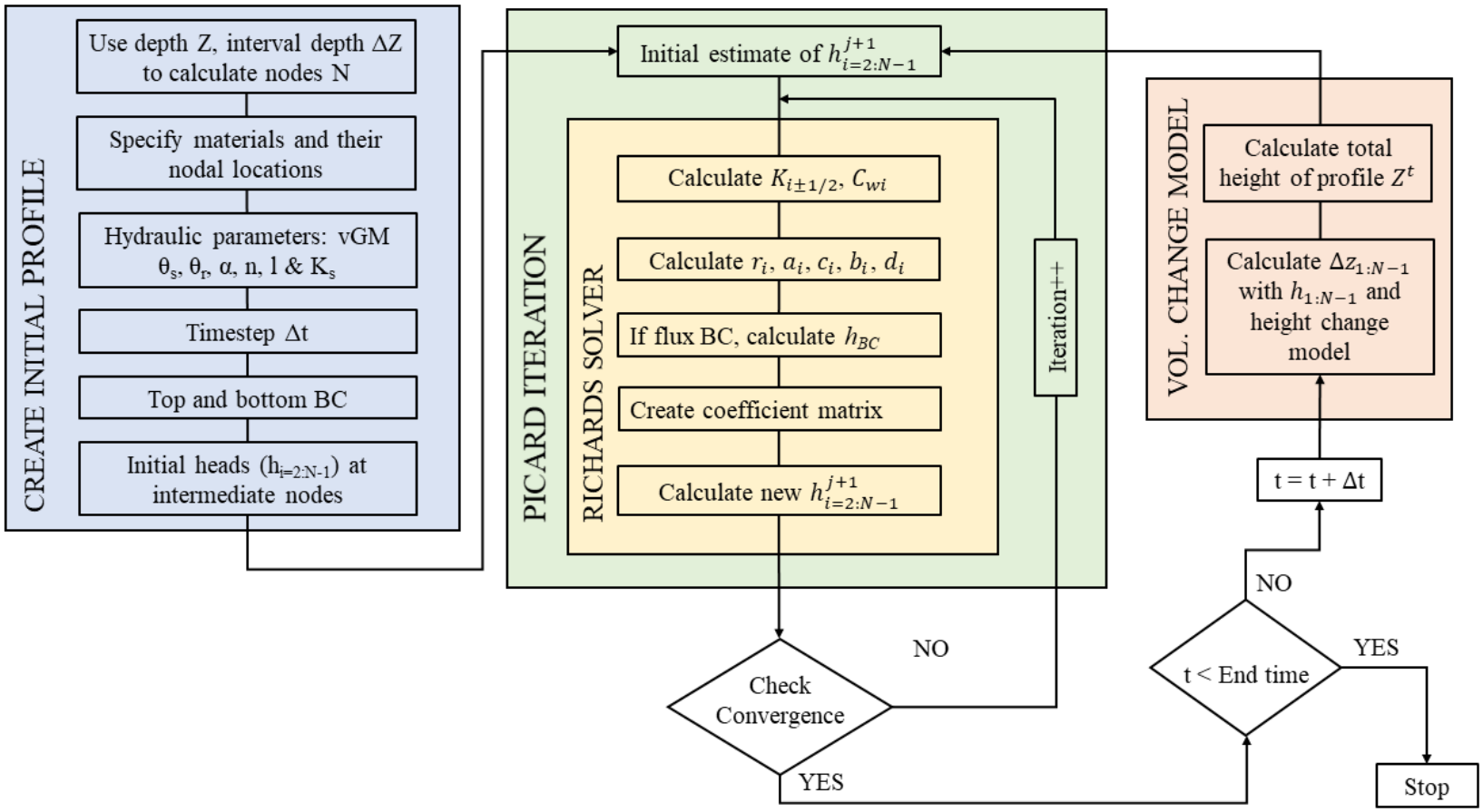

Figure 3-1. Schematic with flow chart of the scripted model.

3.2.1.4. Boundary Conditions

Boundary conditions need to be specified at the surface and the bottom of the soil profile to solve the finite difference scheme proposed in section 3.2.1.3. This section discusses the two main types of boundary conditions used in this study:

(1) System-Independent Boundary Conditions:

System independent boundary conditions do not depend on the moisture status of the soil. A Dirichlet (Type 1) boundary condition is used when the dependent variable, in this case pressure head, at the boundary is known. In the h-based formulation of the RE, it is expressed as:

$$h(z = 0, t) = h_U$$
$$h(z = L, t) = h_L \qquad [3.17]$$

Where h_U is the prescribed pressure head at the upper boundary and h_L is the prescribed pressure head at the lower boundary. The prescribed heads may be constant or varying in time.

In the absence of a prescribed head for the upper boundary condition, h_U can be estimated from meteorological data assuming the soil surface is at equilibrium with the atmosphere using (Feddes et al., 1978):

$$h(z = 0, t) = h_U = \frac{RT(t)}{Mg} \ln [F(t)] \qquad [3.18]$$

Where R is the universal gas constant (J mole^{-1} K^{-1}), M is the molecular weight of water (kg mole^{-1}), g is the acceleration due to gravity (m s^{-1}), $T(t)$ and $F(t)$ are the temperature (K) and the relative humidity of the air fraction with respect to time. This is the minimum pressure head that can be allowed under air-dry conditions.

If the pressure head at the surface is unknown but a flux across the boundary is known, a Neumann (type 2) boundary condition may be used. The Neumann condition specifies the derivative of the pressure head,

$$q(t) = -K(h)\left(\frac{\partial h}{\partial z} + 1\right) \qquad [3.19]$$

The flux equation maybe expanded and applied to the algebraic system of equations to solve. It can be solved either by prescribing the Dirichlet boundary condition as a gradient or the use of ghost nodes.

The flux used in a Neumann condition is known, a priori. It does not depend on the moisture conditions of the soil system.

(2) System-Dependent Boundary Condition:

System-Dependent boundary conditions are used to simulate boundary conditions that depend on the moisture status of the soil. For this type of boundary conditions, the pressure head or the prescribed flux at the boundary node is unknown. The model uses potential flux (from atmospheric or subsurface) to calculate the actual flux across the boundary. For a pressure head of h at the soil surface, it is formulated by (Radcliffe and Simunek, 2010):

$$\left|K(h)\left(\frac{\partial h}{\partial z}+1\right)\right| \leq E \qquad [3.20]$$

and

$$h_A \leq h \leq h_S \qquad [3.21]$$

Where E is the maximum potential evaporation or infiltration, h_A is the minimum allowable pressure head for the soil conditions (calculated from equilibrium conditions of soil and water), and h_S is the maximum allowable pressure head for the soil conditions (set to zero for instantaneous runoff).

3.2.1.5. Model Parameterization

The soil hydraulic model is parameterized using the SWRC. An accurate SWRC is important for unsaturated flow modeling as it defines the unsaturated hydraulic conductivity of the model. The SWRC links the VWC of the soil to the pressure head. The VWC is the ratio of the volume of water to the volume of the soil sample. For the drying SWRC, the volume of the soil sample decreases with increasing pressure head. Not accounting for the volume change in the SWRC through volume-correction results in the underestimating the VWC. For organic soils like peat with porosities greater than 80%, this results in underestimating the VWC as early as 10 kPa. This effect is expected to be more pronounced at higher pressure heads with greater volume loss.

Since soil hydraulic models like the vGM model use the retention data from SWRCs to parametrize the RE, volume corrected SWRCs also affect the hydraulic models. Table 2-4 presents the VWC with and without volume correction for a peat and marl sample from the water retention curves from section 2.2.6, while Figure 2-9 presents the graphical

retention data from the vGM model. In general, accounting for volume change in the vGM model results in a larger air-entry region. The nodal height, Δz for each cell and at each timestep is calculated from a look-up table. The table is created by interpolating between the HCR (Height Change Ratios) values at 0 kPa, 6 kPa, 10 kPa, 50 kPa and 1500 kPa and multiplying by the initial height of the node. HCRs are calculated from section 2.2.6.2 by dividing the height of sample measured after each applied pressure by the height of the sample at saturation. Figure 3-2 presents the mean HCRs for each cluster.

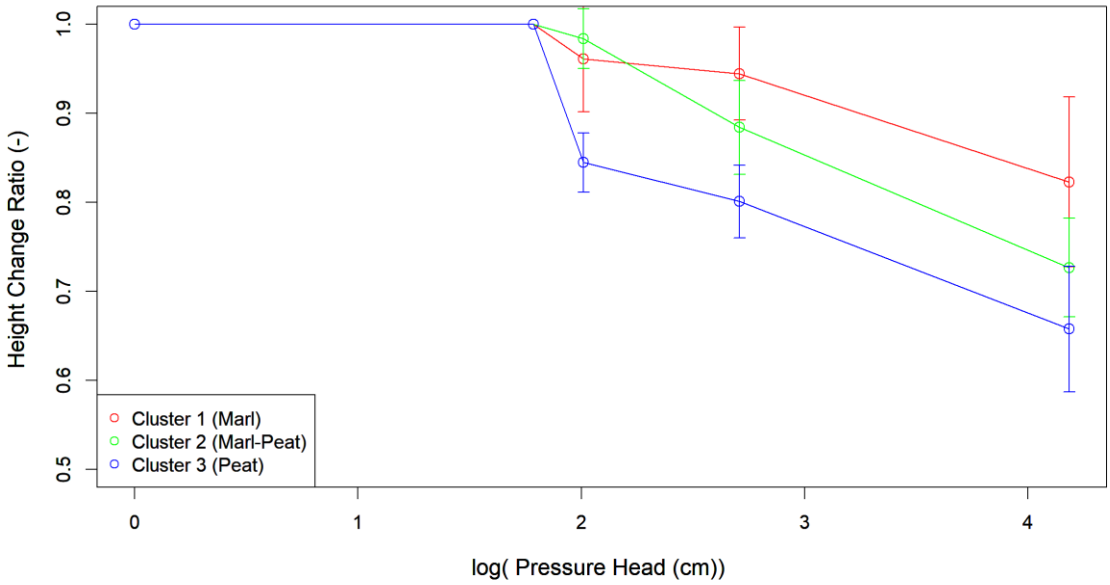

Figure 3-2. Mean Height Change Ratios (HCRs) of each cluster with arrows showing one standard deviation.

3.2.1.6. Comparison to HYDRUS

The Richards' equation code in the R-script was compared to two different examples presented with the HYDRUS package to verify the R-script for constant head boundary conditions simulating upward (*UPINFIL*) and downward (*1INFILTR*) infiltration. In addition, the code for atmospheric boundary condition was tested by comparing to a project created in HYDRUS with identical conditions as no examples with atmospheric boundary conditions were provided in the HYDRUS package. The volume change component of the R-script was disabled to allow for a direct comparison of results generated for all three codes.

Example: UPINFIL

The R-script was tested with an example from HYDRUS simulating upward infiltration with a bottom tension for an 8 cm deep homogenous column of loam. The profile was discretized to 0.1 cm thick depth intervals resulting in 80 depth intervals and 81 nodes. ($\theta_r = 0.078$, $\theta_s = 0.43$, $\alpha = 0.036$, $n = 1.56$, K_{sat} = 0.00029 cm/s, $l = 0.5$). The vGM model with no hysteresis was used to develop unsaturated hydraulic conductivity. The top and bottom boundary conditions were specified as constant pressure heads. The initial head of -750 cm was specified for nodes 1 to 80 except the bottom node at depth 8 cm, node 81 which was assigned a pressure head of -1 to simulate infiltration. The simulation was performed from zero to 10800 seconds with a timestep of one second. Figure 3-3 (a) presents the pressure head across the profile for time steps of 720 (T1), 1440 (T2), 2160 (T3), 3600 (T4), and 10800 (T5) seconds. Comparability was observed between both scripts.

Example: 1INFILTR

Infiltration with a sharp wetting front was simulated in both HYDRUS and the R-Script with the purpose of comparison. The simulation was performed for a homogenous, 600 cm deep soil profile discretized into 120 depth intervals 5 cm thick resulting in 121 nodes. A uniform initial head of -729.7 cm was prescribed across the profile except for the top node (at depth 0 cm) which was prescribed 0 cm to simulate the wetting front. Simulations were performed with constant boundary conditions of 0 cm at the top node (node 1 at depth 0 cm) and -729.7 cm at the bottom node (node 121 at depth 600 cm). The vGM model with no hysteresis was used to parameterize the model ($\theta_r = 0$, $\theta_s = 0.3308$, $\alpha = 0.01433$, $n = 1.506$, K_{sat} = 25 cm/hr, $l =$ 0.5). Simulations were performed from zero to five hours with a time step of 0.001 hours. Figure 3-3 (b) presents the pressure head across the profile for the simulations.

Project: SysBCTest

Simulations for a top atmospheric boundary condition generated by the R-code were compared to a similar profile and boundary conditions in HYDRUS. A 30 cm deep soil profile was discretized into 1 cm deep 30 depth intervals resulting in 31 nodes. Hydrostatic equilibrium with the water table which is assumed to be at the depth of 30 cm was applied as the initial condition. At the first time-step, an atmospheric top boundary condition with evapotranspiration flux of 0.016 cm/hour was applied at the top node (node 1 at depth 0) and this top boundary condition was held constant for the rest of the simulation. A constant head boundary condition of 0 cm was applied as the bottom boundary condition signifying the water table. The vGM model with no hysteresis was

used to parameterize the model ($\theta_r = 0.142$, $\theta_s = 0.786$, $\alpha = 0.012$, $n = 1.415$, K_{sat} = 0.225 cm/hr, $l = 0.5$). Simulations were performed from zero to 100 hours with a time step of one hour. Figure 3-3 (c) presents the pressure head across the profile for the simulations. The R-code and HYDRUS produced similar solutions.

A second simulation was performed to test atmospheric boundary condition with a bottom tension for the profile described above. The bottom boundary condition was changed to a constant boundary condition of -30 cm. An initial condition of -30cm was applied to all the nodes. Simulations were performed from zero to 100 hours with a time step of one hour. Figure 3-3 (d) presents the pressure head across the profile for select time steps during the simulation. Results of the R-code and HYDRUS were comparable.

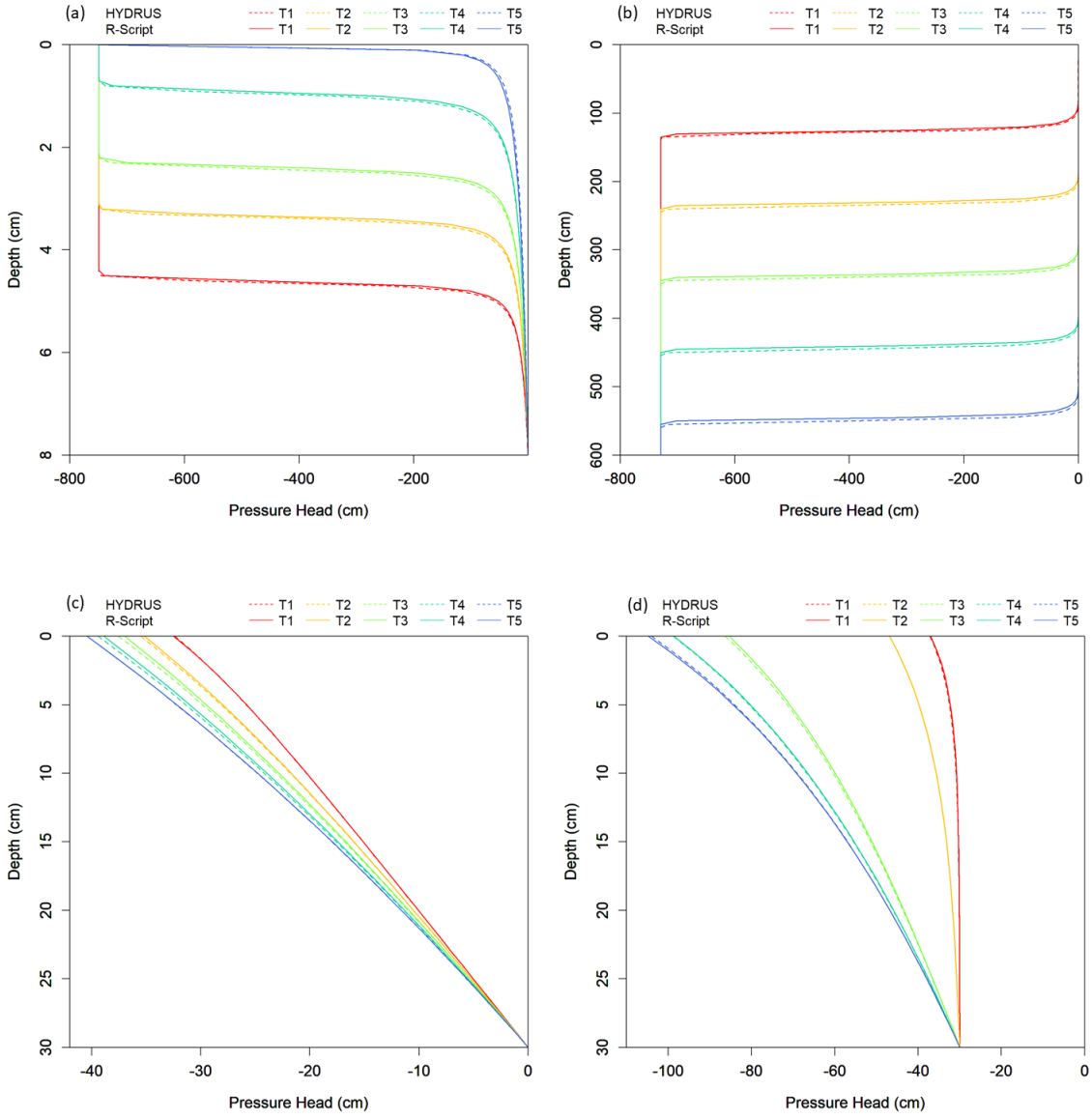

Figure 3-3. Comparison of the REVC model (neglecting shrinkage) with HYDRUS for the tested examples: (a) *UPINFIL* at timesteps T1 (720 seconds), T2 (1440 seconds), T3 (2160 seconds), T4(3600 seconds), and T5 (10800 seconds); (b) *1INFILTR* at timesteps T1 (1 hour), T2 (2 hours), T3 (3 hours), T4 (4 hours), and T5 (5 hours); (c) *SysBCTest* T1 (1 hour), T2 (5 hours), T3 (10 hours), T4 (20 hours), and T5 (100 hours); and (d) *SysBCTest* with bottom tension at timesteps T1 (1 hour), T2 (50 hours), T3 (100 hours), T4 (150 hours), and T5 (300 hours).

3.2.1.7. Mesh Convergence and Stability

Mesh density influences the numerical solution for both implicit and explicit methods. In the case of RE, the selection of cell heights and time steps are known to affect its solutions and, in some cases, cause convergence issues through oscillations (Karthikeyan et al., 2001). In addition, differences between numerical and analytical solutions are known to decrease when Δt and Δz tend to zero (Warrick, 2001); however, finer mesh sizes and time steps can make the solutions computationally intensive. Mesh convergence analysis is s useful method of defining combinations of cell heights and time steps where the solutions are stable. In this section, suitable mesh sizes are investigated with refinement techniques for the case of a shallow vadose zone, and the effect of the time steps on the solution is investigated. Mesh sizes in the following sections will be selected using the results obtained herewith.

3.2.1.7.1 Methodology

Simulations were performed for the case of a shallow unsaturated zone with depth of 20 cm. Homogenous soil columns were assigned soil hydraulic parameter combinations presented in Table 3-1. The top boundary condition was set to atmospheric with a potential flux of 6 mm/day (largest potential flux observed in the Everglades wetland) and the bottom boundary condition was a prescribed pressure head of 0 cm (indicating the water table). The minimum allowable pressure head for the top node was set to -500 cm. Multiple mesh sizes were simulated with by iteratively varying Δz values of 5 cm, 4 cm, 2 cm, 1 cm, 0.5 cm, 0.1 cm, and 0.05 cm (corresponding to 5, 6, 11, 21, 41, 201, and 401 nodes). Figure 3-4 presents the discretization for the mesh sizes with the boundary conditions. For

each mesh size, solutions were obtained for time steps of 10-minute, 1-hour, and 1-day. The total simulation period was set to 5 days. The surficial pressure head and volumetric water content at the end of each simulation were recorded. Solutions were graphed as a function of mesh size for each time step and are considered stable when the variations in surficial pressure head or surficial volumetric water content is low with finer mesh size.

Table 3-1. Combinations of parameters used in the simulations.

Combination	θ_s [-]	θ_r [-]	α [cm^{-1}]	n [-]	K_{sat} [cm d^{-1}]
Marl Max	0.835	0.558	0.038	1.579	18.7
Marl Min	0.772	0	0.002	1.065	0.5
Marl Mean	0.783	0.159	0.017	1.283	5.4
Peat Max	0.948	0.404	0.036	1.401	114.2
Peat Min	0.867	0	0.002	1.074	2.1
Peat Mean	0.927	0.085	0.022	1.227	17.1

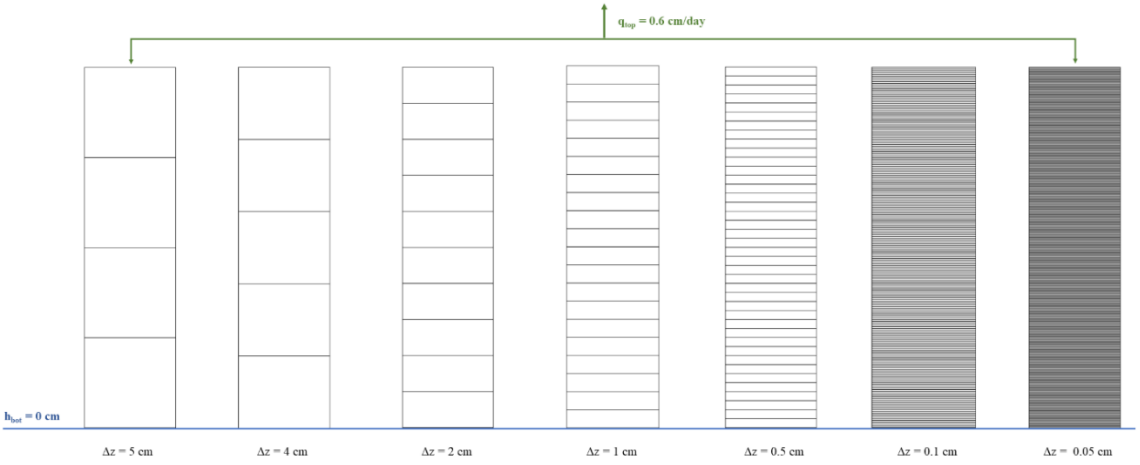

Figure 3-4. Schematic of mesh sizes tested with top atmospheric boundary condition and bottom constant head boundary condition.

3.2.1.7.2 Results

The combination of parameters for marl and peat with maximum values (top panel of Figure 3-5 and Figure 3-6) show differences in the solutions with changes in Δz and Δt. The solution with Δt of 10-minute and 1-hour are very similar for all Δz, but solutions with Δt of 1-day underestimate the surficial pressure head and the surficial volumetric water content. For Marl Max, maximum difference in volumetric water content (of 2.5%) between the 10-minute and 1-day timestep occurs at Δz of 0.05 cm whereas for Peat Max, this difference is 5.2%. Large time steps are advantageous in reducing computation time. Since, at the worst-case scenario, only a difference of 5.2 % volumetric water content is observed at the top node, the use of 1-day time steps to keep computation time low, should not significantly impact solution, and is, therefore, acceptable.

Stability of solution increases with an increase in mesh density; however, significant changes in solution is not observed across the Δz values tested for Marl Max and Peat Max with the 10-minute or 1-hour time step. For Marl Max at 1-day time step, the volumetric water content decreases from 77.8% to 75.0% when mesh density increases from 6 to 41 nodes (Δz from 5 cm to 0.5 cm) but it only decreases by 1% when the mesh density is increased from 41 to 401 nodes (Δz from 0.5 cm to 0.05 cm); hence, stability at 41 nodes (Δz of 0.5 cm) is a reasonable assumption for marl. For Peat Max at 1-day time step, the volumetric water content reduces from 87.4% to 83.5% when mesh density increases from 6 to 201 nodes (Δz from 5 cm to 0.1 cm); however, when the mesh density increases to 401 nodes (Δz of 0.05), only a 1.3% decrease in volumetric water content is observed indicating that for peat mesh stability can be assumed to be from Δz of 0.1 cm and finer.

For marl with the parameter combination derived from the minimum values (bottom panel of Figure 3-5 and Figure 3-6), the pressure head on the surface drops to the minimum allowable pressure head at the end of the 5-day time period for the 10-minute time step; however, non-convergence is observed for larger time steps with finer mesh size. For example, the solution does not converge for Δt of 1-hour at Δz of 0.1 cm and 0.05 cm and for Δt of 1-day timestep Δz of 0.05 cm. Non-convergence with finer mesh sizes and larger time steps is also observed in the case of peat with parameter combination generated from minimum values (bottom panel of Figure 3-6). For small time steps (10-minute and 1-hour) solutions converge from Δz of 1 cm (21 nodes) and finer. For larger time-steps, convergence is observed from Δz of 0.1 cm (201 nodes) and finer.

Non-convergence is a known challenge with RE numerical models and may occur as a result of steep gradients in the solution of state variables. Generally, steep gradients are observed for infiltration problems. In the case of shallow aquifer with evaporation conditions (slow upward water flow), which is of interest in this study, the boundary conditions change very slowly. However, certain combinations in parameters, as observed with the minimum combination for marl and peat, can result in non-convergence through extreme changes in surficial pressure head. Increasing the number of iterations until convergence or reducing the convergence tolerance threshold can force a solution at the risk of increasing computation time and decreasing the accuracy of the solution. Codes like HYDRUS implement a dynamic time stepping method where the time step is varied over a pre-defined range when non-convergence is observed. The advantage of such a method over increasing the number of iterations is that computation time is only affected when non-convergence is encountered. For this effort, due to the slow change in boundary

conditions, non-convergence is not expected to be a significant problem except for a few combinations of hydraulic parameters (when K_{sat} and α are low), and hence, a dynamic time stepping methodology should be applied on a case-by-case basis for scenarios where non-convergence hinders numerical solution.

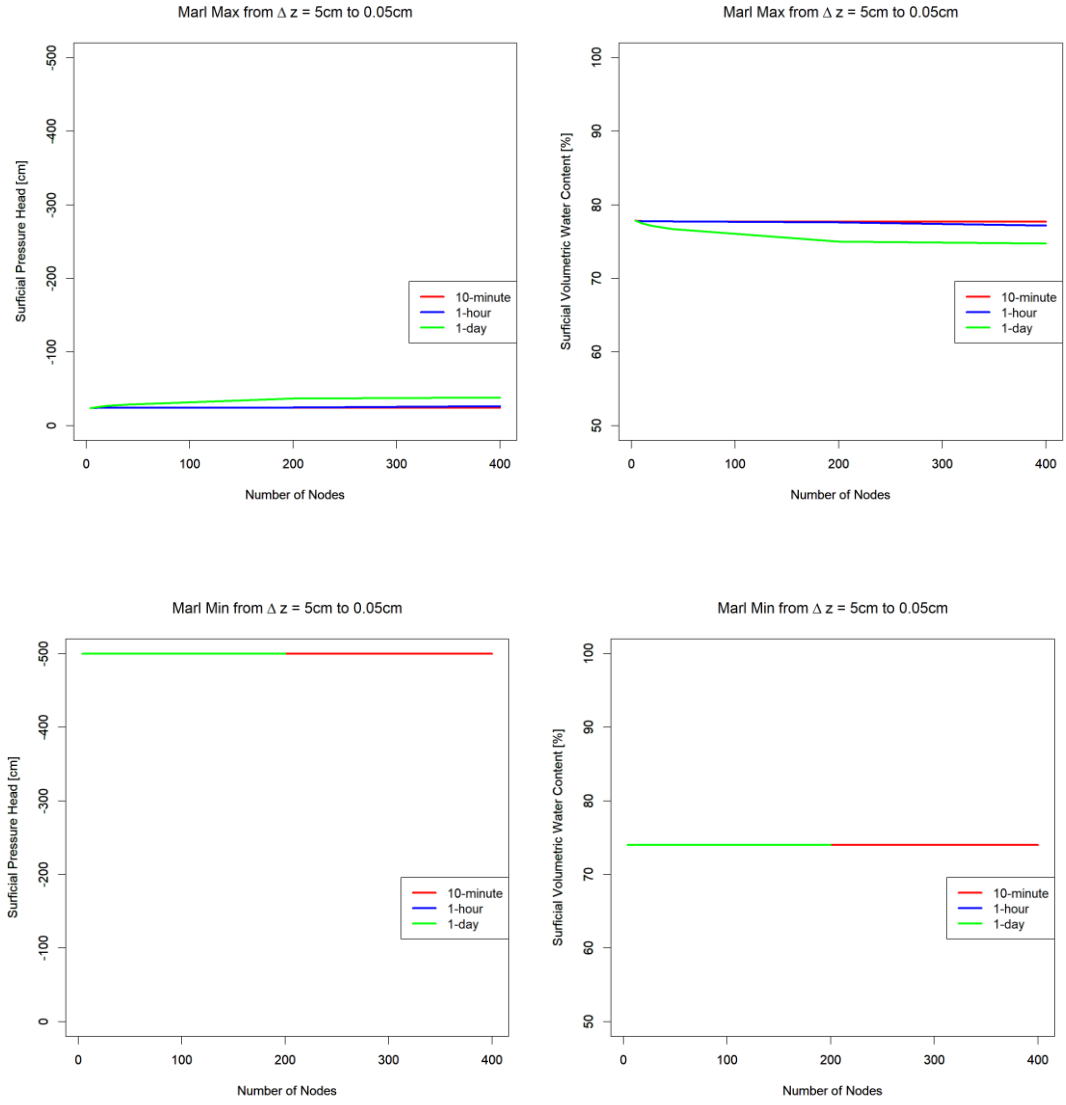

Figure 3-5. The surficial pressure head (left) and surficial volumetric water content (right) for marl with parameter combinations of maximum values (top) and minimum values (bottom) generated for Δz from 5 cm to 0.05 cm at time steps of 10-minute, 1-hour and 1-day.

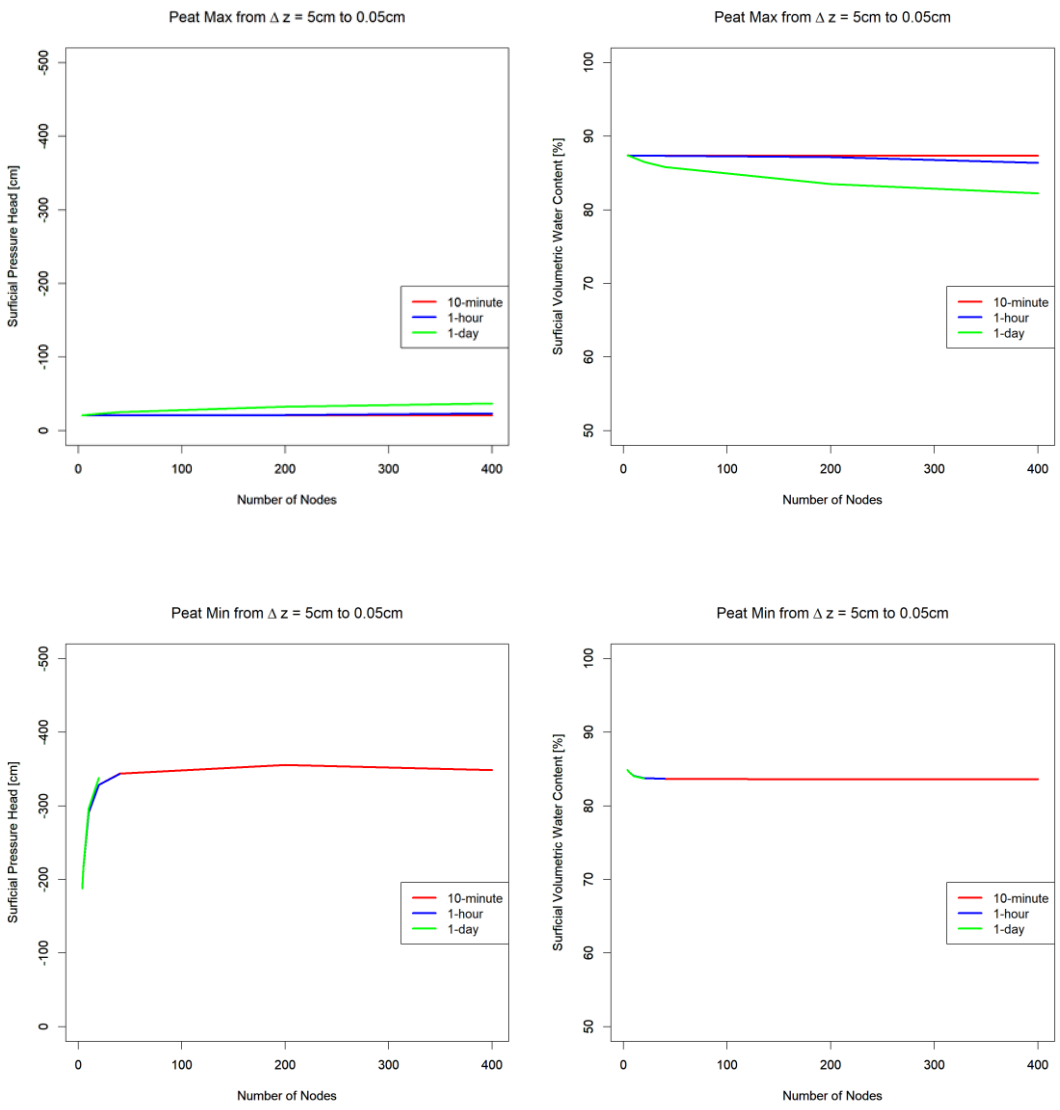

Figure 3-6. The surficial pressure head (left) and surficial volumetric water content (right) for peat with parameter combinations of maximum values (top) and minimum values (bottom) generated for Δz from 5 cm to 0.05 cm at time steps of 10-minute, 1-hour and 1-day.

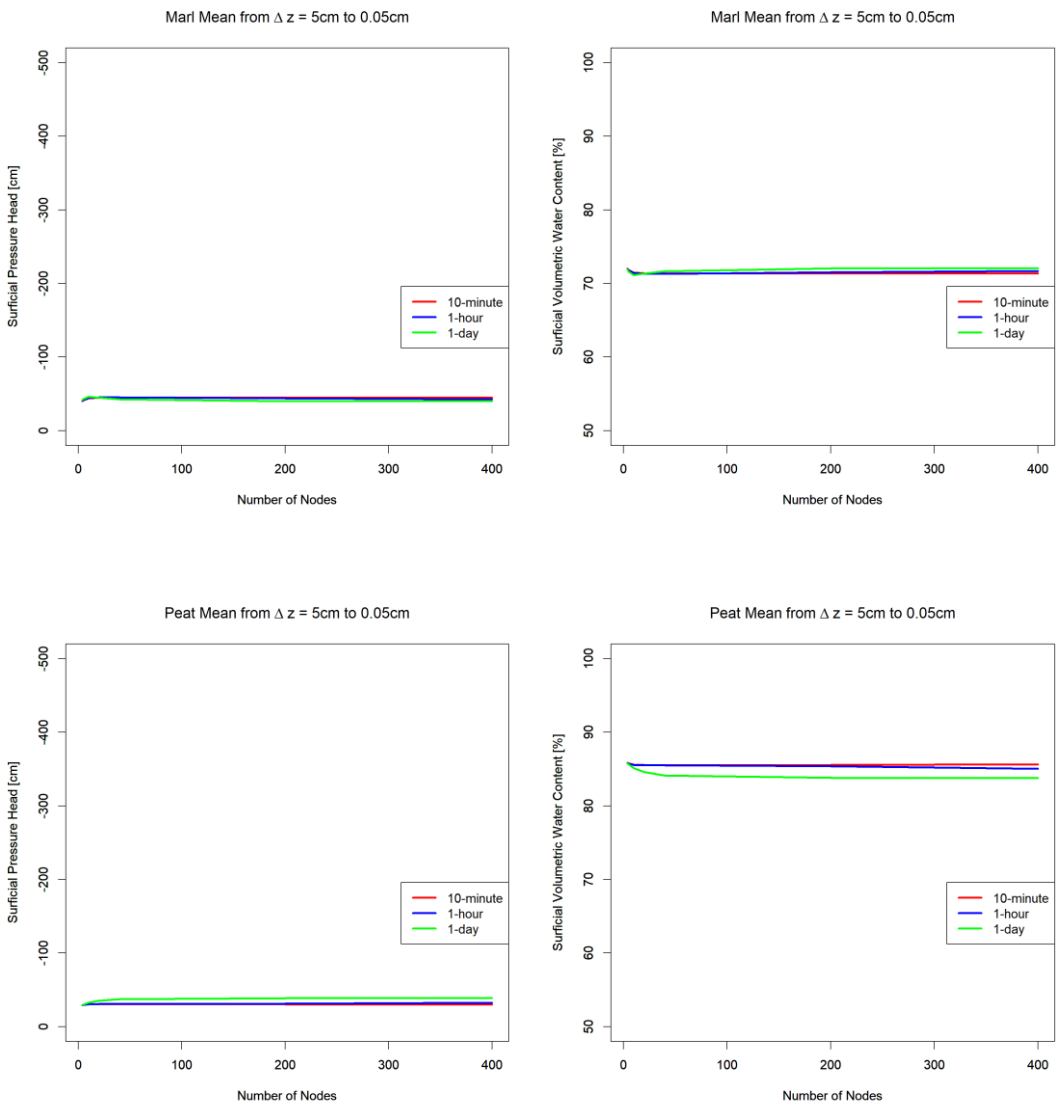

Figure 3-7. The surficial pressure head (left) and surficial volumetric water content (right) for marl (top) and peat (bottom) with parameter combinations of mean values generated for Δz from 5 cm to 0.05 cm at timesteps of 10-minute, 1-hour and 1-day.

3.3 Sensitivity Analysis

This sensitivity analysis was conducted for the case scenario of a typical vadose zone in a wetland system where the water table is not far below the surface of the soil and the flux from the surface of the soil is controlled by evapotranspiration. The vadose zone thickness in such systems is defined as the depth from the surface to the water table. It is believed that with increasing vadose zone thickness, the tendency of the surficial soil to have more negative matric potential increases and in turn, shrinkage of the soil increases. However, the variation in matric potential across the profile and its' rate of change and shrinkage are both determined by the hydraulic parameters of the model. Kettridge et al., 2016 ran HYDRUS simulations using ranges of typical vGM parameters for Canadian peat to determine the time taken to reach a threshold tension of 100 cm of water (approximately 10 kPa), a tension at which wetland plants like *Spaghnum* experience hydrologic stress. This study aims at understanding the equilibrium state of the system, i.e. when no change in tension across the profile is observed. For shallow groundwater systems, capillarity from the water table may provide a continuous source of moisture to the surface of the soil; in such systems, the tension at the surface remains close to hydrostatic equilibrium. However, depending on the soil hydraulic properties, vulnerable soil profiles may experience high equilibrium surface tension. The methodology and results of a sensitivity analysis performed to determine how the equilibrium surficial tension varies with soil hydraulic parameters are presented in this subsection.

3.3.1. Sensitivity Analysis Methodology

The sensitivity of the equilibrium surficial pressure head to soil hydraulic parameters α, n, and K_{sat} were tested at vadose zone depths of 40 cm and 60 cm for homogenous marl and peat soil profiles. Initial testing revealed that parameters θ_s and θ_r did not affect surficial equilibrium pressure head and hence, they were not tested. Parameters θ_s and θ_r were assigned the average values calculated for marl and peat in the previous chapter (Table 3-2). Previous works of peat unsaturated flow modeling have found that parameter l does not strongly affect the Richards solution (Schwärzel et al., 2006; Kettridge et al., 2016; Wallor et al., 2018a); preliminary testing confirmed the same and hence, parameter l is assumed to be a constant of 0.5 for the simulations. The tests were performed for three different models: 1) vGM NonVC RE – vGM parameters were calculated without VC and the transport model does not consider the change in volume of the soil matrix; 2) vGM VC RE – vGM parameters were calculated taking into account the VC but the transport model does not consider the change in volume of the soil matrix; and 3) vGM VC REVC – vGM parameters were calculated taking into account the volume of the soil matrix and the mean HCR model to simulate the change in the height of the soil matrix. To test each parameter, a sequence of equally spaced values was generated using the range of values determined in Chapter 1 without outliers. The parameter to be tested is then varied using the sequence while the other two parameters are assigned their mean values. Table 3-2 presents the ranges of values tested. This results in a total of 150 simulations per soil type per model type and a grand total of 900 simulations.

At the beginning of each run, the depth of the soil profile is set to the depth of water table from the surface, also known as the vadose zone depth (cm). Each profile is discretized with a Δz of 1 cm. Hydrostatic equilibrium with the water table is assumed at the beginning of the run; hence, pressure head is assigned 0 at the bottom node and it decreases by 1 cm of water for each 1 cm increase in height resulting in the highest tension pressure head on the surface. A flux boundary condition is applied at the top boundary. This value is assumed to be 6 mm/day corresponding to the maximum evapotranspiration recorded in the Everglades. A constant head 0 cm is applied at the bottom boundary to simulate the presence of the water table, and this is a no-flux boundary condition. The script is run iteratively until equilibrium with the water table is reached, i.e. the square root of the sum of the squares between the pressure head across the profile of two successive time steps is less than the tolerance of 0.01 cm. At this point, the combination of hydraulic parameters, time to equilibrium (hours), and equilibrium surface tension is written into an output matrix. The script moves on to the next set of parameters and the process is repeated. After the process has run through all the parameters at both the depths for one model type, the output matrix is also written out as a csv file and the script moves on to the next model type.

Table 3-2. Presents the values and ranges of parameters tested in the sensitivity analysis.

Model	Soil	θ_s [cm^3 cm^{-3}]	θ_r [cm^3 cm^{-3}]	α [cm^{-1}]			n [-]			K_{sat} [cm d^{-1}]		
				Min	Max	Mean	Min	Max	Mean	Min	Max	Mean
	Marl	0.787	0.155	0.003	0.019	0.012	1.220	1.726	1.455	0.5	18.7	5.4
vGM NonVC	**Peat**	0.940	0.087	0.013	0.022	0.018	1.415	1.714	1.568	2.1	114.2	17.1
	Marl	0.783	0.159	0.002	0.038	0.017	1.065	1.579	1.283	0.5	18.7	5.4
vGM VC	**Peat**	0.927	0.085	0.002	0.036	0.022	1.074	1.401	1.227	2.1	114.2	17.1

3.3.2. Sensitivity Analysis Results and Discussion

The results from the sensitivity analysis are presented in Figure 3-8, Figure 3-9 and Figure 3-10. For all models and parameters tested, there is a tendency for the surficial equilibrium pressure head to be more negative with increase in vadose depth. In addition, the equilibrium pressure head of marl tends to be more negative than that of peat. Another consistent trend for all parameters is the tendency of the vGM NonVC RE models to predict higher pressure heads than the vGM VC RE or vGM VC REVC models. The vGM REVC model predicts higher pressure heads than the vGM VC RE model.

Figure 3-8 shows that the surficial pressure head decreases with an increase in vGM parameter α, which controls the air-entry potential of the soil. Higher α results in a narrower air-entry region (Radcliffe and Simunek, 2010). Peat and marl have similar ranges of α but marl tends to reach the constrained critical pressure head of -500 cm at lower ranges of α. For overlapping ranges of α between the vGM NonVC RE and vGM VC REVC models, the only difference is vGM parameter n, with lower n for vGM VC RE model (Figure 3-8). A lower n indicates a less steep SWRC with a wider pore-size distribution (Radcliffe and Simunek, 2010). Between the vGM VC RE and vGM VC REVC models, the surficial equilibrium pressure head tends to reach the constrained critical pressure head at lower α for the vGM RE model with major differences observed for peat, which has more significant shrinkage than marl. Overall, the equilibrium surficial pressure head for the vGM VC REVC model is higher than the vGM VC RE model indicating that predicted VWC will be higher for the VGM VC REVC model; this result is

consistent with past observations of the effect of vertical shrinkage (McCarter and Price, 2014b).

For parameter n, the surficial pressure head increases with an increase in n for marl and peat at all depths except for marl at 60 cm (Figure 3-9). Kettridge et al., 2016 found that with an increase in n the time to reach threshold tension of 100 cm increased; this observation along with the observation from this study indicates that lower n caused by a narrower pore-size distribution results in more negative surficial pressure heads for shallow water tables. The equilibrium surficial pressure head of marl at 60 cm reaches the constrained critical pressure head of -500 cm for the vGM VC RE and vGM VC REVC models at all tested values of n (Figure 3-9). For overlapping ranges of n tested, the tendency for marl to have lower surficial pressure heads. A more negative surficial pressure head increases the ability of the matrix to draw soil water from the shallow aquifer while preventing further soil moisture loss to the atmosphere (Kettridge et al., 2016).

Higher equilibrium surficial pressure heads are observed with an increase in K_{sat} for both soil depths and model types (Figure 3-10). With an increase in depth, the range of K_{sat} over which surficial pressure head is sensitive increases. For marl, significant differences are observed between vGM NonVC RE and vGM VC RE over the range of K_{sat} tested. A lower α and higher n of the vGM NonVC RE results in higher equilibrium surficial pressure heads compared to the vGM VC RE model. Between the vGM VC RE and vGM VC REVC models, significant differences in surficial pressure heads are observed at deeper vadose zones for the middle range of K_{sat}. At low K_{sat}, both vGM VC and vGM VC REVC reach the critical constrained pressure head, and no differences in

surficial pressure head are observed; whereas, at high K_{sat}, the surficial pressure head is relatively high, indicating that the pressure head across the profile is never negative enough to induce shrinkage and hence model solutions are similar. A high K_{sat} is capable of continuously providing soil moisture from the shallow aquifer to the atmosphere and can prevent the soil surface from shrinkage due to moisture loss (Kettridge et al., 2016).

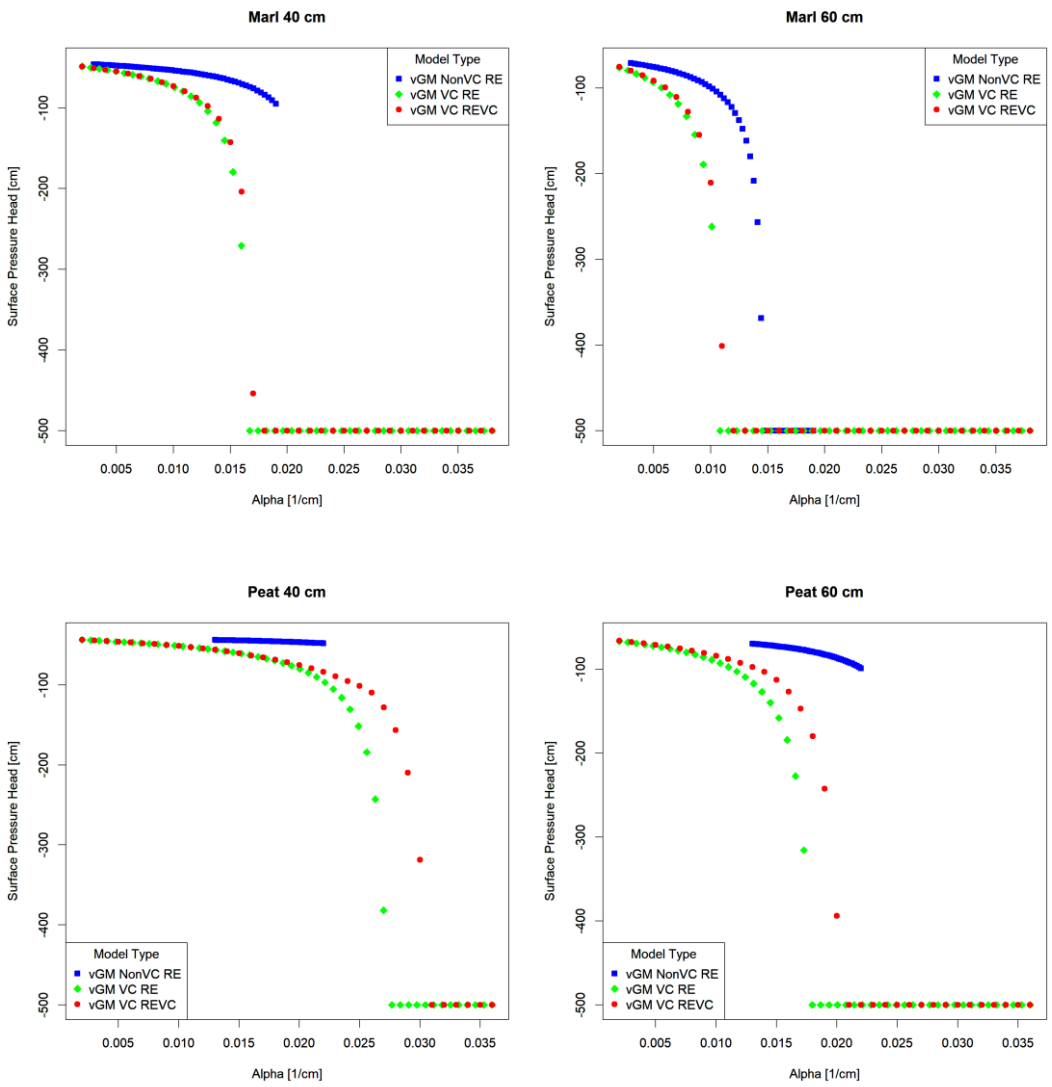

Figure 3-8. Sensitivity results of vGM parameter α for peat and marl for vadose zone thickness of 40 cm and 60 cm.

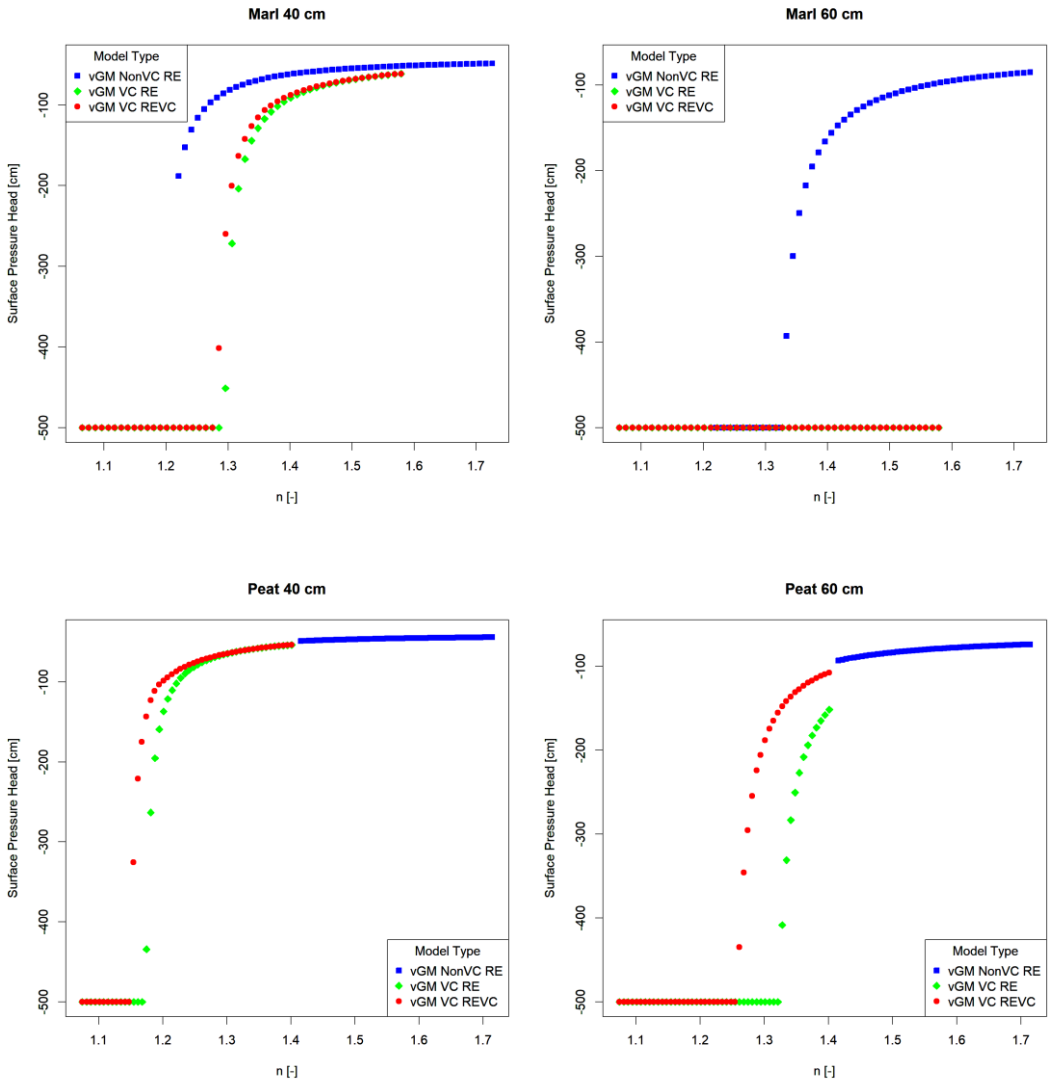

Figure 3-9. Sensitivity results of vGM parameter *n* for peat and marl soils for vadose zone thickness of 40 cm and 60 cm.

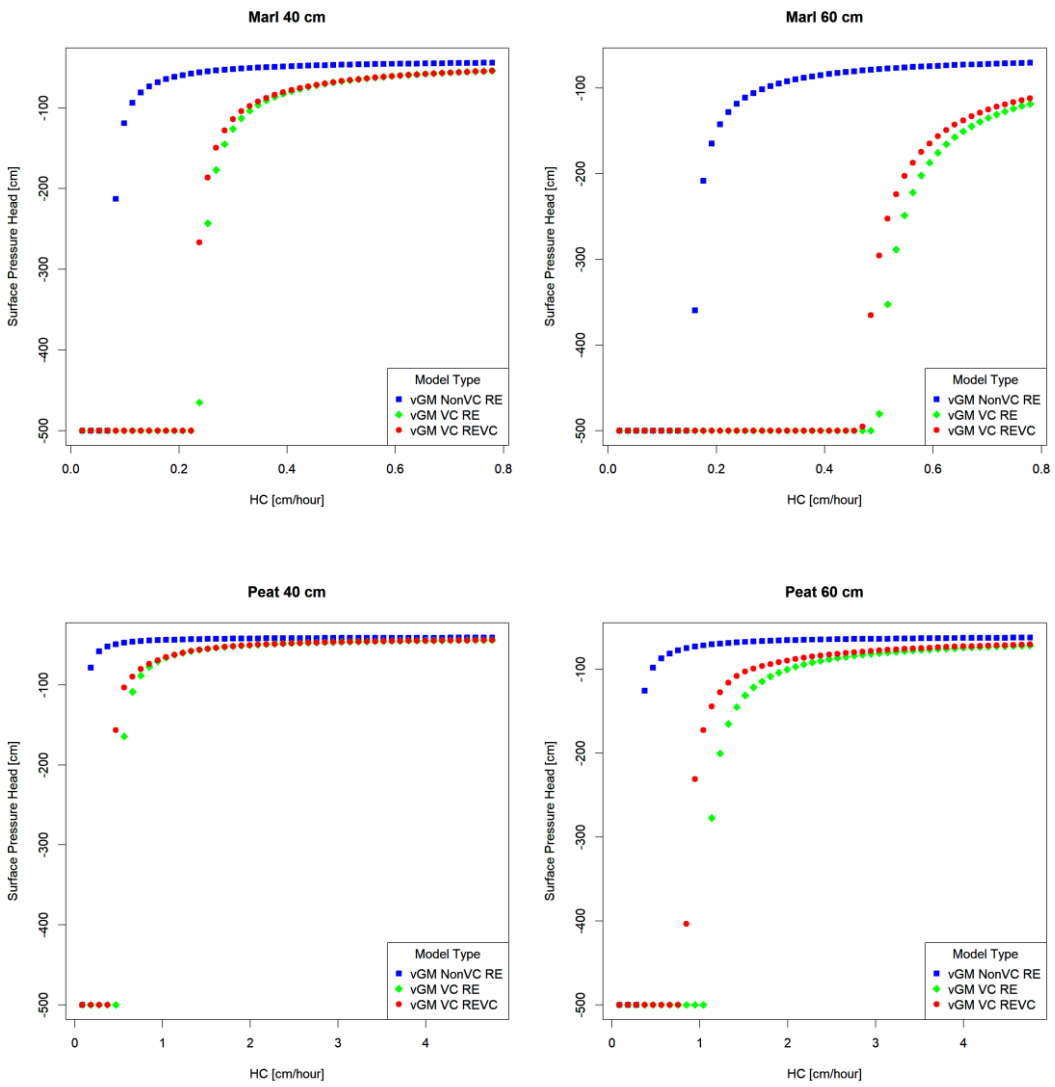

Figure 3-10. Sensitivity results of hydraulic conductivity for peat and marl soils for vadose zone thickness of 40 cm and 60 cm.

3.4 Model Testing with Lysimetry

Typically, vadose zone soil moisture models are validated in the field by measuring the time-varying soil moisture content using tensiometers and TDR probes. In cases where it is not possible to perform field validation, lysimetry may be employed. Lysimeters are

soil-filled containers which can be used for drainage and recharge experiments (Chaberneau, 2006). In this effort, lysimeter tests were used to record the variation in soil moisture in Everglades peat and marl soil profiles to changing water levels.

3.4.1. Calibration of the Time Domain Reflectometry (TDR) sensor

The TDR sensor - Stevens Hydra Probe was used in this study to determine the moisture content of the soil. TDR probes like the Stevens Hydra Probe work on the principle that the dielectric permittivity (ε) of the soil is proportional to its moisture content. The Stevens Hydra Probe consists of four metal tines (45 mm long by 3mm wide) on a base plate of 25mm diameter. The center rod transmits an EM wave created by a 50 MHz signal and measures the return raw signal response in the form of five voltages (first three represent the standing wave, fourth for temperature corrections of the electronics, and fifth for temperature corrections of the soil). Both components of the complex dielectric permittivity – real and imaginary can be measured by the Hydra Probe. For this reason, the Stevens Hydra Probe is a popular choice for vadose zone investigations. The real component called the real dielectric constant is related to the soil moisture while the imaginary component is related to the electrical conductivity and frequency. The Hydra Probe provides calibrated moisture contents for sand, silt, clay and loam. For Everglades peat and marl, no calibration curves exist. This study performed a laboratory-based soil-specific calibration for Everglades peat and marl using the Stevens Hydra Probe.

The laboratory test was performed by collecting a soil core (height 70 mm and diameter 78.67 mm) from the lysimeter of unknown moisture content. The sample was placed on a ceramic disk and saturated for 24 hours (Figure 3-11a). The mass of the sample

was recorded, and the dielectric permittivity was measured by inserting the Stevens Hydra Probe into the sample (Figure 3-11b) . Then the sample was placed in an oven and dried for six one-hour intervals. At each interval, the mass (M_{wet}), and dielectric permittivity were recorded. Finally, the dry mass of the soil (M_{dry}) was obtained after oven-drying the sample for 24 hours. The volume of the dry soil was recorded. VWC s at each of the drying intervals (Table 3-4 and Table 3-5) were calculated as:

$$\theta = \frac{M_{wet} - M_{dry}}{V_{soil}} \quad [3.22]$$

The real dielectric permittivity (ε_r) was plotted as a function of the calculated VWCs to create the calibration curves (Figure 3-12 and Figure 3-13). Prior work has shown that the calibration curves may have the mathematical appearance of a polynomial expression; hence, polynomial equation fit of the data points resulted in the following expressions for marl (Equation 3.23) and peat (Equation 3.24):

$$VWC = 0.00045\varepsilon_r^3 - 0.0528\varepsilon_r^2 + 2.157\varepsilon_r + 38.13 \quad [3.25]$$

$$VWC = 0.00044\varepsilon_r^3 - 0.0604\varepsilon_r^2 + 3.087\varepsilon_r + 18.33 \quad [3.26]$$

The coefficients generated from the polynomial fitting were to calibrate the TDR probe measurements for marl and peat.

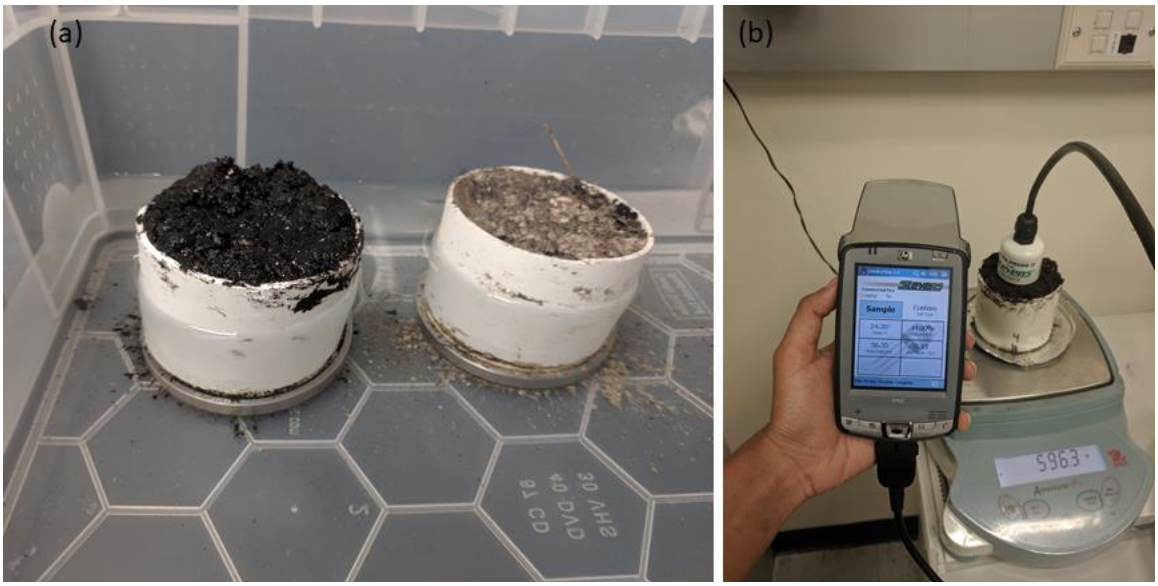

Figure 3-11. Photograph of the measurement of the real dielectric to develop the calibration curve for peat using the Stevens Hydra Probe.

Table 3-3. Tabular data from the cores obtained from the lysimeters for the TDR calibration of marl and peat calibration.

Soil Tested	Ring Weight [g]	Plate Weight [g]	Sample Height [mm]	Sample Diameter [mm]	Oven Dried Soil+Cont. Weight [g]	Container Weight [g]
Marl	51.9	3.6	70	78.67	202.7	19.9
Peat	52.1	3.6	70	78.67	153.9	19.9

Table 3-4. Time Domain Reflectometry (TDR) probe calibration readings for marl soil.

TDR Marl Calibration					
	Sample Lab Readings			Sensor Readings	
Reading	Ring + Wet Soil Wt. [g]	Water Wt. [g]	VWC [%]	Temperature [^{o}C]	Real Dielectric [-]
1	449.1	266.3	78.3	21.9	58.87
2	440.3	257.5	75.7	24.8	53.37
3	432.0	249.2	73.3	26.6	51.50
4	424.9	242.1	71.2	25.3	41.83
5	416.7	233.9	68.8	28.3	30.88
6	413.7	230.9	67.9	27.4	27.89
7	409.3	226.5	66.6	30.9	24.74
8	397.8	215.0	63.2	20.4	17.79
9	389.8	207.0	60.9	24.0	15.98
10	182.8	0.0	0.0	-	-

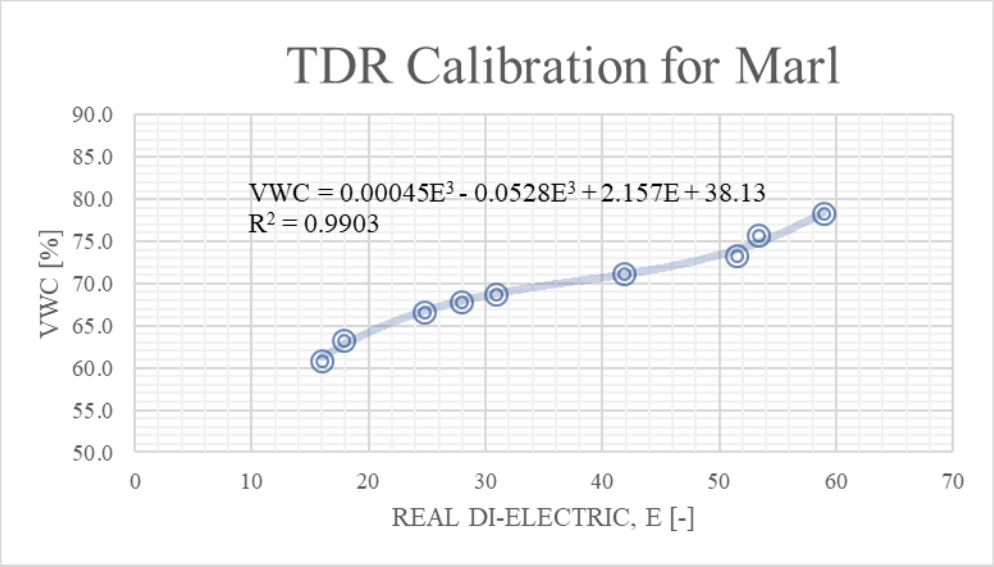

Figure 3-12. Development of the Time Domain Reflectometry (TDR) probe calibration equation for marl.

Table 3-5. Time Domain Reflectometry (TDR) probe calibration readings for peat soil.

TDR Peat Calibration					
	Sample Lab Readings			Sensor Readings	
Reading	Ring + Wet Soil Wt. [g]	Water Wt. [g]	VWC [%]	Temperature [^{o}C]	Real Dielectric E [-]
1	422.2	288.2	84.7	22.0	65.30
2	415.4	281.4	82.7	23.7	64.26
3	405.8	271.8	79.9	24.2	56.35
4	396.2	262.2	77.1	23.9	53.35
6	386.9	252.9	74.4	26.3	45.53
7	383.7	249.7	73.4	26.5	40.22
8	378.3	244.3	71.8	26.5	35.99
9	364.0	230.0	67.6	20.3	28.08
10	356.2	222.2	65.3	22.0	26.39
11	134.0	0.0	0.0	-	-

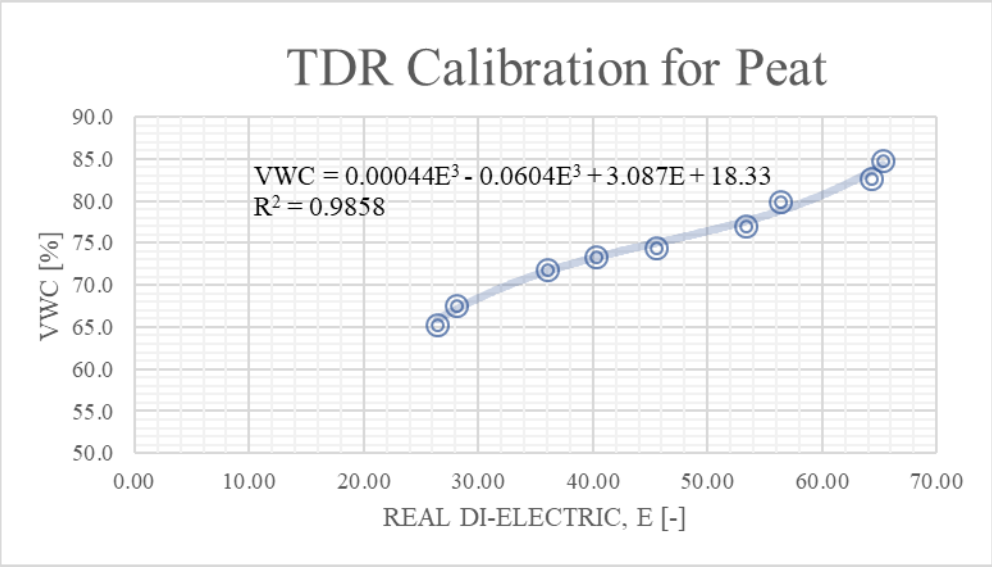

Figure 3-13. Development of the Time Domain Reflectometry (TDR) probe calibration equation for peat.

3.4.2. Sample Collection and Experimental Setup

Figure 3-14. Map of sampling location for collection of lysimeter cores (created using ArcGIS 10.1).

Soil samples were collected from a site south of 8th street. The site was accessed through a service road and then by foot. The site consisted of inundated marl prairies, sparse sawgrass peat marshes, and eleocharis marshes. The soil profile was examined by driving clear acrylic pipes into the ground and retracting intact soil cores of diameter 77 mm and height 200 mm. Examination of soil profile up to 200 mm from the surface showed three types of soil profiles: 1) marl, 2) peat, and 3) layered peat and marl. The layered

profile consisted of a peat topsoil, a middle layer of light-colored marl and a bottom layer of dark peat. The three layers varied from 50 mm to 75 mm thickness.

Large lysimeter cores were collected using a plastic sampler of diameter 300 mm and height 500 mm. The sampler was hammered into the ground until the soil surface was close to the top of the sampler. The soil around the sampler was removed. The sampler was tilted and lifted off the ground with the core intact. The cores were transferred to a container with a No. 40 mesh bottom and transported to the laboratory. The lysimeter cores were placed in a large water tankand were kept inundated in the laboratory until the start of the experiment to ensure complete saturation in the soil profile. The temperature conditions in the lab were regulated to a constant temperature range of 19 to 21^{o}C during the experiment.

Figure 3-15. Photographic record of (a) laboratory set-up of all three lysimeters and (b) reading the surficial di-electric of the lysimeters using a Stevens Hydra Probe.

The VWC was measured using two separate TDR probes – a Stevens Hydra Probe for surficial soil moisture and a Delta-T PR2 Time Domain Reflectometry (TDR) probe at

the bottom of the lysimeter core. TDR probes allow for non-destructive measurement of the soil profile. The Delta-T PR2 probe was inserted into a thin-walled access tube which was installed in each core. The access tube allows for greater penetration of the electromagnetic signal measured by the sensor on the TDR probe. The Stevens HydraProbe measures the real dielectric of the soil while the Delta-T PR2 measures an analog DC voltage. Measurements of the Stevens Hydra Probe were converted to VWC using the calibration curve generated in section 3.4.1; however, the measurements from the Delta-T PR2 probe cannot be converted to VWC using the same calibration curve due to differences in the radio frequency (Hydra Probe – 50 MHz and PR2 – 100 MHz) (Delta-T Devices, 2004; Stevens, 2007). The raw voltage measurements from the Delta-TPR2 are presented in Table A 8 (Appendix A).

3.4.3. Dry-down Experiment

To simulate dry-down of the soil profile, the water level was dropped after the saturated period to a level of 6 cm from the bottom of the core. The water level was maintained at 6 cm from the base to prevent evaporation through the bottom mesh of the core. The initial height of the soil profile was marked on the side of the lysimeter. Using the Stevens Hydra Probe, the real dielectric at the surface was recorded for all three lysimeters, and the PR2 Profile Probe was inserted into an acrylic sleeve to record an output DC voltage at the bottom of the lysimeter. The readings were taken at ten-minute intervals for the first two hours. This was followed by daily readings for the next four days and weekly readings for the next three weeks. The last reading was taken 50 days from the start of the experiment. The real dielectric from the surface was converted to soil moisture using

the soil specific probe calibration equation developed in section 1.3.3.2. The experiment was stopped at the end of a 50-day dry-down. The change in elevation of the soil cores were recorded at the end of the experiment. Table 3-7 presents the calibrated surficial soil moisture recorded with the Stevens Hydra Probe for the three lysimeters during the dry-down experiment.

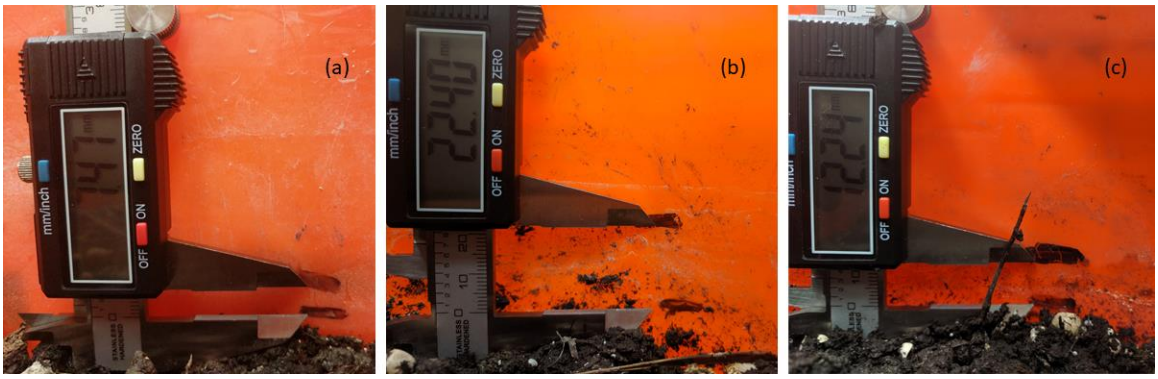

Figure 3-16. Measurement of soil loss in (a) Lysimeter 1 – Layered Marl-Peat, (b) Lysimeter 2 – Peat, and (c) Lysimeter 3 – Layered Peat-Marl.

Table 3-6. Measurement of soil depth and soil loss in the lysimeters.

Lysimeter	Measurement	Depth to Top of Lysimeter [mm]	Subsidence [mm]	Mean Subsidence [mm]
	1	122	6.51	
Lysimeter 1	2	102	7.47	
Layered Marl-Peat	3	119	8.83	7.60
	1	64	22.40	
Lysimeter 2	2	70	23.09	
Peat	3	58	15.61	20.37
	1	80	12.24	
Lysimeter 3	2	65	13.94	
Layered Peat-Marl	3	88	8.47	11.55

3.4.4. Lysimeter Soil Profile

At the end of the experiment, soil cores were collected by inserting an acrylic tube into each lysimeter. The stratigraphy of the lysimeters were obtained from each core. Figure 3-17 presents the photographic record of the soil cores obtained from the lysimeter. Some compression was observed during the insertion of the cores in the sample. Furthermore, some of the soil at the bottom of the core did not stay intact during retrieval. Core 1 from Lysimeter 1 consisted of a top layer of marl soil up to 13 cm deep and a bottom layer of peat soil 10 cm thick. Core 2 from Lysimeter 2 consisted of entirely peat soil 23 cm thick (maximum compression during core retrieval was observed for this sample) whereas lysimeter 3 had a top layer of peat up 16 cm over a 10 cm thick marl layer. The cores were sectioned into 2 cm high cylindrical slices and the bulk density of each slice was obtained through the oven drying experiment described in 2.2.4. The top slice of lysimeters 1 and 2 (surface) were only 1 cm. Figure 3-18 presents the bulk densities of layers examined.

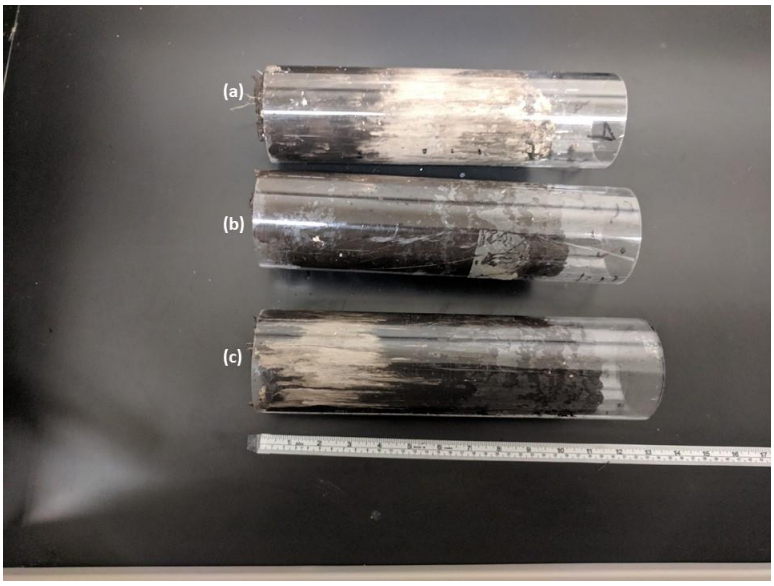

Figure 3-17. Photograph of soil cores obtained from the three lysimeters for stratigraphy - (a) Lysimeter 1, (b) Lysimeter 2, and (c) Lysimeter 3

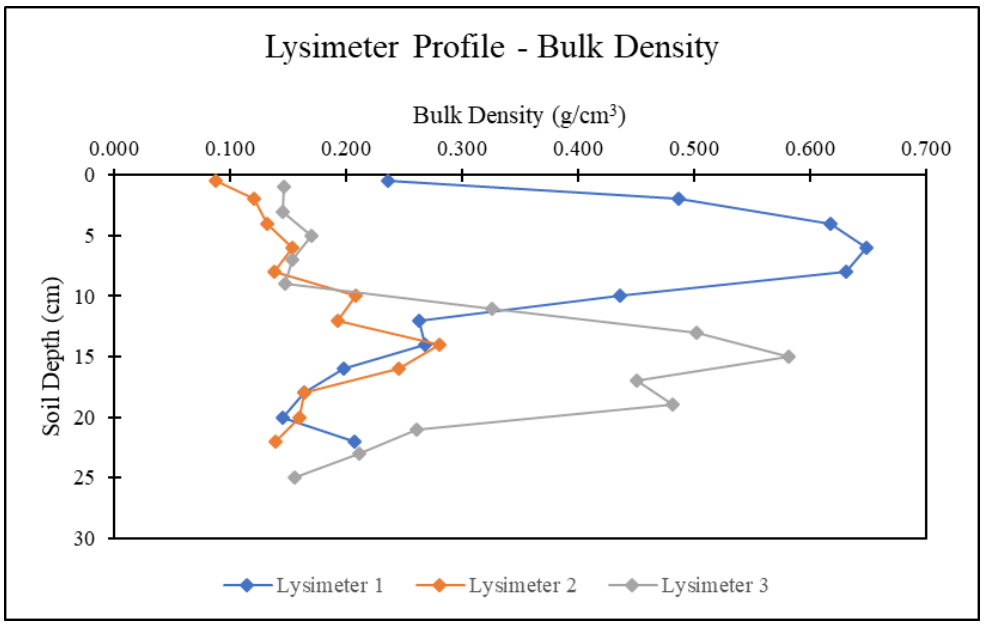

Figure 3-18. Bulk density measured across the soil profile for the three lysimeters after the lysimeter experiment. The surface is at the soil depth of 0 cm.

Table 3-7. Surficial soil moisture observations recorded for all three lysimeters using the Hydra Probe during the 50-day dry-down experiment.

		HydraProbe Surficial Measurments of the Top 5 cm								
		Lysimeter 1			Lysimeter 2			Lysimeter 3		
	Time	Temperature	E	Corrected VWC	Temperature	E	Corrected VWC	Temperature	E	Corrected VWC
Date	[PM]	[^{o}C]	[-]	[%]	[^{o}C]	[-]	[%]	[^{o}C]	[-]	[%]
29-Jan	2:00	21.8	58.46	78.1	19.9	71.91	90.8	19.8	71.48	90.3
29-Jan	2:10	20.5	52.74	74.6	19.9	69.45	88.0	19.8	67.92	86.5
29-Jan	2:20	19.5	47.68	72.6	19.4	69.64	88.2	19.2	60.09	80.7
29-Jan	2:30	19.4	46.93	72.3	19.3	66.41	85.2	19.1	67.04	85.7
29-Jan	2:40	19.5	48.03	72.7	19.3	65.88	84.7	19.1	69.41	88.0
29-Jan	2:50	19.3	39.68	70.6	19.2	62.49	82.2	19.2	54.63	78.1
29-Jan	3:00	19.2	46.54	72.2	19.3	60.97	81.2	19.3	57.98	79.6
29-Jan	3:10	19.3	45.20	71.9	19.1	64.03	83.3	19.1	54.13	77.9
29-Jan	3:20	19.2	39.77	70.7	19.1	58.10	79.7	19.2	51.43	76.9
29-Jan	3:30	19.4	33.53	69.4	19.4	55.14	78.3	19.3	48.11	75.8
29-Jan	3:40	19.5	31.23	68.9	19.5	55.26	78.4	19.5	52.14	77.1
29-Jan	3:50	19.5	33.51	69.4	19.5	48.57	75.9	19.5	43.10	74.2
29-Jan	4:00	19.5	35.45	69.8	19.5	52.94	77.4	19.5	43.10	74.2
30-Jan	2:00	20.4	39.91	70.7	19.9	49.30	76.2	19.7	39.70	73.1
31-Jan	2:00	20.9	33.20	69.3	21.0	47.64	75.7	20.9	41.75	73.8
1-Feb	2:00	19.2	32.26	69.1	19.1	42.20	73.9	19.4	53.50	77.6
2-Feb	2:00	20.4	29.48	68.4	20.6	40.41	73.3	20.9	52.58	77.3
9-Feb	2:00	21.9	26.76	67.5	21.8	39.39	73.0	21.7	46.23	75.2
16-Feb	2:00	20.2	29.65	68.5	20.1	39.42	73.0	20.1	43.27	74.3
23-Feb	2:00	20.6	34.68	69.7	20.6	35.18	71.2	20.5	51.53	76.9
20-Mar	2:00	20.8	38.59	70.4	20.6	56.45	78.9	20.5	60.51	81.0

Table 3-8. Laboratory data used to calculate the saturated volumetric water content (θ_s) for the top 2.5 cm of the three lysimeters.

	Container Weight	Container + Wet Soil	Container +Dry Soil	Volume	VWC	Average	StdDev
Sample	[g]	[g]	[g]	[cm^3]	[%]	[%]	[%]
Lys 1-1	8.901	62.643	28.010	45.216	76.6		
Lys 1-2	8.885	63.875	31.686	45.216	71.2		
Lys 1-3	8.911	70.434	33.720	45.216	81.2	76.3	5.01
Lys 2-1	8.886	59.233	15.968	45.216	95.7		
Lys 2-2	8.896	59.898	18.115	45.216	92.4		
Lys 2-3	8.906	55.065	15.677	45.216	87.1	91.7	4.33
Lys 3-1	8.919	60.154	17.905	45.216	93.4		
Lys 3-2	8.933	58.668	16.400	45.216	93.5		
Lys 3-3	8.886	52.613	15.357	45.216	82.4	89.8	6.39

3.4.5. Lysimetry Simulation Setup

The R-script REVC was combined with an iterative procedure to select the parameters with the best fit to the observational data. The geometry of the soil profile was setup by specifying the depth of the unsaturated profile, the number and thickness of soil layers, and the number of nodes and cells. Since the water level was maintained at 6 cm for each lysimeter, the unsaturated soil depth was calculated by subtracting 6 from the total lysimeter height. In addition, the profiles for each lysimeter were discretized with constant initial cell heights of 0.1 cm; this results in soil profiles with depths of 19.1 cm, 24.1 cm, and 22.6 cm and total nodes of 192, 242, and 226 for lysimeters 1, 2, and 3, respectively. Using the bulk density tests performed in section 3.4.4, the materials of each profile were specified. Lysimeter 1 has a top 13 cm layer of marl (nodes 1 to 131) and bottom 6 cm layer of peat (nodes 132 to 191); lysimeter 2 has a single 24.1 cm thick layer of peat (nodes 1 to 242); and Lysimeter 3 has a top 16 cm layer of peat (nodes 1 to 162) and bottom 6.5 cm of marl (nodes 163 to 227). The parameter assignments are made based on the material type of the nodes.

Due to the differences in the frequency of observations, numerical simulations were conducted as two different models with their own time-steps and time-periods; this method allowed for comparison with observed and simulated values while keeping the model run times low. The first model simulates the first two hours of the experiment with 10-minute time-steps while the second model simulated the 50-day time period with one-day time-steps. For the first model, a pressure head of zero cm of water is prescribed for each node to represent a saturated soil column and both boundary conditions are specified as constant pressure head boundary conditions. At the first timestep, the bottom boundary condition is changed to zero cm and the top boundary condition is set to the negative of the depth of the unsaturated zone (for example, -24.1cm for Lysimeter 2). The boundary conditions are held constant for rest of the two hours simulation. This method assumes that the change in surface pressure head due to evaporation is negligible for the two-hour period. The second model was initialized using the pressure head at each node at the end of the two-hour time-period from the first model. The bottom boundary condition was specified as a constant boundary condition of pressure head zero cm to indicate the presence of the water level, while a system-dependent evaporative boundary condition with flux 0.2 cm/day was specified on the top node.

The range of parameter values obtained from Table 3-2 was used to create sequences of parameters and the two models were run serially to select parameters that best simulated the surficial VWC observed and elevation change. The surficial VWC is considered as the mean VWC of the top 5 cm of the soil profile since the Stevens Hydra Probe data, used as observations, is reported for the top 5 cm of the lysimeters. For the simulation model, this is calculated using the mean pressure head of the top 5 cm (Nodes

1 to 51) and converting this into VWC using the vGM model parameters. The VWCs from the numerical simulation are then compared to the observed VWC using root mean squared error (RMSE) and the normalized root mean squared error ($RMSE_N$), given by,

$$RMSE = \sqrt{\frac{\sum_{i=1}^{X}(S_i - O_i)^2}{x}} \quad [3.27]$$

$$RMSE_N = 100 \times \frac{RMSE}{(maxO_i - minO_i)} \quad [3.28]$$

Where S_i are the simulated values, O_i are the observed values, and x is the total number of samples. An $RMSE_N$ value less than 20% is considered a very good fit. The simulated model predicts the pressure head at each node. The pressure head was converted into VWC using the soil water characteristic curve. The average water content of the top 5 cm was used as S_i while O_i is the observations recorded by the Hydra Probe.

Model selection of Lysimeter 2 was conducted first as it was a purely peat profile followed by Lysimeter 1 and Lysimeter 3. The saturated VWC of top layer of each lysimeter was assigned based on the experiment in 3.4.4 (Table 3-8). The residual VWC, θ_r, was assigned zero to allow for the maximum range of VWCs. The vGM parameters, α and n and the K_{sat} were varied using the sequences generated from the parameter range. Iterations were performed in multiple rounds until a hydraulic model with low $RMSE_N$ was obtained. Following this, the HCR values were varied to fit the observed soil elevation change. The selected model parameters from Lysimeter 2 were applied for the bottom peat

layer of Lysimeter 1 and the iterative procedure was used to calibrate parameters for the top marl. For Lysimeter 3, the calibrated marl parameters from Lysimeter 1 were applied to the bottom marl layer; however due to poor model performance; both layers were calibrated unlike in Lysimeter 2.

3.4.6. Lysimetry Results and Discussion

The results from iterative calibration process are presented in Table 3-9. For Lysimeter 2, the first round involved calibrating the model over a wide range of parameter values. Based on the performance of the model, the ranges of values were narrowed as seen in the consequent model runs. Figure 3-19 presents the normalized $RMSE_N$ over the range of α tested for select combination of n and K_{sat} for Lysimeter 2. The highest $RMSE_N$s were observed with models of low n and low K_{sat}. For low K_{sat} models, with an increase in n, $RMSE_N$ dropped considerably; however, for higher K_{sat} models, significant differences in $RMSE_N$ with n were only observed in the middle range of α values. α was found to have the most influence on the $RMSE_N$ with lower $RMSE_N$ values at higher α. Increasing the K_{sat} was also found to have a considerable effect on the $RMSE_N$; lower $RMSE_N$ is observed with increasing the K_{sat} from 2.1 cm/d to 114.2 cm/d; however, there appears to be a threshold value beyond which the $RMSE_N$ increases. Figure 3-20 presents the observed and modeled VWCs for different combinations of K_{sat} and n with a constant high α of 0.036 cm^{-1}. For models with low n, the VWC at the end of the first two-hour observation period is higher than the observed VWC (Figure 3-20). Models with high n had a better fit to the observed data. K_{sat} influences the surficial VWC of the lysimeters at the end of the 50-day period, with higher VWC at higher K_{sat}; this indicates that there is

an increased delivery of soil moisture to the surface with higher K_{sat}. The second model script run (Table 3-9) was performed using a targeted range of high α, high n and the lower middle range of K_{sat}. The third run was conducted keeping the α at 0.036 cm^{-1} but varying K_{sat} from 35 cm/d to 39 cm/d, n from 1.401 to 1.500, and HCR from 0.55 to 0.59 (Table 3-9). The HCR values at higher pressure heads were not varied as the absolute value of pressure head at the surface did not increase beyond 6 kPa for the targeted runs. The HCR values were selected using percent difference between the measured soil loss and the calculated soil loss. The selected hydraulic model for Lysimeter 2 (K_{sat}=36.0 cm/d, α= 0.036 cm^{-1}, n=1.475) has an RMSE of 2.6% VWC, an $RMSE_N$ of 13.1% and a soil elevation percent error of 0.14% (Table 3-10).

Lysimeter 1 consisted of layered marl over peat. The soil hydraulic parameters from Lysimeter 2 were applied to the bottom layer and three rounds iterations were performed for only the top layer to determine the best fitting parameters for the marl top layer. Figure 3-21 demonstrates that model performance was found to improve with increase in α; however, when both n and K_{sat} are low, the $RMSE_N$ is consistently high and increases with α. Figure 3-22 presents select combinations of n and K_{sat} for an α of 0.026 cm^{-1}. When n and K_{sat} are low, the simulated surficial VWC is higher than the observed in the first two hours; however, over time, the simulated surficial VWC drops below the observed VWC. If the n value is increased to 1.293, the simulated surficial VWC is lowered. When the K_{sat} is increased to 6.6 cm/d and the n value is low at 1.179, the simulated surficial VWC is consistently higher than the observed VWC. If the n value is increased to 1.293, the fit with the observed data is improved. The selected model (K_{sat}=15.3 cm/d, α= 0.026 cm^{-1},

n=1.293) has an RMSE of 0.8% VWC and an $RMSE_N$ of 7.9% (Table 3-10). Like Lysimeter 2, the absolute value of the pressure head is never higher than 6 kPa; hence, the elevation change model was parametrized with only the HCR at 6 kPa. An HCR at 6 kPa of 0.79 for marl combined with an HCR at 6 kPa of 0.58 for peat resulted in a subsidence percent error of 0.13%.

The iterative process for determining the unsaturated hydraulic parameters of the layered Lysimeter 3 was more intensive than the other two lysimeters. The initial run with the entire range of peat parameter values and the constant specified values for the marl layer obtained from Lysimeter 2 only produced a minimum $RMSE_N$ of 57.7% (Table 3-9). For the second run, the parameters of the bottom marl layer were varied iteratively while the top peat layer was assigned a constant parameter set with the lowest $RMSE_N$; this was performed with the intention of producing a better fitting set of parameters for the lower marl layer. When the parameters of the second layer are varied, the $RMSE_N$ of the model varies between 39.0% and 81.6% with the lowest $RMSE_N$ at K_{sat}=18.7 cm/d, α=0.002 cm^{-1}, and n=1.450. The model with the lowest $RMSE_N$ for the marl layer was selected and the first run was repeated to produce a minimum $RMSE_N$ of 29.4% indicating that the model fit is better.

An analysis of the $RMSE_N$ with α for select combinations of hydraulic parameters for the top peat layer shows the model performance is consistently better at higher values of (Figure 3-23). The surficial VWC for select combinations of K_{sat} and n with a constant α of 0.036 cm^{-1} is presented in Figure 3-24. Increasing n resulted in a better model fit to the observations.

Figure 3-25 presents the vGM curves generated with the parameters selected for the soil materials of each lysimeter. The vGM curve of the peat in Lysimeter 2 is very similar to that of top-layer peat in Lysimeter 3. The bottom layer marl from Lysimeter 3 has a significantly broader air-entry region (as a result of a much lower α) than the marl top layer of Lysimeter 1. Generally, a lower layer is expected to have a higher BD, and in turn, a lower α and wide air-entry (Schwarzel et al., 2002; Wallor et al., 2018b); however, the BD of the marl layer in Lysimeter 3 was not higher than the marl layer in Lysimeter 1. Figure 3-26 shows that the wider air-entry region between the two marl layers results in a significantly higher unsaturated hydraulic conductivity for the marl in Lysimeter 3.

Table 3-9. Ranges of parameters tested for selection of lysimeter parameters and their model performance.

					Parameter Range															
			θ_s	θ_r	α [cm^{-1}]			n [-]			K_{sat} [$cm\ d^{-1}$]			HCR 6 kPa [-]			RMSE [%]		$RMSE_N$ [%]	
Lysimeter	Script Run	Layer	[$cm^3\ cm^{-3}$]	[$cm^3\ cm^{-3}$]	Min	Max	Increments	Min	Max	Increments	Min	Max	Increments	Min	Max	Increments	Min	Max	Min	Max
	1	1	0.92	0.00	0.002	0.036	10	1.074	1.401	10	2.1	114.2	10	-	1.00	-	2.8	90.5	14.2	461.8
	2	1	0.92	0.00	0.034	0.036	3	-	1.401	-	27.0	64.0	10	0.50	0.60	10	3.3	4.9	16.9	24.9
Lysimeter 2 Peat	3	1	0.92	0.00	-	0.036	-	1.401	1.500	5	35.0	39.0	5	0.55	0.59	5	2.5	3.5	12.9	17.7
		1	0.76	0.00	0.002	0.038	10	1.065	1.579	10	0.5	18.7	10	-	1.00	-				
	1	2	0.92	0.00	-	0.036	-	-	1.475	-	-	36.0	-	-	0.58	-	0.8	62.0	7.5	583.9
Lysimeter 1		1	0.76	0.00	0.022	0.038	4	1.293	1.579	4	8.6	18.7	4	0.78	0.81	4				
Layered Marl-Peat	2	2	0.92	0.00	-	0.036	-	-	1.475	-	-	36.0	-	-	0.58	1	0.8	13.0	7.9	122.9
		1	0.90	0.00	0.002	0.036	10	1.074	1.401	10	2.1	114.2	5	-	0.58	-				
	1	2	0.76	0.00	-	0.027	-	-	1.293	-	-	15.3	-	-	0.79	-	9.9	72.1	57.7	419.0
		1	0.90	0.00	-	0.036	-	-	1.328	-	-	114.2	-	-	0.58	-				
	2	2	0.76	0.00	0.002	0.038	5	1.065	1.579	5	0.5	18.7	5	-	0.79	-	6.7	14.0	39.0	81.6
		1	0.90	0.00	-	0.036	-	1.256	1.401	10	58.2	114.2	10	0.50	0.70	5				
	3	2	0.76	0.00	-	0.002	-	-	1.450	-	-	18.7	-	-	1.00	-	5.1	9.8	29.4	56.7
Lysimeter 3		1	0.90	0.00	-	0.036	-	1.320	1.401	10	-	58.2	1	0.60	0.80	22				
Layered Peat-Marl	4	2	0.76	0.00	-	0.002	-	-	1.450	-	-	18.7	-	-	1.00	-	5.1	6.3	29.4	36.7

Table 3-10. Selected model parameters for the layers of all three lysimeters.

Lysimeter	Soil Type	Depth [cm]	θ_s [cm^3 cm^{-3}]	θ_r [cm^3 cm^{-3}]	α [cm^{-1}]	n [-]	K_{sat} [cm d^{-1}]	HCR 6kPa [-]	RMSE [%]	$RMSE_N$ [%]	Subsidence Percent Error [%]
Lysimeter 2											
Peat	Peat	0.0 - 24.1	0.92	0.00	0.036	1.475	36.0	0.58	2.6	13.1	0.14
Lysimeter 1	Marl	0.0 - 13.0	0.76	0.00	0.027	1.293	15.3	0.79			
Layered Marl-Peat	Peat	13.1 - 19.1	0.92	0.00	0.036	1.475	36.0	0.58	0.8	7.7	0.13
Lysimeter 3	Peat	0.0 - 16.0	0.90	0.00	0.036	1.392	58.2	0.69			
Layered Peat-Marl	Marl	16.1 - 22.6	0.76	0.00	0.002	1.45	18.7	1.00	5.1	29.9	0.08

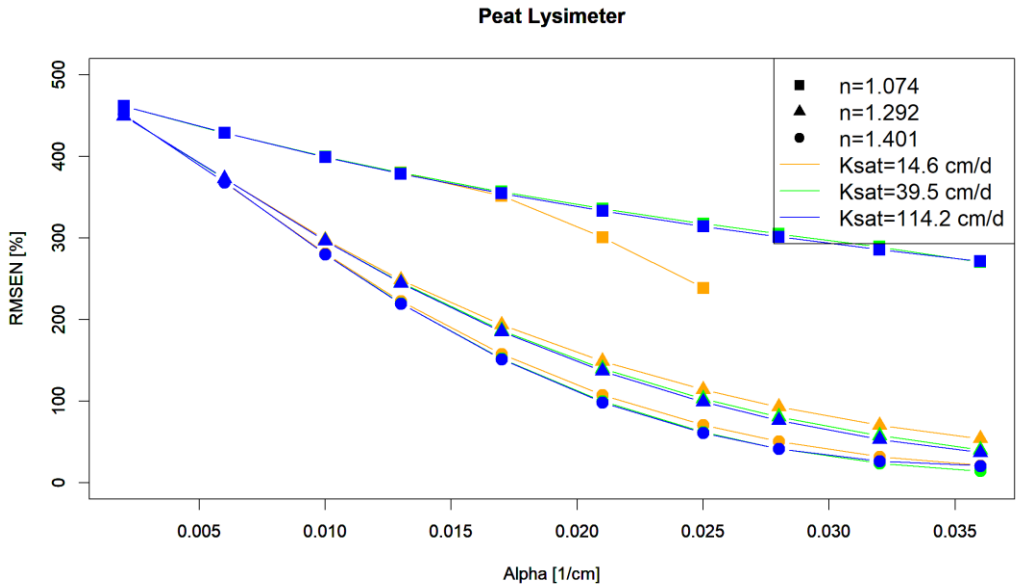

Figure 3-19. The normalized root mean squared errors ($RMSE_N$) for select combinations of K_{sat} and n over the range of α for Lysimeter 2.

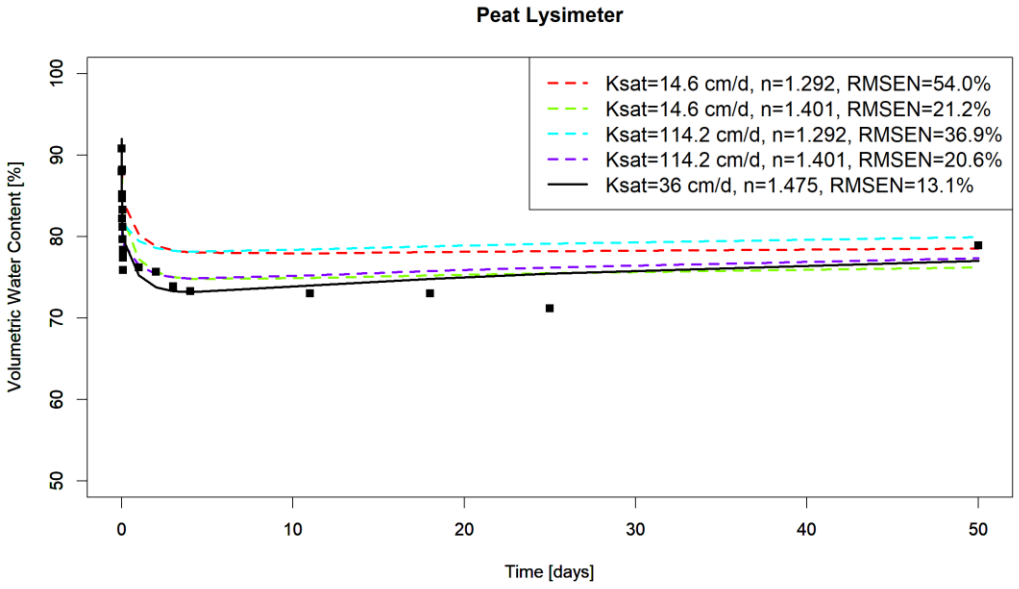

Figure 3-20. The observed (black squares) and modeled volumetric water contents for different combinations of K_{sat} and n with an α of 0.036 cm^{-1} for Lysimeter 2.

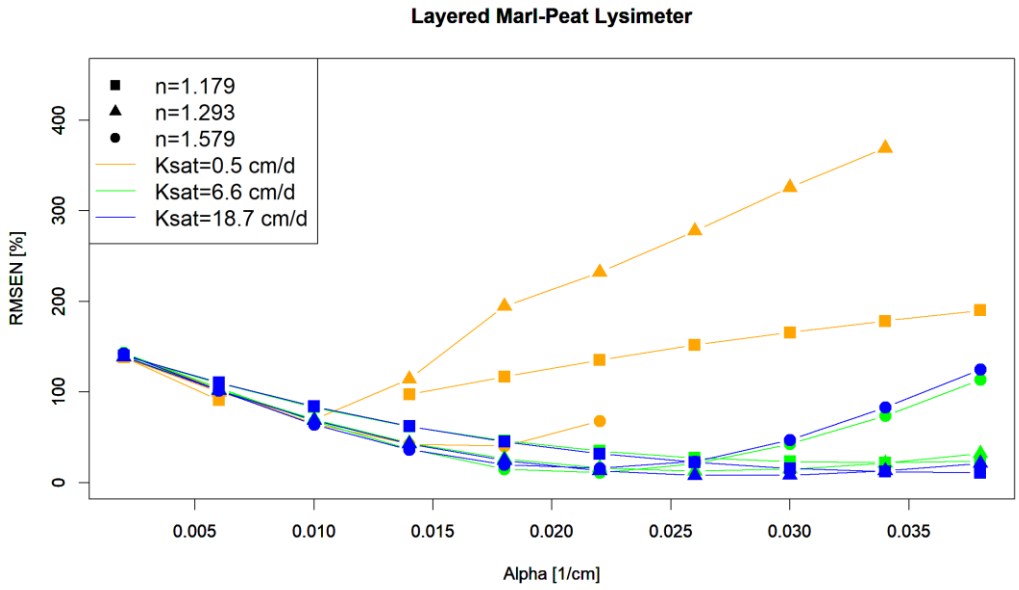

Figure 3-21. The normalized root mean squared errors ($RMSE_N$) for select combinations of K_{sat} and n over the range of α for Lysimeter 1.

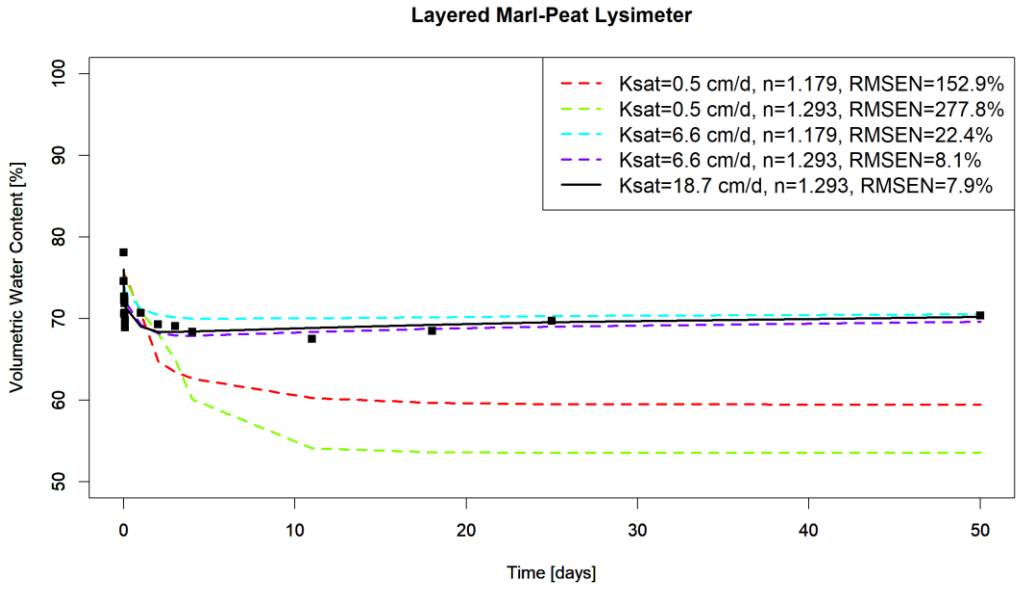

Figure 3-22. The observed (black squares) and modeled volumetric water contents different combinations of K_{sat} and n with an α of 0.026 cm^{-1} for Lysimeter 2.

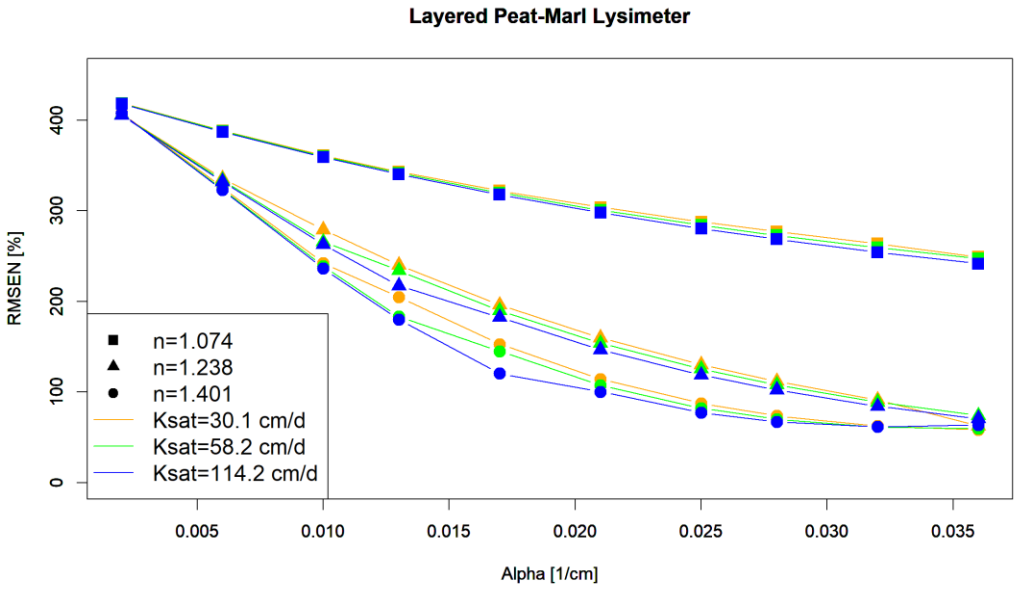

Figure 3-23. The normalized root mean squared errors ($RMSE_N$) for select combinations of K_{sat} and n over the range of α for Lysimeter 3 for the first run.

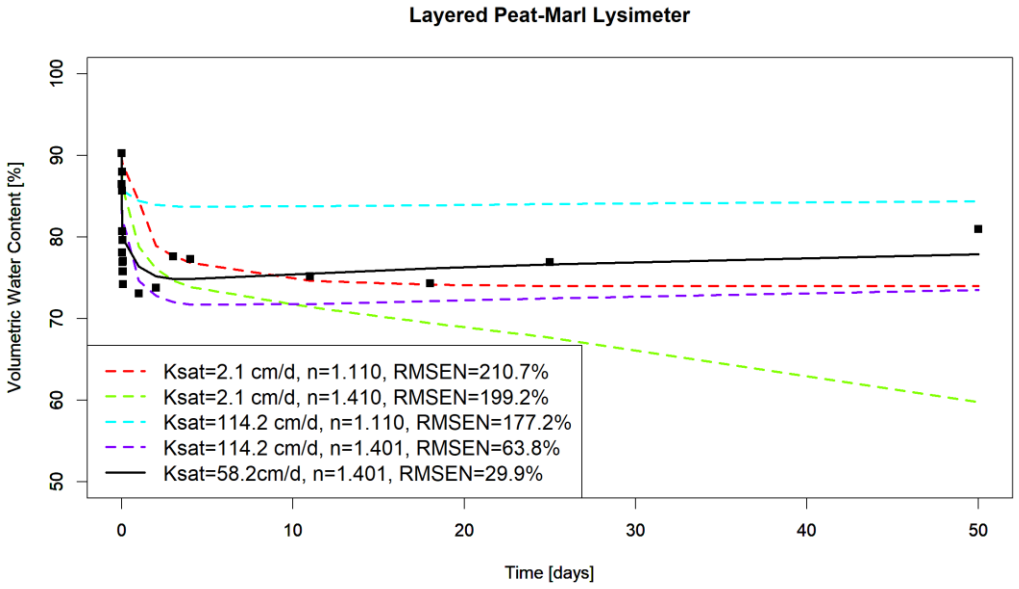

Figure 3-24. The observed (black squares) and modeled volumetric water contents different combinations of K_{sat} and n with an α of 0.036 cm^{-1} for the peat layer of Lysimeter 3.

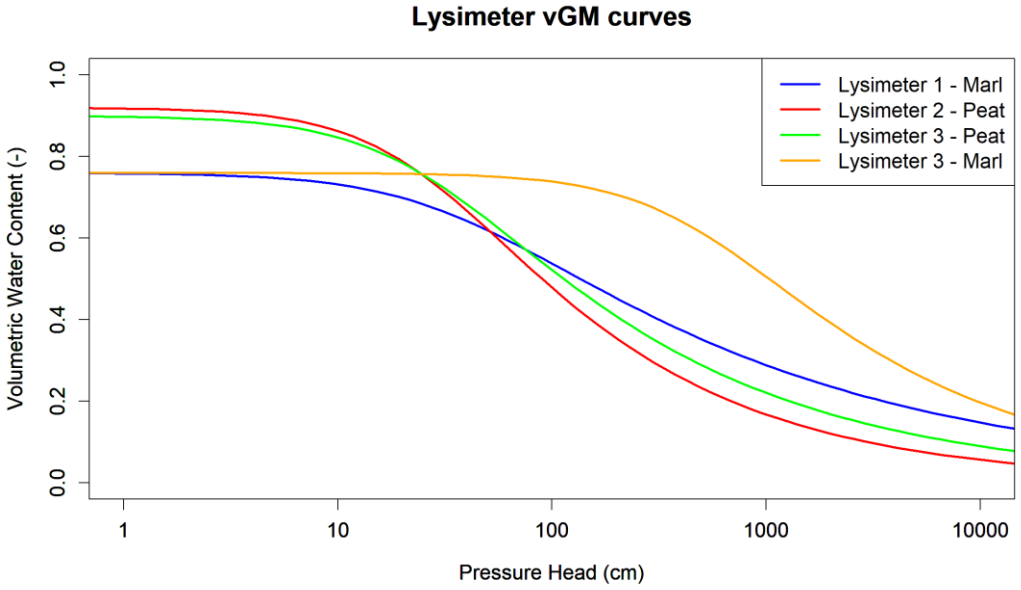

Figure 3-25. The vGM curves generated from parameters obtained using the iterative model fitting process for each lysimeter.

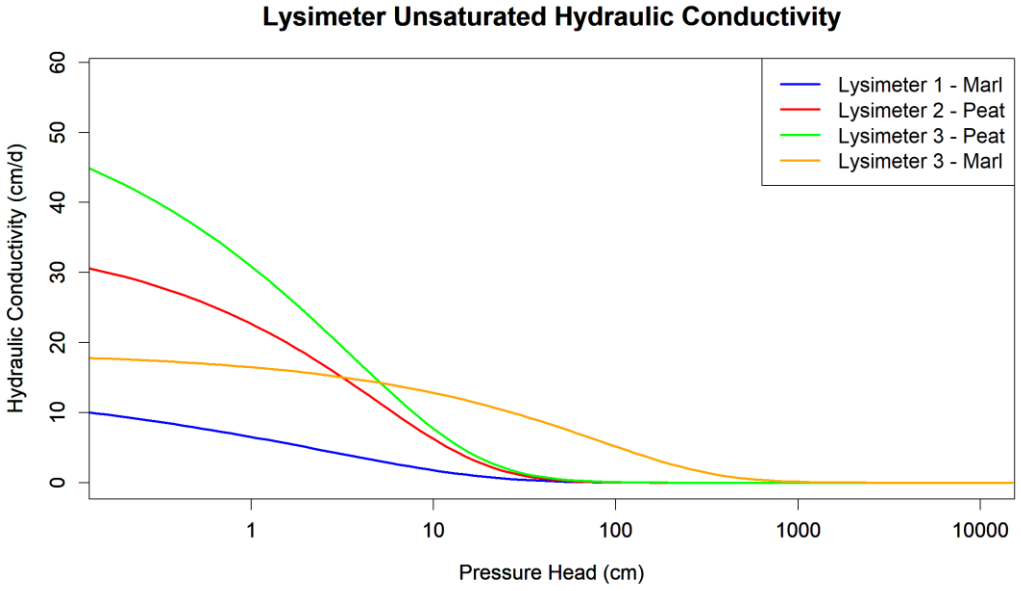

Figure 3-26. The unsaturated hydraulic conductivity curves generated from parameters obtained using the iterative model fitting process for each lysimeter.

3.4.7. Lysimetry Limitations and Future Recommendations

A major limitation of the lysimeter testing was the inability to verify if the surficial pressure head or the pressure head across the soil profile is, infact, the value predicted by the models. Comparisons were only performed with the surficial VWC. For future work, a depth based sampling of both the pressure head (using tensiometers) and VWC (using TDR probes) is recommended. Such a set up would also facilitate the simulatneous measurement of the SWRC (using the data pairs of pressure head and VWC). The only major disadvantage of determining the SWRC from the lysimeter is that data is limited to the range of the conditions experienced by the lysimeter, and cannot then be extrapolated to prediction models with different conditions (Schwärzel et al., 2006). In addition, soil samples may be retrieved from the lysimeters at the end of the experiment to determine the SWRC through oedometer testing; however, such processes generally involve destroying the structure of the sample to some extent. In the case of peat, extraction of cores for testing can result in compression of the soil sample which will increase its BD.

The TDR probe sampling method is also known to cause errors in reading VWCs. The probe rods can create long cracks on the soil surface (Stevens, 2007). In cases where the soil matrix is relatively wet, water from the soil matrix pool into these cracks resulting in overestimating the VWCs, whereas in drier conditions air-pockets around the prongs can result in underestimating the VWCs. There is no known solution to dealing with this type of issue. For highly compressive soils like peat, inserting the TDR probes must be done with care as compression can result in recording higher VWCs. It is also recommended that the probes once inserted should remain inserted until the end of the experiment.

The measurement of shrinkage or swelling of the lysimeter samples should be performed with the surface elevation tables (SETs) or it may be automated with displacement transducers, which can measure to an accuracy of ±0.125 mm (Camporese et al., 2006). An automated method would provide precise, real-time measurement of the change in lysimeter thickness.

Extracting of lysimeter cores from the field should be done with maximum care especially in the case of peat as compression during field work can alter the sample. It is recommended that large blocks be extracted from the ground and frozen. Lysimeter cores can be cut out of the frozen blocks prior to testing. Freezing will minimize compression experienced by sample during core extraction, and the source of error caused by freezing is negligable (Branham and Strack, 2014; Weber et al., 2017).

3.5 Conclusions

Many studies have confirmed the importance of including volume change behavior in unsaturated mineral soils like clay and organic soils like peat. In the deterministic modeling of the unsaturated zone, volume-change affects both the soil hydraulic parameterization model (like the vGM model) and the transport model (like the RE model). However, unsaturated models, particularly of organic soils tend to neglect the volume change behavior of the soil possibly due to the additional data required (volume change lab data, constitutive relationships) and the prevalence of established codes which do not incorporate volume-change in the soil. This study proposed a simple look-up table method which incorporates volume change in the RE by updating nodal heights in the numerical

discretization at every time step. The proposed model was scripted in R-Studio and the script was verified for a non-volume changing matrix with examples from HYDRUS.

The modeled case study of a shallow water table is different from typical unsaturated zone environments; hence, a sensitivity analysis performed for the equilibrium of matric head across the soil profile of shallow vadose zones (as observed in wetlands) found differences in the solution based on model type. Models that do not incorporate volume change both at the model parameterization level as well as at the transport model level predicted higher surficial equilibrium pressure heads; and hence a higher VWC. Models that incorporate volume-change at the parameterization level but not at the transport level produced similar solutions to the models that incorporate volume-change at both levels, except for narrow ranges of parameters α, n, and K_{sat}, in which significantly higher pressure head and VWC is predicted by the models that consider volume-change at parameterization and transport. Overall, a high α, low n, and low K_{sat} can contribute to the low surficial pressure heads, and the tendency for low surficial pressure heads increased with vadose zone depth.

Three lysimeter cores with varying soil profiles and a 50-day dry-down were used to test the REVC script. An iterative procedure was used to generate parameters and the resulting simulations were compared to the lysimeter observations using RMSEs and $RMSE_N$s. $RMSE_N$ varied significantly with α for all three lysimeter tests; $RMSE_N$s were found to be lower at higher values of α. For the pure peat lysimeter, models with low K_{sat} and low n tended to overestimates the VWC for the 50-day period. The best fitting model had an $RMSE_N$ of 13.1%, RMSE of 2.6% VWC, and an HCR at 6 kPa of 0.58 with an

elevation percent error of 0.14%. For the layered marl-peat lysimeter, model performance increased with α. Models with low K_{sat} and low n severly underpredict the surficial VWC, while the model with the highest K_{sat} with n of 1.293 and an α of 0.027, had the lowest RMSE of 7.7%, and when combined with an HCR of 0.79 for the marl layer resulted in an elevation percent error of 0.13%. For the layered peat-marl lysimeter, the optimal vGM model selected could only provide a fair fit ($RMSE_N$ of 29.9%) to the observed surficial VWC. In addition, an HCR at 6 kPa of 0.69 for the peat layer resulted in an elevation percent error of 0.8% for Lysimeter 3; it is not entirely clear why this HCR is significantly lower than the HCR for the peat lysimeter. The SWRC of the two lysimeters with peat were similar; however, the lower marl layer in Lysimeter 3 had a significantly lower air-entry values indicating that the effect of layering is strong. This work was limited to the parameterization dataset, which was generated only from soil samples from the top 10 cm. It was also limited by the data collected at each depth in the lysimeter, future work should study how the SWRC parameters vary with depth for soil profiles and include this in the lysimeter tests.

References

Adem, H.H., Vanapalli, S.K., 2015. Review of methods for predicting in situ volume change movement of expansive soil over time. J. Rock Mech. Geotech. Eng. 7, 73–86. https://doi.org/10.1016/j.jrmge.2014.11.002

Adem, H.H., Vanapalli, S.K., 2013. Constitutive modeling approach for estimating *1-D* heave with respect to time for expansive soils. Int. J. Geotech. Eng. 7, 199–204. https://doi.org/10.1179/1938636213Z.00000000024

Branham, J.E., Strack, M., 2014. Saturated hydraulic conductivity in Sphagnum-dominated peatlands: Do microforms matter? Hydrol. Process. 28, 4352–4362. https://doi.org/10.1002/hyp.10228

Briaud, J.-L., Zhang, X., Moon, S., 2003. Shrink Test–Water Content Method for Shrink and Swell Predictions. J. Geotech. Geoenvironmental Eng. 129, 590–600. https://doi.org/10.1061/(ASCE)1090-0241(2003)129:7(590)

Camporese, M., Ferraris, S., Putti, M., Salandin, P., Teatini, P., 2006. Hydrological modeling in swelling/shrinking peat soils. Water Resour. Res. 42, 1–15. https://doi.org/10.1029/2005WR004495

Caviedes-Voullième, D., Garcí a-Navarro, P., Murillo, J., 2013. Verification, conservation, stability and efficiency of a finite volume method for the 1D Richards equation. J. Hydrol. 480. https://doi.org/10.1016/j.jhydrol.2012.12.008

Chaberneau, R.J., 2006. Groundwater Hydraulics and Pollutant Transport. Waveland Press, Long Grove, IL.

Chen, F., Ren, L., 2008. Application of the finite difference heterogeneous multiscale method to the Richards' equation 44, 7413. https://doi.org/10.1029/2007WR006275

Cumming, B., Moroney, T., Turner, I., 2011. A mass-conservative control volume-finite element method for solving Richards' equation in heterogeneous porous media. BIT Numer. Math. 51, 845–864. https://doi.org/10.1007/s10543-011-0335-3

Delta-T Devices, 2004. User manual for the profile probe (type PR2). Delta-T Devices Ltd., Cambridge, UK.土.

Dixon, S.J., Kettridge, N., Moore, P.A., Devito, K.J., Tilak, A.S., Petrone, R.M., Mendoza, C.A., Waddington, J.M., 2017. Peat depth as a control on moss water availability under evaporative stress. Hydrol. Process. 31, 4107–4121. https://doi.org/10.1002/hyp.11307

Feddes, R.A., Kowalik, P.J., Zaradny, H., 1978. Simulation of field water use and crop yield. John Wiley & Sons, Wageningen, Netherlands.

He, X., Ren, L., 2009. An adaptive multiscale finite element method for unsaturated flow problems in heterogeneous porous media. J. Hydrol. 374, 56–70. https://doi.org/10.1016/j.jhydrol.2009.05.021

Karthikeyan, M., Tan, T.-S., Phoon, K.-K., 2001. Numerical oscillation in seepage analysis of unsaturated soils. Can. Geotech. J. https://doi.org/10.1139/t01-018

Kennedy, G.W., Price, J.S., 2005. A conceptual model of volume-change controls on the hydrology of cutover peats. J. Hydrol. 302, 13–27. https://doi.org/10.1016/j.jhydrol.2004.06.024

Kettridge, N., Tilak, A.S., Devito, K.J., Petrone, R.M., Mendoza, C.A., Waddington, J.M., 2016. Moss and peat hydraulic properties are optimized to maximize peatland water use efficiency. Ecohydrology 9, 1039–1051. https://doi.org/10.1002/eco.1708

Kroes, J., Dam, J. van, 2003. Reference manual SWAP version 3.0. 3.

List, F., Radu, F.A., 2016. A study on iterative methods for solving Richards' equation. Comput. Geosci. 20. https://doi.org/10.1007/s10596-016-9566-3

McCarter, C.P.R., Price, J.S., 2014a. Ecohydrology of *Sphagnum* moss hummocks: mechanisms of capitula water supply and simulated effects of evaporation. Ecohydrology 7, 33–44. https://doi.org/10.1002/eco.1313

McCarter, C.P.R., Price, J.S., 2014b. Ecohydrology of *Sphagnum* moss hummocks: mechanisms of capitula water supply and simulated effects of evaporation. Ecohydrology 7, 33–44. https://doi.org/10.1002/eco.1313

McCarter, C.P.R., Price, J.S., 2013. The hydrology of the Bois-des-Bel bog peatland restoration: 10 years post-restoration. Ecol. Eng. 55. https://doi.org/10.1016/j.ecoleng.2013.02.003

Oh, W.T., Vanapalli, S.K., Puppala, A.J., 2009. Semi-empirical model for the prediction of modulus of elasticity for unsaturated soils. Can. Geotech. J. 46, 903–914. https://doi.org/10.1139/T09-030

Paniconi, C., Aldama, A.A., Wood, E.F., 1991. Numerical Evaluation of Iterative and Noniterative Methods for the Solution of the Nonlinear Richards Equation, WATER RESOURCES RESEARCH.

Pyatt, D.G., John, A.L., 1989. Modelling volume changes in peat under conifer plantations. Soil Sci. 40, 695–706. https://doi.org/10.1111/j.1365-2389.1989.tb01310.x

Radcliffe, D.E., Simunek, J., 2010. Soil Physics with HYDRUS: Modeling and Applications [Hardcover]. CRC Press.

Schwarzel, K., Renger, M., Sauerbrey, R., Wessolek, G., 2002. Soil physical characteristics of peat soils. Plant Nutr. Soil 479–486.

Schwärzel, K., Šimůnek, J., Stoffregen, H., Wessolek, G., van Genuchten, M.T., 2006. Estimation of the Unsaturated Hydraulic Conductivity of Peat Soils. Vadose Zo. J. 5, 628. https://doi.org/10.2136/vzj2005.0061

Šimůnek, J., Šejna, M., Saito, H., Sakai, M., van Genuchten, M.T., 2013. The Hydrus-1D Software Package for Simulating the Movement of Water, Heat, and Multiple Solutes in Variably Saturated Media.

Stevens, 2007. The Hydra Probe Soil Sensor - Comprehensive Stevens Hydra Probe Users Manual.

Vu, H.Q., Fredlund, D.G., 2004. The prediction of one-, two-, and three-dimensional heave in expansive soils. Can. Geotech. J. 41, 713–737. https://doi.org/10.1139/t04-023

Wallor, E., Herrmann, A., Zeitz, J., 2018a. Hydraulic properties of drained and cultivated fen soils part II — Model-based evaluation of generated van Genuchten parameters using experimental field data. Geoderma 319, 208–218. https://doi.org/10.1016/J.GEODERMA.2017.12.012

Wallor, E., Rosskopf, N., Zeitz, J., 2018b. Hydraulic properties of drained and cultivated fen soils part I -Horizon- based evaluation of van Genuchten parameters considering the state of moorsh-forming process. https://doi.org/10.1016/j.geoderma.2017.10.026

Warrick, A.W., 2001. Soil physics companion, Soil Physics Companion. https://doi.org/10.2136/vzj2004.0727

Weber, T.K.D., Iden, S.C., Durner, W., 2017. A pore-size classification for peat bogs derived from unsaturated hydraulic properties. Hydrol. Earth Syst. Sci. 21, 6185–6200. https://doi.org/10.5194/hess-21-6185-2017

Wray, W.K., El-Garhy, B.M., Youssef, A.A., 2005. Three-Dimensional Model for Moisture and Volume Changes Prediction in Expansive Soils. J. Geotech. Geoenvironmental Eng. https://doi.org/10.1061/(asce)1090-0241(2005)131:3(311)

4. FIELD APPLICATION AT A STUDY SITE IN SHARK RIVER, EVERGLADES

4.1 Introduction

Several processes contribute to the changes in soil elevation observed in coastal peatlands and wetlands rendering ecosystems vulnerable to sea-level rise. As explained in section 1.1.4, they may be reversible processes like pore drainage and refilling or irreversible processes like compaction from matrix collapse, mass loss through bio-chemical oxidation, subsidence from plant root network collapse or surface elevation loss through the dissolution of carbonates (Szajdak and Szatylowicz, 2002; Camporese et al., 2006; Lane et al., 2016; Crump, 2017; Wang et al., 2017; Chambers et al., 2019). Hydrology and the unsaturation of the soil matrix directly and indirectly affects all the above-mentioned processes. Deterministic models which can simulate water distribution and transport in the soil matrix can serve as important tools for conservation, restoration and management of these ecologically peatlands.

Many studies have attempted to quantify subsidence in the Everglades through surveys and remote sensing (Jones, 1948; Stephens and Johnson, 1951; Stephens et al., 1984; Glaz, 1995; USEPA, 1997; Whelan et al., 2005; Dreschel et al., 2018). Although it has been understood that hydrology plays an important role in Everglades subsidence, very few studies have attempted to quantify this relationship. Whelan et al., 2005 studied the relationship between surface elevation change and groundwater changes in a mangrove forest in Shark River, Everglades. Change in the soil thickness of three layers of soil were measured- shallow zone, middle zone and bottom using Surface Elevation Tables (SETs).

This chapter applies the model developed in the preceding chapter to simulate daily root-zone VWC and root-zone subsidence at this site in Shark River Slough where monthly surface elevation measurements were obtained through SETs and presented in the study by Whelan et al., 2005.

4.2 Methodology

4.2.1. Study Site

The study site was in a brackish mangrove forest located at the mouth of Shark River in the Everglades (25º21'50.3"N 81º4'42.2"W) (Smith and Cahoon, 2003; Whelan et al., 2005). The predominant vegetation at the site consisted of Rhizophora mangle (L.) (red mangrove), Laguncularia racemose (L.) Gaertn. (white mangrove), and the Avicennia germinans (L.) Stearn (black mangrove) (Whelan et al., 2005). The soil profile at the site consists of 5.5 m of marine mangrove peat (dominated by *Rhizophora mangle*) which overlays a limestone bedrock. Hydrology at the site is affected by daily tidal activity. Whelan et al., 2005 found that the conductivity varied between 25 mS cm^{-1} and 51 mS cm^{-1}. The study site was a hydrological and meteorological station called SH3 operated by USGS with data available in the EDEN. Evapotranspiration (Figure 4-3) and rainfall data (Figure 4-4) are available from June 1995 to December 2017 and January 2002 to March 2019. Water level data was only available from January 2008 to September 2010. Since this did not cover the study period, water levels (Figure 4-5) were determined from a hydrological monitoring station 2.37 km downstream of SH3 called Shark River Before Gunboat Island.

Figure 4-1. Map shows station SH3 where the surface elevation study was conducted by Whelan et al., 2006. The hydrological data of this work was obtained from station SRBG (Shark River Before Gunboat) which is 2.37 miles downstream of SH3.

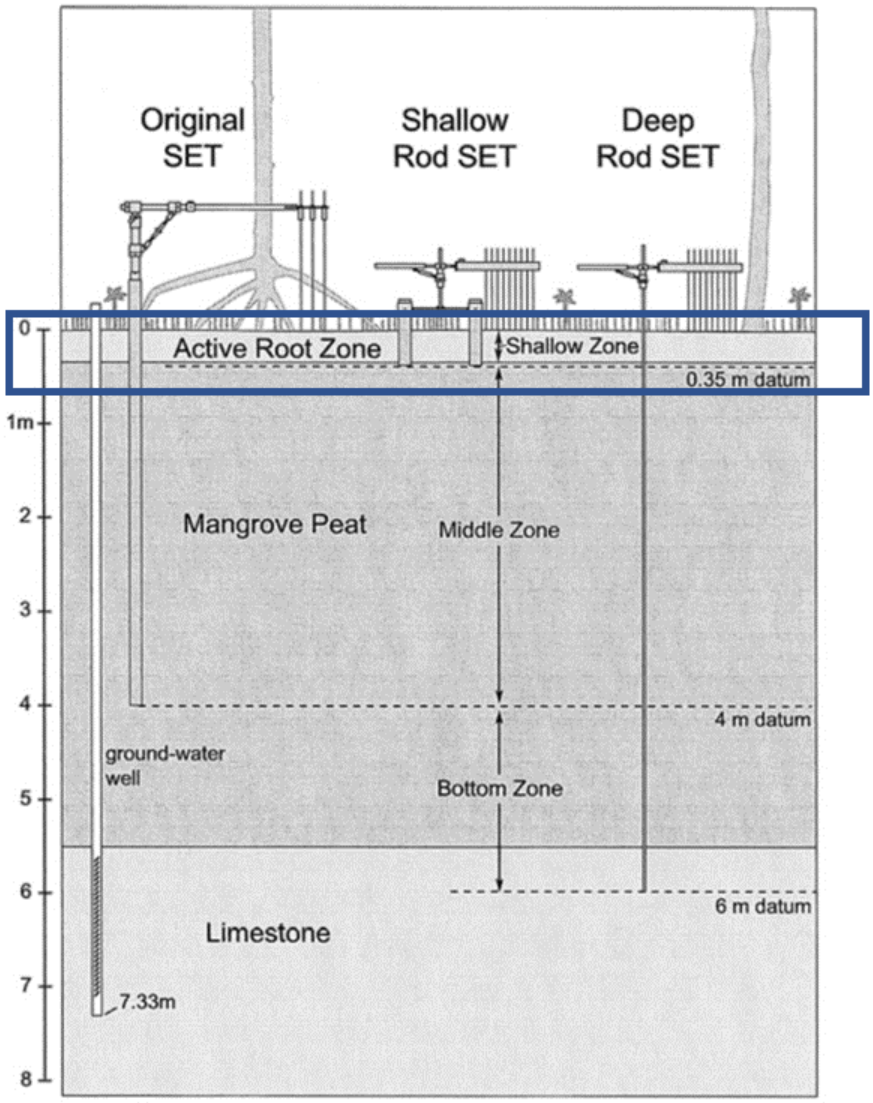

Figure 4-2. Experimental setup of the Surface Elevation Tables (SETs) at the study site of Whelan et al., 2005. The blue box represents the simulated zone. (Modified from Whelan et al., 2005).

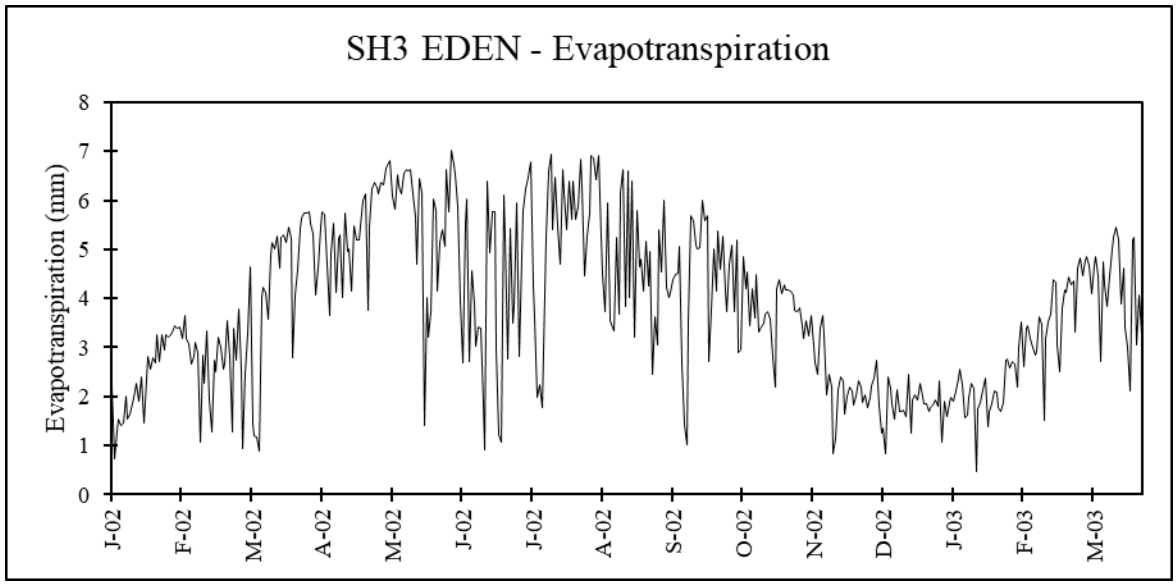

Figure 4-3. Daily potential evapotranspiration in mm at EDEN SH3 from January 2002 to March 2003.

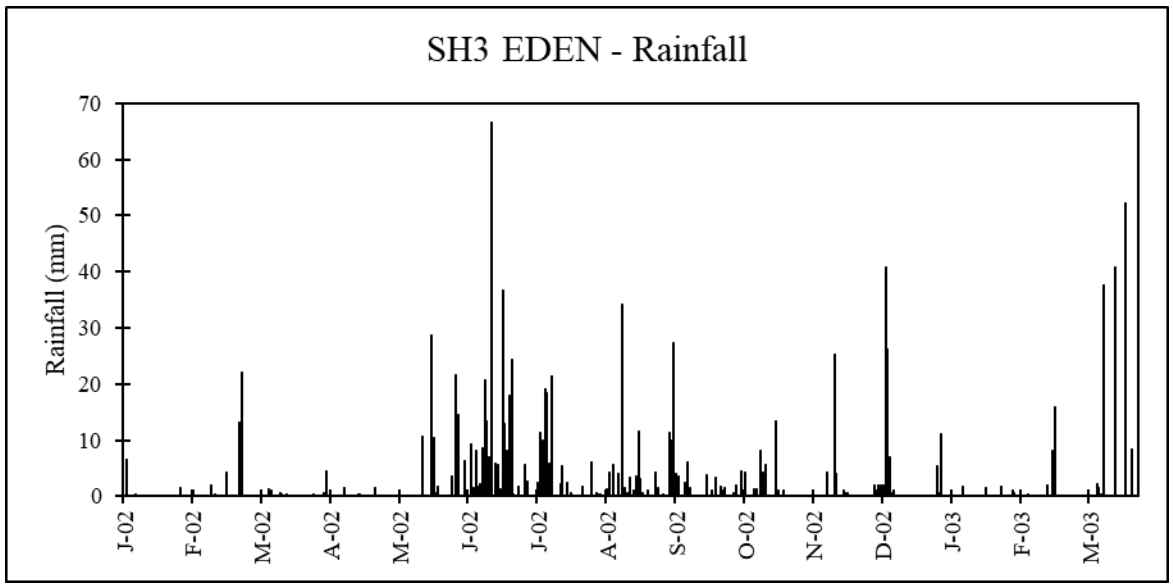

Figure 4-4. Daily measured rainfall in mm at EDEN SH3 from January 2002 to March 2003.

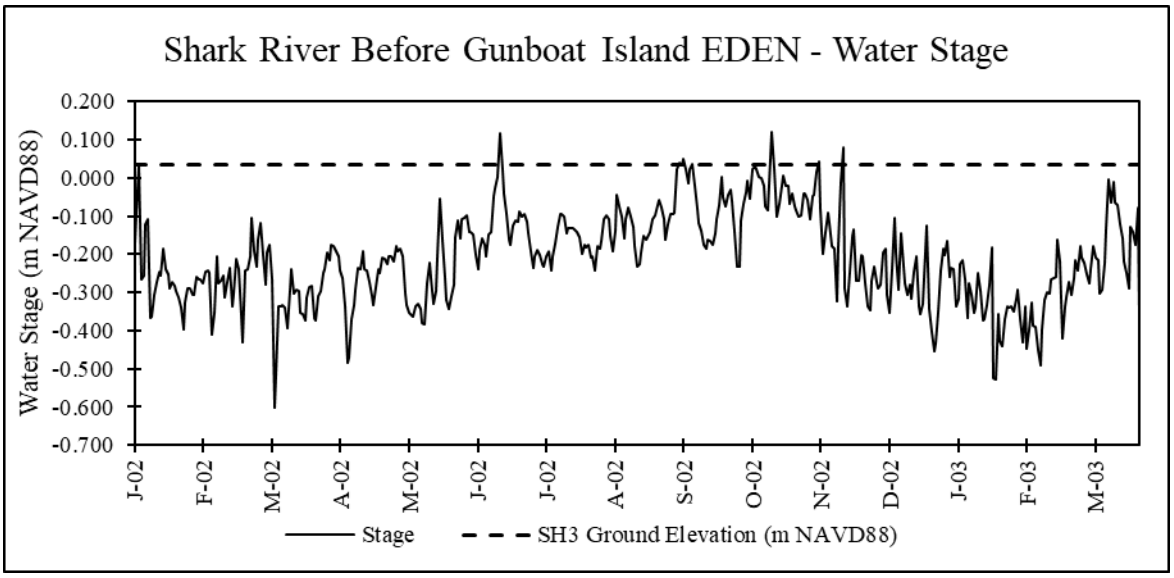

Figure 4-5. Daily water stage reported in NAVD 88 (black solid line) from January 2002 to March 2003 at the nearest EDEN station Shark River Before Gunboat Island and the ground elevation in NAVD 88 (black dashed line) at the study site EDEN SH3.

4.2.2. Observational Data

The observational data used in this study was published in a study conducted by Whelan et al., 2005 to determine the contribution of hydrology to three depths of a peat soil profile: shallow zone (0-0.35 m), middle zone (0.35-4 m), and bottom zone (4-6 m). Surface elevation data at each of the depths of the soil profile were measured using Surface Elevation Tables (SETs) (Figure 4-2). SETs consisted of a fixed, leveled benchmark to which four mechanical arms are attached (in four fixed directions). Each arm had nine measuring pins (total of 36 pins for all four arms) which could measure the relative soil elevation. This work used the data obtained from the shallow-rod surface elevation table (shallow-RSET). Three shallow-RSETs were installed at a depth of 35 cm within 18 m of each other on February 28, 2002. Four feldspar markers were installed with each shallow-RSET to measure soil accretion. Monthly measurements were taken at all three groups and

at the feldspar markers between March 18, 2002 to Mach 21, 2003 on the same day. The mean elevation of all three shallow-RSETs (Figure 4-6 b) and mean accretion (Figure 4-6 a) at all feldspar markers was calculated on the sampled days. The change in thickness of the shallow zone (Figure 4-6 c) was calculated as the difference between the surface elevations. The elevation of the shallow-RSETs were resurveyed on November 9, 2002 and February 10, 2005 and no movement in the RSET benchmarks were observed for during these surveys; therefore, a stable benchmark was assumed. The data published in Whelan et al., 2005 was extracted using WebPlotDigitizer (Rohatgi, 2019).

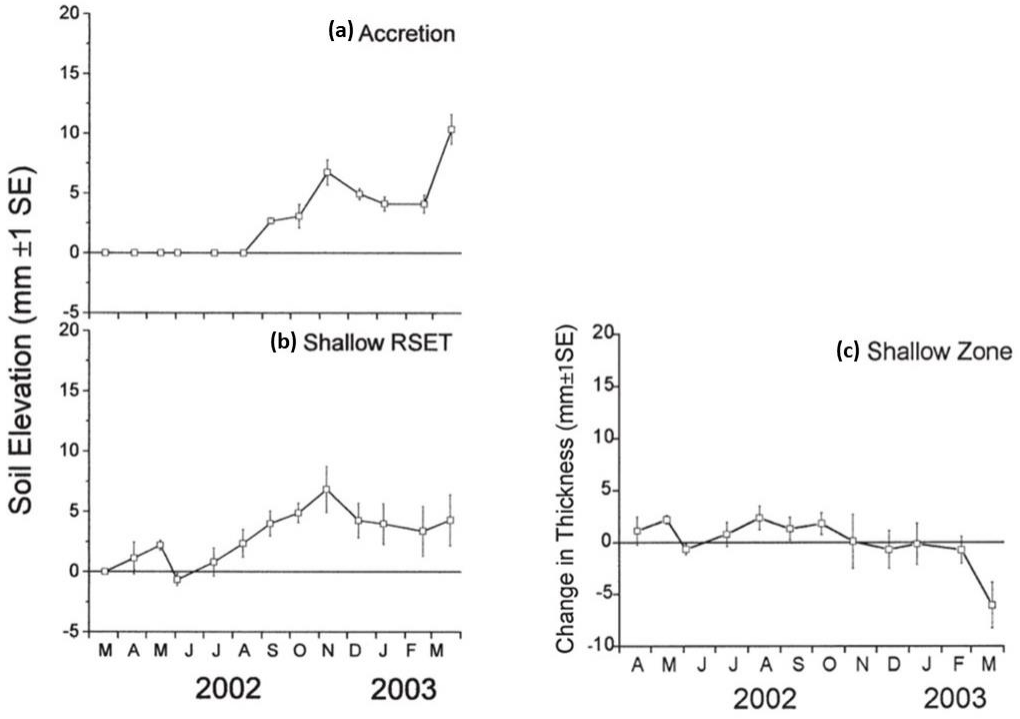

Figure 4-6. Observational data used from study by Whelan et al., 2005. The soil accretion (a) was measured using Feldspar markers. The elevation change in the shallow zone (b) was measured using Rod Surface Elevation Tables (RSETs). Shallow Zone change in thickness (c) was calculated as the difference between soil elevation and soil accretion (Modified from Whelan et al., 2005).

4.2.3. Defining Soil Surface Elevation and Water Table Height

Defining the soil profile was done using information available from the Whelan et al., 2005 study and the site information for SH3. To calculate the water table heights in the soil profile, it was necessary to first determine the elevation of the soil surface. SH3 was surveyed by USGS in July 2008 and the average ground elevation was reported as 0.082 m (NAVD88). Since the site is prone to changes in elevation due to accretion, the annual accretion rate reported by Whelan et al., 2005 of 6.64 ± 0.56 mm yr^{-1} was used to back-calculate the average elevation of the site in Jan 2002 as 0.036 m (NAVD88). This method assumes that the accretion rates were constant from Jan 2002 to July 2008. Since the USGS ground survey was conducted in July 2008, seven accretion cycles shown in Figure 4-6a (totaling an accretion of 46.48 mm) were used to make this calculation. The shallow ground zone defined by Whelan et al., 2005 was 0.350 m deep hence, the bottom of the soil profile is calculated to be at -0.314 m (NAVD88). The water level at the nearest EDEN site named Shark River Before Gunboat Island is reported in m (NAVD88) as shown in Figure 4-5. The water level (m NAVD88) was subtracted from the elevation at the bottom of the profile (m NAVD88) to obtain water table heights with respect to the bottom node and define the lower boundary condition.

4.2.4. Initial Conditions, Profile Discretization and Time Discretization

The soil profile is assigned an initial height of 35 cm with a Δz of 0.1 cm resulting in 350 cells and 351 nodes. The soil profile is assumed to be completely saturated at the start of the simulation, i.e. all the nodes are assigned an initial pressure head of 0 cm of water. This restricts the maximum modeled height of the profile to 35 cm since 0 cm of

water corresponds to the maximum HCR of 1 assigned to the model. Another approach would be to assume a zero-pressure head at the phreatic surface and assume a linear (with a slope of 1) decrease in pressure head with increase in elevation. From this distribution, the HCR for each cell can be computed. The sum of the ratios multiplied by a factor should result in the initial soil depth. The HCR of each cell times the factor will result in the initial cells heights.

The first approach was selected for this study for two reasons: (1) the observational data is provided as a change in thickness; (2) the simulation data is for the period for January 2002 to March 2003 while the observations are monthly for the period of March 2002 to March 2003. The RE is computed only for the nodes where the soil is unsaturated. There are three conditions associated with this calculation: Condition 1 – water table is above the top surface of the soil profile; Condition 2 – water table is between the top surface and the bottom surface of the soil profile; and Condition 3 – water table is below the bottom surface of the profile. For Condition 1, a pressure head of 0 cm of water is assigned to all nodes in the profile, and all cells are assigned a maximum Δz of 0.1 cm. For Condition 2, the number of nodes to run the Richards code is calculated as the difference between maximum profile depth and the water table height divided by the initial Δz of 0.1. For Condition 3, the number of nodes is set to the initial maximum number of nodes as the entire profile is unsaturated.

The simulations were conducted with a daily timestep for a period from January 1, 2002 to March 31, 2003, a total of 455 days. The maximum number of iterations until convergence was set to 100. Convergence is assumed when the sum of the squares of the

difference between the predicted pressure head and the solved pressure head is less than a prescribed tolerance of 1 cm of water.

4.2.5. Boundary conditions

The boundary conditions are specified to reflect the time dependent variation in evapotranspiration, rainfall, and water-table depth. A system-dependent flux boundary condition was specified as the upper-boundary condition at the top node, while a variable pressure head boundary condition is specified at the bottom node. The meteorological data from the site was obtained through EDEN. The dataset of total daily potential evapotranspiration at the site was calculated from Geostationary Operational Environmental Satellites (GOES) and climate data from the Florida Automated Weather Network and presented in mmd^{-1}. The total daily rainfall was also available on EDEN, this dataset is obtained from Next Generation Radar (NEXRAD) data from the U.S. National Weather Service. The NEXRAD rainfall data was enhanced using a local rain-gauge to increase accuracy and presented in EDEN as total daily rainfall in cm. Monthly quality assurance is performed on the EDEN datasets. The top flux from the soil was calculated by summing the rainfall and the potential evapotranspiration. A negative value for top flux would indicate evaporation from the soil while a positive value would indicate infiltration into the soil surface. The code is programmed to then search for positive values of flux and prescribe a constant head of -1. This value was chosen because a value of zero caused numerical instability in the code. A value of -1 has been used to model infiltration in HYDRUS for the examples of Skagg's Infiltration Test with bottom tension and is a

reasonable assumption to obtain numerical stability without making major changes to the code (Šimůnek et al., 2013).

For evaporation from the surface (when flux is negative), the flux considered is a potential flux, i.e. the maximum possible flux from the soil surface. However, the actual flux delivered out of the soil surface will depend on the antecedent conditions of the soil. Hence, a framework was included to calculate this actual flux. For this method, at the first iteration the potential flux is used to calculate the pressure head at the upper boundary condition node. This calculated pressure head is compared to the minimum allowable pressure head under air-dry conditions which is calculated using the temperature and relative humidity of air. If the calculated pressure head is lower than the minimum allowable pressure head, a prescribed pressure head with the minimum allowable head is used as the top boundary condition, and if it is higher than the minimum allowable pressure head, the actual flux is calculated. Since the actual flux cannot be greater than the potential flux out the soil, the lower value of the two values is assigned as the actual flux. At each time step, the pressure head at the top boundary condition is the sum of the hydrostatic equilibrium pressure head at the surface (calculated using the phreatic surface) and the change in pressure head from flux.

The lower boundary condition is specified as a time-varying pressure head calculated using the phreatic surface. The daily time-series water stage data at the site available through EDEN is used to calculate the water table heights with the bottom node (considered at a depth of 35cm) of the soil profile as a reference point. Positive water table heights indicate that the water level is above the bottom node while negative heights

indicate the water table is below the bottom node. At each timestep, if the water table height is greater than or equal to zero, the bottom node is prescribed a pressure head of zero. If the calculated water table height is less than zero, the depth in cm below the bottom node (a negative value – same value as the calculated water table height) is assigned as the prescribed pressure head at the bottom node.

4.2.6. Parameters and their Testing

Due to the absence of known hydraulic parameters for this site, the calibrated vGM model and hydraulic conductivity from the lysimeter tests from the preceding chapter were used to parameterize the unsaturated flow model. It was not possible to calibrate the hydraulic model due to the lack of observed VWC or pressure head distribution for the soil profile, hence these values were kept constant for all simulations. The average HCRs from Chapter 1 were used to create the look-up table for the elevation change model. During simulations, it was observed that the HCR value at 6 kPa was most sensitive to the elevation change model. Hence, this value was varied and the mean monthly change in profile thickness was compared to the observational data made using RMSE and $RMSE_N$. In addition, since the observational data was taken on one day of each month during study duration and it is not a monthly average, the minimum and maximum simulated change in profile thickness for each month were calculated and compared to the observational data.

4.3 Results and Discussion

Table 4-1 presents the RMSE and $RMSE_N$ between the mean simulated monthly change in thickness and the observed monthly change in thickness for the shallow-RSETs at the tested HCRs. Figure 4-7 presents the mean monthly simulated change in profile

thickness and its range along with the observed monthly readings. The results from the RMSE and the $RMSE_N$ for the simulations conducted with different values of HCR are presented in Table 1-1 and the number of observations that lie in the simulated range were also calculated since the exact day of the data collection each month is unknown. Hence the minimum and maximum change in vadose zone thickness were also used as metrics for model evaluation. With increasing the HCR from 0.93 to 0.98, a decrease in the RMSE and $RMSE_N$ was observed. The number of observations in the simulated range increased with the HCR of 0.93 and 0.96 resulting in 8 observations within the simulated range. When the HCR is increased to 0.97, the RMSE and $RMSE_N$ decrease; however, the number of observations in the simulated range decreases to 8. As the HCR is increased, there is a tendency of the graph of simulated change in thickness to flatten. For an HCR of 1 (not presented in the figures), no change in soil thickness is observed. An HCR of 0.96 was selected as the model with the lowest RMSE and $RMSE_N$ and the highest number of observations in the simulated range. This value is much higher than the HCR fitted to the laboratory lysimeter value of 0.58 but closer to the oedometer HCR value of 1 at 6 kPa. It is also worth noting that the oedometer tests were performed with 1 cm high samples standard sample rings provided by F 1-15 Pressure Plate Apparatus, and hence, a change of 0.04 mm would not have been visually observed during testing.

For June 2002 and March 2003, the model predicts an increase in soil height compared the preceding month; however, the observations indicate a decrease in shallow zone thickness. Since the change in vadose zone thickness of the model prediction is only influenced by the flux out of the soil and water table height, the model trend will never reflect a decreasing profile height for both June 2002 and March 2003 as they're both

months with higher water tables. The bottom panel of Figure 4-8 presents the soil profile height (with an HCR of 0.96) and water table depth (measured from the bottom of the soil profile) with time for the simulation period while the top panel presents the potential and calculated flux out of the soil profile. The water depth is strongly correlated to the soil profile height. This is expected as the water table height is used to calculate the top boundary condition and to define the depth of the soil profile for the model.

Figure 4-9 presents the degree of saturation with time in the soil profile with an HCR of 0.96. The black solid line indicates the phreatic surface. For the entire duration of the simulation period, the degree of saturation (VWC divided by saturated VWC) in the profile ranges between 0.78 to 1 with 1 indicating complete saturation. The VWC s are highest at the bottom of the profile (below the water table). Complete saturation is also observed above the phreatic surface (dark blue shading) in an area known as the capillary fringe or the capillary zone. Capillarity draws water from the water table resulting in completely saturated pores; however, the water is still held under tension unlike the saturated zone. For the transport model, the height of the capillary zone is directly influenced by the vGM parameter, α, which controls the air-entry pressure head. Thicker capillary fringes are observed with the lower α values. Infiltration into the soil is observed for periods of rainfall (dark blue lines on surface).

The shallowest unsaturated zones and highest simulated soil profiles are observed in the period from June-November (wet-season) when the water table heights are high. Due to the capillary fringe, there are multiple days in this period when the soil column is fully saturated despite the water table being below the soil surface. This effect is intensified by

the high rainfall rates from June to July 2002. The deepest unsaturated zone and shallowest soil profiles are simulated for January 2002 to May 2002 and November 2002 to March 2002. During this period high evaporative flux and low infiltration from rainfall is also observed. Figure 4-10 presents cell heights for the soil profile at each simulation. The lowest cell height is observed on the top boundary and they increase with depth as they are specified as a function of the pressure head which too increases with depth.

During the March 2003, an increase in the water table height was observed. This resulted in higher soil profile height for this time-period. However, the observational data reports a decrease in soil thickness. Soil thickness was calculated by Whelan et al., 2005 using soil elevation and accretion. The high accretion rate observed in March resulted in the low soil thickness reported.

Table 4-1. The Root Mean Squared Error (RMSE) and normalized RMSE ($RMSE_N$) between the mean simulated monthly change in thickness and the observed monthly change in thickness for the shallow-Rod Surface Elevation Table (shallow-RSET) at the tested Height Change Ratios (HCRs). The number of observations in the simulated range is also presented.

HCR at 6 kPa [-]	RMSE [mm]	$RMSE_N$ [%]	Observations in Simulated Range [-]
0.93	6.07	72.0	7
0.94	5.12	60.7	7
0.95	4.02	47.7	8
0.96	3.54	42.0	9
0.97	2.75	32.6	8
0.98	2.52	29.9	6

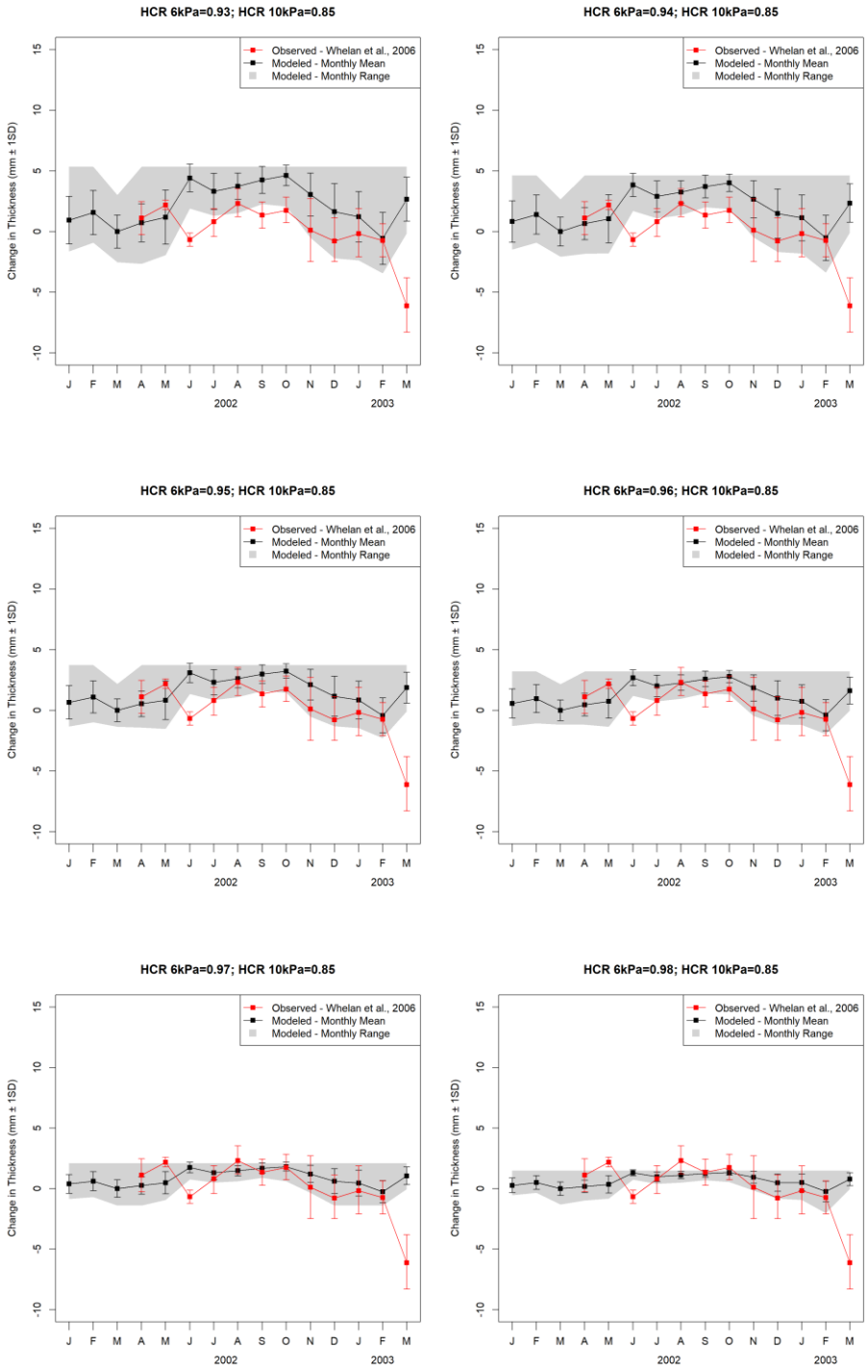

Figure 4-7. Change in root-zone thickness simulated with the REVC model and observed by Whelan et al., 2005.

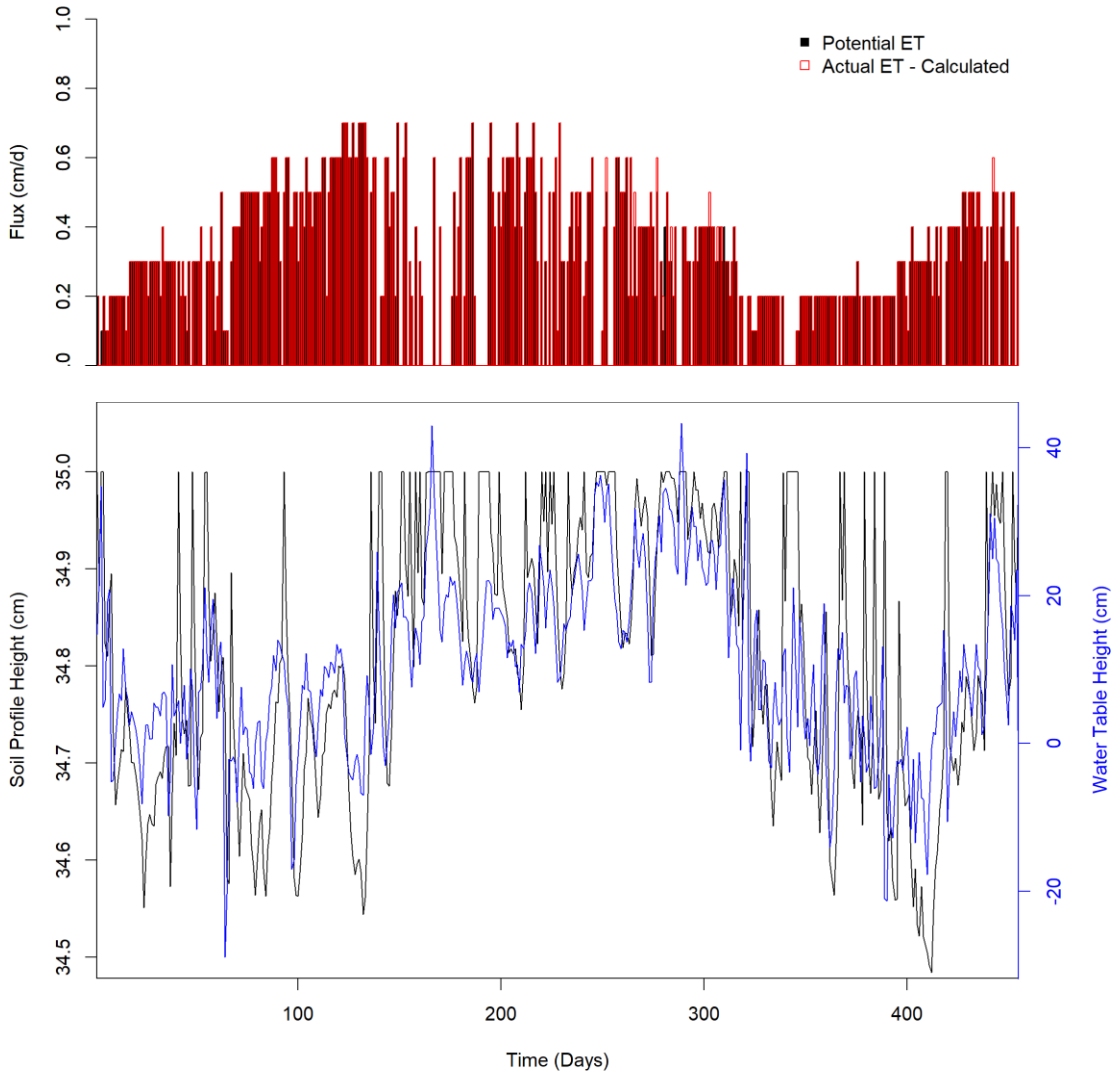

Figure 4-8. (Top) Potential evapotranspiration (black bars) and the calculated actual evapotranspiration (red boxes) used to determine the top boundary condition of the model. (Bottom) the simulated profile heights (black lines) with an HCR of 0.96 and the calculated water table heights (blue lines).

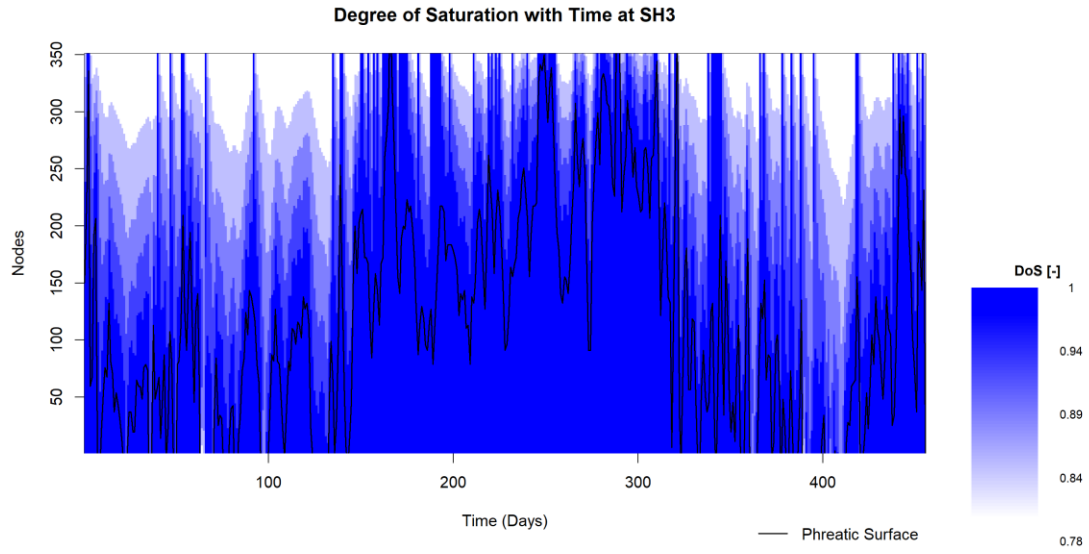

Figure 4-9. Simulated volumetric water content [-] at site SH3 using an HCR of 0.96 for the duration of the study period (455 days). Node 1 is at the bottom of the soil profile while Node 351 is at the top of the profile. The black solid line shows the phreatic surface.

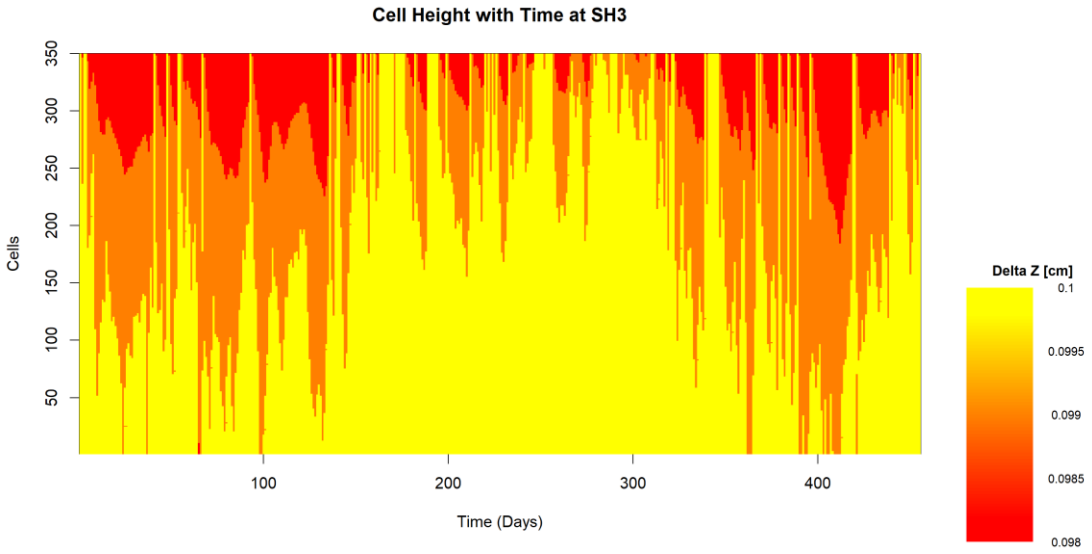

Figure 4-10. The cell heights calculated at site SH3 for the duration of the study period (455 days) using the look-up table method with an HCR of 0.96 for all 350 cells in the soil profile. Cell 1 is at the bottom of the soil profile and Cell 350 is at the top of the soil profile.

4.4 Assumptions and Limitations

As the observational data was not collected by this study but obtained from a previous work, assumptions had to be made about the study site and hydraulic properties of the soil in addition to the assumptions of the physical model. The surface elevation of the study was required to calculate the depth of the unsaturated soil profile at each timestep. The surface elevation at the site was available from a 2008 USGS survey; however, since the site is prone to peat accretion, accretion rates measured by Whelan et al., 2005 were used to back-calculate the surface elevation. This required the assumption that the annual accretion rates were constant from 2002 to 2008.

Although it was known that the shallow zone consisted of 35 cm of mangrove peat, the vGM parameters of the soil were not reported. Anderson et al., 2006 had unpublished data on the hydraulic conductivity of mangrove peat at the site, however this report is no available longer in the USGS repository. Due to these reasons, this study used the calibrated vGM parameters and hydraulic conductivity from section 3.4. It was not possible to calibrate these parameters for the SH3 study site since there was no time-series tensiometer data or VWC data available for the study period.

At the start of simulations, the model soil is assumed to be fully saturated i.e., a pressure head of 0 cm of water is prescribed at all the nodes. The cell heights for all 350 nodes corresponding to this assumption is 0.1 cm which results in a profile height of 35 cm. This 35 cm is the maximum possible simulated profile height since the maximum HCR value is 1 at 0 cm of water. For this type of model, the maximum soil thickness is known, a priori.

The simulations were performed for a 455-day period during for which the pressure head across the soil profile changes as result of the changing boundary conditions. For the top boundary condition, a system dependent boundary condition was employed. For infiltration into the soil, the top boundary condition changes to a pressure head of -1 cm of water instead of 0. This was done for the stability of the code at the specified timestep of one day. For larger timesteps, large changes in gradient can cause non-convergence. This limitation can be overcome by reducing the timestep. However, such solutions become computationally intensive. An assumption of -1 cm of water instead of zero does not affect the VWC of the profile and its effect on the calculated subsidence is negligible; hence, it a reasonable assumption.

4.5 Conclusions

The unsaturated volume change model was applied to a site in Shark River with unsteady boundary conditions. The boundary conditions were calculated from meteorological data and hydrological data obtained through EDEN. Daily VWC and surface elevation were predicted for a period from January 2002 to March 2003 using different values of HCR at 6 kPa. The change in unsaturated zone thickness was compared to monthly observations by Whelan et al., 2005. It was observed that HCR of 0.96 at 6 kPa presented the best fit to the observational data with 10 observations in the simulated; the selected HCR is much higher than the HCR obtained for peat through lysimeter testing; however, it is comparable to the laboratory generated value. The full calibration and validation at this site were not possible due to the lack of daily observational data. The overall monthly modeled trend in surface elevation change matched observed trends. The

works shows promise in the application of REVC to present coupled solutions of subsidence and hydrology. Improvements to REVC through the incorporation of irreversible shrinkage in the HCR model can be made.

Acknowledgements

The authors acknowledge the Everglades Depth Estimation Network (EDEN) project and the United States Geological Survey for providing the meteorological and station data for this research.

References

Camporese, M., S. Ferraris, M. Putti, P. Salandin, and P. Teatini. 2006. Hydrological modeling in swelling/shrinking peat soils. Water Resour. Res. 42(6): 1–15.

Chambers, L.G., H.E. Steinmuller, and J.L. Breithaupt. 2019. Toward a mechanistic understanding of "peat collapse" and its potential contribution to coastal wetland loss. Ecology: e02720Available at https://onlinelibrary.wiley.com/doi/abs/10.1002/ecy.2720 (verified 24 May 2019).

Crump, J. 2017. Smoke on Water - Countering Global Threats From Peatland Loss and Degradation. A UNEP Rapid Response Assessment. Nairobi.

Dreschel, T.W., S. Hohner, S. Aich, and C.W. McVoy. 2018. Peat Soils of the Everglades of Florida, USA. *In* Peat. InTech.

Glaz, B. 1995. Research seeking agricultural and ecological benefits in the Everglades: J. Soil Water Conserv. 50: 609–612.

Jones, L.A. 1948. Soils, geology, and water control in the Everglades region: University of Florida Agricultural Experiment Station Bulletin 442.

Lane, R.R., S.K. Mack, J.W. Day, R.D. DeLaune, M.J. Madison, and P.R. Precht. 2016. Fate of Soil Organic Carbon During Wetland Loss. Wetlands 36(6): 1167–1181Available at http://link.springer.com/10.1007/s13157-016-0834-8 (verified 18 June 2019).

Rohatgi, A. 2019. WebPlotDigitizer. Available at https://automeris.io/WebPlotDigitizer.

Šimůnek, J., M. Šejna, H. Saito, M. Sakai, and M.T. van Genuchten. 2013. The Hydrus-1D Software Package for Simulating the Movement of Water, Heat, and Multiple Solutes in Variably Saturated Media. : 342.

Smith, T.J., and D.R. Cahoon. 2003. Wetland Sediment Elevation in the Florida Everglades: Response to Surface Water Stage Variation. *In* Proceedings of the International Conference on Coastal Sediments. Clearwater Beach, Florida.

Stephens, J.C., A.L. H., and E. Chen. 1984. Organic soil subsidence, in Holzer, T.L., ed., Man-induced land subsidence. Geol. Soc. Am. Rev. Eng. Geol. 6: 107–112.

Stephens, J.C., and L. Johnson. 1951. Subsidence of organic Soils in the upper Everglades region of Florida. Soil Sci. Soc. Florida Proc. XI: 191–237.

Szajdak, L., and J. Szatylowicz. 2002. Impact of Drainage on Hydrophobicity of Fen Peat-Moorsh Soils. Mires Peat: 158–174.

USEPA. 1997. South Florida Ecosystem Assessment: Monitoring for Adaptive Management: Implications for Ecosystem Restoration: Final Technical Report - Phase I.

Wang, C., C. Tong, L.G. Chambers, and X. Liu. 2017. Identifying the Salinity Thresholds that Impact Greenhouse Gas Production in Subtropical Tidal Freshwater Marsh Soils. Wetlands 37(3): 559–571Available at http://link.springer.com/10.1007/s13157-017-0890-8 (verified 18 June 2019).

Whelan, K.R.T., T.J. Smith, D.R. Cahoon, J.C. Lynch, and G.H. Anderson. 2005. Groundwater control of mangrove surface elevation: Shrink and swell varies with soil depth. Estuaries 28(6): 833–843.

5. APPLICATION OF REVC TO STUDY RIDGE AND SLOUGH ENVIRONMENT IN THE EVERGLADES

5.1 Introduction

Ridge and slough environments are habitats with contrasting hydrology and vegetation that occur next to each other and contribute to the biological diversity in the Everglades (Gawlik, 2002; Ogden, 2005; Trexler and Goss, 2009; Harvey et al., 2017). Visually, they can be identified from topography and vegetation. Ridges are topographically elevated with sparse to dense *Cladium Jamaicense* (sawgrass) and typha, whereas, sloughs are topographically lower with sparser vegetation and floating and submergent macrophytes (Watts et al., 2010). Due to the local differences in topography of ridges of slough, differences in hydrology is also observed. During the dry season, the topographically elevated ridges are subject to dry-down whereas the sloughs remain inundated year round (Jorczak, 2006). While there is a lack of clarity on their formation in the landscape, their persistence is attributed to the feedbacks from vegetation production, aeration, and hydrology (Givnish et al., 2008).

Due to the isolated appearance of ridges parallel to the direction of water flow, water scouring and sediment deposition are hypothesized to maintain the elevation of ridges (DeAngelis et al., 1998; Sklar et al., 2000; SCT, 2003; Ogden, 2005). Soil accretion occurs through the decomposition of plant litter in peatlands. Differences in plant productivity may affect the accretion rates observed in different habitats. Typically, the hydrology of sloughs, which remain inundated year round, is expected to provide anoxic conditions with low microbial activity (Watts et al., 2010); hence greater soil accretion is

expected in the slough compared to the ridge. However, the plant productivity of ridge vegetation is higher, and therefore, accretion rates are expected to be higher at the ridges (Lewis, 2005; Jorczak, 2006). Plant productivity also increases with nutrient concentrations in the water, a known issue in the Everglades from agricultural run-off (Gaiser et al., 2005; Hagerthey et al., 2010).

Modifications to the natural flow have resulted in impoundments with high water stages or extremely drained wetlands (Watts et al., 2010). Soil aeration acts as an opposing process to soil accretion. Aeration of the soil causes the lowering of soil elevation through increased microbial action, soil oxidation, and soil shrinkage (Oleszczuk et al., 2003; Jorczak, 2006; Chambers et al., 2019). With rewetting, peat is known to only regain a portion of the elevation change. Subsidence and conversion to other land uses is estimated to have caused almost half of the degradation of the ridge and slough landscape (McVoy et al., 2012). Topographic flattening attributed to the accretion in sloughs (from increased nutrient loads) and aeration of ridges (resulting in irreversible shrinkage) is observed (Givnish et al., 2008; Larsen and Harvey, 2010). One of the key indications of Everglades restoration success is the microtopography of ridge and slough landscape (Harvey et al., 2017). The ideal water conditions for the ridge and slough landscape is somewhere between excessively drained and excessively impounded (Watts et al., 2010).

In this chapter, the practical application of the REVC model to simulate the changes in the elevation as a result of hydrologic dry-down is demonstrated through the case scenarios of a 1) low accretion, low reversible shrinkage model, 2) high accretion,

moderate reversible shrinkage model, and 3) moderate accretion, moderate reversible shrinkage model.

5.2 Methodology

Figure 5-1 presents a 2m x 2m spectrally derived vegetation map of WCA-3B, and the vegetation types with their broad classification (ridge vs. slough) are presented in Table 5-1. The vegetation types of WCA-3B can be broadly classified as sloughs (broadleaf floating, sparse graminoid marshes, open water) or ridges (graminoid Cladium marshes, graminoid typha marshes, shrubs, trees). A 20 m by 50 m study site was selected. Figure 5-2 presents the detailed vegetation map of the site. Using the broad classification in Table 5-1, a ridge and slough map was generated (Figure 5-3). Due to the lack of detailed elevation data of the study site, the 104 ridge cells were assigned heights generated from a random normal distribution, with a mean height of 30 cm and a standard deviation of 5 cm (Figure 5-4). The metrics for the distribution were estimated from surveys conducted by Jorczak, 2006 for the WCA-3B. The slough heights are assigned a zero elevation at the start of the simulation.

Simulations were performed to evaluate changes in ridge and slough heights for three different scenarios: 1) Scenario 1 – no reversible shrinkage with low accretion, 2) Scenario 2 - moderate reversible shrinkage with high soil accretion, and 3) Scenario 3 - moderate reversible shrinkage with moderate soil accretion (Table 5-2). Accretion rates were assumed from previous estimates found in literature (Watts et al., 2010). The REVC code was applied to the ridge cells to simulate a 30-day dry-down called the dry season, followed by an 11-month wet season with fully inundated ridges. The code is only applied

to the 30-day dry season, following which the reversible shrinkage coefficient and accretion rates are used to calculate a new soil profile, for which another 30-day dry season is simulated. This process is repeated for 10 dry seasons mimicking a 10-year period.

For the purpose of assigning soil hydraulic parameters, the soil profile was divided into five layers: 1) Accretion, 2) Fibric, 3) Hemic, and 4) Sapric. Using the FC and BC of the soil samples in WCA-3 from the dataset in Chapter 2, four SWRCs were selected for each layer (Table 5-3 and Figure 5-5). Soil hydraulic conductivity was assumed to be the highest for the accretion layer and decreased with depth. Each layer was assigned the same HCR model (Table 5-4). The HCR at 6 kPa from Chapter 4 along with mean HCRs at other applied pressures from the WCA-3B peats was used to create the HCR model.

Reversible shrinkage, calculated by adding the height of the soil at the end of the dry season to the total shrinkage multiplied by the reversible shrinkage coefficient, is added to the soil at the start of the wet season. On the other hand, accretion is assumed to increase linearly over the course of the wet season and added to the soil profile height at the start of the next dry season. Accretion is also applied to the slough, but shrinkage is not, as sloughs are assumed to remain inundated year-round. During the dry season, the water level is assumed to be 5 cm from the base of the ridge to mimic an inundated slough during the dry season. The unsaturated zone height is calculated by subtracting 5 cm from the ridge height. The bottom node is assigned a constant pressure head boundary value of zero cm to indicate the presence of a constant water table during the dry season. The top node was assigned a system-dependent atmospheric boundary condition with a constant daily

evapotranspiration rate of 6 mm/day. Cell heights were specified at 0.05 cm and the number of nodes are calculated at the start of every dry season using the updated soil profile height.

Table 5-1. Vegetation Classes in WCA-3B (Source: FIU RS&GIS).

Vegetation Class	Class Name	Ridge	Slough
blF	Broadleaf Floating		x
gM	Graminoid Marsh		x
gM_S	Graminoid Marsh Sparse		x
gMCl	Graminoid Marsh Cladium	x	
gMCl_D	Graminoid Marsh Dense Cladium	x	
gMCl_S	Graminoid Marsh Sparse Cladium	x	
gMClTy	Graminoid Marsh Cladium & Typha	x	
gMTy	Graminoid Marsh Typha	x	
hM	Herbaceous Marsh	x	
s_hM	Shrub and Herbaceous Marsh	x	
s_t	Shrub and Tree	x	
zWtr	Water		x

Table 5-2. Scenarios tested for ridge soil shrinkage and accretion.

	Reversible Shrinkage Coefficient [-]	Peat Accretion [cm/year]
Scenario 1	0	0.1
Scenario 2	50	0.5
Scenario 3	50	0.3

Table 5-3. Soil hydraulic parameters selected for each layer of the ridge soil profile.

Layer	Depth [cm]	θ_s [$cm^3\ cm^{-3}$]	θ_r [$cm^3\ cm^{-3}$]	α [cm^{-1}]	n [-]	K_{sat} [$cm\ d^{-1}$]
Accretion	0.0 - 0.5	0.940	0.000	0.027	1.259	51.9
Fibric	0.5 - 2.5	0.939	0.251	0.01	1.401	51.9
Hemic	2.5 - 7.5	0.923	0.000	0.036	1.178	36.0
Sapric	>7.5	0.921	0.000	0.03	1.158	10.0

Table 5-4. Height change ratios (HCRs) for each layer.

Layer	Depth [cm]	HCR 6kPa [-]	HCR 10kPa [-]	HCR 50kPa [-]	HCR 1500kPa [-]
Accretion	0.0 - 0.5	0.96	0.85	0.80	0.67
Fibric	0.5 - 2.5	0.96	0.85	0.80	0.67
Hemic	2.5 - 7.5	0.96	0.85	0.80	0.67
Sapric	>7.5	0.96	0.85	0.80	0.67

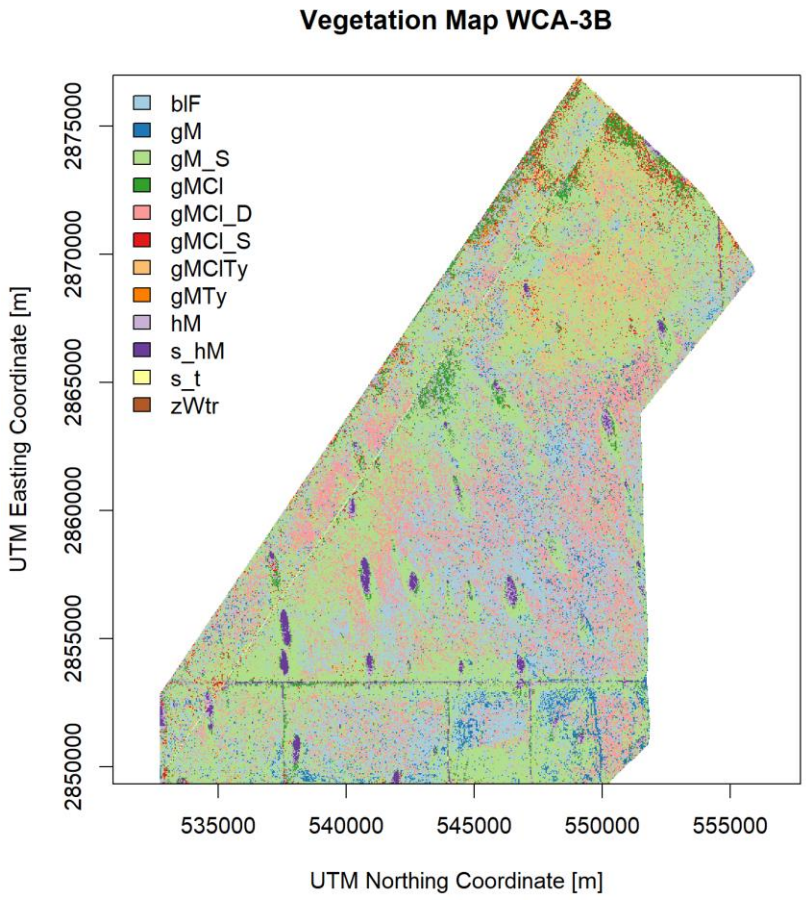

Figure 5-1. Vegetation map of WCA-3B derived from spectral data (Shapefile Source: FIU RS&GIS).

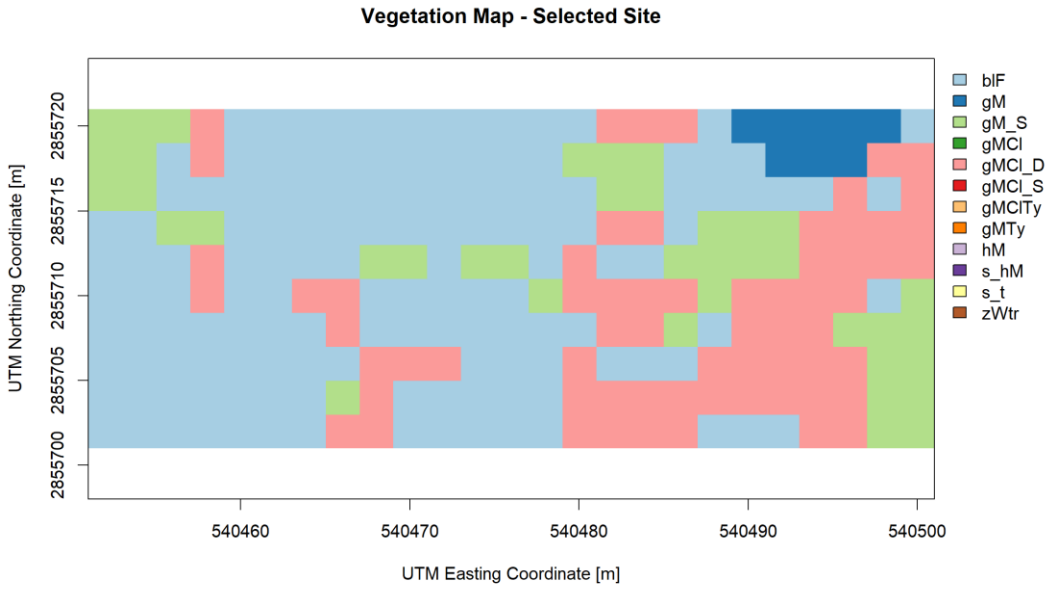

Figure 5-2. Vegetation map of 20 m x 50 m study site in WCA-3B.

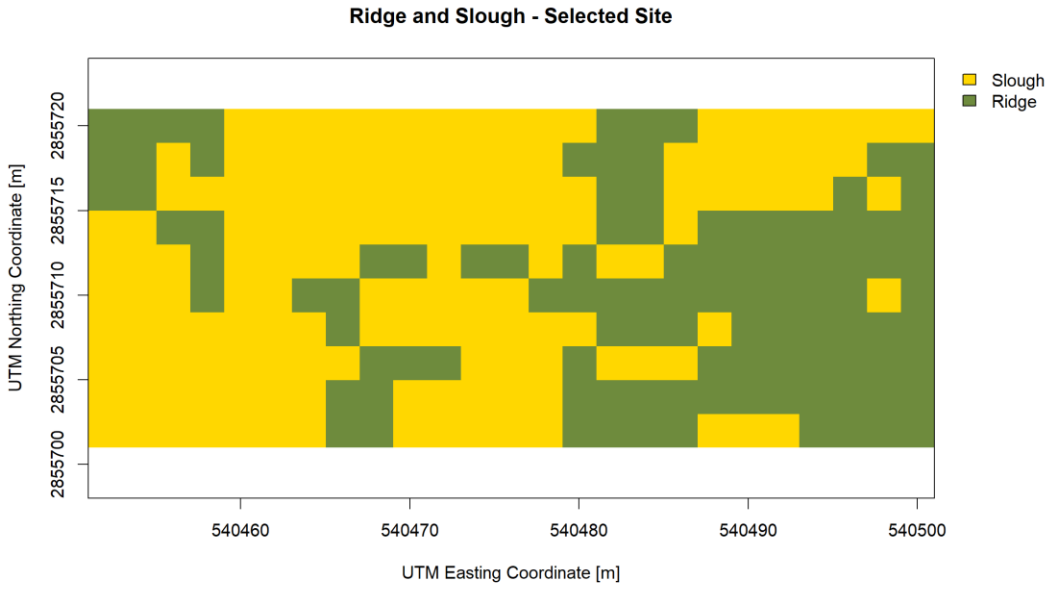

Figure 5-3. Ridge and slough classification at the study site.

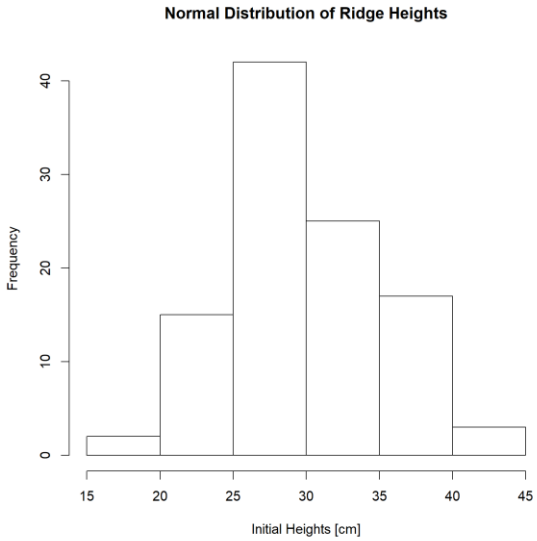

Figure 5-4. Random normal distribution (mean = 30 cm, standard deviation = 5 cm) of ridge heights for 104 ridge cells in the study site.

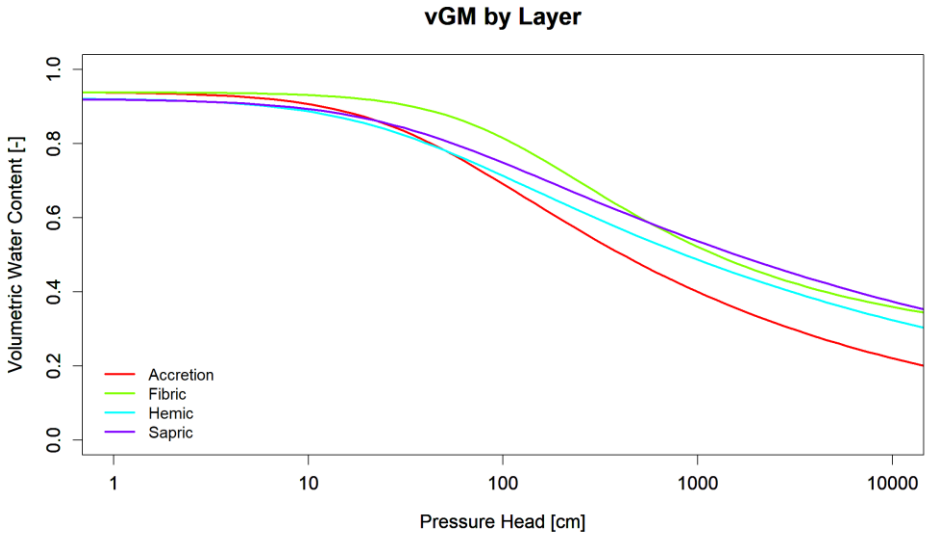

Figure 5-5. Soil water retention curves from generated parameters for each layer of the ridge soil profile.

5.3 Results and Discussion

The 5-year and 10-year change in elevation of the site under the three simulated scenarios is presented in Figure 5-6. Scenario 1 with no reversible shrinkage and low accretion rate produces the highest negative change in elevation. There is also a considerable decline in ridge elevation over the 10-year time period. For Scenario 2, accretion is the dominant process. Sloughs which do not experience any shrinkage have a net accretion of 5 cm over the ten-year period in Scenario 2. In the case of the moderate Scenario 3, overall accretion is the dominant process with some shrinkage observed in ridges with high initial elevations. Figure 5-7 presents the 5-year and 10-year change in ridge heights for all three scenarios. Shrinkage is more dominant in higher ridge elevations. Unlike Scenario 2 and Scenario 3, a net shrinkage is observed consistently in Scenario 1 indicating that an accretion rate of 0.1 cm/year accretion is not sufficient to balance the zero reversible shrinkage. For Scenario 2 and Scenario 3, net change in thickness is consistently positive but there is tempering of the curve with increasing ridge height. For Scenario 3, some ridges (ridge heights in the 35-40 cm range) experience shrinkage or no change.

The simulated change in ridge elevation over the 10-year period for three ridge cells with heights 19.6 cm, 27.6 cm, and 38 cm are presented in Figure 5-8. For the 38 cm sample, there is an 11% drop in ridge height with Scenario 1 compared to a 3% drop for the 27.6 cm ridge cell and no change for the 19.6 cm ridge cell. The lack of change in the 19.6 cm ridge cell is attributed to rounding errors in the model. Cell heights are fixed at 0.05 cm and the calculated ridge heights are rounded to the nearest mm prior to each run.

Over the 10-year period for Scenario 2, ridge height increases by 22% for the 19.6 cm cell, 14% for the 27.6 cm cell, and 2% for the 38 cm cell. Cell heights change moderately for Scenario 3 with increases of 13% for 19.6 cm cell, 7% for the 27.6 cm cell and 1% for the 38 cm cell.

Ridges that shrunk drastically also experienced an increased surficial VWC. Under Scenario 1, the VWC of the 38 cm cell increased from 70.7% at the end of the first dry season to 75.6% at the end of the 10^{th} dry season. For Scenario 3, the VWC of the same cell increases moderately to 71.4%, whereas, for Scenario 2, the VWC decreases to 68.4%. Similar trends are observed with the 19 cm and 27.6 cm cells; however, the changes are not as drastic as the 38 cm cell. Figure 5-9 presents the distribution of surficial VWC across the site. Ridge cells with higher elevation have lower surficial VWC. Significant differences are observed between Scenario 1 and Scenario 2 with Scenario 1 showing higher VWC overall. Overall increase in VWC is observed for Scenario 1 from year 5 to year 10; however, for Scenario 2, overall VWC decreases from year 5 to year 10.

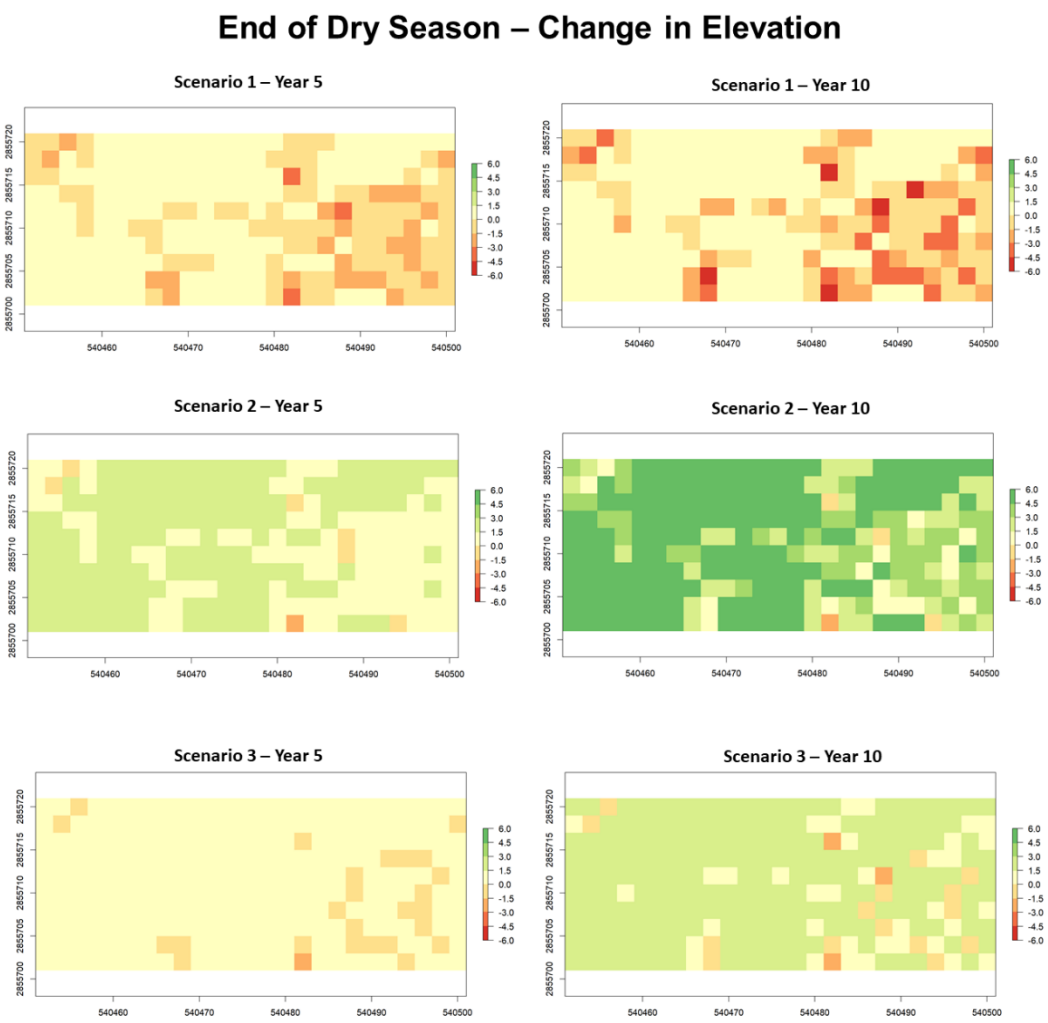

Figure 5-6. The 5-year and 10-year change in elevation for the study site is presented for all three scenarios.

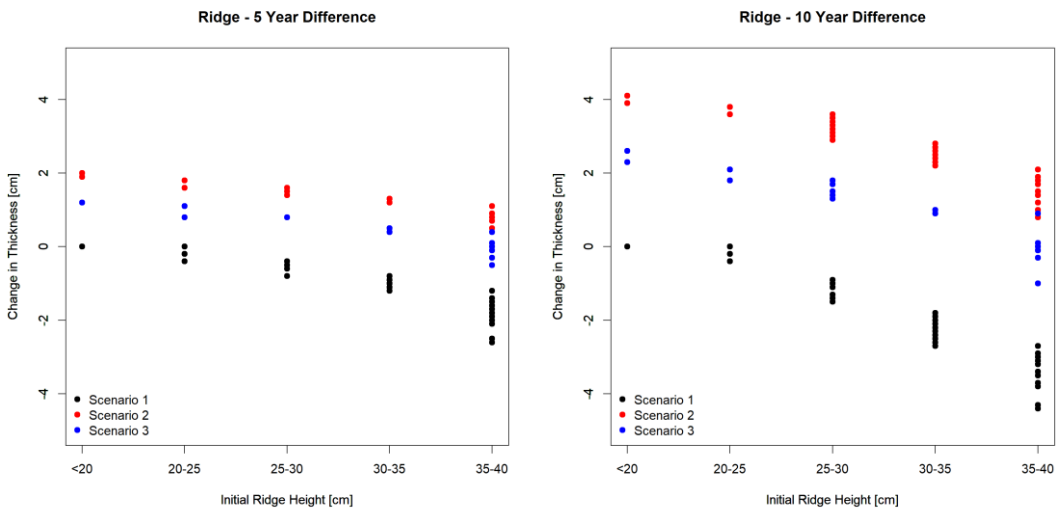

Figure 5-7. The 5-year and 10-year difference in ridge heights for all three scenarios. The 40-45 cm range is not presented due to non-convergence of model.

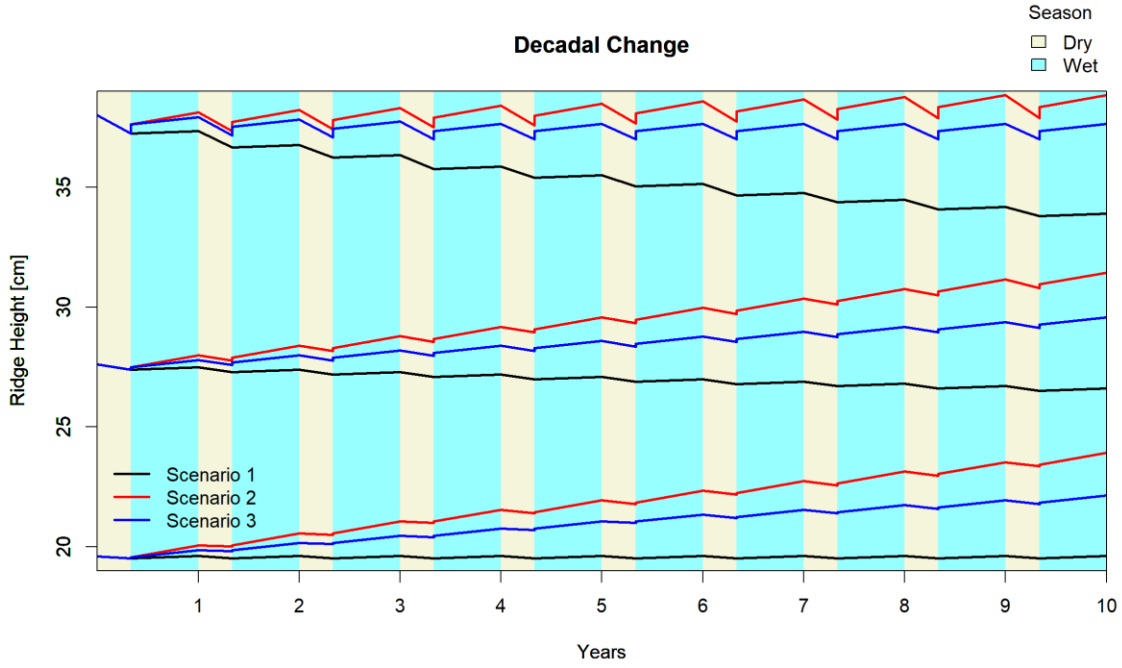

Figure 5-8. Decadal ridge heights of three soil profiles with initial heights 19.6 cm, 27.6 cm and 38 cm under all three model scenarios.

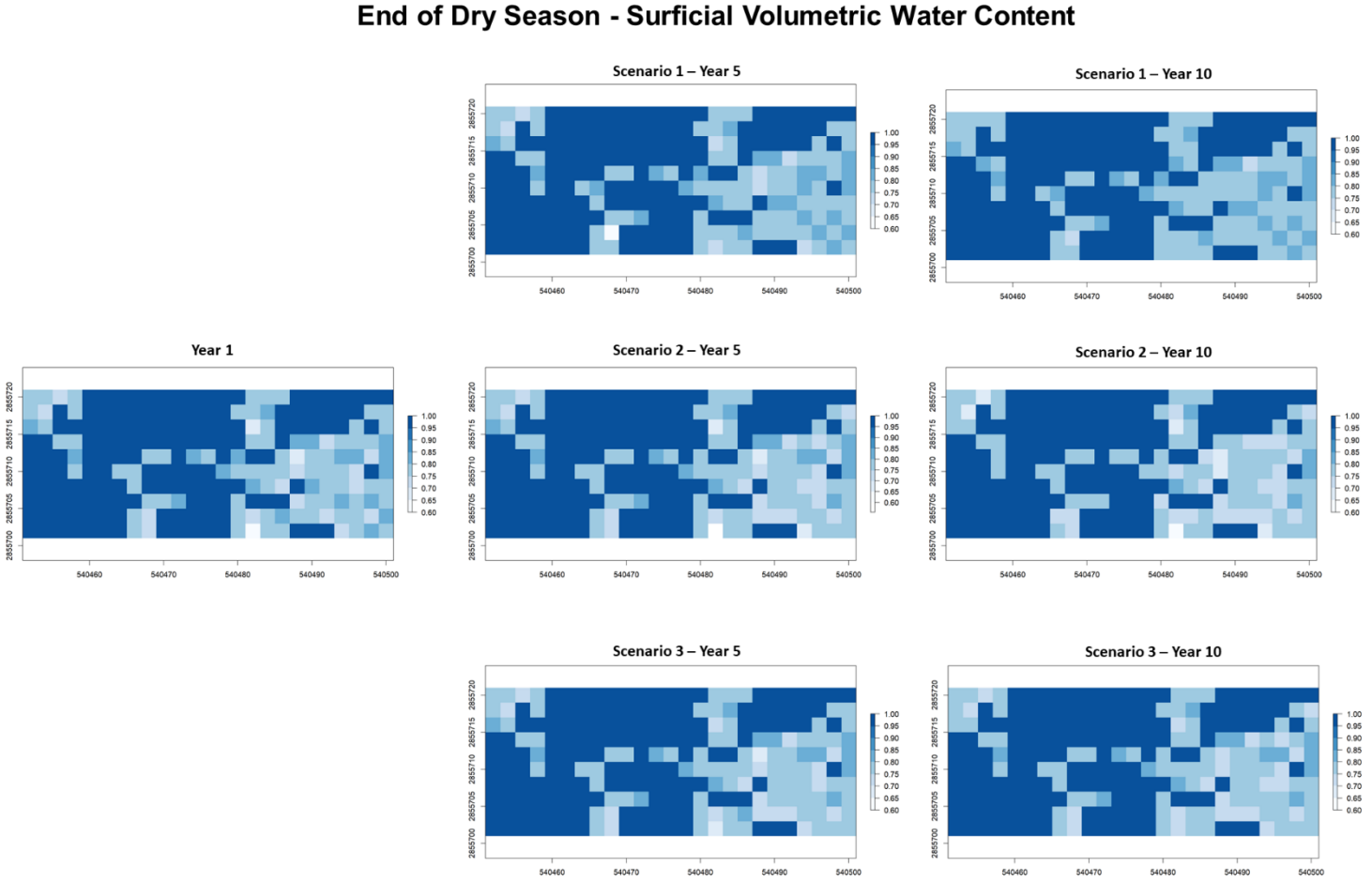

Figure 5-9. The 5-year and 10-year surficial volumetric water content for the study site is presented for all three scenarios.

5.4 Conclusion

In wetlands, accretion and aeration are processes with opposing effects on the soil elevation and the soil moisture content. Ridges, which are at a higher elevation from sloughs, periodically dry-down in the dry season, while sloughs remain inundated. The magnitude of dry-down and accretion in the Everglades post-drainage have resulted in the loss of the ridge and slough habitat – an important indicator of wetland health. This work demonstrated the applicability of the REVC model to simulate accretion and shrinkage from aeration for a decadal timescale for the ridge and slough landscape. Three different scenarios are modeled – 1) low accretion, no reversible shrinkage, 2) high accretion, moderate reversible shrinkage, and 3) moderate accretion, moderate reversible shrinkage. Although Scenario 2 and Scenario 3 had higher accretion than Scenario 1, net elevation increase for ridges with higher elevation was dampened by the shrinkage, which is higher for higher elevations, indicating that accretion and shrinkage can work together to reach an equilibrium state (Larsen et al., 2007). For Scenario 1, net elevation decrease is highest at the high elevation ridges compared to lower elevation ridges indicating that presence of the water table close to the soil surface prevents the low elevation ridges from shrinking further; however, topographical flattening of the high elevation ridges is to be expected with low accretion.

Acknowledgments

The author thanks Florida International University's GIS&RS for the shapefile of the vegetation classes in WCA-3B.

References

Chambers, L.G., H.E. Steinmuller, and J.L. Breithaupt. 2019. Toward a mechanistic understanding of “peat collapse” and its potential contribution to coastal wetland loss. Ecology: e02720Available at https://onlinelibrary.wiley.com/doi/abs/10.1002/ecy.2720 (verified 24 May 2019).

DeAngelis, D.L., L.J. Gross, M. a. Huston, W.F. Wolff, D.M. Fleming, E.J. Comiskey, and S.M. Sylvester. 1998. Landscape Modeling for Everglades Ecosystem Restoration. Ecosystems 1(1): 64–75.

Gaiser, E.E., J.C. Trexler, J.H. Richards, D.L. Childers, D. Lee, A.L. Edwards, L.J. Scinto, K. Jayachandran, G.B. Noe, and R.D. Jones. 2005. Cascading Ecological Effects of Low-Level Phosphorus Enrichment in the Florida Everglades. J. Environ. Qual.

Gawlik, D.E. 2002. The effects of prey availability on the numerical response of wading birds. Ecol. Monogr.

Givnish, T.J., J.C. Volin, V.D. Owen, V.C. Volin, J.D. Muss, and P.H. Glaser. 2008. Vegetation differentiation in the patterned landscape of the central Everglades: importance of local and landscape drivers. Glob. Ecol. Biogeogr. 17(3): 384–402Available at http://dx.doi.org/10.1111/j.1466-8238.2007.00371.x.

Hagerthey, S.E., J.J. Cole, and D. Kilbane. 2010. Aquatic metabolism in the Everglades: Dominance of water column heterotrophy. Limnol. Oceanogr. 55(2): 653–666.

Harvey, J.W., P.R. Wetzel, T.E. Lodge, V.C. Engel, and M.S. Ross. 2017. Role of a naturally varying flow regime in Everglades restoration. Restor. Ecol. 25: S27–S38.

Jorczak, E. 2006. Influence Of Hydrology on Everglades Ridge and Slough Soil Topography.

Larsen, L.G., and J.W. Harvey. 2010. How vegetation and sediment transport feedbacks drive landscape change in the Everglades and wetlands worldwide. Am. Nat.

Larsen, L.G., J.W. Harvey, and J.P. Crimaldi. 2007. A delicate balance: Ecohydrological feedbacks governing landscape morphology in a lotic peatland. Ecol. Monogr.

Lewis, C.G. 2005. Linkages among vegetative substrate quality, biomass production, and decomposition in maintaining Everglades ridge and slough vegetative communities.

McVoy, C., W. Park Said, J. Obeysekera, J. VanArman, and T. Dreschel. 2012. Landscapes and Hydrology of the Predrainage Everglades.

Ogden, J.C. 2005. Everglades ridge and slough conceptual ecological model. Wetlands 25(4): 810–820.

Oleszczuk, R., K. Bohne, J. Szatylowicz, T. Brandyk, and T. Gnatowski. 2003. Influence of load on shrinkage behavior of peat soils. J. Plant Nutr. Soil Sci. 166(2): 220–224.

SCT. 2003. The Role of Flow in the Everglades Ridge and Slough Pattern.

Sklar, F., C. Mcvoy, R. Van Zee, D. Gawlik, W. Park, C. Fitz, Y. Wu, D. Rudnick, S. Miao, A. Ferriter, S. Krupa, T. Armentano, K. Tarboton, K. Rutchey, Q. Dong, and S. Newman. 2000. Everglades Consolidated Report Chapter 2 : Hydrologic Needs : The Effects of Altered Hydrology on the Everglades. : 2:1–68.

Trexler, J.C., and C.W. Goss. 2009. Aquatic fauna as indicators for Everglades restoration: Applying dynamic targets in assessments. Ecol. Indic.

Watts, D.L., M.J. Cohen, J.B. Heffernan, and T.Z. Osborne. 2010. Hydrologic modification and the loss of self-organized patterning in the ridge-slough mosaic of the Everglades. Ecosystems 13(6): 813–827.

6. CONCLUSIONS AND RECOMMENDATIONS

6.1 Summary of Conclusions

Peatlands are a valuable ecosystem – the loss of which has been exacerbated through anthropogenic effects. The Everglades in South Florida is one such peatland where competing demands from agriculture, urbanization, and flood control among others have resulted in the intense management and subsequent loss of horizontal and vertical spatial extent of the wetland. There is strong evidence that the draining of peatlands results in their subsidence and this has been the case for the Everglades as well. Losses of up to 12 feet have been reported in parts of the system like the EAAs where water levels have been consistently lowered for cultivation for close to a century. Peat loss through draining occurs through the compaction of voids, bio-chemical oxidation, collapse of the plant root network (from plant death), or dissolution of carbonates in the soil column. Some of this loss is reversible since peat is a highly porous soil matrix that deforms with the changes in the water table. Hydrology controls the processes that result in peat loss and is the key to the restoration of peatlands.

This work focused on the development of a deterministic model which couples unsaturated flow in the vadose zone with subsidence of soil. The overall objective of this research was to study the vadose zone hydrology in the Everglades environment using numerical methods. This required a comprehensive approach which involved investigating soil physical properties, soil hydraulic properties, soil volume changing behavior, parameterization model, unsaturated zone transport model and unsaturated subsidence models. Described herewith is a summary of the objectives.

The overall objective of the second chapter was to characterize and investigate the physical properties (OC, FC and BD), the hydraulic properties and shrinkage of soils in the Everglades (K_{sat} and SWRC), with the intention of developing a dataset of soil hydraulic parameters to be used in the numerical modeling effort. Laboratory methods were employed to determine the OC, FC, BD, K_{sat}, SWRC and shrinkage of 53 Everglades soils.

Agglomerative clustering with oedometer raw data was used to characterize the soil properties resulting in three distinct clusters of marl, peat and mixed marl-peat. Differences between the hydraulic behavior of the three media were established. To study the effect of volume change on the SWRC, vGM models were generated with and without volume change. In general, it was found that ignoring volume change results in severe underestimation of the VWC of the sample particularly at higher applied pressure heads. Some deviations from the expected SWRC models were observed for the vGM models generated with volume change. Peat SWRCs tended to deviate more than marl when volume change was considered. The deviations were attributed to the collapse of macropores which results in significant change in the total volume of the sample; hence, for some samples, the VWC at a higher applied pressure was found to be higher than the previous applied pressure. Similar behavior was reported for reed-sedge peat in Germany. A comparison of the peat properties across the Everglades system found that peat of the northern marshes are more fibric compared to the southern marshes as a result of the longer wetting cycles in the north; however, the sample size of this study was insufficient to draw conclusions on the effect of vegetation type on peat.

The overall objective of the third chapter was to propose, develop and test a one-dimensional unsaturated flow model for a volume-changing matrix. A finite-difference solution to the widely applied RE was presented, and a model, called REVC, which incorporates the height change of the soil matrix using a look-up table created from HCR to update the cell heights at each timestep of the numerical model was proposed and implemented in RStudio. Since it was not possible to verify the code with the height change component (lack of examples in literature for comparison), the code was verified using four HYDRUS examples (1) downward infiltration, 2) upward infiltration, 3) system-dependent atmospheric boundary condition, and 4) system-dependent atmospheric boundary condition with bottom tension). An HCR value of 1 at all pressure heads was applied to produce simulation with no-change in the height of the soil matrix, as is the case in the examples; the model results produced similar distributions of pressure head with time as the examples. The three typical cases with the application of volume-change in vadose zone models were tested; these are - 1) vGM NonVC RE, 2) vGM NonVC RE, and vGM VC REVC. The tests were performed for the case of a shallow aquifer with a system dependent upper boundary condition and a constant saturation (water table) lower boundary condition. Models that do not incorporate volume change both at the model parameterization level as well as at the transport model level predicted lower surface pressure heads; and hence a lower VWC. Models that incorporate volume-change at the parameterization level but not at the transport level produced similar solutions to the models that incorporate volume-change at both levels, except for narrow ranges of parameters α, n, and K_{sat} which cause a significant change drop in the surficial pressure

head. A high α, low n, and low K_{sat} can contribute to the low surficial pressure head resulting in significant differences in solutions based on transport model type.

Testing of the developed model with lysimeter cores showed good results for the peat lysimeter and the layered marl-peat lysimeter. Using the range of parameters generated in Chapter 2, a combination of vGM parameters that could model the surficial VWC with an $RMSE_N$ less than 13.1% was obtained; however, for the layered peat-marl lysimeter the best fit model had an $RMSE_N$ of 29.9% indicating a fair fit. The combination of vGM parameters selected for the top peat layer of layered peat-marl was almost identical to top layer of the peat lysimeter; however, the former had a much higher K_{sat} than the latter. For this reason, the observed VWC at the end of the 50-day period of the layered peat-marl lysimeter is higher than the peat lysimeter. According to the simulations, for shallow vadose zones, a higher K_{sat} delivers more moisture from the water table to the soil surface over time. The HCR values estimated to produce the observed subsidence in the lysimeter cores are much lower than the laboratory derived values. For the selected soil hydraulic models of the lysimeter cores, the pressure head at the surface is never more negative than 6 kPa; hence, the HCR values of 0.58 (Lysimeter 2 - Peat), 0.79 (Lysimeter 1 - Marl), and 0.69 (Lysimeter 3 - Peat) at 6 kPa are required to produce the measured subsidence whereas, the lab derived HCR is 1 indicating no change. It is possible that when HCR values were determined in the laboratory with the oedometer test, minor changes in the sample height might have gone unnoticed; however, there is no justification for the magnitude of difference in the HCR values generated by the two methods. The only explanation possible explanations are: 1) the matric pressure at the surface may actually be

lower than that predicted by the model; or 2) the process of sampling the lysimeter cores may have compromised the structure of the sample resulting in significant consolidation of the sample once the water table is dropped.

The overall objective of the fourth chapter was to apply the developed model with non-steady boundary conditions to a site in Shark River Slough, Everglades where the subsidence of the root zone was measured. Using the characterization of the site by the previous study, the geometry of the soil profile was set up with a single layer of peat with an initial soil height of 35 cm. Top and bottom boundary conditions were calculated from daily evapotranspiration and water stage data, respectively. The soil hydraulic property model of peat obtained from the peat lysimeter in Chapter 2 was applied. The model was run for a period of 455 days with different HCR at 6 kPa values (from 0.93 to 0.98). It was observed that HCR of 0.96 at 6 kPa presented the best fit to the observational data with 10 observations in the simulated; the selected HCR is much higher than the HCR obtained for peat through lysimeter testing; however, it is comparable to the laboratory generated value. Using an HCR 0.96 at 6 kPa, the degree of saturation of the soil profile, soil profile height, and cell thickness were generated. Strong correlation between the water table height and soil profile height was observed. The degree of saturation varied between 0.77 and 1 with 1 indicating complete saturation. Complete saturation is also observed above the phreatic surface in an area known as the capillary fringe or the capillary zone, in which water is still held under tension. The full calibration and validation of the HCR model at this site was not possible due to the unavailability of daily observational subsidence data. Furthermore, the soil hydraulic model could not be calibrated to this specific site due to the lack of soil moisture data.

The overall objective of the fifth chapter was to demonstrate the practical application of REVC to model hydrological subsidence and study the changes in the topography of the ridge and slough landscape. Three scenarios were modeled: 1) low accretion, no reversible shrinkage, 2) high accretion, moderate reversible shrinkage, and 3) moderate accretion, moderate reversible shrinkage. A decrease in ridge height with time, particularly for the higher elevation ridge cells was observed under Scenario 1; however, interestingly, the surficial VWC at the end of the dry season for the high elevation ridge cells significantly increased over the 10-year time period. Net increase in elevation was observed for Scenario 2 and Scenario 3; however, higher elevation ridge cells did not see significant increase in ridge elevation compared to low elevation ridge cells, indicating a state of possible equilibrium between accretion and shrinkage maybe observed with time.

6.2 Recommendations

- This work used soil samples collected from the R-EMAP sampling effort which employed a probability-based sampling scheme to retrieve metrics for wetland health. While the scale of the sampling efforts was used to derive useful information about overall soil hydraulic properties of peat, marl and marl-peat, it can result in over sampling of some areas compared to the others. A more focused soil sampling effort – one that takes into consideration the vegetation and hydrological patterns at each site could be used to establish differences in the soil hydraulic properties as a result of these drivers within the presently developed soil classification. Furthermore, a more robust, depth-based sampling effort could establish the vertical variability in soil properties. Since the decomposition of the soil varies considerably with depth, the effect of

decomposition on soil hydraulic properties can be studied with a depth-based sampling approach; this would further the knowledge of this study which only samples the top 10 cm of the soil. Depth-based parametrization is also expected to increase transport model accuracy.

- The current study used the closed-chamber oedometer method (using the F1-15 Pressure Plate Apparatus) to develop the SWRCs and corresponding shrinkage at applied pressure heads. This device applies an incremental pressure following which the soils are allowed to equilibrate before readings of VWC and shrinkage are taken. This method assumes that, at equilibrium, the applied pressure and the matric pressure are equal. While this is a common assumption, the continuous measurement of VWC using outflow tubes while recording the corresponding matric pressure head of the soil using a tensiometer would result in a more accurate estimation of the SWRC. A method to measure the continuous shrinkage during desaturation could result in the development of a continuous function which can relate both matric head and VWC to the soil shrinkage.
- Due to the lack of sufficient soil samples and time, this work used the saturated VWC along with the VWC at four incremental pressure heads of 6 kPa, 10 kPa, 50 kPa and 1500 kPa to develop SWRCs capable of modeling the overall range of pressures expected in unsaturated zones. However, for wetland soils, since matric pressure head on the surface is rarely very negative – as confirmed by the modeling efforts, the development of SWRC should focus on the lower range of the applied pressure head with more data points in the 0 kPa to 50 kPa range.

- Some deviations from typical SWRC behavior were observed, particularly for peat, when volume change was included in the calculation of VWC of the sample. The abrupt change in the volume of the sample compared to the preceding recorded volume is the cause of this behavior. Previous studies that have investigated the shrinkage of reed-sedge peats in Germany have reported similar observations. The exact cause of these deviations is not obvious. Due to the low range of applied pressure head at which these deviations are typically observed, the collapse of large pores called macropores is hypothesized. Future work to investigate this phenomenon using continuously measuring shrinkage and VWC at applied pressures should be employed. Furthermore, computed tomography technology can be used to develop scans of the soil matrix at the incremental pressures to investigate the hypothesized phenomenon. The conventional SWRC models need to be modified to be able to handle the deviations from volume-change.
- The present study was tested using experimental data from a 50-day dry-down of three lysimeters whose surficial moisture content was observed with TDR sensors and the subsidence at the end of the experimental period was recorded. This method of data collection does not measure the matric head. Future work should also simultaneously measure the matric potential of the soil using tensiometers preferable at multiple depths. Such an experimental set-up would allow the non-destructive estimation of the SWRC. In addition, the elevation change of the soil surface should be estimated using a SET, which can measure minor changes in the surface elevation. The present study conducted the tests with large cores to allow for greater control over the water table depth than field tests. However, the extraction of cores can result in loss of structural

integrity of the soil, despite the best efforts to ameliorate them. Ideally, a model calibration and validation at a field site using tensiometers (to measure matric potential), TDR probes (to measure VWC), and SETs (to measure surface elevation) is recommended.

APPENDICES

APPENDIX A – Data Tables with Laboratory Raw Data and Calculations

Appendix A provides the raw data and calculations for the following laboratory tests

- Soil Organic Content
- Fiber Content
- Saturated Hydraulic Conductivity
- Saturated Volumetric Water Content
- 1500 F Pressure Plate at 6 kPa, 10 kPa, 50 kPa and 1500 kPa

Table A 1. Raw laboratory data and calculations to determine soil organic content.

Sample	Container Weight [g]	Soil + Container Weight [g]	Post Burn Weight [g]	Ash Weight [g]	Organic Weight [g]	OC [%]	OC Mean [%]	OC SD [%]
22-1	73.70	87.12	85.49	11.79	1.63	12.1	11.7	0.4
22-2	69.04	81.44	79.98	10.94	1.46	11.8		
22-3	87.05	97.81	96.59	9.54	1.22	11.4		
23-1	73.70	87.39	83.98	10.28	3.41	24.9	25.2	0.3
23-2	69.04	82.04	78.73	9.69	3.31	25.5		
23-3	87.05	99.11	96.05	9.00	3.06	25.3		
24-1	74.77	83.01	80.48	5.71	2.53	30.7	30.0	1.0
24-2	69.85	79.54	76.59	6.74	2.95	30.5		
24-3	38.27	47.48	44.82	6.55	2.67	28.9		
25-1	73.70	76.83	74.14	0.44	2.69	85.9	86.5	0.5
25-2	69.04	71.75	69.40	0.35	2.35	86.9		
25-3	87.05	89.82	87.42	0.37	2.40	86.6		
27-1	69.04	83.80	82.37	13.33	1.43	9.7	9.7	0.2
27-2	69.85	84.92	83.44	13.59	1.48	9.8		
27-3	83.64	97.98	96.62	12.98	1.36	9.5		
29-1	74.77	78.82	76.64	1.87	2.18	53.8	56.0	2.3
29-2	69.85	74.36	71.73	1.88	2.63	58.3		
29-3	38.27	42.55	40.15	1.88	2.40	56.0		
30-1	73.70	83.11	81.38	7.68	1.73	18.4	18.3	0.2
30-2	69.04	78.45	76.74	7.70	1.71	18.1		
30-3	87.05	95.80	94.18	7.14	1.61	18.4		
31-1	73.70	82.85	81.59	7.89	1.26	13.8	14.0	0.2
31-2	69.04	79.32	77.87	8.83	1.45	14.1		
31-3	87.05	97.31	95.86	8.82	1.45	14.1		
33-1	74.77	78.91	76.05	1.28	2.86	69.1	68.8	0.3
33-2	69.85	74.04	71.16	1.31	2.88	68.6		
33-3	83.64	87.75	84.93	1.29	2.82	68.7		
36-1	87.05	89.55	87.31	0.26	2.24	89.6	89.0	0.6
36-2	73.70	76.04	73.97	0.27	2.07	88.5		
36-3	69.04	71.45	69.31	0.27	2.14	88.8		
37-1	73.70	75.77	73.92	0.22	1.85	89.5	89.4	0.1
37-2	69.04	71.25	69.28	0.24	1.97	89.3		
37-3	87.05	89.49	87.31	0.26	2.18	89.4		

Table A 1. Contd.

Sample	Container Weight [g]	Soil + Container Weight [g]	Post Burn Weight [g]	Ash Weight [g]	Organic Weight [g]	OC [%]	OC Mean [%]	OC SD [%]
38-1	74.77	78.18	75.74	0.96	2.44	71.7	72.0	0.6
38-2	83.64	86.89	84.53	0.89	2.36	72.7		
38-3	69.85	73.38	70.85	1.00	2.53	71.6		
40-1	69.85	85.42	83.80	13.95	1.62	10.4	10.6	0.3
40-2	83.64	98.73	97.07	13.43	1.66	11.0		
40-3	74.77	90.64	88.99	14.22	1.65	10.4		
94-1	87.05	90.27	87.42	0.37	2.85	88.5	88.6	0.1
94-2	77.77	80.59	78.09	0.32	2.50	88.7		
94-3	69.85	72.97	70.20	0.35	2.77	88.8		
96-1	74.77	77.30	75.00	0.23	2.30	90.9	89.1	1.5
96-2	69.04	71.52	69.33	0.29	2.19	88.3		
96-3	73.70	75.99	73.97	0.27	2.02	88.2		
97-1	87.05	88.84	87.24	0.19	1.60	89.4	89.0	0.5
97-2	77.77	79.51	77.97	0.20	1.54	88.5		
97-3	69.85	71.60	70.04	0.19	1.56	89.1		
104-1	77.70	80.90	78.11	0.41	2.79	87.2	88.4	1.1
104-2	69.85	72.91	70.18	0.33	2.73	89.2		
104-3	74.77	77.54	75.08	0.31	2.46	88.8		
108-1	74.78	77.53	75.08	0.31	2.44	88.8	88.8	0.1
108-2	83.64	86.08	83.92	0.28	2.16	88.7		
108-3	69.85	72.77	70.17	0.33	2.60	88.9		
112-1	74.77	78.14	75.30	0.53	2.84	84.3	84.3	0.2
112-2	69.04	72.18	69.54	0.50	2.64	84.1		
112-3	87.05	90.15	87.53	0.48	2.62	84.5		
113-1	73.70	79.09	77.00	3.30	2.10	38.9	37.0	2.7
113-2	68.04	74.19	72.10	4.06	2.09	33.9		
113-3	87.05	92.29	90.30	3.25	2.00	38.1		
116-1	69.85	72.83	70.11	0.26	2.72	91.3	89.6	1.4
116-2	74.77	77.72	75.09	0.32	2.63	89.2		
116-3	69.04	72.00	69.38	0.34	2.62	88.5		
155-1	87.05	89.49	87.38	0.33	2.11	86.5	86.3	0.4
155-2	77.77	80.14	78.09	0.32	2.05	86.5		
155-3	73.70	76.03	74.03	0.33	2.00	85.8		
156-1	83.64	87.17	84.39	0.75	2.78	78.8	80.2	1.4
156-2	74.77	78.00	75.41	0.64	2.59	80.2		
156-3	69.04	72.19	69.62	0.58	2.57	81.6		

Table A 1. Contd.

Sample	Container Weight [g]	Soil + Container Weight [g]	Post Burn Weight [g]	Ash Weight [g]	Organic Weight [g]	OC [%]	OC Mean [%]	OC SD [%]
157-1	87.05	89.52	87.31	0.26	2.21	89.5	89.0	0.4
157-2	77.77	80.23	78.05	0.28	2.18	88.6		
157-3	73.70	76.03	73.96	0.26	2.07	88.8		
158-1	73.70	76.26	74.05	0.35	2.21	86.3	86.8	0.5
158-2	83.64	86.13	83.97	0.33	2.16	86.7		
158-3	69.85	72.45	70.18	0.33	2.27	87.3		
159-1	69.04	71.67	69.71	0.67	1.96	74.5	73.2	1.4
159-2	87.04	89.70	87.75	0.71	1.95	73.3		
159-3	77.77	80.49	78.54	0.77	1.95	71.7		
161-1	73.70	83.75	80.13	6.43	3.62	36.0	37.0	0.9
161-2	83.64	93.01	89.48	5.84	3.53	37.7		
161-3	69.04	78.27	74.83	5.79	3.44	37.3		
176-1	87.04	88.74	87.16	0.12	1.58	92.9	92.6	0.3
176-2	69.04	71.05	69.19	0.15	1.86	92.5		
176-3	73.70	75.65	73.85	0.15	1.80	92.3		
177-1	69.85	71.68	69.94	0.09	1.74	95.1	94.8	0.3
177-2	74.77	76.47	74.86	0.09	1.61	94.7		
177-3	83.64	85.45	83.74	0.10	1.71	94.5		
178-1	87.04	88.95	87.17	0.13	1.78	93.2	93.4	0.2
178-2	69.04	70.70	69.15	0.11	1.55	93.4		
178-3	73.70	75.55	73.82	0.12	1.73	93.5		
179-1	69.85	72.40	70.12	0.27	2.28	89.4	89.5	0.2
179-2	74.77	77.44	75.05	0.28	2.39	89.5		
179-3	83.64	86.07	83.89	0.25	2.18	89.7		
202-1	73.69	83.51	81.96	8.26	1.55	15.8	15.5	0.2
202-2	69.04	78.18	76.76	7.72	1.41	15.5		
202-3	87.04	96.82	95.31	8.27	1.50	15.4		
203-1	74.77	83.79	82.04	7.27	1.75	19.4	18.6	0.8
203-2	73.70	81.82	80.34	6.64	1.48	18.3		
203-3	69.04	77.79	76.21	7.17	1.57	18.0		
204-1	87.05	93.92	92.75	5.70	1.16	17.0	18.4	1.6
204-2	74.77	81.73	80.47	5.69	1.27	18.2		
204-3	83.64	91.19	89.67	6.03	1.52	20.1		
206-1	69.04	74.85	72.78	3.74	2.07	35.6	40.6	4.9
206-2	87.05	92.01	89.76	2.71	2.25	45.4		
206-3	77.77	83.24	81.00	3.23	2.24	41.0		

Table A 1. Contd.

Sample	Container Weight [g]	Soil + Container Weight [g]	Post Burn Weight [g]	Ash Weight [g]	Organic Weight [g]	OC [%]	OC Mean [%]	OC SD [%]
207-1	73.70	83.42	81.63	7.94	1.79	18.4	19.5	1.6
207-2	69.04	78.11	76.41	7.37	1.70	18.7		
207-3	87.03	95.46	93.67	6.64	1.79	21.3		
209-1	74.77	78.92	76.76	1.99	2.16	52.0	51.6	0.7
209-2	83.64	87.21	85.36	1.72	1.86	51.9		
209-3	69.85	73.80	71.79	1.94	2.01	50.8		
213-1	73.70	76.41	74.03	0.33	2.38	87.7	87.8	0.1
213-2	69.04	71.65	69.36	0.32	2.30	87.9		
213-3	87.04	89.60	87.35	0.31	2.25	87.8		
214-1	74.77	77.49	75.22	0.45	2.27	83.5	83.0	0.8
214-2	83.64	86.06	84.04	0.40	2.02	83.4		
214-3	69.85	72.51	70.32	0.48	2.19	82.1		
217-1	74.71	81.96	79.95	5.24	2.02	27.8	28.0	0.7
217-2	83.64	91.63	89.45	5.81	2.19	27.3		
217-3	69.84	77.21	75.09	5.24	2.12	28.8		
218-1	73.70	77.27	74.36	0.66	2.90	81.4	81.7	0.2
218-2	69.04	72.71	69.71	0.67	3.00	81.8		
218-3	87.05	90.53	87.68	0.63	2.85	81.8		
219-1	74.77	80.43	78.55	3.77	1.88	33.3	32.2	1.2
219-2	83.64	89.47	87.67	4.03	1.80	30.9		
219-3	69.85	75.48	73.66	3.81	1.82	32.3		
220-1	73.70	77.39	74.41	0.70	2.99	80.9	81.0	0.1
220-2	69.04	73.39	69.87	0.83	3.52	80.9		
220-3	87.05	91.39	87.87	0.82	3.53	81.2		
221-1	74.77	85.52	83.18	8.40	2.34	21.8	21.8	0.0
221-2	83.64	93.28	91.18	7.54	2.11	21.8		
221-3	69.85	79.94	77.74	7.90	2.20	21.8		
252-1	73.70	78.36	75.30	1.60	3.06	65.6	64.3	1.2
252-2	69.04	73.31	70.60	1.55	2.71	63.6		
252-3	87.04	91.49	88.66	1.61	2.83	63.7		
260-1	69.04	71.67	69.34	0.30	2.33	88.6	88.5	0.6
260-2	74.77	77.16	75.06	0.29	2.10	87.9		
260-3	77.77	80.76	78.10	0.33	2.66	89.0		
264-1	69.85	74.56	72.66	2.81	1.90	40.3	40.0	0.6
264-2	87.04	92.49	90.29	3.25	2.20	40.4		
264-3	73.70	78.82	76.81	3.11	2.01	39.3		

Table A 1. Contd.

Sample	Container Weight [g]	Soil + Container Weight [g]	Post Burn Weight [g]	Ash Weight [g]	Organic Weight [g]	OC [%]	OC Mean [%]	OC SD [%]
267-1	69.04	75.34	72.76	3.72	2.58	41.0	42.5	1.8
267-2	74.77	81.10	78.43	3.66	2.67	42.2		
267-3	83.64	89.54	86.92	3.28	2.62	44.4		
268-1	69.85	73.15	70.21	0.36	2.94	89.1	89.0	0.1
268-2	87.05	90.58	87.44	0.39	3.14	89.0		
268-3	73.70	77.30	74.10	0.40	3.20	88.9		
270-1	69.04	71.43	69.31	0.27	2.12	88.7	88.4	0.3
270-2	74.77	77.20	75.05	0.28	2.15	88.5		
270-3	83.64	85.98	83.92	0.28	2.06	88.0		
300-1	69.04	70.70	69.22	0.18	1.48	89.2	89.0	0.3
300-2	87.05	88.71	87.23	0.18	1.48	89.2		
300-3	77.77	79.43	77.96	0.19	1.47	88.6		
302-1	73.70	81.29	79.00	5.30	2.29	30.2	30.4	0.2
302-2	83.64	91.71	89.25	5.61	2.46	30.5		
302-3	69.85	77.47	75.14	5.29	2.33	30.6		
303-1	69.04	71.11	69.26	0.22	1.85	89.4	86.9	3.4
303-2	87.04	88.22	87.24	0.20	0.98	83.1		
303-3	77.77	79.73	78.00	0.23	1.73	88.3		
305-1	77.77	80.00	78.05	0.28	1.95	87.4	87.4	0.2
305-2	69.85	72.12	70.13	0.28	1.99	87.7		
305-3	74.77	76.88	75.04	0.27	1.84	87.2		
312-1	69.85	71.38	69.94	0.09	1.44	94.1	93.7	0.3
312-2	74.77	76.31	74.87	0.10	1.44	93.5		
312-3	83.64	85.34	83.75	0.11	1.59	93.5		
313-1	87.05	88.68	87.13	0.08	1.55	95.1	95.2	0.2
313-2	69.04	70.78	69.12	0.08	1.66	95.4		
313-3	73.70	75.50	73.79	0.09	1.71	95.0		
314-1	69.85	72.01	69.98	0.13	2.03	94.0	94.1	0.1
314-2	87.05	89.10	87.17	0.12	1.93	94.1		
314-3	73.70	75.88	73.83	0.13	2.05	94.0		
315-1	69.04	70.88	69.19	0.15	1.69	91.8	91.8	0.2
315-2	74.77	76.44	74.91	0.14	1.53	91.6		
315-3	83.64	85.40	83.78	0.14	1.62	92.0		

Table A 2. Raw laboratory data and calculations to determine fiber content.

	Moisture Content Calculations				Fiber Content Calculations			
Code	Container Wt [g]	Pre-Oven [g]	Post-Oven [g]	MC [%]	Initial Mass [g]	Paper Wt [g]	End Wt [g]	FC [%]
25	6.609	71.291	13.589	89.2	107.028	4.348	9.482	44.5
36	6.677	77.387	12.956	91.1	111.463	4.284	8.767	45.3
94	6.494	64.379	13.575	87.8	101.881	4.257	7.274	24.2
96	6.572	64.379	13.575	87.9	100.533	4.261	6.115	15.2
97	6.475	74.610	12.047	91.8	104.284	4.310	7.221	34.1
104	6.632	78.537	13.738	90.1	108.517	4.317	7.325	28.0
108	6.686	76.926	13.932	89.7	100.083	4.342	9.265	47.7
112	6.694	79.093	14.291	89.5	109.691	4.203	5.998	15.6
116	6.665	74.525	13.672	89.7	115.001	4.193	5.261	9.0
155	6.686	62.534	13.051	88.6	110.426	4.292	7.919	28.8
157	6.663	63.733	12.844	89.2	101.471	4.135	7.314	28.9
176	6.486	62.686	10.293	93.2	99.466	4.321	6.911	38.4
177	6.549	60.448	10.542	92.6	102.531	4.275	8.653	57.6
178	6.529	72.510	11.261	92.8	102.64	4.285	6.663	32.3
179	6.563	59.691	12.732	88.4	105.934	4.219	10.456	50.7
213	6.684	57.993	12.075	89.5	108.619	4.362	8.506	36.3
218	6.631	59.092	14.791	84.4	117.394	4.380	8.255	21.2
253	6.665	74.525	12.795	91.0	107.471	4.286	7.678	34.9
260	6.691	68.049	14.200	87.8	102.254	4.398	7.565	25.3
268	6.557	77.607	15.277	87.7	102.952	4.253	7.078	22.4
270	6.564	72.481	12.841	90.5	102.758	4.178	5.819	16.8
300	6.735	64.898	12.140	90.7	103.368	4.262	6.525	23.6
303	6.686	74.662	12.551	91.4	107.022	4.330	7.365	32.9
305	6.551	73.842	13.291	90.0	100.186	4.313	7.496	31.7
312	6.444	67.678	10.925	92.7	101.109	4.196	7.094	39.2
314	6.469	58.246	11.164	90.9	102.877	4.284	6.887	27.9
316	6.659	76.158	12.901	91.0	113.329	4.228	8.911	46.0

Table A 3. Raw laboratory data for the calculation of saturated hydraulic conductivity

Saturation Date	10/23/2017	**Saturation Time**	1:21PM
Sample Code	23	**Container**	2
Sample Diameter (mm)	76.51	**Room Temperature (^{o}C)**	20
Sample Height (mm)	76.89	**Calculated Avg K_{sat} (cm/d)**	0.5
Test Date	10/26/2017	**Standard Deviation (cm/d)**	0.2

Trial	Column Height (mm)	Volume (mL)	Time (min)	K_{sat} (cm/d)
1	50	1	60	0.3
2	50	1	60	0.3
3	50	1	60	0.3
4	75	2	60	0.5
5	75	2	60	0.5
6	75	2	60	0.5
7	100	3	60	0.7
8	100	3	60	0.7
9	100	3	60	0.7

Saturation Date	10/23/2017	**Saturation Time**	1:30PM
Sample Code	25	**Container**	4
Sample Diameter (mm)	76.51	**Room Temperature (^{o}C)**	20
Sample Height (mm)	78.41	**Calculated Avg K_{sat} (cm/d)**	124.2
Test Date	10/31/2017	**Standard Deviation (cm/d)**	4.2

Trial	Column Height (mm)	Volume (mL)	Time (min)	K_{sat} (cm/d)
1	50	20	3	127.6
2	50	20	3	127.6
3	50	20	3	127.6
4	75	24	3	128.1
5	75	22	3	117.5
6	75	22	3	117.5
7	100	27	3	124.0
8	100	27	3	124.0
9	100	27	3	124.0

Table A 3. Contd.

Saturation Date	10/23/2017	**Saturation Time**	1:40PM
Sample Code	26	**Container**	5
Sample Diameter (mm)	76.51	**Room Temperature (^{o}C)**	22
Sample Height (mm)	78.41	**Calculated Avg K_{sat} (cm/d)**	19.2
Test Date	10/31/2017	**Standard Deviation (cm/d)**	0.1

Trial	Column Height (mm)	Volume (mL)	Time (min)	K_{sat} (cm/d)
1	50	5	5	19.1
2	50	5	5	19.1
3	50	5	5	19.1
4	75	6	5	19.2
5	75	6	5	19.2
6	75	6	5	19.2
7	100	7	5	19.3
8	100	7	5	19.3
9	100	7	5	19.3

Saturation Date	10/2/2016	**Saturation Time**	3:40PM
Sample Code	27	**Container**	1
Sample Diameter (mm)	76.51	**Room Temperature (^{o}C)**	20
Sample Height (mm)	82.34	**Calculated Avg K_{sat} (cm/d)**	3.2
Test Date	10/8/2016	**Standard Deviation (cm/d)**	1.0

Trial	Column Height (mm)	Volume (mL)	Time (min)	K_{sat} (cm/d)
1	50	1	10	1.9
2	50	1	10	1.9
3	50	1	10	1.9
4	75	2	10	3.3
5	75	2	10	3.3
6	75	2	10	3.3
7	100	3	10	4.2
8	100	3	10	4.2
9	100	3	10	4.2

Table A 3. Contd.

Saturation Date	10/23/2017	**Saturation Time**	5:15PM
Sample Code	29	**Container**	1
Sample Diameter (mm)	76.51	**Room Temperature (^{o}C)**	22
Sample Height (mm)	80.91	**Calculated Avg K_{sat} (cm/d)**	6.3
Test Date	10/26/2017	**Standard Deviation (cm/d)**	2.0

Trial	Column Height (mm)	Volume (mL)	Time (min)	K_{sat} (cm/d)
1	50	1	5	3.9
2	50	1	5	3.9
3	50	1	5	3.9
4	75	2	5	6.5
5	75	2	5	6.5
6	75	2	5	6.5
7	100	3	5	8.4
8	100	3	5	8.4
9	100	3	5	8.4

Saturation Date	10/26/2017	**Saturation Time**	3:00PM
Sample Code	30	**Container**	1
Sample Diameter (mm)	76.51	**Room Temperature (^{o}C)**	21
Sample Height (mm)	77.46	**Calculated Avg K_{sat} (cm/d)**	2.1
Test Date	10/29/2017	**Standard Deviation (cm/d)**	0.5

Trial	Column Height (mm)	Volume (mL)	Time (min)	K_{sat} (cm/d)
1	50	1	10	1.9
2	50	1	10	1.9
3	50	1	10	1.9
4	75	1	10	1.6
5	75	1	10	1.6
6	75	1	10	1.6
7	100	2	10	2.7
8	100	2	10	2.7
9	100	2	10	2.7

Table A 3. Contd.

Saturation Date	10/26/2017	**Saturation Time**	3:00PM
Sample Code	31	**Container**	2
Sample Diameter (mm)	76.51	**Room Temperature (^{o}C)**	21
Sample Height (mm)	77.83	**Calculated Avg K_{sat} (cm/d)**	2.1
Test Date	10/29/2017	**Standard Deviation (cm/d)**	0.5

Trial	Column Height (mm)	Volume (mL)	Time (min)	K_{sat} (cm/d)
1	50	1	10	1.9
2	50	1	10	1.9
3	50	1	10	1.9
4	75	1	10	1.6
5	75	1	10	1.6
6	75	1	10	1.6
7	100	2	10	2.7
8	100	2	10	2.7
9	100	2	10	2.7

Saturation Date	11/8/2017	**Saturation Time**	1:30PM
Sample Code	33	**Container**	6
Sample Diameter (mm)	76.51	**Room Temperature (^{o}C)**	20
Sample Height (mm)	77.23	**Calculated Avg K_{sat} (cm/d)**	6.3
Test Date	11/12/2017	**Standard Deviation (cm/d)**	0.5

Trial	Column Height (mm)	Volume (mL)	Time (min)	K_{sat} (cm/d)
1	50	3	10	5.7
2	50	3	10	5.7
3	50	3	10	5.7
4	75	4	10	6.4
5	75	4	10	6.4
6	75	4	10	6.4
7	100	5	10	6.8
8	100	5	10	6.8
9	100	5	10	6.8

Table A 3. Contd.

Saturation Date	10/2/2016	**Saturation Time**	3:40PM
Sample Code	34	**Container**	2
Sample Diameter (mm)	76.51	**Room Temperature (^{o}C)**	20
Sample Height (mm)	79.14	**Calculated Avg K_{sat} (cm/d)**	7.3
Test Date	10/8/2016	**Standard Deviation (cm/d)**	0.7

Trial	Column Height (mm)	Volume (mL)	Time (min)	K_{sat} (cm/d)
1	50	4	10	7.7
2	50	4	10	7.7
3	50	4	10	7.7
4	75	4	10	6.4
5	75	4	10	6.4
6	75	5	10	8.0
7	100	6	10	8.3
8	100	5	10	6.9
9	100	5	10	6.9

Saturation Date	10/2/2016	**Saturation Time**	3:40PM
Sample Code	36	**Container**	4
Sample Diameter (mm)	76.51	**Room Temperature (^{o}C)**	20
Sample Height (mm)	83.16	**Calculated Avg K_{sat} (cm/d)**	31.4
Test Date	10/10/2016	**Standard Deviation (cm/d)**	1.2

Trial	Column Height (mm)	Volume (mL)	Time (min)	K_{sat} (cm/d)
1	50	16	10	31.3
2	50	16	10	31.3
3	50	16	10	31.3
4	75	18	10	29.7
5	75	19	10	31.3
6	75	18	10	29.7
7	100	23	10	32.7
8	100	23	10	32.7
9	100	23	10	32.7

Table A 3. Contd.

Saturation Date	10/26/2017	**Saturation Time**	3:00PM
Sample Code	94	**Container**	3
Sample Diameter (mm)	76.51	**Room Temperature (^{o}C)**	21
Sample Height (mm)	79.91	**Calculated Avg K_{sat} (cm/d)**	22.4
Test Date	10/29/2017	**Standard Deviation (cm/d)**	1.1

Trial	Column Height (mm)	Volume (mL)	Time (min)	K_{sat} (cm/d)
1	50	6	5	23.1
2	50	6	5	23.1
3	50	6	5	23.1
4	75	7	5	22.6
5	75	7	5	22.6
6	75	7	5	22.6
7	100	8	5	22.3
8	100	7	5	19.5
9	100	8	5	22.3

Saturation Date	11/15/2017	**Time**	2:30PM
Sample Code	97	**Container**	1
Sample Diameter (mm	76.51	**Room Temperature (^{o}C)**	22
Sample Height (mm)	76.42	**Calculated Avg K_{sat} (cm/d)**	8.1
Test Date	11/18/2017	**Standard Deviation (cm/d)**	0.6

Trial	Column Height (mm)	Volume (mL)	Time (min)	K_{sat} (cm/d)
1	50	5	10	9.5
2	50	4	10	7.6
3	50	4	10	7.6
4	75	5	10	7.9
5	75	5	10	7.9
6	75	5	10	7.9
7	100	6	10	8.1
8	100	6	10	8.1
9	100	6	10	8.1

Table A 3. Contd.

Saturation Date	11/15/2017	**Time**	2:30PM
Sample Code	104	**Container**	2
Sample Diameter (mm	76.51	**Room Temperature (^{o}C)**	22
Sample Height (mm)	77.89	**Calculated Avg K_{sat} (cm/d)**	3.7
Test Date	11/18/2017	**Standard Deviation (cm/d)**	0.4

Trial	Column Height (mm)	Volume (mL)	Time (min)	K_{sat} (cm/d)
1	50	2	10	3.8
2	50	2	10	3.8
3	50	2	10	3.8
4	75	2	10	3.2
5	75	2	10	3.2
6	75	2	10	3.2
7	100	3	10	4.1
8	100	3	10	4.1
9	100	3	10	4.1

Saturation Date	10/2/2016	**Saturation Time**	3:40PM
Sample Code	108	**Container**	6
Sample Diameter (mm)	76.51	**Room Temperature (^{o}C)**	20
Sample Height (mm)	85.97	**Calculated Avg K_{sat} (cm/d)**	10.9
Test Date	10/10/2016	**Standard Deviation (cm/d)**	0.9

Trial	Column Height (mm)	Volume (mL)	Time (min)	K_{sat} (cm/d)
1	50	6	10	11.9
2	50	5	10	9.9
3	50	5	10	9.9
4	75	6	10	10.0
5	75	7	10	11.7
6	75	6	10	10.0
7	100	8	10	11.6
8	100	8	10	11.6
9	100	8	10	11.6

Table A 3. Contd.

Saturation Date	11/15/2017	**Time**	2:30PM
Sample Code	112	**Container**	3
Sample Diameter (mm	76.51	**Room Temperature (^{o}C)**	22
Sample Height (mm)	76.64	**Calculated Avg K_{sat} (cm/d)**	2.6
Test Date	11/18/2017	**Standard Deviation (cm/d)**	0.6

Trial	Column Height (mm)	Volume (mL)	Time (min)	K_{sat} (cm/d)
1	50	1	10	1.9
2	50	1	10	1.9
3	50	1	10	1.9
4	75	2	10	3.2
5	75	2	10	3.2
6	75	2	10	3.2
7	100	2	10	2.7
8	100	2	10	2.7
9	100	2	10	2.7

Saturation Date	11/15/2017	**Time**	2:30PM
Sample Code	113	**Container**	4
Sample Diameter (mm	76.51	**Room Temperature (^{o}C)**	21
Sample Height (mm)	79.34	**Calculated Avg K_{sat} (cm/d)**	2.6
Test Date	11/18/2017	**Standard Deviation (cm/d)**	0.6

Trial	Column Height (mm)	Volume (mL)	Time (min)	K_{sat} (cm/d)
1	50	1	10	1.9
2	50	1	10	1.9
3	50	1	10	1.9
4	75	2	10	3.2
5	75	2	10	3.2
6	75	2	10	3.2
7	100	2	10	2.8
8	100	2	10	2.8
9	100	2	10	2.8

Table A 3. Contd.

Saturation Date	11/15/2017	**Time**	2:30PM
Sample Code	116	**Container**	5
Sample Diameter (mm	76.51	**Room Temperature (^{o}C)**	21
Sample Height (mm)	78.69	**Calculated Avg K_{sat} (cm/d)**	3.7
Test Date	11/18/2017	**Standard Deviation (cm/d)**	0.4

Trial	Column Height (mm)	Volume (mL)	Time (min)	K_{sat} (cm/d)
1	50	2	10	3.8
2	50	2	10	3.8
3	50	2	10	3.8
4	75	2	10	3.2
5	75	2	10	3.2
6	75	2	10	3.2
7	100	3	10	4.1
8	100	3	10	4.1
9	100	3	10	4.1

Saturation Date	9/22/2016	**Saturation Time**	2:30PM
Sample Code	155	**Container**	1
Sample Diameter (mm)	76.51	**Room Temperature (^{o}C)**	20
Sample Height (mm)	79.14	**Calculated Avg K_{sat} (cm/d)**	13.74
Test Date	9/29/2016	**Standard Deviation (cm/d)**	0.52

Trial	Column Height (mm)	Volume (mL)	Time (min)	K_{sat} (cm/d)
1	50	7	10	13.44
2	50	7	10	13.44
3	50	7	10	13.44
4	75	9	10	14.48
5	75	9	10	14.48
6	75	8	10	12.87
7	100	10	10	13.84
8	100	10	10	13.84
9	100	10	10	13.84

Table A 3. Contd.

Saturation Date	9/22/2016	**Saturation Time**	2:30PM
Sample Code	156	**Container**	2
Sample Diameter (mm)	76.51	**Room Temperature (^{o}C)**	20
Sample Height (mm)	81.00	**Calculated Avg K_{sat} (cm/d)**	9.76
Test Date	9/28/2016	**Standard Deviation (cm/d)**	0.06

Trial	Column Height (mm)	Volume (mL)	Time (min)	K_{sat} (cm/d)
1	50	5	10	9.69
2	50	5	10	9.69
3	50	5	10	9.69
4	75	6	10	9.76
5	75	6	10	9.76
6	75	6	10	9.76
7	100	7	10	9.82
8	100	7	10	9.82
9	100	7	10	9.82

Saturation Date	9/22/2016	**Saturation Time**	2:30PM
Sample Code	158	**Container**	4
Sample Diameter (mm)	76.51	**Room Temperature (^{o}C)**	20
Sample Height (mm)	79.03	**Calculated Avg K_{sat} (cm/d)**	14.4
Test Date	9/30/2016	**Standard Deviation (cm/d)**	0.8

Trial	Column Height (mm)	Volume (mL)	Time (min)	K_{sat} (cm/d)
1	50	7	10	13.4
2	50	7	10	13.4
3	50	7	10	13.4
4	75	9	10	14.5
5	75	9	10	14.5
6	75	9	10	14.5
7	100	11	10	15.2
8	100	11	10	15.2
9	100	11	10	15.2

Table A 3. Contd.

Saturation Date	9/22/2016	**Saturation Time**	2:30PM
Sample Code	159	**Container**	5
Sample Diameter (mm)	76.51	**Room Temperature (^{o}C)**	20
Sample Height (mm)	74.71	**Calculated Avg K_{sat} (cm/d)**	14.6
Test Date	9/28/2016	**Standard Deviation (cm/d)**	0.4

Trial	Column Height (mm)	Volume (mL)	Time (min)	K_{sat} (cm/d)
1	50	8	10	15.0
2	50	8	10	15.0
3	50	8	10	15.0
4	75	9	10	14.1
5	75	9	10	14.1
6	75	9	10	14.1
7	100	11	10	14.7
8	100	11	10	14.7
9	100	11	10	14.7

Saturation Date	9/22/2016	**Saturation Time**	2:30PM
Sample Code	161	**Container**	6
Sample Diameter (mm)	76.51	**Room Temperature (^{o}C)**	20
Sample Height (mm)	85.77	**Calculated Avg K_{sat} (cm/d)**	18.7
Test Date	9/29/2016	**Standard Deviation (cm/d)**	0.8

Trial	Column Height (mm)	Volume (mL)	Time (min)	K_{sat} (cm/d)
1	50	10	10	19.8
2	50	9	10	17.8
3	50	9	10	17.8
4	75	12	10	20.1
5	75	11	10	18.4
6	75	11	10	18.4
7	100	13	10	18.8
8	100	13	10	18.8
9	100	13	10	18.8

Table A 3. Contd.

Saturation Date	10/26/2016	**Saturation Time**	2:00PM
Sample Code	176	**Container**	5
Sample Diameter (mm)	76.51	**Room Temperature (^{o}C)**	20
Sample Height (mm)	77.64	**Calculated Avg K_{sat} (cm/d)**	2.1
Test Date	10/29/2016	**Standard Deviation (cm/d)**	0.5

Trial	Column Height (mm)	Volume (mL)	Time (min)	K_{sat} (cm/d)
1	50	1	10	1.9
2	50	1	10	1.9
3	50	1	10	1.9
4	75	1	10	1.6
5	75	1	10	1.6
6	75	1	10	1.6
7	100	2	10	2.7
8	100	2	10	2.7
9	100	2	10	2.7

Saturation Date	10/26/2016	**Saturation Time**	2:00PM
Sample Code	177	**Container**	6
Sample Diameter (mm)	76.51	**Room Temperature (^{o}C)**	20
Sample Height (mm)	79.24	**Calculated Avg K_{sat} (cm/d)**	7.0
Test Date	10/29/2016	**Standard Deviation (cm/d)**	0.5

Trial	Column Height (mm)	Volume (mL)	Time (min)	K_{sat} (cm/d)
1	50	4	10	7.7
2	50	4	10	7.7
3	50	4	10	7.7
4	75	4	10	6.4
5	75	4	10	6.4
6	75	4	10	6.4
7	100	5	10	6.9
8	100	5	10	6.9
9	100	5	10	6.9

Table A 3. Contd.

Saturation Date	10/26/2016	**Saturation Time**	2:00PM
Sample Code	178	**Container**	1
Sample Diameter (mm)	76.51	**Room Temperature (^{o}C)**	20
Sample Height (mm)	88.25	**Calculated Avg K_{sat} (cm/d)**	3.3
Test Date	10/29/2016	**Standard Deviation (cm/d)**	1.0

Trial	Column Height (mm)	Volume (mL)	Time (min)	K_{sat} (cm/d)
1	50	1	10	2.0
2	50	1	10	2.0
3	50	1	10	2.0
4	75	2	10	3.4
5	75	2	10	3.4
6	75	2	10	3.4
7	100	3	10	4.4
8	100	3	10	4.4
9	100	3	10	4.4

Saturation Date	10/26/2016	**Saturation Time**	2:00PM
Sample Code	179	**Container**	3
Sample Diameter (mm)	76.51	**Room Temperature (^{o}C)**	20
Sample Height (mm)	77.46	**Calculated Avg K_{sat} (cm/d)**	114.2
Test Date	10/29/2016	**Standard Deviation (cm/d)**	29.4

Trial	Column Height (mm)	Volume (mL)	Time (min)	K_{sat} (cm/d)
1	50	8	1	152.4
2	50	8	1	152.4
3	50	8	1	152.4
4	75	11	2	87.6
5	75	11	2	87.6
6	75	11	2	87.6
7	100	15	2	102.6
8	100	15	2	102.6
9	100	15	2	102.6

Table A 3. Contd.

Saturation Date	3/21/2017	**Saturation Time**	5:10PM
Sample Code	180	**Container**	2
Sample Diameter (mm)	76.51	**Room Temperature (^{o}C)**	20
Sample Height (mm)	78.56	**Calculated Avg K_{sat} (cm/d)**	6.2
Test Date	3/24/2017	**Standard Deviation (cm/d)**	1.9

Trial	Column Height (mm)	Volume (mL)	Time (min)	K_{sat} (cm/d)
1	50	1	5	3.8
2	50	1	5	3.8
3	50	1	5	3.8
4	75	2	5	6.4
5	75	2	5	6.4
6	75	2	5	6.4
7	100	3	5	8.3
8	100	3	5	8.3
9	100	3	5	8.3

Saturation Date	11/8/2017	**Saturation Time**	1:30PM
Sample Code	202	**Container**	1
Sample Diameter (mm)	76.51	**Room Temperature (^{o}C)**	20
Sample Height (mm)	77.71	**Calculated Avg K_{sat} (cm/d)**	2.1
Test Date	11/11/2017	**Standard Deviation (cm/d)**	0.5

Trial	Column Height (mm)	Volume (mL)	Time (min)	K_{sat} (cm/d)
1	50	1	10	1.9
2	50	1	10	1.9
3	50	1	10	1.9
4	75	1	10	1.6
5	75	1	10	1.6
6	75	1	10	1.6
7	100	2	10	2.7
8	100	2	10	2.7
9	100	2	10	2.7

Table A 3. Contd.

Saturation Date	11/8/2017	**Saturation Time**	1:30PM
Sample Code	203	**Container**	2
Sample Diameter (mm)	76.51	**Room Temperature (^{o}C)**	20
Sample Height (mm)	78.87	**Calculated Avg K_{sat} (cm/d)**	1.0
Test Date	11/11/2017	**Standard Deviation (cm/d)**	0.3

Trial	Column Height (mm)	Volume (mL)	Time (min)	K_{sat} (cm/d)
1	50	1	20	1.0
2	50	1	20	1.0
3	50	1	20	1.0
4	75	1	20	0.8
5	75	1	20	0.8
6	75	1	20	0.8
7	100	2	20	1.4
8	100	2	20	1.4
9	100	2	20	1.4

Saturation Date	11/8/2017	**Saturation Time**	1:30PM
Sample Code	204	**Container**	3
Sample Diameter (mm)	76.51	**Room Temperature (^{o}C)**	20
Sample Height (mm)	76.51	**Calculated Avg K_{sat} (cm/d)**	2.1
Test Date	11/11/2017	**Standard Deviation (cm/d)**	0.5

Trial	Column Height (mm)	Volume (mL)	Time (min)	K_{sat} (cm/d)
1	50	1	10	1.9
2	50	1	10	1.9
3	50	1	10	1.9
4	75	1	10	1.6
5	75	1	10	1.6
6	75	1	10	1.6
7	100	2	10	2.7
8	100	2	10	2.7
9	100	2	10	2.7

Table A 3. Contd.

Saturation Date	11/8/2017	**Saturation Time**	1:30PM
Sample Code	206	**Container**	4
Sample Diameter (mm)	76.51	**Room Temperature (^{o}C)**	20
Sample Height (mm)	76.57	**Calculated Avg K_{sat} (cm/d)**	4.0
Test Date	11/12/2017	**Standard Deviation (cm/d)**	1.6

Trial	Column Height (mm)	Volume (mL)	Time (min)	K_{sat} (cm/d)
1	50	1	10	1.9
2	50	1	10	1.9
3	50	1	10	1.9
4	75	3	10	4.7
5	75	3	10	4.7
6	75	3	10	4.7
7	100	4	10	5.4
8	100	4	10	5.4
9	100	4	10	5.4

Saturation Date	11/8/2017	**Saturation Time**	1:30PM
Sample Code	207	**Container**	5
Sample Diameter (mm)	76.51	**Room Temperature (^{o}C)**	20
Sample Height (mm)	80.37	**Calculated Avg K_{sat} (cm/d)**	1.6
Test Date	11/12/2017	**Standard Deviation (cm/d)**	0.2

Trial	Column Height (mm)	Volume (mL)	Time (min)	K_{sat} (cm/d)
1	50	1	10	1.9
2	50	1	10	1.9
3	50	1	10	1.9
4	75	1	10	1.6
5	75	1	10	1.6
6	75	1	10	1.6
7	100	1	10	1.4
8	100	1	10	1.4
9	100	1	10	1.4

Table A 3. Contd.

Saturation Date	11/1/2017	**Saturation Time**	11:00AM
Sample Code	209	**Container**	1
Sample Diameter (mm)	76.51	**Room Temperature (^{o}C)**	20
Sample Height (mm)	91.81	**Calculated Avg K_{sat} (cm/d)**	4.0
Test Date	11/4/2017	**Standard Deviation (cm/d)**	0.5

Trial	Column Height (mm)	Volume (mL)	Time (min)	K_{sat} (cm/d)
1	50	2	10	4.1
2	50	2	10	4.1
3	50	2	10	4.1
4	75	2	10	3.4
5	75	2	10	3.4
6	75	2	10	3.4
7	100	3	10	4.5
8	100	3	10	4.5
9	100	3	10	4.5

Saturation Date	10/2/2016	**Saturation Time**	3:40PM
Sample Code	211	**Container**	5
Sample Diameter (mm)	76.51	**Room Temperature (^{o}C)**	20
Sample Height (mm)	79.81	**Calculated Avg K_{sat} (cm/d)**	323.2
Test Date	10/10/2016	**Standard Deviation (cm/d)**	21.8

Trial	Column Height (mm)	Volume (mL)	Time (min)	K_{sat} (cm/d)
1	50	32	2	308.3
2	50	30	2	289.0
3	50	31	2	298.6
4	75	20	1	323.1
5	75	20	1	323.1
6	75	20	1	323.1
7	100	25	1	347.7
8	100	25	1	347.7
9	100	25	1	347.7

Table A 3. Contd.

Saturation Date	10/26/2017	**Saturation Time**	3:00PM
Sample Code	213	**Container**	4
Sample Diameter (mm)	76.51	**Room Temperature (^{o}C)**	21
Sample Height (mm)	76.72	**Calculated Avg K_{sat} (cm/d)**	9.7
Test Date	10/29/2017	**Standard Deviation (cm/d)**	0.5

Trial	Column Height (mm)	Volume (mL)	Time (min)	K_{sat} (cm/d)
1	50	5	10	9.5
2	50	5	10	9.5
3	50	5	10	9.5
4	75	6	10	9.5
5	75	6	10	9.5
6	75	6	10	9.5
7	100	8	10	10.9
8	100	7	10	9.5
9	100	7	10	9.5

Saturation Date	11/1/2017	**Saturation Time**	11:00AM
Sample Code	214	**Container**	2
Sample Diameter (mm)	76.51	**Room Temperature (^{o}C)**	21
Sample Height (mm)	82.84	**Calculated Avg K_{sat} (cm/d)**	9.9
Test Date	11/4/2017	**Standard Deviation (cm/d)**	0.1

Trial	Column Height (mm)	Volume (mL)	Time (min)	K_{sat} (cm/d)
1	50	5	10	9.8
2	50	5	10	9.8
3	50	5	10	9.8
4	75	6	10	9.9
5	75	6	10	9.9
6	75	6	10	9.9
7	100	7	10	9.9
8	100	7	10	9.9
9	100	7	10	9.9

Table A 3. Contd.

Saturation Date	11/1/2017	**Saturation Time**	11:00AM
Sample Code	217	**Container**	3
Sample Diameter (mm)	76.51	**Room Temperature (^{o}C)**	21
Sample Height (mm)	77.89	**Calculated Avg K_{sat} (cm/d)**	2.1
Test Date	11/4/2017	**Standard Deviation (cm/d)**	0.5

Trial	Column Height (mm)	Volume (mL)	Time (min)	K_{sat} (cm/d)
1	50	1	10	1.9
2	50	1	10	1.9
3	50	1	10	1.9
4	75	1	10	1.6
5	75	1	10	1.6
6	75	1	10	1.6
7	100	2	10	2.7
8	100	2	10	2.7
9	100	2	10	2.7

Saturation Date	10/26/2017	**Saturation Time**	3:00PM
Sample Code	218	**Container**	5
Sample Diameter (mm)	76.51	**Room Temperature (^{o}C)**	21
Sample Height (mm)	72.52	**Calculated Avg K_{sat} (cm/d)**	3.1
Test Date	10/30/2017	**Standard Deviation (cm/d)**	0.5

Trial	Column Height (mm)	Volume (mL)	Time (min)	K_{sat} (cm/d)
1	50	2	10	3.7
2	50	2	10	3.7
3	50	2	10	3.7
4	75	2	10	3.1
5	75	2	10	3.1
6	75	2	10	3.1
7	100	2	10	2.6
8	100	2	10	2.6
9	100	2	10	2.6

Table A 3. Contd.

Saturation Date	11/1/2017	**Saturation Time**	11:00AM
Sample Code	252	**Container**	4
Sample Diameter (mm)	76.51	**Room Temperature (^{o}C)**	21
Sample Height (mm)	77.85	**Calculated Avg K_{sat} (cm/d)**	9.6
Test Date	11/4/2017	**Standard Deviation (cm/d)**	0.0

Trial	Column Height (mm)	Volume (mL)	Time (min)	K_{sat} (cm/d)
1	50	5	10	9.5
2	50	5	10	9.5
3	50	5	10	9.5
4	75	6	10	9.6
5	75	6	10	9.6
6	75	6	10	9.6
7	100	7	10	9.6
8	100	7	10	9.6
9	100	7	10	9.6

Saturation Date	10/26/2017	**Saturation Time**	3:00PM
Sample Code	260	**Container**	6
Sample Diameter (mm)	76.51	**Room Temperature (^{o}C)**	21
Sample Height (mm)	79.14	**Calculated Avg K_{sat} (cm/d)**	13.2
Test Date	10/30/2017	**Standard Deviation (cm/d)**	0.7

Trial	Column Height (mm)	Volume (mL)	Time (min)	K_{sat} (cm/d)
1	50	7	10	13.4
2	50	7	10	13.4
3	50	6	10	11.5
4	75	8	10	12.9
5	75	8	10	12.9
6	75	8	10	12.9
7	100	10	10	13.8
8	100	10	10	13.8
9	100	10	10	13.8

Table A 3. Contd.

Saturation Date	10/2/2016	**Saturation Time**	3:40PM
Sample Code	264	**Container**	3
Sample Diameter (mm)	76.51	**Room Temperature (^{o}C)**	20
Sample Height (mm)	35.78	**Calculated Avg K_{sat} (cm/d)**	2.1
Test Date	10/8/2016	**Standard Deviation (cm/d)**	0.5

Trial	Column Height (mm)	Volume (mL)	Time (min)	K_{sat} (cm/d)
1	50	1	10	1.3
2	50	2	10	2.6
3	50	1	10	1.3
4	75	2	10	2.0
5	75	2	10	2.0
6	75	2	10	2.0
7	100	3	10	2.5
8	100	3	10	2.5
9	100	3	10	2.5

Saturation Date	11/1/2017	**Saturation Time**	11:00AM
Sample Code	267	**Container**	5
Sample Diameter (mm)	76.51	**Room Temperature (^{o}C)**	21
Sample Height (mm)	73.38	**Calculated Avg K_{sat} (cm/d)**	2.0
Test Date	11/4/2017	**Standard Deviation (cm/d)**	0.5

Trial	Column Height (mm)	Volume (mL)	Time (min)	K_{sat} (cm/d)
1	50	1	10	1.9
2	50	1	10	1.9
3	50	1	10	1.9
4	75	1	10	1.5
5	75	1	10	1.5
6	75	1	10	1.5
7	100	2	10	2.7
8	100	2	10	2.7
9	100	2	10	2.7

Table A 3. Contd.

Saturation Date	11/1/2017	**Saturation Time**	11:00AM
Sample Code	270	**Container**	6
Sample Diameter (mm)	76.51	**Room Temperature (^{o}C)**	21
Sample Height (mm)	79.63	**Calculated Avg K_{sat} (cm/d)**	16.1
Test Date	11/4/2017	**Standard Deviation (cm/d)**	0.6

Trial	Column Height (mm)	Volume (mL)	Time (min)	K_{sat} (cm/d)
1	50	8	10	15.4
2	50	8	10	15.4
3	50	8	10	15.4
4	75	10	10	16.1
5	75	10	10	16.1
6	75	10	10	16.1
7	100	12	10	16.7
8	100	12	10	16.7
9	100	12	10	16.7

Saturation Date	10/12/2016	**Saturation Time**	2:00PM
Sample Code	300	**Container**	1
Sample Diameter (mm)	76.51	**Room Temperature (^{o}C)**	20
Sample Height (mm)	80.89	**Calculated Avg K_{sat} (cm/d)**	12.0
Test Date	10/15/2016	**Standard Deviation (cm/d)**	0.9

Trial	Column Height (mm)	Volume (mL)	Time (min)	K_{sat} (cm/d)
1	50	7	10	13.6
2	50	6	10	11.6
3	50	6	10	11.6
4	75	8	10	13.0
5	75	7	10	11.4
6	75	7	10	11.4
7	100	9	10	12.6
8	100	8	10	11.2
9	100	8	10	11.2

Table A 3. Contd.

Saturation Date	10/12/2016	**Saturation Time**	2:00PM
Sample Code	302	**Container**	2
Sample Diameter (mm)	76.51	**Room Temperature (^{o}C)**	20
Sample Height (mm)	78.69	**Calculated Avg K_{sat} (cm/d)**	15.7
Test Date	10/15/2016	**Standard Deviation (cm/d)**	0.5

Trial	Column Height (mm)	Volume (mL)	Time (min)	K_{sat} (cm/d)
1	50	8	10	15.3
2	50	8	10	15.3
3	50	8	10	15.3
4	75	10	10	16.0
5	75	10	10	16.0
6	75	10	10	16.0
7	100	11	10	15.2
8	100	12	10	16.6
9	100	11	10	15.2

Saturation Date	10/12/2016	**Saturation Time**	2:00PM
Sample Code	303	**Container**	3
Sample Diameter (mm)	76.51	**Room Temperature (^{o}C)**	20
Sample Height (mm)	76.8	**Calculated Avg K_{sat} (cm/d)**	66.9
Test Date	10/15/2016	**Standard Deviation (cm/d)**	2.7

Trial	Column Height (mm)	Volume (mL)	Time (min)	K_{sat} (cm/d)
1	50	11	3	69.6
2	50	11	3	69.6
3	50	10	3	63.3
4	75	13	3	68.7
5	75	12	3	63.4
6	75	12	3	63.4
7	100	15	3	68.1
8	100	15	3	68.1
9	100	15	3	68.1

Table A 3. Contd.

Saturation Date	10/12/2016	**Saturation Time**	2:00PM
Sample Code	305	**Container**	4
Sample Diameter (mm)	76.51	**Room Temperature (^{o}C)**	20
Sample Height (mm)	78.32	**Calculated Avg K_{sat} (cm/d)**	11.3
Test Date	10/15/2016	**Standard Deviation (cm/d)**	1.1

Trial	Column Height (mm)	Volume (mL)	Time (min)	K_{sat} (cm/d)
1	50	6	10	11.5
2	50	6	10	11.5
3	50	5	10	9.6
4	75	7	10	11.2
5	75	7	10	11.2
6	75	6	10	9.6
7	100	9	10	12.4
8	100	9	10	12.4
9	100	9	10	12.4

Saturation Date	3/21/2017	**Saturation Time**	5:00PM
Sample Code	312	**Container**	6
Sample Diameter (mm)	76.51	**Room Temperature (^{o}C)**	21
Sample Height (mm)	75.60	**Calculated Avg K_{sat} (cm/d)**	17.9
Test Date	3/24/2017	**Standard Deviation (cm/d)**	2.3

Trial	Column Height (mm)	Volume (mL)	Time (min)	K_{sat} (cm/d)
1	50	4	5	15.1
2	50	4	5	15.1
3	50	4	5	15.1
4	75	6	5	18.9
5	75	6	5	18.9
6	75	6	5	18.9
7	100	8	5	21.6
8	100	7	5	18.9
9	100	7	5	18.9

Table A 3. Contd.

Saturation Date	3/21/2017	**Saturation Time**	5:00PM
Sample Code	313	**Container**	1
Sample Diameter (mm)	76.51	**Room Temperature (^{o}C)**	20
Sample Height (mm)	88.25	**Calculated Avg K_{sat} (cm/d)**	3.3
Test Date	3/24/2017	**Standard Deviation (cm/d)**	1.0

Trial	Column Height (mm)	Volume (mL)	Time (min)	K_{sat} (cm/d)
1	50	1	10	2.0
2	50	1	10	2.0
3	50	1	10	2.0
4	75	2	10	3.4
5	75	2	10	3.4
6	75	2	10	3.4
7	100	3	10	4.4
8	100	3	10	4.4
9	100	3	10	4.4

Saturation Date	3/21/2017	**Saturation Time**	5:25PM
Sample Code	314	**Container**	3
Sample Diameter (mm)	76.51	**Room Temperature (^{o}C)**	20
Sample Height (mm)	77.39	**Calculated Avg K_{sat} (cm/d)**	2.1
Test Date	3/21/2017	**Standard Deviation (cm/d)**	0.5

Trial	Column Height (mm)	Volume (mL)	Time (min)	K_{sat} (cm/d)
1	50	1	10	1.9
2	50	1	10	1.9
3	50	1	10	1.9
4	75	1	10	1.6
5	75	1	10	1.6
6	75	1	10	1.6
7	100	2	10	2.7
8	100	2	10	2.7
9	100	2	10	2.7

Table A 4. Raw data from the pressure plate extractor at 6 kPa

	0.06 BAR							Post Experiment			Calculations				
Sample	Soil+Ring [g]	D1 [mm]	D2 [mm]	D3 [mm]	H1 [mm]	H2 [mm]	H3 [mm]	Box Weight [g]	Box + Dry Soil [g]	Ring Weight [g]	Average D [mm]	Average H [mm]	Average Volume [cm^3]	VC Ratio	VWC
22-1	33.094	52.50	52.50	52.50	10.00	10.00	10.00	6.660	19.752	4.034	51.50	10.00	20.820	1.00	0.767
22-2	33.919	51.50	51.50	51.50	10.00	10.00	10.00	6.751	20.489	4.470	51.50	10.00	20.820	1.00	0.755
22-3	30.296	51.50	51.50	51.50	10.00	10.00	10.00	6.695	19.067	4.034	51.50	10.00	20.820	1.00	0.667
23-1	33.200	51.50	51.50	51.50	10.00	10.00	10.00	8.902	22.228	4.023	51.50	10.00	20.820	1.00	0.761
23-2	31.836	51.50	51.50	51.50	10.00	10.00	10.00	73.700	86.381	4.005	51.50	10.00	20.820	1.00	0.728
23-3	29.994	51.50	51.50	51.50	10.00	10.00	10.00	69.043	80.790	4.239	51.50	10.00	20.820	1.00	0.673
24-1	27.935	51.50	51.50	51.50	10.00	10.00	10.00	6.741	15.365	4.054	51.50	10.00	20.820	1.00	0.733
24-2	28.952	51.50	51.50	51.50	10.00	10.00	10.00	6.695	15.497	4.133	51.50	10.00	20.820	1.00	0.769
24-3	28.289	51.50	51.50	51.50	10.00	10.00	10.00	6.560	15.213	4.052	51.50	10.00	20.820	1.00	0.749
25-1	23.793	51.50	51.50	51.50	10.00	10.00	10.00	6.556	9.575	3.976	51.50	10.00	20.820	1.00	0.807
25-2	23.011	51.50	51.50	51.50	10.00	10.00	10.00	6.516	9.340	3.978	51.50	10.00	20.820	1.00	0.779
25-3	23.741	51.50	51.50	51.50	10.00	10.00	10.00	6.586	9.514	4.027	51.50	10.00	20.820	1.00	0.806
29-1	24.648	51.50	51.50	51.50	10.00	10.00	10.00	6.487	10.715	4.128	51.50	10.00	20.820	1.00	0.783
29-2	24.670	51.50	51.50	51.50	10.00	10.00	10.00	6.505	10.955	4.020	51.50	10.00	20.820	1.00	0.778
29-3	24.358	51.50	51.50	51.50	10.00	10.00	10.00	6.425	10.815	4.015	51.50	10.00	20.820	1.00	0.766
30-1	29.523	51.50	51.50	51.50	10.00	10.00	10.00	6.440	16.485	4.329	51.50	10.00	20.820	1.00	0.728
30-2	30.085	51.50	51.50	51.50	10.00	10.00	10.00	6.533	16.944	4.049	51.50	10.00	20.820	1.00	0.750
30-3	30.412	51.50	51.50	51.50	10.00	10.00	10.00	6.475	17.035	4.219	51.50	10.00	20.820	1.00	0.751
31-1	28.016	51.50	51.50	51.50	10.00	10.00	10.00	6.400	15.514	4.005	51.50	10.00	20.820	1.00	0.716
31-2	31.345	51.50	51.50	51.50	10.00	10.00	10.00	6.498	16.737	4.247	51.50	10.00	20.820	1.00	0.810
31-3	30.932	51.50	51.50	51.50	10.00	10.00	10.00	6.444	16.671	3.978	51.50	10.00	20.820	1.00	0.803
33-1	23.931	51.50	51.50	51.50	10.00	10.00	10.00	6.445	10.297	3.888	51.50	10.00	20.820	1.00	0.778
33-2	24.249	51.50	51.50	51.50	10.00	10.00	10.00	6.553	10.362	4.104	51.50	10.00	20.820	1.00	0.785
33-3	23.668	51.50	51.50	51.50	10.00	10.00	10.00	6.540	10.292	3.990	51.50	10.00	20.820	1.00	0.765
37-1	20.67	51.50	51.50	51.50	10.00	10.00	10.00	6.480	8.571	3.882	51.50	10.00	20.820	1.00	0.706
37-2	20.583	51.50	51.50	51.50	10.00	10.00	10.00	6.521	8.605	3.920	51.50	10.00	20.820	1.00	0.700
37-3	21.705	51.50	51.50	51.50	10.00	10.00	10.00	6.665	8.895	3.970	51.50	10.00	20.820	1.00	0.745
38-1	24.564	51.50	51.50	51.50	10.00	10.00	10.00	69.845	73.441	4.045	51.50	10.00	20.820	1.00	0.813
38-2	24.588	51.50	51.50	51.50	10.00	10.00	10.00	87.992	91.374	3.873	51.50	10.00	20.820	1.00	0.833
38-3	24.172	51.50	51.50	51.50	10.00	10.00	10.00	38.266	41.509	3.983	51.50	10.00	20.820	1.00	0.814

Table A 4. Contd.

	0.06 BAR							Post Experiment			Calculations				
Sample	Soil+Ring [g]	D1 [mm]	D2 [mm]	D3 [mm]	H1 [mm]	H2 [mm]	H3 [mm]	Box Weight [g]	Box + Dry Soil [g]	Ring Weight [g]	Average D [mm]	Average H [mm]	Average Volume [cm^3]	VC Ratio	VWC
94-1	26.735	51.50	51.50	51.50	10.00	10.00	10.00	6.548	9.142	3.999	51.50	10.00	20.820	1.00	0.967
94-2	25.635	51.50	51.50	51.50	10.00	10.00	10.00	6.530	9.183	3.783	51.50	10.00	20.820	1.00	0.922
94-3	25.449	51.50	51.50	51.50	10.00	10.00	10.00	6.485	9.027	3.998	51.50	10.00	20.820	1.00	0.908
96-1	22.889	51.50	51.50	51.50	10.00	10.00	10.00	6.419	9.016	3.879	51.50	10.00	20.820	1.00	0.788
96-2	21.713	51.50	51.50	51.50	10.00	10.00	10.00	6.534	8.760	4.146	51.50	10.00	20.820	1.00	0.737
96-3	19.373	51.50	51.50	51.50	10.00	10.00	10.00	6.507	8.530	3.904	51.50	10.00	20.820	1.00	0.646
97-1	22.299	51.50	51.50	51.50	10.00	10.00	10.00	6.453	8.339	3.984	51.50	10.00	20.820	1.00	0.789
97-2	19.784	51.50	51.50	51.50	10.00	10.00	10.00	6.489	8.089	3.866	51.50	10.00	20.820	1.00	0.688
97-3	20.701	51.50	51.50	51.50	10.00	10.00	10.00	6.644	8.353	4.078	51.50	10.00	20.820	1.00	0.716
104-1	20.144	51.50	51.50	51.50	10.00	10.00	10.00	6.641	8.951	3.974	51.50	10.00	20.820	1.00	0.666
104-2	21.887	51.50	51.50	51.50	10.00	10.00	10.00	6.688	9.233	4.079	51.50	10.00	20.820	1.00	0.733
104-3	18.745	51.50	51.50	51.50	10.00	10.00	10.00	6.659	8.780	4.116	51.50	10.00	20.820	1.00	0.601
112-1	21.787	51.50	51.50	51.50	10.00	10.00	10.00	6.684	9.427	4.104	51.50	10.00	20.820	1.00	0.718
112-2	20.647	51.50	51.50	51.50	10.00	10.00	10.00	6.737	9.192	3.966	51.50	10.00	20.820	1.00	0.683
112-3	20.733	51.50	51.50	51.50	10.00	10.00	10.00	6.663	9.043	4.132	51.50	10.00	20.820	1.00	0.683
116-1	22.983	51.50	51.50	51.50	10.00	10.00	10.00	6.763	9.303	3.934	51.50	10.00	20.820	1.00	0.793
116-2	21.622	51.50	51.50	51.50	10.00	10.00	10.00	6.689	9.044	3.864	51.50	10.00	20.820	1.00	0.740
116-3	23.309	51.50	51.50	51.50	10.00	10.00	10.00	6.559	9.091	4.085	51.50	10.00	20.820	1.00	0.802
155-1	20.725	51.50	51.50	51.50	10.00	10.00	10.00	6.451	8.585	4.177	51.50	10.00	20.820	1.00	0.692
155-2	19.955	51.50	51.50	51.50	10.00	10.00	10.00	6.557	8.595	3.922	51.50	10.00	20.820	1.00	0.672
155-3	22.035	51.50	51.50	51.50	10.00	10.00	10.00	6.547	8.957	4.154	51.50	10.00	20.820	1.00	0.743
156-1	24.818	51.50	51.50	51.50	10.00	10.00	10.00	6.399	9.212	3.847	51.50	10.00	20.820	1.00	0.872
156-2	26.210	51.50	51.50	51.50	10.00	10.00	10.00	6.499	9.492	3.976	51.50	10.00	20.820	1.00	0.924
156-3	23.752	51.50	51.50	51.50	10.00	10.00	10.00	6.437	9.011	3.969	51.50	10.00	20.820	1.00	0.827
157-1	21.096	51.50	51.50	51.50	10.00	10.00	10.00	6.484	8.521	4.131	51.50	10.00	20.820	1.00	0.717
157-2	21.299	51.50	51.50	51.50	10.00	10.00	10.00	6.525	8.498	4.187	51.50	10.00	20.820	1.00	0.727
157-3	21.725	51.50	51.50	51.50	10.00	10.00	10.00	6.668	8.727	4.147	51.50	10.00	20.820	1.00	0.745
158-1	25.828	51.50	51.50	51.50	10.00	10.00	10.00	6.418	9.200	3.850	51.50	10.00	20.820	1.00	0.922
158-2	24.864	51.50	51.50	51.50	10.00	10.00	10.00	6.533	9.199	3.775	51.50	10.00	20.820	1.00	0.885
158-3	24.845	51.50	51.50	51.50	10.00	10.00	10.00	6.506	9.078	4.029	51.50	10.00	20.820	1.00	0.876

Table A 4. Contd.

	0.06 BAR							Post Experiment			Calculations				
Sample	Soil+Ring [g]	D1 [mm]	D2 [mm]	D3 [mm]	H1 [mm]	H2 [mm]	H3 [mm]	Box Weight [g]	Box + Dry Soil [g]	Ring Weight [g]	Average D [mm]	Average H [mm]	Average Volume [cm^3]	VC Ratio	VWC
159-1	25.652	51.50	51.50	51.50	10.00	10.00	10.00	6.444	8.978	3.770	51.50	10.00	20.820	1.00	0.929
159-2	27.090	51.50	51.50	51.50	10.00	10.00	10.00	6.462	8.951	3.995	51.50	10.00	20.820	1.00	0.990
159-3	24.723	51.50	51.50	51.50	10.00	10.00	10.00	6.409	9.103	3.992	51.50	10.00	20.820	1.00	0.866
161-1	27.884	51.50	51.50	51.50	10.00	10.00	10.00	6.672	15.763	4.030	51.50	10.00	20.820	1.00	0.709
161-2	25.300	51.50	51.50	51.50	10.00	10.00	10.00	6.718	14.467	4.397	51.50	10.00	20.820	1.00	0.632
161-3	25.697	51.50	51.50	51.50	10.00	10.00	10.00	6.685	14.951	4.127	51.50	10.00	20.820	1.00	0.639
176-1	21.813	51.50	51.50	51.50	10.00	10.00	10.00	6.682	8.309	3.981	51.50	10.00	20.820	1.00	0.778
176-2	21.571	51.50	51.50	51.50	10.00	10.00	10.00	6.765	8.337	3.970	51.50	10.00	20.820	1.00	0.770
176-3	20.065	51.50	51.50	51.50	10.00	10.00	10.00	6.701	8.109	4.159	51.50	10.00	20.820	1.00	0.696
177-1	19.715	51.50	51.50	51.50	10.00	10.00	10.00	6.748	8.299	3.884	51.50	10.00	20.820	1.00	0.686
177-2	20.209	51.50	51.50	51.50	10.00	10.00	10.00	6.695	8.345	3.958	51.50	10.00	20.820	1.00	0.701
177-3	21.748	51.50	51.50	51.50	10.00	10.00	10.00	6.566	8.359	3.912	51.50	10.00	20.820	1.00	0.771
178-1	21.264	51.50	51.50	51.50	10.00	10.00	10.00	6.569	8.310	4.132	51.50	10.00	20.820	1.00	0.739
178-2	21.766	51.50	51.50	51.50	10.00	10.00	10.00	6.522	8.134	3.997	51.50	10.00	20.820	1.00	0.776
178-3	21.631	51.50	51.50	51.50	10.00	10.00	10.00	6.591	8.196	4.124	51.50	10.00	20.820	1.00	0.764
179-1	22.676	51.50	51.50	51.50	10.00	10.00	10.00	6.492	9.090	4.176	51.50	10.00	20.820	1.00	0.764
179-2	22.176	51.50	51.50	51.50	10.00	10.00	10.00	6.511	8.991	3.992	51.50	10.00	20.820	1.00	0.754
179-3	23.057	51.50	51.50	51.50	10.00	10.00	10.00	6.428	9.159	4.116	51.50	10.00	20.820	1.00	0.779
202-1	31.045	51.50	51.50	51.50	10.00	10.00	10.00	6.664	18.518	4.067	51.50	10.00	20.820	1.00	0.726
202-2	30.549	51.50	51.50	51.50	10.00	10.00	10.00	6.712	18.654	4.147	51.50	10.00	20.820	1.00	0.695
202-3	31.743	51.50	51.50	51.50	10.00	10.00	10.00	6.683	19.053	4.131	51.50	10.00	20.820	1.00	0.732
203-1	28.988	51.50	51.50	51.50	10.00	10.00	10.00	6.658	17.130	4.117	51.50	10.00	20.820	1.00	0.692
203-2	30.149	51.50	51.50	51.50	10.00	10.00	10.00	8.925	19.618	4.002	51.50	10.00	20.820	1.00	0.742
203-3	30.392	51.50	51.50	51.50	10.00	10.00	10.00	8.934	19.654	4.014	51.50	10.00	20.820	1.00	0.752
204-1	29.808	51.50	51.50	51.50	10.00	10.00	10.00	8.915	19.676	3.905	51.50	10.00	20.820	1.00	0.727
204-2	29.412	51.50	51.50	51.50	10.00	10.00	10.00	8.891	19.191	4.020	51.50	10.00	20.820	1.00	0.725
204-3	29.822	51.50	51.50	51.50	10.00	10.00	10.00	8.913	19.382	4.076	51.50	10.00	20.820	1.00	0.734
206-1	26.048	51.50	51.50	51.50	10.00	10.00	10.00	6.558	12.275	3.966	51.50	10.00	20.820	1.00	0.786
206-2	23.294	51.50	51.50	51.50	10.00	10.00	10.00	6.495	11.398	3.907	51.50	10.00	20.820	1.00	0.696
206-3	25.361	51.50	51.50	51.50	10.00	10.00	10.00	6.575	12.395	3.956	51.50	10.00	20.820	1.00	0.749

Table A 4. Contd.

	0.06 BAR							Post Experiment			Calculations				
Sample	Soil+Ring [g]	D1 [mm]	D2 [mm]	D3 [mm]	H1 [mm]	H2 [mm]	H3 [mm]	Box Weight [g]	Box + Dry Soil [g]	Ring Weight [g]	Average D [mm]	Average H [mm]	Average Volume [cm^3]	VC Ratio	VWC
207-1	30.461	51.50	51.50	51.50	10.00	10.00	10.00	6.610	16.377	3.994	51.50	10.00	20.820	1.00	0.802
207-2	28.965	51.50	51.50	51.50	10.00	10.00	10.00	6.680	15.780	4.023	51.50	10.00	20.820	1.00	0.761
207-3	28.964	51.50	51.50	51.50	10.00	10.00	10.00	6.660	15.117	3.874	51.50	10.00	20.820	1.00	0.799
209-1	26.891	51.50	51.50	51.50	10.00	10.00	10.00	6.990	10.885	4.036	51.50	10.00	20.820	1.00	0.911
209-2	24.046	51.50	51.50	51.50	10.00	10.00	10.00	6.880	10.301	3.880	51.50	10.00	20.820	1.00	0.804
209-3	25.650	51.50	51.50	51.50	10.00	10.00	10.00	6.551	10.544	3.973	51.50	10.00	20.820	1.00	0.849
213-1	23.501	51.50	51.50	51.50	10.00	10.00	10.00	6.531	9.314	3.875	51.50	10.00	20.820	1.00	0.809
213-2	22.649	51.50	51.50	51.50	10.00	10.00	10.00	6.488	9.170	3.775	51.50	10.00	20.820	1.00	0.778
213-3	22.716	51.50	51.50	51.50	10.00	10.00	10.00	6.562	9.186	4.016	51.50	10.00	20.820	1.00	0.772
214-1	25.583	51.50	51.50	51.50	10.00	10.00	10.00	6.443	9.232	4.012	51.50	10.00	20.820	1.00	0.902
214-2	22.993	51.50	51.50	51.50	10.00	10.00	10.00	6.462	8.938	3.983	51.50	10.00	20.820	1.00	0.794
214-3	25.331	51.50	51.50	51.50	10.00	10.00	10.00	6.408	9.136	3.997	51.50	10.00	20.820	1.00	0.894
217-1	26.293	51.50	51.50	51.50	10.00	10.00	10.00	6.417	13.673	4.034	51.50	10.00	20.820	1.00	0.721
217-2	26.230	51.50	51.50	51.50	10.00	10.00	10.00	6.531	14.593	3.847	51.50	10.00	20.820	1.00	0.688
217-3	26.389	51.50	51.50	51.50	10.00	10.00	10.00	6.506	13.935	3.876	51.50	10.00	20.820	1.00	0.724
218-1	24.180	51.50	51.50	51.50	10.00	10.00	10.00	6.454	9.670	3.854	51.50	10.00	20.820	1.00	0.822
218-2	25.535	51.50	51.50	51.50	10.00	10.00	10.00	6.490	9.800	4.013	51.50	10.00	20.820	1.00	0.875
218-3	24.133	51.50	51.50	51.50	10.00	10.00	10.00	6.645	9.781	3.780	51.50	10.00	20.820	1.00	0.827
219-1	26.912	51.50	51.50	51.50	10.00	10.00	10.00	6.639	12.069	3.992	51.50	10.00	20.820	1.00	0.840
219-2	26.329	51.50	51.50	51.50	10.00	10.00	10.00	6.687	12.291	3.854	51.50	10.00	20.820	1.00	0.810
219-3	26.261	51.50	51.50	51.50	10.00	10.00	10.00	6.659	12.067	4.035	51.50	10.00	20.820	1.00	0.808
220-1	23.027	51.50	51.50	51.50	10.00	10.00	10.00	6.647	9.966	3.774	51.50	10.00	20.820	1.00	0.765
220-2	25.913	51.50	51.50	51.50	10.00	10.00	10.00	8.921	12.824	3.869	51.50	10.00	20.820	1.00	0.871
220-3	26.257	51.50	51.50	51.50	10.00	10.00	10.00	8.918	12.823	4.034	51.50	10.00	20.820	1.00	0.880
221-1	29.644	51.50	51.50	51.50	10.00	10.00	10.00	8.906	19.223	3.870	51.50	10.00	20.820	1.00	0.742
221-2	27.203	51.50	51.50	51.50	10.00	10.00	10.00	6.608	15.881	3.887	51.50	10.00	20.820	1.00	0.674
221-3	28.713	51.50	51.50	51.50	10.00	10.00	10.00	6.678	16.367	3.874	51.50	10.00	20.820	1.00	0.728
252-1	27.567	51.50	51.50	51.50	10.00	10.00	10.00	6.399	11.144	4.029	51.50	10.00	20.820	1.00	0.903
252-2	25.569	51.50	51.50	51.50	10.00	10.00	10.00	6.498	10.844	3.999	51.50	10.00	20.820	1.00	0.827
252-3	25.886	51.50	51.50	51.50	10.00	10.00	10.00	6.438	10.964	3.973	51.50	10.00	20.820	1.00	0.835

Table A 4. Contd.

	0.06 BAR							Post Experiment			Calculations				
Sample	Soil+Ring [g]	D1 [mm]	D2 [mm]	D3 [mm]	H1 [mm]	H2 [mm]	H3 [mm]	Box Weight [g]	Box + Dry Soil [g]	Ring Weight [g]	Average D [mm]	Average H [mm]	Average Volume [cm^3]	VC Ratio	VWC
260-1	22.718	51.50	51.50	51.50	10.00	10.00	10.00	6.484	9.139	3.868	51.50	10.00	20.820	1.00	0.778
260-2	21.679	51.50	51.50	51.50	10.00	10.00	10.00	6.486	8.867	3.981	51.50	10.00	20.820	1.00	0.736
260-3	23.548	51.50	51.50	51.50	10.00	10.00	10.00	6.408	9.047	3.982	51.50	10.00	20.820	1.00	0.813
264-1	22.218	51.50	51.50	51.50	10.00	10.00	10.00	6.645	10.771	4.094	51.50	10.00	20.820	1.00	0.672
264-2	25.085	51.50	51.50	51.50	10.00	10.00	10.00	8.918	14.132	4.249	51.50	10.00	20.820	1.00	0.750
264-3	26.405	51.50	51.50	51.50	10.00	10.00	10.00	8.917	14.356	4.117	51.50	10.00	20.820	1.00	0.809
267-1	27.304	51.50	51.50	51.50	10.00	10.00	10.00	6.536	12.174	3.870	51.50	10.00	20.820	1.00	0.855
267-2	27.508	51.50	51.50	51.50	10.00	10.00	10.00	6.49	12.181	3.968	51.50	10.00	20.820	1.00	0.857
267-3	28.599	51.50	51.50	51.50	10.00	10.00	10.00	6.565	12.289	3.873	51.50	10.00	20.820	1.00	0.913
268-1	24.897	51.50	51.50	51.50	10.00	10.00	10.00	6.454	9.407	3.769	51.50	10.00	20.820	1.00	0.873
268-2	27.042	51.50	51.50	51.50	10.00	10.00	10.00	6.49	9.654	4.009	51.50	10.00	20.820	1.00	0.954
268-3	26.036	51.50	51.50	51.50	10.00	10.00	10.00	6.644	9.633	3.850	51.50	10.00	20.820	1.00	0.922
270-1	20.444	51.50	51.50	51.50	10.00	10.00	10.00	8.906	11.001	3.990	51.50	10.00	20.820	1.00	0.690
270-2	20.765	51.50	51.50	51.50	10.00	10.00	10.00	8.893	11.022	3.934	51.50	10.00	20.820	1.00	0.706
270-3	23.705	51.50	51.50	51.50	10.00	10.00	10.00	8.912	11.43	4.078	51.50	10.00	20.820	1.00	0.822
300-1	23.2	51.50	51.50	51.50	10.00	10.00	10.00	6.666	8.741	4.035	51.50	10.00	20.820	1.00	0.821
300-2	22.438	51.50	51.50	51.50	10.00	10.00	10.00	8.930	10.870	4.191	51.50	10.00	20.820	1.00	0.783
300-3	23.476	51.50	51.50	51.50	10.00	10.00	10.00	8.939	11.015	3.953	51.50	10.00	20.820	1.00	0.838
302-1	29.546	51.50	51.50	51.50	10.00	10.00	10.00	6.722	16.087	3.784	51.50	10.00	20.820	1.00	0.788
302-2	30.513	51.50	51.50	51.50	10.00	10.00	10.00	6.693	16.176	3.847	51.50	10.00	20.820	1.00	0.825
302-3	30.790	51.50	51.50	51.50	10.00	10.00	10.00	6.553	16.003	3.981	51.50	10.00	20.820	1.00	0.834
303-1	20.531	51.50	51.50	51.50	10.00	10.00	10.00	8.916	10.555	3.948	51.50	10.00	20.820	1.00	0.718
303-2	20.809	51.50	51.50	51.50	10.00	10.00	10.00	8.893	10.515	4.058	51.50	10.00	20.820	1.00	0.727
303-3	20.837	51.50	51.50	51.50	10.00	10.00	10.00	8.914	10.617	4.069	51.50	10.00	20.820	1.00	0.724
305-1	20.134	51.50	51.50	51.50	10.00	10.00	10.00	8.866	10.669	4.028	51.50	10.00	20.820	1.00	0.687
305-2	21.593	51.50	51.50	51.50	10.00	10.00	10.00	8.876	10.852	4.005	51.50	10.00	20.820	1.00	0.750
305-3	21.114	51.50	51.50	51.50	10.00	10.00	10.00	8.889	10.828	3.985	51.50	10.00	20.820	1.00	0.730
312-1	22.320	51.50	51.50	51.50	10.00	10.00	10.00	6.664	8.321	3.873	51.50	10.00	20.820	1.00	0.806
312-2	23.437	51.50	51.50	51.50	10.00	10.00	10.00	6.694	8.462	4.016	51.50	10.00	20.820	1.00	0.848
312-3	23.555	51.50	51.50	51.50	10.00	10.00	10.00	6.686	8.419	4.012	51.50	10.00	20.820	1.00	0.855

Table A 4. Contd.

	0.06 BAR							Post Experiment				Calculations			
Sample	Soil+Ring [g]	D1 [mm]	D2 [mm]	D3 [mm]	H1 [mm]	H2 [mm]	H3 [mm]	Box Weight [g]	Box + Dry Soil [g]	Ring Weight [g]	Average D [mm]	Average H [mm]	Average Volume [cm^3]	VC Ratio	VWC
313-1	22.429	51.50	51.50	51.50	10.00	10.00	10.00	6.639	7.985	3.983	51.50	10.00	20.820	1.00	0.821
313-2	23.113	51.50	51.50	51.50	10.00	10.00	10.00	6.687	8.129	3.997	51.50	10.00	20.820	1.00	0.849
313-3	21.692	51.50	51.50	51.50	10.00	10.00	10.00	6.660	7.985	3.973	51.50	10.00	20.820	1.00	0.787
314-1	20.928	51.50	51.50	51.50	10.00	10.00	10.00	6.457	8.223	4.130	51.50	10.00	20.820	1.00	0.722
314-2	22.556	51.50	51.50	51.50	10.00	10.00	10.00	6.537	8.625	4.139	51.50	10.00	20.820	1.00	0.784
314-3	24.219	51.50	51.50	51.50	10.00	10.00	10.00	6.482	8.659	4.245	51.50	10.00	20.820	1.00	0.855
315-1	22.382	51.50	51.50	51.50	10.00	10.00	10.00	6.645	8.317	4.046	51.50	10.00	20.820	1.00	0.800
315-2	22.969	51.50	51.50	51.50	10.00	10.00	10.00	8.919	10.654	4.035	51.50	10.00	20.820	1.00	0.826
315-3	23.202	51.50	51.50	51.50	10.00	10.00	10.00	8.919	10.685	3.776	51.50	10.00	20.820	1.00	0.848

Table A 5. Raw data from the pressure plate extractor at 10 kPa.

	0.10 BAR							Post Experiment				Calculations			
Sample	Soil+Ring [g]	D1 [mm]	D2 [mm]	D3 [mm]	H1 [mm]	H2 [mm]	H3 [mm]	Box Weight [g]	Box + Dry Soil [g]	Ring Weight [g]	Average D [mm]	Average H [mm]	Average Volume [cm^3]	VC Ratio	VWC
22-1	32.381	49.03	49.10	49.03	10.00	10.00	10.00	6.608	19.861	4.011	49.05	10.00	18.889	0.91	0.800
22-2	29.599	48.66	48.12	48.91	10.00	10.00	10.00	6.681	18.927	3.965	48.56	10.00	18.513	0.89	0.723
22-3	25.734	49.11	48.37	49.16	10.00	10.00	10.00	6.663	17.269	3.833	48.88	10.00	18.756	0.90	0.602
23-1	31.371	51.50	51.50	51.50	10.00	10.00	10.00	8.902	22.228	4.023	51.50	10.00	20.820	1.00	0.673
23-2	30.041	51.50	51.50	51.50	10.00	10.00	10.00	73.700	86.381	4.005	51.50	10.00	20.820	1.00	0.641
23-3	28.361	51.50	51.50	51.50	10.00	10.00	10.00	69.043	80.790	4.239	51.50	10.00	20.820	1.00	0.594
24-1	25.738	51.50	51.50	51.50	10.00	10.00	10.00	6.700	14.545	4.263	51.50	10.00	20.820	1.00	0.655
24-2	29.706	51.50	51.50	51.50	10.00	10.00	10.00	6.689	15.916	3.881	51.50	10.00	20.820	1.00	0.797
24-3	28.398	51.50	51.50	51.50	10.00	10.00	10.00	6.551	15.359	4.060	51.50	10.00	20.820	1.00	0.746
25-1	20.406	51.50	51.50	51.50	9.58	9.56	8.88	6.532	9.268	3.962	51.50	9.34	19.446	0.93	0.705
25-2	19.954	51.50	51.50	51.50	9.55	9.22	9.27	6.488	8.879	3.917	51.50	9.35	19.460	0.93	0.701
25-3	20.050	51.50	51.50	51.50	9.14	8.63	9.42	6.564	9.001	4.035	51.50	9.06	18.870	0.91	0.720
29-1	20.818	49.98	50.00	49.76	8.38	9.53	8.55	6.444	10.187	4.135	49.91	8.82	17.249	0.83	0.750
29-2	22.522	50.29	50.41	49.75	9.73	8.40	9.03	6.462	10.586	4.139	50.15	9.05	17.874	0.86	0.798
29-3	22.213	49.64	50.18	49.53	9.76	8.51	8.91	6.409	10.341	4.084	49.78	9.06	17.626	0.85	0.805
30-1	26.803	51.50	51.50	51.50	10.00	10.00	10.00	6.400	15.533	4.019	51.50	10.00	20.820	1.00	0.656
30-2	26.740	51.50	51.50	51.50	10.00	10.00	10.00	6.499	15.640	3.996	51.50	10.00	20.820	1.00	0.653
30-3	24.889	51.50	51.50	51.50	10.00	10.00	10.00	6.437	14.947	3.887	51.50	10.00	20.820	1.00	0.600
31-1	26.594	51.50	51.50	51.50	10.00	10.00	10.00	6.400	15.514	4.005	51.50	10.00	20.820	1.00	0.647
31-2	29.667	51.50	51.50	51.50	10.00	10.00	10.00	6.498	16.737	4.247	51.50	10.00	20.820	1.00	0.729
31-3	29.329	51.50	51.50	51.50	10.00	10.00	10.00	6.444	16.671	3.978	51.50	10.00	20.820	1.00	0.726
33-1	22.433	48.65	49.25	48.55	10.00	10.00	10.00	6.417	10.162	3.987	48.82	10.00	18.707	0.90	0.786
33-2	23.083	48.77	48.58	48.72	10.00	10.00	10.00	6.533	10.327	4.031	48.69	10.00	18.610	0.89	0.820
33-3	22.501	48.21	49.75	48.88	10.00	10.00	10.00	6.507	10.228	4.113	48.95	10.00	18.807	0.90	0.780
37-1	17.015	48.67	48.03	47.66	8.01	8.30	7.96	6.454	8.237	4.005	48.12	8.09	14.705	0.71	0.763
37-2	17.799	50.30	47.24	46.70	7.91	8.80	8.16	6.490	8.393	4.132	48.08	8.29	15.044	0.72	0.782
37-3	18.829	46.78	49.27	47.91	9.24	7.94	8.38	6.645	8.752	4.219	47.99	8.52	15.401	0.74	0.812
38-1	21.750	48.59	48.65	47.18	10.00	10.00	10.00	69.845	73.441	4.045	48.14	10.00	18.192	0.87	0.776
38-2	21.910	48.10	49.66	48.47	10.00	10.00	10.00	87.992	91.374	3.873	48.74	10.00	18.651	0.90	0.786
38-3	20.341	48.00	48.62	48.96	10.00	10.00	10.00	38.266	41.509	3.983	48.53	10.00	18.485	0.89	0.709

Table A 5. Contd.

	0.10 BAR							Post Experiment				Calculations			
Sample	Soil+Ring [g]	D1 [mm]	D2 [mm]	D3 [mm]	H1 [mm]	H2 [mm]	H3 [mm]	Box Weight [g]	Box + Dry Soil [g]	Ring Weight [g]	Average D [mm]	Average H [mm]	Average Volume [cm^3]	VC Ratio	VWC
94-1	23.191	51.50	51.50	51.50	10.00	10.00	10.00	6.548	9.142	3.999	51.50	10.00	20.820	1.00	0.797
94-2	22.540	51.50	51.50	51.50	10.00	10.00	10.00	6.530	9.183	3.783	51.50	10.00	20.820	1.00	0.773
94-3	22.349	51.50	51.50	51.50	10.00	10.00	10.00	6.485	9.027	3.998	51.50	10.00	20.820	1.00	0.759
96-1	20.203	49.78	49.26	49.26	8.27	9.04	7.92	6.419	9.016	3.879	49.43	8.41	16.133	0.77	0.851
96-2	19.218	48.14	49.62	48.27	8.12	7.50	8.60	6.534	8.760	4.146	48.68	8.07	15.016	0.72	0.855
96-3	17.024	47.92	50.47	48.46	7.38	8.05	8.00	6.507	8.530	3.904	48.95	7.81	14.690	0.71	0.755
97-1	18.391	48.58	48.29	48.58	8.92	8.45	8.63	6.453	8.339	3.984	48.48	8.67	15.992	0.77	0.783
97-2	17.061	49.71	48.89	49.61	9.79	8.62	7.74	6.489	8.089	3.866	49.40	8.72	16.701	0.80	0.694
97-3	18.153	49.70	49.16	47.18	8.41	8.72	8.37	6.644	8.353	4.078	48.68	8.50	15.812	0.76	0.782
104-1	17.870	46.65	46.12	45.65	7.83	8.47	7.86	6.641	8.951	3.974	46.14	8.05	13.459	0.65	0.861
104-2	19.518	46.07	47.10	48.26	7.37	7.87	7.00	6.688	9.233	4.079	47.14	7.41	12.934	0.62	0.997
104-3	16.582	46.71	44.86	48.22	6.69	6.81	6.91	6.659	8.780	4.116	46.60	6.80	11.596	0.56	0.892
112-1	18.879	48.96	48.90	48.09	8.68	8.20	7.78	6.684	9.427	4.104	48.65	8.22	15.272	0.73	0.788
112-2	17.744	48.58	46.40	48.54	9.03	7.57	8.44	6.737	9.192	3.966	47.84	8.35	14.996	0.72	0.755
112-3	17.974	46.55	47.86	48.16	9.31	8.38	7.94	6.663	9.043	4.132	47.52	8.54	15.146	0.73	0.757
116-1	20.324	49.32	47.91	49.48	8.76	7.34	8.69	6.763	9.303	4.126	48.90	8.26	15.513	0.75	0.880
116-2	18.931	48.31	48.76	47.27	8.07	8.54	8.26	6.689	9.044	4.006	48.11	8.29	15.065	0.72	0.834
116-3	20.378	47.11	48.30	47.16	8.52	8.63	8.66	6.559	9.091	4.235	47.52	8.60	15.253	0.73	0.892
155-1	18.373	50.80	48.03	49.06	8.44	8.97	8.44	6.451	8.585	4.177	49.30	8.62	16.438	0.79	0.734
155-2	17.800	48.15	49.76	49.47	9.28	8.11	8.73	6.557	8.595	3.922	49.13	8.71	16.495	0.79	0.718
155-3	20.609	49.05	49.38	49.90	9.62	9.36	8.56	6.547	8.957	4.154	49.44	9.18	17.617	0.85	0.797
156-1	20.558	49.66	49.39	49.55	10.00	10.00	10.00	6.399	9.212	3.847	49.53	10.00	19.260	0.93	0.722
156-2	21.817	48.83	50.98	49.53	10.00	10.00	10.00	6.499	9.492	3.976	49.78	10.00	19.453	0.93	0.763
156-3	19.606	50.66	48.61	50.73	10.00	10.00	10.00	6.437	9.011	3.969	50.00	10.00	19.625	0.94	0.666
157-1	19.039	51.50	51.50	51.50	9.42	8.80	8.28	6.484	8.521	4.131	51.50	8.83	18.391	0.88	0.700
157-2	19.236	51.50	51.50	51.50	8.73	9.14	8.73	6.525	8.498	4.187	51.50	8.87	18.461	0.89	0.708
157-3	19.710	51.50	51.50	51.50	9.07	7.67	8.32	6.668	8.727	4.147	51.50	8.35	17.392	0.84	0.776
158-1	21.241	48.51	49.94	48.10	10.00	10.00	10.00	6.418	9.200	3.850	48.85	10.00	18.733	0.90	0.780
158-2	19.925	50.02	48.70	50.42	10.00	10.00	10.00	6.533	9.199	3.775	49.71	10.00	19.401	0.93	0.695
158-3	20.097	50.46	50.47	50.40	10.00	10.00	10.00	6.506	9.078	4.029	50.44	10.00	19.975	0.96	0.676

Table A 5. Contd.

	0.10 BAR							Post Experiment				Calculations			
Sample	Soil+Ring [g]	D1 [mm]	D2 [mm]	D3 [mm]	H1 [mm]	H2 [mm]	H3 [mm]	Box Weight [g]	Box + Dry Soil [g]	Ring Weight [g]	Average D [mm]	Average H [mm]	Average Volume [cm^3]	VC Ratio	VWC
159-1	19.793	48.55	46.91	46.81	10.00	10.00	10.00	6.444	8.978	3.770	47.42	10.00	17.654	0.85	0.764
159-2	19.083	46.00	49.16	48.26	10.00	10.00	10.00	6.462	8.951	3.995	47.81	10.00	17.941	0.86	0.702
159-3	20.771	49.91	48.70	48.49	10.00	10.00	10.00	6.409	9.103	3.992	49.03	10.00	18.874	0.91	0.746
161-1	26.581	51.50	51.50	51.50	10.00	10.00	10.00	6.672	15.763	4.030	51.50	10.00	20.820	1.00	0.646
161-2	23.873	51.50	51.50	51.50	10.00	10.00	10.00	6.718	14.467	4.397	51.50	10.00	20.820	1.00	0.563
161-3	24.353	51.50	51.50	51.50	10.00	10.00	10.00	6.685	14.951	4.127	51.50	10.00	20.820	1.00	0.574
176-1	19.453	49.65	49.29	50.08	8.77	7.98	7.61	6.682	8.309	3.981	49.67	8.12	15.728	0.76	0.880
176-2	19.173	50.67	48.54	49.28	8.12	8.66	7.25	6.765	8.337	3.970	49.50	8.01	15.405	0.74	0.885
176-3	17.511	46.06	49.22	50.46	7.84	8.79	8.02	6.701	8.109	4.159	48.58	8.22	15.222	0.73	0.785
177-1	17.026	51.50	51.50	51.50	8.13	9.25	8.25	6.748	8.299	3.884	51.50	8.54	17.787	0.85	0.652
177-2	17.647	51.50	51.50	51.50	8.02	9.23	8.00	6.695	8.345	3.958	51.50	8.42	17.524	0.84	0.687
177-3	18.738	51.50	51.50	51.50	8.33	7.64	8.68	6.566	8.359	3.912	51.50	8.22	17.107	0.82	0.762
178-1	18.39	50.82	47.59	48.59	7.30	8.26	7.58	6.569	8.310	4.132	49.00	7.71	14.538	0.70	0.861
178-2	18.937	48.83	50.26	49.58	9.32	8.25	9.16	6.522	8.134	3.997	49.56	8.91	17.177	0.83	0.776
178-3	18.789	47.60	48.44	48.93	8.64	9.29	8.30	6.591	8.196	4.124	48.32	8.74	16.027	0.77	0.815
179-1	20.108	49.30	48.93	49.91	9.09	8.33	8.84	6.492	9.090	4.176	49.38	8.75	16.755	0.80	0.796
179-2	19.551	50.96	49.75	49.13	8.16	8.65	8.23	6.511	8.991	3.992	49.95	8.35	16.345	0.79	0.800
179-3	20.423	48.80	50.63	48.12	9.35	8.89	8.04	6.428	9.159	4.116	49.18	8.76	16.634	0.80	0.816
202-1	25.602	50.13	48.74	49.98	9.50	8.37	8.60	6.645	16.249	3.823	49.62	8.82	17.051	0.82	0.714
202-2	24.289	50.25	49.63	50.88	9.44	8.50	9.43	8.918	17.894	4.166	50.25	9.12	18.086	0.87	0.616
202-3	23.536	50.25	50.30	48.21	8.24	10.15	8.01	8.918	18.524	3.985	49.59	8.80	16.986	0.82	0.585
203-1	23.513	49.75	50.93	50.97	10.02	8.82	9.42	8.903	17.692	4.065	50.55	9.42	18.896	0.91	0.564
203-2	24.911	49.36	50.65	50.28	9.42	9.73	8.76	73.700	81.822	4.214	50.10	9.30	18.328	0.88	0.686
203-3	24.839	49.61	50.81	49.36	9.60	8.12	9.93	69.043	77.785	4.035	49.93	9.22	18.035	0.87	0.669
204-1	23.962	49.27	49.36	49.95	8.21	8.53	8.24	87.047	94.916	3.789	49.53	8.33	16.033	0.77	0.767
204-2	24.228	49.96	50.86	49.61	9.43	8.37	8.59	74.774	82.732	3.996	50.14	8.80	17.363	0.83	0.707
204-3	26.025	50.44	50.79	49.62	8.58	7.94	9.15	3.254	11.641	4.137	50.28	8.56	16.983	0.82	0.795
206-1	23.918	51.50	51.50	51.50	10.00	10.00	10.00	6.558	12.275	3.966	51.50	10.00	20.820	1.00	0.684
206-2	21.377	51.50	51.50	51.50	10.00	10.00	10.00	6.495	11.398	3.907	51.50	10.00	20.820	1.00	0.604
206-3	23.358	51.50	51.50	51.50	10.00	10.00	10.00	6.575	12.395	3.956	51.50	10.00	20.820	1.00	0.652

Table A 5. Contd.

	0.10 BAR							Post Experiment				Calculations			
Sample	Soil+Ring [g]	D1 [mm]	D2 [mm]	D3 [mm]	H1 [mm]	H2 [mm]	H3 [mm]	Box Weight [g]	Box + Dry Soil [g]	Ring Weight [g]	Average D [mm]	Average H [mm]	Average Volume [cm^3]	VC Ratio	VWC
207-1	29.103	51.50	51.50	51.50	10.00	10.00	10.00	6.610	16.377	3.994	51.50	10.00	20.820	1.00	0.737
207-2	27.562	51.50	51.50	51.50	10.00	10.00	10.00	6.680	15.780	4.023	51.50	10.00	20.820	1.00	0.694
207-3	27.315	51.50	51.50	51.50	10.00	10.00	10.00	6.660	15.117	3.874	51.50	10.00	20.820	1.00	0.720
209-1	23.455	48.55	49.64	47.98	10.00	10.00	10.00	6.990	10.885	4.036	48.72	10.00	18.636	0.90	0.833
209-2	20.950	49.01	49.21	51.05	10.00	10.00	10.00	6.880	10.301	3.880	49.76	10.00	19.434	0.93	0.702
209-3	22.380	50.76	48.16	50.81	10.00	10.00	10.00	6.551	10.544	3.973	49.91	10.00	19.554	0.94	0.737
213-1	20.392	49.31	49.14	49.01	10.00	10.00	10.00	6.531	9.314	3.875	49.15	10.00	18.966	0.91	0.724
213-2	19.652	48.92	48.36	48.76	10.00	10.00	10.00	6.488	9.170	3.775	48.68	10.00	18.602	0.89	0.709
213-3	19.653	48.90	49.63	49.07	10.00	10.00	10.00	6.562	9.186	4.016	49.20	10.00	19.002	0.91	0.685
214-1	20.963	45.98	48.96	48.36	10.00	10.00	10.00	6.443	9.232	4.012	47.77	10.00	17.911	0.86	0.791
214-2	19.202	45.95	47.18	47.54	10.00	10.00	10.00	6.462	8.938	3.983	46.89	10.00	17.260	0.83	0.738
214-3	20.705	48.03	48.04	48.13	10.00	10.00	10.00	6.408	9.136	3.997	48.07	10.00	18.137	0.87	0.771
217-1	24.767	51.36	48.96	50.44	10.00	10.00	10.00	6.417	13.673	4.034	50.25	10.00	19.824	0.95	0.680
217-2	26.585	49.86	48.51	49.88	10.00	10.00	10.00	6.531	14.593	3.847	49.42	10.00	19.170	0.92	0.766
217-3	24.986	49.93	50.96	50.84	10.00	10.00	10.00	6.506	13.935	3.876	50.58	10.00	20.080	0.96	0.681
218-1	22.146	51.50	51.50	51.50	10.00	10.00	10.00	6.454	9.670	3.854	51.50	10.00	20.820	1.00	0.724
218-2	23.499	51.50	51.50	51.50	10.00	10.00	10.00	6.490	9.800	4.013	51.50	10.00	20.820	1.00	0.777
218-3	21.950	51.50	51.50	51.50	10.00	10.00	10.00	6.645	9.781	3.780	51.50	10.00	20.820	1.00	0.722
219-1	23.933	48.91	48.81	48.24	10.00	10.00	10.00	6.639	12.069	3.992	48.65	10.00	18.582	0.89	0.781
219-2	23.493	48.81	48.00	48.36	10.00	10.00	10.00	6.687	12.291	3.854	48.39	10.00	18.381	0.88	0.764
219-3	23.380	47.21	49.21	46.74	10.00	10.00	10.00	6.659	12.067	4.035	47.72	10.00	17.876	0.86	0.780
220-1	19.921	47.77	48.74	49.02	9.51	8.93	8.25	6.647	9.966	3.774	48.51	8.90	16.435	0.79	0.781
220-2	22.541	49.36	47.61	49.09	9.73	8.06	9.43	8.921	12.824	3.869	48.69	9.07	16.883	0.81	0.875
220-3	22.757	51.00	48.68	47.71	9.60	9.18	10.06	8.918	12.823	4.034	49.13	9.61	18.215	0.87	0.813
221-1	27.726	48.92	48.68	49.71	9.12	9.11	8.67	8.906	19.223	3.870	49.10	8.97	16.972	0.82	0.798
221-2	25.410	50.16	49.62	48.99	9.30	8.29	7.82	6.608	15.881	3.887	49.59	8.47	16.351	0.79	0.749
221-3	26.302	50.02	49.75	49.77	7.85	9.03	8.09	6.678	16.367	3.874	49.85	8.32	16.235	0.78	0.785
252-1	24.809	50.08	50.35	49.41	10.00	10.00	10.00	6.399	11.144	4.029	49.95	10.00	19.583	0.94	0.819
252-2	22.988	50.09	50.32	49.23	10.00	10.00	10.00	6.498	10.844	3.999	49.88	10.00	19.531	0.94	0.750
252-3	23.429	50.01	49.95	50.17	10.00	10.00	10.00	6.438	10.964	3.973	50.04	10.00	19.659	0.94	0.759

Table A 5. Contd.

	0.10 BAR							Post Experiment			Calculations				
Sample	Soil+Ring [g]	D1 [mm]	D2 [mm]	D3 [mm]	H1 [mm]	H2 [mm]	H3 [mm]	Box Weight [g]	Box + Dry Soil [g]	Ring Weight [g]	Average D [mm]	Average H [mm]	Average Volume [cm^3]	VC Ratio	VWC
260-1	19.977	48.51	48.78	48.17	8.96	8.64	8.08	6.484	9.139	3.868	48.49	8.56	15.797	0.76	0.852
260-2	19.091	47.92	49.59	48.60	8.62	9.44	8.84	6.486	8.867	3.981	48.70	8.97	16.696	0.80	0.762
260-3	20.900	49.41	48.01	49.21	9.17	9.97	8.93	6.408	9.047	3.982	48.88	9.36	17.547	0.84	0.814
264-1	20.575	51.50	51.50	51.50	7.17	9.03	8.09	6.645	10.771	4.094	51.50	8.10	16.857	0.81	0.733
264-2	23.598	51.50	51.50	51.50	10.00	10.00	10.00	8.918	14.132	4.249	51.50	10.00	20.820	1.00	0.679
264-3	24.759	51.50	51.50	51.50	10.00	10.00	10.00	8.917	14.356	4.117	51.50	10.00	20.820	1.00	0.730
267-1	23.569	51.50	51.50	51.50	10.00	10.00	10.00	6.536	12.174	3.870	51.50	10.00	20.820	1.00	0.675
267-2	23.652	51.50	51.50	51.50	10.00	10.00	10.00	6.49	12.181	3.968	51.50	10.00	20.820	1.00	0.672
267-3	24.971	51.50	51.50	51.50	10.00	10.00	10.00	6.565	12.289	3.873	51.50	10.00	20.820	1.00	0.738
268-1	20.502	51.50	51.50	51.50	10.00	10.00	10.00	6.454	9.407	3.769	51.50	10.00	20.820	1.00	0.662
268-2	22.517	51.50	51.50	51.50	10.00	10.00	10.00	6.49	9.654	4.009	51.50	10.00	20.820	1.00	0.737
268-3	21.779	51.50	51.50	51.50	10.00	10.00	10.00	6.644	9.633	3.850	51.50	10.00	20.820	1.00	0.718
270-1	18.353	49.02	49.70	48.19	8.08	6.98	7.78	8.906	11.001	3.990	48.97	7.61	14.332	0.69	0.856
270-2	18.566	50.36	48.56	48.80	8.28	8.28	8.72	8.893	11.022	3.934	49.24	8.43	16.038	0.77	0.780
270-3	21.840	48.78	49.12	48.86	9.42	8.14	9.11	8.912	11.43	4.078	48.92	8.89	16.701	0.80	0.913
300-1	20.297	48.97	47.90	47.74	9.34	8.89	8.61	6.666	8.741	4.035	48.20	8.95	16.319	0.78	0.869
300-2	19.585	48.03	46.28	47.00	8.30	8.25	8.74	8.930	10.870	4.191	47.10	8.43	14.683	0.71	0.916
300-3	20.518	48.80	47.67	46.76	8.65	8.06	9.07	8.939	11.015	3.953	47.74	8.59	15.376	0.74	0.942
302-1	26.419	49.92	50.43	50.43	10.00	10.00	10.00	6.722	16.087	3.784	50.26	10.00	19.830	0.95	0.669
302-2	26.883	50.07	50.64	50.44	10.00	10.00	10.00	6.693	16.176	3.847	50.38	10.00	19.927	0.96	0.680
302-3	27.035	50.26	50.06	47.65	10.00	10.00	10.00	6.553	16.003	3.981	49.32	10.00	19.097	0.92	0.712
303-1	17.467	46.39	48.53	47.27	8.63	9.19	8.42	8.916	10.555	3.948	47.40	8.75	15.424	0.74	0.770
303-2	17.81	46.78	46.55	48.84	9.19	8.27	6.18	8.893	10.515	4.058	47.39	7.88	13.892	0.67	0.873
303-3	17.919	48.87	48.61	46.74	8.97	8.39	7.47	8.914	10.617	4.069	48.07	8.28	15.015	0.72	0.809
305-1	17.839	48.70	50.86	50.00	9.00	8.13	8.20	8.866	10.669	4.028	49.85	8.44	16.473	0.79	0.729
305-2	19.387	49.76	50.53	47.68	8.44	8.11	8.52	8.876	10.852	4.005	49.32	8.36	15.959	0.77	0.840
305-3	18.887	50.36	50.52	50.21	8.16	8.59	8.73	8.889	10.828	3.985	50.36	8.49	16.911	0.81	0.767
312-1	18.333	47.01	48.88	49.23	8.43	7.48	8.46	6.664	8.321	3.873	48.37	8.12	14.922	0.72	0.858
312-2	19.459	49.32	48.60	48.98	9.84	8.22	7.84	6.694	8.462	4.016	48.97	8.63	16.250	0.78	0.842
312-3	19.470	49.13	48.72	49.13	9.59	8.72	9.12	6.686	8.419	4.012	48.99	9.14	17.229	0.83	0.797

Table A 5. Contd.

	0.10 BAR							Post Experiment				Calculations			
Sample	Soil+Ring [g]	D1 [mm]	D2 [mm]	D3 [mm]	H1 [mm]	H2 [mm]	H3 [mm]	Box Weight [g]	Box + Dry Soil [g]	Ring Weight [g]	Average D [mm]	Average H [mm]	Average Volume [cm^3]	VC Ratio	VWC
313-1	16.766	46.94	48.56	47.44	7.83	9.75	6.86	6.639	7.985	3.983	47.65	8.15	14.518	0.70	0.788
313-2	17.118	48.53	49.64	50.17	8.19	9.53	8.83	6.687	8.129	3.997	49.45	8.85	16.986	0.82	0.688
313-3	16.098	48.40	50.63	49.27	9.65	9.57	8.61	6.660	7.985	3.973	49.43	9.28	17.795	0.85	0.607
314-1	18.468	50.60	49.15	50.42	8.35	7.31	8.16	6.457	8.223	4.130	50.06	7.94	15.618	0.75	0.805
314-2	19.912	48.89	50.01	49.09	9.52	9.34	8.86	6.537	8.625	4.139	49.33	9.24	17.651	0.85	0.775
314-3	21.486	50.44	48.10	49.29	9.47	8.94	8.86	6.482	8.659	4.245	49.28	9.09	17.327	0.83	0.869
315-1	17.147	49.47	49.39	48.22	6.48	7.59	8.95	6.645	8.317	4.046	49.03	7.67	14.478	0.70	0.789
315-2	17.626	49.58	48.46	49.75	9.61	8.01	8.08	8.919	10.654	4.035	49.26	8.57	16.320	0.78	0.726
315-3	17.562	49.90	49.68	49.24	8.84	8.10	8.71	8.919	10.685	3.776	49.61	8.55	16.516	0.79	0.728

Table A 6. Raw data from the pressure plate extractor at 50 kPa.

	0.50 BAR							Post Experiment			Calculations				
Sample	Soil+Ring [g]	D1 [mm]	D2 [mm]	D3 [mm]	H1 [mm]	H2 [mm]	H3 [mm]	Box Weight [g]	Box + Dry Soil [g]	Ring Weight [g]	Average D [mm]	Average H [mm]	Average Volume [cm^3]	VC Ratio	VWC
22-1	30.182	48.44	47.80	47.20	10.00	10.00	10.00	6.608	19.861	4.011	47.81	10.00	17.946	0.91	0.720
22-2	27.474	48.06	47.63	46.64	10.00	10.00	10.00	6.681	18.927	3.965	47.44	10.00	17.669	0.90	0.637
22-3	23.945	47.76	47.12	46.43	10.00	10.00	10.00	6.663	17.269	3.833	47.10	10.00	17.417	0.89	0.546
23-1	29.240	49.11	47.93	47.80	10.00	10.00	10.00	8.902	22.228	4.023	48.28	10.00	18.298	0.93	0.650
23-2	27.605	47.88	49.08	47.97	10.00	10.00	10.00	73.700	86.381	4.005	48.31	10.00	18.321	0.93	0.596
23-3	25.851	49.04	48.06	48.49	10.00	10.00	10.00	69.043	80.790	4.239	48.53	10.00	18.488	0.94	0.534
24-1	22.841	46.49	46.07	46.83	10.00	10.00	10.00	6.700	14.545	4.263	46.46	10.00	16.947	0.86	0.633
24-2	25.913	45.79	47.66	47.02	10.00	10.00	10.00	6.689	15.916	3.881	46.82	10.00	17.211	0.88	0.744
24-3	25.053	45.85	46.22	46.26	10.00	10.00	10.00	6.551	15.359	4.060	46.11	10.00	16.690	0.85	0.730
25-1	15.890	46.71	47.93	47.43	8.85	8.13	8.57	6.532	9.268	3.962	47.36	8.52	14.993	0.76	0.613
25-2	14.436	47.38	47.81	48.36	9.17	9.65	4.08	6.488	8.879	3.917	47.85	7.63	13.720	0.70	0.592
25-3	15.007	47.12	44.46	46.64	9.56	9.11	9.10	6.564	9.001	4.035	46.07	9.26	15.425	0.79	0.553
29-1	16.184	44.99	45.81	45.89	9.47	7.59	9.35	6.444	10.187	4.139	45.56	8.80	14.347	0.73	0.579
29-2	18.016	46.40	45.92	45.77	9.57	9.00	8.55	6.462	10.586	4.084	46.03	9.04	15.036	0.77	0.652
29-3	16.999	46.68	46.58	45.02	9.38	10.32	8.67	6.409	10.341	4.019	46.09	9.46	15.772	0.80	0.574
30-1	23.557	46.88	46.27	46.37	9.22	9.22	8.85	6.400	15.533	4.019	46.51	9.10	15.445	0.79	0.674
30-2	23.600	46.65	46.18	45.70	8.97	8.90	9.52	6.499	15.640	3.996	46.18	9.13	15.282	0.78	0.685
30-3	21.065	47.52	47.53	46.25	9.63	9.40	9.54	6.437	14.947	3.887	47.10	9.52	16.584	0.85	0.523
31-1	23.502	46.79	45.36	45.28	9.59	8.60	9.18	6.400	15.514	4.005	45.81	9.12	15.029	0.77	0.691
31-2	26.094	45.97	45.47	45.09	9.95	9.04	9.94	6.498	16.737	4.247	45.51	9.64	15.679	0.80	0.740
31-3	25.887	46.08	45.48	46.46	9.85	9.29	9.96	6.444	16.671	3.978	46.01	9.70	16.117	0.82	0.725
33-1	17.059	43.40	43.51	43.69	9.58	9.98	8.87	6.417	10.162	3.987	43.53	9.48	14.098	0.72	0.662
33-2	17.770	43.74	44.41	42.74	9.23	9.33	8.25	6.533	10.327	4.031	43.63	8.94	13.354	0.68	0.745
33-3	17.259	43.65	42.45	42.12	8.82	9.11	9.58	6.507	10.228	4.113	42.74	9.17	13.149	0.67	0.717
37-1	12.495	45.33	44.30	43.30	9.52	8.63	7.98	6.454	8.237	4.005	44.31	8.71	13.424	0.64	0.500
37-2	12.853	43.67	44.56	44.79	8.41	8.20	7.23	6.490	8.393	4.132	44.34	7.95	12.264	0.59	0.556
37-3	13.750	45.98	45.52	40.76	9.16	8.27	7.49	6.645	8.752	4.219	44.09	8.31	12.674	0.61	0.586
38-1	17.886	44.96	43.34	44.44	9.07	8.79	9.30	69.845	73.441	4.045	44.25	9.05	13.914	0.67	0.736
38-2	18.134	45.07	45.49	43.88	9.41	8.32	9.43	87.992	91.374	3.873	44.81	9.05	14.272	0.69	0.762
38-3	16.796	43.67	43.55	43.02	8.81	9.01	8.21	38.266	41.509	3.983	43.41	8.68	12.837	0.62	0.745

Table A 6. Contd.

	0.50 BAR							Post Experiment				Calculations			
Sample	Soil+Ring [g]	D1 [mm]	D2 [mm]	D3 [mm]	H1 [mm]	H2 [mm]	H3 [mm]	Box Weight [g]	Box + Dry Soil [g]	Ring Weight [g]	Average D [mm]	Average H [mm]	Average Volume [cm^3]	VC Ratio	VWC
94-1	16.541	44.01	45.28	45.57	7.93	9.59	8.80	6.548	9.142	3.999	44.95	8.77	13.917	0.67	0.715
94-2	15.618	46.09	44.91	44.83	8.50	9.72	8.59	6.530	9.183	3.783	45.28	8.94	14.381	0.69	0.638
94-3	15.515	42.12	44.21	45.92	9.46	8.35	8.98	6.485	9.027	3.998	44.08	8.93	13.623	0.65	0.659
96-1	14.085	41.70	42.61	41.63	7.83	8.93	7.32	6.419	9.016	3.879	41.98	8.03	11.104	0.53	0.685
96-2	13.318	45.51	44.75	41.37	8.38	7.22	8.13	6.534	8.760	4.146	43.88	7.91	11.954	0.57	0.581
96-3	11.889	42.23	42.14	43.71	9.25	7.63	8.41	6.507	8.530	3.904	42.69	8.43	12.062	0.58	0.494
97-1	12.009	42.21	44.13	42.25	7.45	8.07	8.32	6.453	8.339	3.984	42.86	7.95	11.461	0.55	0.536
97-2	11.379	45.09	44.56	42.81	7.68	7.25	7.60	6.489	8.089	3.866	44.15	7.51	11.493	0.55	0.514
97-3	12.035	45.07	44.03	42.73	7.60	8.00	7.59	6.644	8.353	4.078	43.94	7.73	11.718	0.56	0.533
104-1	12.987	41.82	42.78	40.28	7.43	7.71	7.07	6.641	8.951	3.974	41.63	7.40	10.070	0.48	0.666
104-2	13.879	42.76	41.11	44.38	7.21	7.60	8.22	6.688	9.233	4.079	42.75	7.68	11.013	0.53	0.659
104-3	12.406	39.91	41.90	42.44	7.65	6.72	7.13	6.659	8.780	4.116	41.42	7.17	9.650	0.46	0.639
112-1	13.772	41.17	40.99	40.00	8.45	8.83	7.96	6.684	9.427	4.104	40.72	8.41	10.951	0.53	0.632
112-2	12.828	39.42	39.46	41.10	7.83	8.60	8.29	6.737	9.192	3.966	39.99	8.24	10.346	0.50	0.619
112-3	12.671	41.60	39.40	41.31	7.50	6.88	7.96	6.663	9.043	4.132	40.77	7.45	9.717	0.47	0.634
116-1	14.242	46.60	42.51	39.75	8.13	8.52	8.74	6.763	9.303	3.934	42.95	8.46	12.258	0.59	0.634
116-2	13.280	40.09	40.89	40.81	8.03	7.95	8.33	6.689	9.044	3.864	40.60	8.10	10.484	0.50	0.674
116-3	14.362	40.85	40.18	40.51	8.55	8.04	7.51	6.559	9.091	4.085	40.51	8.03	10.351	0.50	0.748
155-1	12.963	40.10	43.10	42.53	7.50	7.78	7.43	6.451	8.585	4.177	41.91	7.57	10.438	0.50	0.637
155-2	12.461	43.03	42.39	42.24	7.31	7.59	8.08	6.557	8.595	3.922	42.55	7.66	10.888	0.52	0.597
155-3	14.204	41.23	41.64	42.17	8.68	8.18	7.76	6.547	8.957	4.154	41.68	8.21	11.192	0.54	0.683
156-1	16.897	44.39	45.01	42.72	9.47	9.43	8.59	6.399	9.212	3.847	44.04	9.16	13.951	0.67	0.734
156-2	16.942	43.65	42.62	43.96	9.02	9.92	9.58	6.499	9.492	3.976	43.41	9.51	14.063	0.68	0.709
156-3	15.108	43.15	44.87	43.36	8.30	7.51	9.61	6.437	9.011	3.969	43.79	8.47	12.757	0.61	0.671
157-1	13.064	43.40	44.08	42.49	7.03	7.71	8.07	6.484	8.521	4.131	43.32	7.60	11.203	0.54	0.616
157-2	12.898	45.79	44.46	45.66	7.63	7.79	8.22	6.525	8.498	4.187	45.30	7.88	12.696	0.61	0.531
157-3	13.33	42.86	46.54	42.94	8.09	7.75	8.49	6.668	8.727	4.147	44.11	8.11	12.389	0.60	0.575
158-1	16.376	43.64	43.83	44.37	8.48	8.80	7.28	6.418	9.200	3.850	43.95	8.19	12.412	0.60	0.785
158-2	15.353	44.64	42.72	45.03	8.40	8.82	9.58	6.533	9.199	3.775	44.13	8.93	13.657	0.66	0.653
158-3	15.669	44.54	43.97	43.91	8.95	8.63	8.33	6.506	9.078	4.029	44.14	8.64	13.209	0.63	0.686

Table A 6. Contd.

	0.50 BAR							Post Experiment			Calculations				
Sample	Soil+Ring [g]	D1 [mm]	D2 [mm]	D3 [mm]	H1 [mm]	H2 [mm]	H3 [mm]	Box Weight [g]	Box + Dry Soil [g]	Ring Weight [g]	Average D [mm]	Average H [mm]	Average Volume [cm^3]	VC Ratio	VWC
159-1	16.432	43.77	43.37	43.16	10.00	10.00	10.00	6.444	8.978	3.770	43.43	10.00	14.809	0.71	0.684
159-2	14.940	42.69	42.58	40.98	10.00	10.00	10.00	6.462	8.951	3.995	42.08	10.00	13.902	0.67	0.608
159-3	16.332	42.69	43.87	42.37	10.00	10.00	10.00	6.409	9.103	3.992	42.98	10.00	14.499	0.70	0.665
161-1	22.332	46.45	48.11	46.91	9.51	9.54	9.32	6.672	15.763	4.030	47.16	9.46	16.508	0.79	0.558
161-2	19.542	46.66	47.58	46.98	9.32	8.39	8.52	6.718	14.467	4.397	47.07	8.74	15.209	0.73	0.486
161-3	20.417	46.94	46.89	47.59	9.10	9.11	8.91	6.685	14.951	4.127	47.14	9.04	15.769	0.76	0.509
176-1	13.101	42.41	41.38	40.03	7.41	7.75	8.16	6.682	8.309	3.981	41.27	7.77	10.395	0.50	0.721
176-2	12.861	40.74	41.99	40.88	8.81	7.68	8.00	6.765	8.337	3.970	41.20	8.16	10.879	0.52	0.673
176-3	12.24	42.17	38.27	38.60	7.63	7.46	7.44	6.701	8.109	4.159	39.68	7.51	9.282	0.45	0.719
177-1	11.521	43.97	45.13	44.88	7.77	8.83	9.05	6.748	8.299	3.884	44.66	8.55	13.387	0.64	0.455
177-2	12.045	46.08	46.64	45.27	7.39	8.77	7.79	6.695	8.345	3.958	46.00	7.98	13.259	0.64	0.485
177-3	12.609	44.63	45.84	46.23	8.42	7.60	8.86	6.566	8.359	3.912	45.57	8.29	13.517	0.65	0.511
178-1	12.374	37.71	42.94	40.01	7.62	8.02	7.58	6.569	8.310	4.132	40.22	7.74	9.829	0.47	0.661
178-2	12.479	43.89	39.53	42.67	7.81	6.99	7.99	6.522	8.134	3.997	42.03	7.60	10.534	0.51	0.652
178-3	12.527	41.60	42.85	40.37	8.89	8.25	7.02	6.591	8.196	4.124	41.61	8.05	10.944	0.53	0.621
179-1	14.404	45.97	45.36	46.07	8.92	9.26	9.25	6.492	9.090	4.176	45.80	9.14	15.056	0.72	0.507
179-2	13.669	44.10	43.68	45.22	8.14	9.05	8.73	6.511	8.991	3.992	44.33	8.64	13.330	0.64	0.540
179-3	14.668	44.98	46.36	47.49	8.31	9.20	7.77	6.428	9.159	4.116	46.28	8.43	14.166	0.68	0.552
202-1	22.726	46.35	47.02	45.14	9.80	9.54	7.59	6.645	16.249	3.823	46.17	8.98	15.021	0.72	0.619
202-2	21.669	47.34	48.70	46.67	9.06	7.82	8.06	8.918	17.894	4.166	47.57	8.31	14.768	0.71	0.577
202-3	22.809	43.92	48.78	47.41	8.77	9.15	10.48	8.918	18.524	3.985	46.70	9.47	16.209	0.78	0.569
203-1	20.185	47.12	46.72	46.58	8.38	9.04	8.45	8.903	17.692	4.065	46.81	8.62	14.831	0.71	0.494
203-2	20.429	46.36	46.25	47.71	8.46	8.88	9.96	73.700	81.822	4.214	46.77	9.10	15.628	0.75	0.518
203-3	21.291	46.44	45.78	44.92	8.79	8.98	9.65	69.043	77.785	4.035	45.71	9.14	14.993	0.72	0.568
204-1	21.318	46.31	46.09	46.45	8.94	7.34	9.73	87.047	94.916	3.789	46.28	8.67	14.579	0.70	0.663
204-2	21.661	43.81	45.29	46.05	9.40	9.80	7.67	74.774	82.732	3.996	45.05	8.96	14.269	0.69	0.680
204-3	22.989	47.30	46.14	44.87	9.48	8.12	8.53	3.254	11.641	4.137	46.10	8.71	14.533	0.70	0.720
206-1	18.250	43.27	44.09	41.93	9.21	8.49	8.72	6.558	12.275	3.966	43.10	8.81	12.840	0.62	0.667
206-2	16.443	43.68	43.37	43.97	8.11	8.17	7.14	6.495	11.398	3.907	43.67	7.81	11.689	0.56	0.653
206-3	18.008	42.80	43.18	43.55	8.93	9.58	9.62	6.575	12.395	3.956	43.18	9.38	13.722	0.66	0.600

Table A 6. Contd.

	0.50 BAR							Post Experiment			Calculations				
Sample	Soil+Ring [g]	D1 [mm]	D2 [mm]	D3 [mm]	H1 [mm]	H2 [mm]	H3 [mm]	Box Weight [g]	Box + Dry Soil [g]	Ring Weight [g]	Average D [mm]	Average H [mm]	Average Volume [cm^3]	VC Ratio	VWC
207-1	24.987	48.08	45.84	46.98	10.00	10.00	10.00	6.610	16.377	3.994	46.97	10.00	17.316	0.83	0.648
207-2	23.484	46.71	46.68	46.25	10.00	10.00	10.00	6.680	15.780	4.023	46.55	10.00	17.008	0.82	0.609
207-3	22.773	46.80	47.84	46.94	10.00	10.00	10.00	6.660	15.117	3.874	47.19	10.00	17.484	0.84	0.597
209-1	16.489	43.10	43.17	43.20	8.85	8.47	9.11	6.990	10.885	4.036	43.16	8.81	12.881	0.62	0.664
209-2	15.169	42.27	46.41	43.75	8.18	8.62	9.04	6.880	10.301	3.880	44.14	8.61	13.176	0.63	0.597
209-3	16.334	42.88	42.75	43.16	8.65	7.72	8.41	6.551	10.544	3.973	42.93	8.26	11.950	0.57	0.700
213-1	14.650	42.31	42.17	43.18	9.06	7.52	7.84	6.531	9.314	3.875	42.55	8.14	11.571	0.56	0.691
213-2	14.041	41.71	43.86	42.34	8.37	7.47	6.92	6.488	9.170	3.775	42.64	7.59	10.826	0.52	0.701
213-3	13.764	42.28	42.97	42.82	7.94	8.24	7.91	6.562	9.186	4.016	42.69	8.03	11.488	0.55	0.620
214-1	14.781	40.64	41.42	40.72	8.71	9.52	8.44	6.443	9.232	4.012	40.93	8.89	11.689	0.56	0.683
214-2	13.483	37.57	40.47	39.65	8.16	7.24	7.51	6.462	8.938	3.983	39.23	7.64	9.226	0.44	0.761
214-3	14.415	40.21	41.66	41.25	7.90	7.85	8.42	6.408	9.136	3.997	41.04	8.06	10.652	0.51	0.722
217-1	20.900	46.84	42.46	44.74	9.90	8.88	8.69	6.417	13.673	4.034	44.68	9.16	14.349	0.69	0.670
217-2	22.610	45.95	44.20	45.40	8.74	9.50	8.65	6.531	14.593	3.847	45.18	8.96	14.365	0.69	0.745
217-3	21.110	44.52	45.34	45.60	9.52	9.03	8.79	6.506	13.935	3.876	45.15	9.11	14.586	0.70	0.672
218-1	16.419	45.64	45.73	45.97	8.10	9.50	9.19	6.454	9.670	3.854	45.78	8.93	14.692	0.71	0.636
218-2	17.109	47.06	47.11	44.20	8.72	8.80	8.11	6.490	9.800	4.013	46.12	8.54	14.267	0.69	0.686
218-3	16.148	45.45	45.33	45.93	8.29	8.57	7.70	6.645	9.781	3.780	45.57	8.19	13.345	0.64	0.692
219-1	18.388	43.52	43.53	42.41	8.97	7.43	8.03	6.639	12.069	3.992	43.15	8.14	11.904	0.57	0.753
219-2	18.479	41.97	42.16	42.71	8.13	8.14	7.42	6.687	12.291	3.854	42.28	7.90	11.081	0.53	0.814
219-3	18.143	40.22	43.77	42.84	8.82	7.84	8.68	6.659	12.067	4.035	42.28	8.45	11.851	0.57	0.734
220-1	15.677	42.18	42.34	43.97	9.19	8.62	9.10	6.647	9.966	3.774	42.83	8.97	12.917	0.62	0.665
220-2	17.465	43.36	43.24	43.38	8.71	7.50	8.98	8.921	12.824	3.869	43.33	8.40	12.373	0.59	0.783
220-3	17.344	42.57	45.71	45.37	9.43	8.25	9.04	8.918	12.823	4.034	44.55	8.91	13.877	0.67	0.678
221-1	24.487	45.65	44.90	46.52	9.26	9.28	9.86	8.906	19.223	3.870	45.69	9.47	15.513	0.75	0.664
221-2	22.354	45.92	45.52	45.55	7.86	9.56	8.47	6.608	15.881	3.887	45.66	8.63	14.126	0.68	0.651
221-3	23.152	46.25	45.42	45.87	8.60	7.89	9.15	6.678	16.367	3.874	45.85	8.55	14.102	0.68	0.680
252-1	18.985	44.19	44.02	43.23	9.51	9.37	9.37	6.399	11.144	4.029	43.81	9.42	14.190	0.68	0.720
252-2	17.671	43.67	44.64	43.81	9.31	9.52	8.19	6.498	10.844	3.999	44.04	9.01	13.713	0.66	0.680
252-3	18.055	44.01	43.76	44.99	8.83	9.60	9.42	6.438	10.964	3.973	44.25	9.28	14.271	0.69	0.670

Table A 6. Contd.

	0.50 BAR							Post Experiment			Calculations				
Sample	Soil+Ring [g]	D1 [mm]	D2 [mm]	D3 [mm]	H1 [mm]	H2 [mm]	H3 [mm]	Box Weight [g]	Box + Dry Soil [g]	Ring Weight [g]	Average D [mm]	Average H [mm]	Average Volume [cm^3]	VC Ratio	VWC
260-1	13.536	43.25	42.97	42.85	9.34	7.45	7.98	6.484	9.139	3.868	43.02	8.26	11.997	0.58	0.585
260-2	12.994	42.47	41.25	41.37	7.54	8.17	8.18	6.486	8.867	3.981	41.70	7.96	10.868	0.52	0.610
260-3	14.004	41.96	42.32	42.98	8.56	8.11	7.54	6.408	9.047	3.982	42.42	8.07	11.399	0.55	0.648
264-1	17.590	45.08	46.67	43.84	8.11	8.61	8.19	6.645	10.771	4.094	45.20	8.30	13.315	0.64	0.704
264-2	19.495	46.85	46.37	46.55	7.64	8.92	8.65	8.918	14.132	4.249	46.59	8.40	14.319	0.69	0.701
264-3	19.893	46.91	46.27	45.38	9.64	8.99	8.87	8.917	14.356	4.117	46.19	9.17	15.350	0.74	0.673
267-1	19.938	46.13	45.22	45.10	10.00	10.00	10.00	6.536	12.174	3.870	45.48	10.00	16.240	0.78	0.642
267-2	20.578	44.36	47.43	46.96	10.00	10.00	10.00	6.490	12.181	3.968	46.25	10.00	16.792	0.81	0.650
267-3	20.739	45.62	46.68	45.67	10.00	10.00	10.00	6.565	12.289	3.873	45.99	10.00	16.603	0.80	0.671
268-1	16.017	44.56	46.01	44.90	9.56	8.09	8.41	6.454	9.407	3.769	45.16	8.69	13.905	0.67	0.668
268-2	17.080	46.68	44.82	43.75	9.23	8.67	8.60	6.490	9.654	4.009	45.08	8.83	14.094	0.68	0.703
268-3	16.691	47.13	44.80	46.29	9.66	9.13	8.56	6.644	9.633	3.850	46.07	9.12	15.192	0.73	0.649
270-1	13.126	42.52	43.29	40.96	7.61	8.04	7.50	8.906	11.001	3.990	42.26	7.72	10.817	0.52	0.651
270-2	13.091	41.63	43.29	41.55	6.91	7.28	7.95	8.893	11.022	3.934	42.16	7.38	10.296	0.49	0.683
270-3	14.868	42.67	41.17	42.88	8.42	7.82	8.54	8.912	11.430	4.078	42.24	8.26	11.569	0.56	0.715
300-1	14.913	41.35	43.07	42.08	9.00	9.67	8.62	6.666	8.741	4.035	42.17	9.10	12.697	0.61	0.693
300-2	13.873	39.96	43.32	41.94	8.79	8.32	8.66	8.930	10.870	4.191	41.74	8.59	11.748	0.56	0.659
300-3	14.286	40.02	41.23	39.90	9.04	9.49	7.94	8.939	11.015	3.953	40.38	8.82	11.296	0.54	0.731
302-1	22.965	47.94	47.32	48.53	10.00	10.00	10.00	6.722	16.087	3.784	47.93	10.00	18.034	0.87	0.544
302-2	22.857	46.67	47.99	47.79	10.00	10.00	10.00	6.693	16.176	3.847	47.48	10.00	17.699	0.85	0.538
302-3	22.368	46.30	49.92	46.62	10.00	10.00	10.00	6.553	16.003	3.981	47.61	10.00	17.796	0.85	0.502
303-1	12.137	40.69	39.95	39.44	8.55	7.61	8.29	8.916	10.555	3.948	40.03	8.15	10.250	0.49	0.639
303-2	12.015	40.72	42.33	38.79	7.23	7.72	8.22	8.893	10.515	4.058	40.61	7.72	10.000	0.48	0.633
303-3	12.285	40.69	40.72	39.01	8.04	8.41	8.41	8.914	10.617	4.069	40.14	8.29	10.481	0.50	0.621
305-1	12.34	42.72	44.96	42.83	7.96	8.06	9.06	8.866	10.669	4.028	43.50	8.36	12.420	0.60	0.524
305-2	13.192	43.02	45.81	41.95	8.05	8.50	7.52	8.876	10.852	4.005	43.59	8.02	11.969	0.57	0.602
305-3	12.911	44.89	43.24	45.42	8.96	7.82	8.28	8.889	10.828	3.985	44.52	8.35	12.995	0.62	0.538
312-1	12.439	44.32	43.92	43.33	7.71	7.87	7.45	6.664	8.321	3.873	43.86	7.68	11.591	0.56	0.596
312-2	12.959	43.67	44.46	42.66	8.50	8.09	8.35	6.694	8.462	4.016	43.60	8.31	12.404	0.60	0.578
312-3	12.880	42.63	43.14	43.48	7.90	8.80	7.86	6.686	8.419	4.012	43.08	8.19	11.929	0.57	0.598

Table A 6. Contd.

	0.50 BAR							Post Experiment			Calculations				
Sample	Soil+Ring [g]	D1 [mm]	D2 [mm]	D3 [mm]	H1 [mm]	H2 [mm]	H3 [mm]	Box Weight [g]	Box + Dry Soil [g]	Ring Weight [g]	Average D [mm]	Average H [mm]	Average Volume [cm^3]	VC Ratio	VWC
313-1	11.766	45.07	44.39	41.17	6.90	7.56	6.42	6.639	7.985	4.130	43.54	6.96	10.359	0.50	0.607
313-2	12.040	44.65	43.67	42.97	6.77	6.93	6.37	6.687	8.129	4.139	43.76	6.69	10.058	0.48	0.642
313-3	11.349	43.52	42.55	43.74	7.11	6.56	7.62	6.660	7.985	4.245	43.27	7.10	10.430	0.50	0.554
314-1	12.975	42.12	43.65	44.08	6.87	7.26	7.45	6.457	8.223	3.983	43.28	7.19	10.579	0.51	0.683
314-2	14.236	43.32	42.04	43.07	8.74	7.76	8.12	6.537	8.625	3.997	42.81	8.21	11.807	0.57	0.690
314-3	14.983	41.78	40.93	41.89	8.93	7.80	8.43	6.482	8.659	3.973	41.53	8.39	11.357	0.55	0.778
315-1	12.350	44.16	43.45	42.51	8.33	7.61	8.55	6.645	8.317	4.046	43.37	8.16	12.055	0.58	0.550
315-2	12.721	43.18	44.70	44.00	7.47	7.68	8.40	8.919	10.654	4.035	43.96	7.85	11.908	0.57	0.584
315-3	13.011	42.83	43.24	41.61	7.88	8.41	8.98	8.919	10.685	3.776	42.56	8.42	11.977	0.58	0.624

Table A 7. Raw data from the pressure plate extractor at 1500 kPa.

	15 BAR							Post Experiment			Calculations				
Sample	Soil+Ring [g]	D1 [mm]	D2 [mm]	D3 [mm]	H1 [mm]	H2 [mm]	H3 [mm]	Box Weight [g]	Box + Dry Soil [g]	Ring Weight [g]	Average D [mm]	Average H [mm]	Average Volume [cm^3]	VC Ratio	VWC
22-1	20.872	46.62	44.41	45.66	8.58	8.88	7.56	6.608	19.861	4.011	45.56	8.34	13.591	0.65	0.265
22-2	20.316	45.35	45.07	46.14	7.84	8.79	8.42	6.681	18.927	3.965	45.52	8.35	13.582	0.65	0.302
22-3	18.508	45.80	45.84	45.14	7.88	6.99	6.39	6.663	17.269	3.833	45.59	7.09	11.564	0.56	0.352
23-1	27.102	46.74	47.67	47.06	10.00	10.00	10.00	8.902	22.228	4.023	47.16	10.00	17.456	0.84	0.559
23-2	25.484	48.55	46.43	47.18	10.00	10.00	10.00	73.700	86.381	4.005	47.39	10.00	17.627	0.85	0.499
23-3	23.446	46.81	47.52	46.62	10.00	10.00	10.00	69.043	80.790	4.239	46.98	10.00	17.328	0.83	0.431
24-1	17.919	44.58	43.63	44.65	8.85	8.25	8.34	6.700	14.545	4.263	44.29	8.48	13.056	0.63	0.445
24-2	21.919	43.47	47.36	45.30	8.35	8.88	9.33	6.689	15.916	4.106	45.38	8.85	14.310	0.69	0.600
24-3	22.560	44.48	44.73	44.80	9.39	8.91	9.51	6.551	15.359	4.060	44.67	9.27	14.520	0.70	0.667
25-1	11.399	44.98	47.17	45.82	8.26	7.35	8.75	6.532	9.268	3.962	45.99	8.12	13.482	0.65	0.349
25-2	11.361	45.34	46.41	47.71	7.97	8.56	9.06	6.488	8.879	3.917	46.49	8.53	14.470	0.70	0.349
25-3	11.495	45.44	44.09	43.88	7.43	8.33	8.44	6.564	9.001	4.035	44.47	8.07	12.523	0.60	0.401
29-1	12.240	42.99	43.80	41.41	7.36	8.65	5.81	6.444	10.187	4.000	42.73	7.27	10.426	0.50	0.431
29-2	13.488	45.05	42.33	44.61	8.18	7.40	8.63	6.462	10.586	4.000	44.00	8.07	12.263	0.59	0.437
29-3	13.257	40.80	43.26	43.10	9.03	7.55	7.19	6.409	10.341	4.000	42.39	7.92	11.175	0.54	0.477
30-1	20.082	43.01	44.30	43.71	8.23	8.01	7.12	6.440	15.533	4.019	43.67	7.79	11.659	0.56	0.598
30-2	19.048	43.62	42.47	42.28	8.28	7.89	8.05	6.533	15.640	3.996	42.79	8.07	11.604	0.56	0.512
30-3	18.938	43.92	44.51	44.60	8.26	6.80	7.91	6.475	14.947	3.887	44.34	7.66	11.819	0.57	0.557
31-1	17.382	44.13	43.49	44.67	8.08	7.59	7.93	6.672	16.468	3.942	44.10	7.87	12.008	0.58	0.303
31-2	21.105	43.65	45.59	44.06	8.19	8.17	8.52	6.754	17.320	3.956	44.43	8.29	12.853	0.62	0.512
31-3	21.210	43.70	44.05	44.01	8.32	7.83	7.86	6.703	16.898	4.078	43.92	8.00	12.119	0.58	0.572
33-1	14.514	40.74	41.75	41.74	8.26	6.51	7.73	6.417	10.162	4.000	41.41	7.50	10.096	0.48	0.670
33-2	15.983	41.81	41.12	42.47	7.36	8.97	7.94	6.533	10.327	4.000	41.80	8.09	11.096	0.53	0.738
33-3	15.086	40.49	40.37	41.79	8.89	8.26	7.75	6.507	10.228	4.000	40.88	8.30	10.890	0.52	0.676
37-1	9.734	43.51	43.13	41.20	6.61	5.06	8.02	6.454	8.237	4.000	42.61	6.56	9.356	0.45	0.422
37-2	9.871	37.31	40.85	39.53	7.48	6.78	6.80	6.490	8.393	4.000	39.23	7.02	8.481	0.41	0.468
37-3	10.371	44.15	37.85	40.26	6.86	7.63	6.16	6.645	8.752	4.000	40.75	6.88	8.974	0.43	0.475
38-1	13.510	40.74	41.78	40.87	7.40	8.08	7.00	6.640	9.708	4.045	41.13	7.49	9.951	0.48	0.643
38-2	13.553	40.18	41.27	40.08	7.59	7.93	6.90	6.687	9.607	4.056	40.51	7.47	9.627	0.46	0.661
38-3	13.811	41.14	41.76	41.29	7.29	6.67	7.65	6.660	9.837	4.061	41.40	7.20	9.690	0.47	0.661

Table A 7. Contd.

	15 BAR							Post Experiment				Calculations			
Sample	Soil+Ring [g]	D1 [mm]	D2 [mm]	D3 [mm]	H1 [mm]	H2 [mm]	H3 [mm]	Box Weight [g]	Box + Dry Soil [g]	Ring Weight [g]	Average D [mm]	Average H [mm]	Average Volume [cm^3]	VC Ratio	VWC
94-1	9.757	40.74	40.27	40.03	6.29	8.32	5.92	6.548	9.142	3.999	40.35	6.84	8.745	0.42	0.362
94-2	9.498	41.11	44.64	40.79	6.87	6.88	6.03	6.530	9.183	3.783	42.18	6.59	9.208	0.44	0.333
94-3	9.344	36.28	36.27	38.04	5.55	6.58	6.58	6.485	9.027	3.998	36.86	6.24	6.653	0.33	0.421
96-1	8.669	35.04	41.22	38.04	6.07	5.55	5.91	6.566	9.090	3.841	38.10	5.84	6.659	0.32	0.346
96-2	8.364	35.04	41.22	38.04	6.07	5.55	5.91	6.534	8.760	4.146	38.10	5.84	6.659	0.32	0.299
96-3	8.563	35.04	41.22	38.04	6.07	5.55	5.91	6.507	8.530	3.904	38.10	5.84	6.659	0.32	0.396
97-1	7.644	41.17	39.59	39.78	6.58	7.20	6.05	6.525	8.296	3.841	40.18	6.61	8.377	0.40	0.243
97-2	8.298	42.18	42.75	41.13	6.36	7.00	6.54	6.683	9.038	4.047	42.02	6.63	9.194	0.44	0.226
97-3	8.184	38.17	38.34	42.00	7.26	7.20	6.68	6.755	9.123	3.899	39.50	7.05	8.632	0.41	0.229
104-1	9.780	37.74	37.18	37.39	7.80	7.01	6.19	6.596	9.274	4.065	37.44	7.00	7.701	0.37	0.394
104-2	10.659	37.67	36.70	36.58	6.39	7.70	6.81	6.699	9.912	4.044	36.98	6.97	7.480	0.36	0.442
104-3	10.779	36.00	37.12	36.46	6.76	6.82	6.29	6.739	9.875	4.006	36.53	6.62	6.937	0.33	0.472
112-1	9.426	36.75	35.82	36.04	6.67	6.17	6.23	6.514	9.307	3.917	36.20	6.36	6.540	0.31	0.415
112-2	10.355	36.56	35.41	38.43	6.29	6.30	6.29	6.761	9.998	3.893	36.80	6.29	6.690	0.32	0.493
112-3	9.853	35.98	35.54	36.68	6.91	6.51	5.84	6.568	9.619	3.883	36.07	6.42	6.556	0.31	0.446
116-1	9.050	35.32	37.64	35.09	6.10	6.12	6.38	6.486	9.006	3.939	36.02	6.20	6.313	0.30	0.410
116-2	10.138	35.74	34.44	36.39	6.31	6.86	6.99	6.577	9.396	4.047	35.52	6.72	6.657	0.32	0.518
116-3	9.109	35.42	34.43	34.36	5.91	5.62	6.06	6.527	9.159	3.884	34.74	5.86	5.554	0.27	0.411
155-1	9.076	37.46	34.13	39.00	6.48	5.82	6.74	6.451	8.585	4.046	36.86	6.35	6.770	0.33	0.428
155-2	8.273	37.46	34.13	39.00	6.48	5.82	6.74	6.557	8.595	3.922	36.86	6.35	6.770	0.33	0.342
155-3	9.214	37.46	34.13	39.00	6.48	5.82	6.74	6.547	8.957	4.154	36.86	6.35	6.770	0.33	0.391
156-1	12.248	42.49	44.77	43.50	7.24	7.25	8.23	6.641	9.419	3.847	43.59	7.57	11.294	0.54	0.498
156-2	11.596	42.82	42.78	43.21	8.21	7.56	8.61	6.686	9.416	3.976	42.94	8.13	11.761	0.56	0.416
156-3	11.607	43.64	42.31	42.81	6.95	7.01	7.60	6.661	9.472	3.969	42.92	7.19	10.392	0.50	0.464
157-1	8.646	39.55	40.23	42.06	6.40	6.95	6.22	6.507	8.881	3.852	40.61	6.52	8.446	0.41	0.287
157-2	8.831	42.25	37.34	39.14	6.35	5.86	5.29	6.597	9.159	4.033	39.58	5.83	7.172	0.34	0.265
157-3	9.043	39.95	36.53	37.32	7.01	5.97	5.97	6.491	9.111	3.912	37.93	6.32	7.135	0.34	0.297
158-1	9.816	43.87	42.72	43.33	7.35	7.24	7.33	6.447	8.681	3.850	43.31	7.31	10.757	0.52	0.347
158-2	9.899	42.91	40.92	44.02	6.55	6.23	6.56	6.464	8.538	3.775	42.62	6.45	9.191	0.44	0.441
158-3	9.815	43.11	43.35	42.70	7.43	8.01	7.62	6.413	8.736	4.029	43.05	7.69	11.185	0.54	0.310

Table A 7. Contd.

	15 BAR							Post Experiment				Calculations			
Sample	Soil+Ring [g]	D1 [mm]	D2 [mm]	D3 [mm]	H1 [mm]	H2 [mm]	H3 [mm]	Box Weight [g]	Box + Dry Soil [g]	Ring Weight [g]	Average D [mm]	Average H [mm]	Average Volume [cm^3]	VC Ratio	VWC
159-1	10.486	42.23	43.38	41.46	7.34	8.05	7.43	6.400	8.485	3.770	42.36	7.61	10.713	0.51	0.432
159-2	10.183	40.57	41.23	41.89	7.55	7.50	6.55	6.503	8.691	3.995	41.23	7.20	9.608	0.46	0.416
159-3	10.813	42.18	40.93	42.37	8.00	7.68	7.04	6.442	8.623	3.992	41.83	7.57	10.401	0.50	0.446
161-1	17.607	45.76	45.54	45.12	8.00	8.40	7.71	6.448	15.991	3.956	45.47	8.04	13.045	0.63	0.315
161-2	21.789	46.79	48.19	46.65	9.28	9.21	8.64	6.523	17.645	4.063	47.21	9.04	15.822	0.76	0.506
161-3	19.673	44.90	47.50	47.71	8.54	8.92	8.71	6.436	17.392	3.860	46.70	8.72	14.936	0.72	0.372
176-1	7.156	35.05	36.76	37.97	6.35	5.86	6.11	6.682	8.309	3.981	36.59	6.11	6.419	0.31	0.241
176-2	7.774	35.05	36.76	37.97	6.35	5.86	6.11	6.496	8.202	3.970	36.59	6.11	6.419	0.31	0.327
176-3	8.241	35.05	36.76	37.97	6.35	5.86	6.11	6.653	8.455	4.159	36.59	6.11	6.419	0.31	0.355
177-1	7.523	42.15	43.04	45.99	7.12	7.89	7.33	6.543	8.408	4.086	43.73	7.45	11.177	0.54	0.141
177-2	8.174	46.22	43.92	45.27	9.34	8.77	8.79	6.459	8.795	3.808	45.14	8.97	14.340	0.69	0.182
177-3	8.859	45.33	41.38	44.06	7.72	8.57	7.91	6.543	9.011	4.001	43.59	8.07	12.032	0.58	0.214
178-1	7.326	38.75	38.16	37.90	6.07	6.50	5.78	6.484	8.129	4.047	38.27	6.12	7.032	0.34	0.232
178-2	7.374	33.57	34.45	34.21	6.72	6.58	6.34	6.499	8.207	4.046	34.08	6.55	5.968	0.29	0.230
178-3	7.410	36.39	35.19	35.92	6.46	7.17	6.04	6.457	8.272	3.890	35.83	6.56	6.609	0.32	0.242
179-1	9.707	39.77	42.66	40.99	7.19	7.62	6.96	6.522	9.384	4.081	41.14	7.26	9.641	0.46	0.287
179-2	9.056	39.77	42.66	40.99	7.19	7.62	6.96	6.467	9.008	3.992	41.14	7.26	9.641	0.46	0.262
179-3	9.499	39.77	42.66	40.99	7.19	7.62	6.96	6.416	8.950	4.116	41.14	7.26	9.641	0.46	0.295
202-1	17.722	42.37	43.44	45.13	7.55	8.30	7.50	6.645	16.249	4.000	43.65	7.78	11.640	0.56	0.354
202-2	18.037	45.93	44.41	45.02	7.40	6.50	7.55	8.918	17.894	4.000	45.12	7.15	11.427	0.55	0.443
202-3	18.783	42.86	45.69	45.91	7.44	6.94	7.86	8.918	18.524	4.000	44.82	7.41	11.690	0.56	0.443
203-1	16.755	46.07	46.80	46.96	7.92	6.51	6.51	8.903	17.692	4.000	46.61	6.98	11.904	0.57	0.333
203-2	16.745	44.89	45.74	45.63	6.59	8.39	7.34	73.700	81.822	4.000	45.42	7.44	12.049	0.58	0.384
203-3	18.015	45.99	44.76	46.16	7.92	8.26	8.32	69.043	77.785	4.000	45.64	8.17	13.352	0.64	0.395
204-1	16.883	43.08	43.81	44.69	6.83	7.44	7.78	87.047	94.916	3.864	43.86	7.35	11.099	0.53	0.464
204-2	18.769	43.06	43.31	44.76	6.31	7.70	7.92	74.774	82.732	4.166	43.71	7.31	10.963	0.53	0.606
204-3	18.183	43.67	42.45	42.61	7.78	6.21	8.03	3.254	11.641	3.985	42.91	7.34	10.609	0.51	0.548
206-1	13.750	38.76	39.03	39.31	6.65	7.22	6.81	6.667	13.354	4.078	39.03	6.89	8.245	0.40	0.362
206-2	13.475	38.76	39.03	39.31	6.65	7.22	6.81	6.687	12.342	3.907	39.03	6.89	8.245	0.40	0.475
206-3	13.504	38.76	39.03	39.31	6.65	7.22	6.81	6.659	12.41	3.956	39.03	6.89	8.245	0.40	0.461

Table A 7. Contd.

	15 BAR							Post Experiment				Calculations			
Sample	Soil+Ring [g]	D1 [mm]	D2 [mm]	D3 [mm]	H1 [mm]	H2 [mm]	H3 [mm]	Box Weight [g]	Box + Dry Soil [g]	Ring Weight [g]	Average D [mm]	Average H [mm]	Average Volume [cm^3]	VC Ratio	VWC
207-1	18.481	45.09	45.27	45.49	7.25	8.18	7.63	6.610	16.377	3.994	45.28	7.69	12.373	0.59	0.381
207-2	17.259	45.25	43.34	44.44	9.26	7.71	7.10	6.680	15.780	4.023	44.34	8.02	12.385	0.59	0.334
207-3	16.803	44.62	44.08	46.50	7.70	7.69	8.45	6.660	15.117	3.874	45.07	7.95	12.670	0.61	0.353
209-1	11.694	38.45	37.84	35.90	6.93	5.89	6.67	6.990	10.885	4.036	37.40	6.50	7.132	0.34	0.528
209-2	11.340	41.59	38.01	38.64	6.28	6.61	5.45	6.880	10.301	3.880	39.41	6.11	7.455	0.36	0.542
209-3	12.073	38.83	36.66	37.82	6.65	7.12	6.75	6.551	10.544	3.973	37.77	6.84	7.660	0.37	0.536
213-1	11.170	38.64	37.66	38.77	6.32	6.76	7.44	6.531	9.314	3.875	38.36	6.84	7.900	0.38	0.571
213-2	10.027	37.25	37.96	37.54	6.26	7.39	6.31	6.488	9.170	3.775	37.58	6.65	7.377	0.35	0.484
213-3	9.993	36.58	40.16	37.00	6.35	7.05	6.33	6.562	9.186	4.016	37.91	6.58	7.421	0.36	0.452
214-1	11.399	36.30	36.53	37.85	7.09	6.68	7.21	6.443	9.232	4.012	36.89	6.99	7.472	0.36	0.615
214-2	9.349	32.72	32.83	33.48	6.00	6.68	5.13	6.462	8.938	3.983	33.01	5.94	5.078	0.24	0.569
214-3	10.218	35.65	35.37	35.38	6.30	6.66	7.28	6.408	9.136	3.997	35.47	6.75	6.662	0.32	0.524
217-1	15.642	43.88	41.61	43.18	6.96	9.03	7.06	6.417	13.673	4.034	42.89	7.68	11.095	0.53	0.392
217-2	16.516	42.46	41.67	40.07	7.65	8.09	6.91	6.531	14.593	3.847	41.40	7.55	10.158	0.49	0.454
217-3	15.897	42.20	42.41	41.94	8.35	7.71	8.41	6.506	13.935	3.876	42.18	8.16	11.394	0.55	0.403
218-1	12.242	41.21	41.69	41.22	7.36	6.41	7.06	6.454	9.670	3.854	41.37	6.94	9.330	0.45	0.554
218-2	12.161	44.80	40.34	42.71	6.49	7.48	7.12	6.490	9.800	4.013	42.62	7.03	10.023	0.48	0.483
218-3	11.241	41.06	40.72	40.82	6.66	6.87	6.24	6.645	9.781	3.780	40.87	6.59	8.640	0.41	0.501
219-1	13.332	37.72	37.82	38.42	6.30	7.34	7.27	6.639	12.069	3.992	37.99	6.97	7.895	0.38	0.495
219-2	14.411	37.91	38.29	37.51	6.82	6.43	7.46	6.687	12.291	3.854	37.90	6.90	7.785	0.37	0.636
219-3	13.538	35.37	39.10	36.47	6.01	5.22	5.80	6.659	12.067	4.035	36.98	5.68	6.094	0.29	0.672
220-1	11.359	37.30	38.40	39.15	7.24	6.95	6.10	6.647	9.966	3.774	38.28	6.76	7.781	0.37	0.548
220-2	11.914	36.88	38.23	36.84	7.25	6.79	7.13	8.921	12.824	3.869	37.32	7.06	7.714	0.37	0.537
220-3	11.683	35.90	41.48	38.44	7.73	6.96	7.90	8.918	12.823	4.034	38.61	7.53	8.810	0.42	0.425
221-1	17.854	43.35	43.47	43.21	8.32	9.02	7.57	8.906	19.223	3.870	43.34	8.30	12.245	0.59	0.299
221-2	16.397	42.59	44.30	45.16	7.64	6.42	6.56	6.608	15.881	3.887	44.02	6.87	10.454	0.50	0.310
221-3	16.981	43.84	44.97	44.04	7.26	5.91	6.68	6.678	16.367	3.874	44.28	6.62	10.186	0.49	0.336
252-1	13.604	39.12	38.21	39.33	7.00	8.08	7.06	6.399	11.144	4.029	38.89	7.38	8.760	0.42	0.551
252-2	13.636	40.85	39.43	39.90	7.54	6.20	7.48	6.498	10.844	3.999	40.06	7.07	8.911	0.43	0.594
252-3	14.097	40.45	39.93	40.42	6.79	7.42	6.33	6.438	10.964	3.973	40.27	6.85	8.714	0.42	0.642

Table A 7. Contd.

	15 BAR							Post Experiment				Calculations			
Sample	Soil+Ring [g]	D1 [mm]	D2 [mm]	D3 [mm]	H1 [mm]	H2 [mm]	H3 [mm]	Box Weight [g]	Box + Dry Soil [g]	Ring Weight [g]	Average D [mm]	Average H [mm]	Average Volume [cm^3]	VC Ratio	VWC
260-1	7.973	35.84	37.67	36.10	5.97	5.71	5.74	6.666	8.748	4.072	36.54	5.81	6.085	0.29	0.299
260-2	9.364	37.85	34.62	38.26	7.25	7.59	7.59	6.565	9.239	4.036	36.91	7.48	7.996	0.38	0.436
260-3	9.933	39.56	37.46	37.63	8.20	8.20	7.28	6.548	9.614	4.028	38.22	7.89	9.050	0.43	0.467
264-1	12.254	41.72	39.59	41.95	7.24	7.30	7.52	6.645	10.771	3.843	41.09	7.35	9.744	0.47	0.440
264-2	12.852	45.90	46.25	45.02	6.79	7.47	6.56	6.485	11.749	4.066	45.72	6.94	11.390	0.55	0.361
264-3	15.602	41.18	44.28	41.15	7.78	8.63	7.76	6.524	12.448	4.053	42.20	8.06	11.265	0.54	0.577
267-1	15.336	44.96	44.84	43.76	7.73	7.99	7.63	6.536	12.174	3.870	44.52	7.78	12.110	0.58	0.481
267-2	15.183	45.36	44.05	46.13	7.46	8.01	8.31	6.490	12.181	3.968	45.18	7.93	12.701	0.61	0.435
267-3	15.191	45.05	43.47	44.05	8.77	8.82	7.93	6.565	12.289	3.873	44.19	8.51	13.040	0.63	0.429
268-1	11.294	43.69	44.45	44.83	7.30	7.55	8.06	6.454	9.407	3.769	44.32	7.64	11.777	0.57	0.388
268-2	12.001	43.70	44.24	45.12	7.31	8.17	7.69	6.490	9.654	4.009	44.35	7.72	11.927	0.57	0.405
268-3	12.014	44.93	45.24	46.30	7.62	7.34	7.81	6.644	9.633	3.850	45.49	7.59	12.329	0.59	0.420
270-1	8.799	38.79	33.00	36.99	6.34	6.67	6.00	6.689	9.059	3.857	36.26	6.34	6.540	0.31	0.393
270-2	10.594	35.93	37.63	37.22	8.20	7.83	7.84	6.668	9.227	3.906	36.93	7.96	8.517	0.41	0.631
270-3	10.467	36.49	37.95	36.35	7.46	6.89	6.90	6.665	9.36	4.019	36.93	7.08	7.583	0.36	0.574
300-1	8.683	32.40	32.87	33.00	6.01	5.66	5.68	6.662	8.820	4.048	32.76	5.78	4.871	0.23	0.508
300-2	8.222	32.40	32.87	33.00	6.01	5.66	5.68	8.930	10.870	4.191	32.76	5.78	4.871	0.23	0.429
300-3	8.276	32.40	32.87	33.00	6.01	5.66	5.68	8.939	11.015	3.953	32.76	5.78	4.871	0.23	0.461
302-1	15.858	47.64	47.03	47.90	10.00	10.00	10.00	6.714	15.562	3.784	47.52	10.00	17.729	0.85	0.182
302-2	15.320	46.53	48.07	47.03	10.00	10.00	10.00	6.701	15.246	3.847	47.21	10.00	17.496	0.84	0.167
302-3	16.428	48.14	45.28	45.95	10.00	10.00	10.00	6.559	15.768	3.981	46.46	10.00	16.942	0.81	0.191
303-1	7.376	37.84	34.34	36.06	8.06	7.15	6.69	8.926	10.713	3.902	36.08	7.30	7.460	0.36	0.226
303-2	9.099	36.63	39.11	37.63	7.99	6.88	6.55	6.718	9.047	4.018	37.79	7.14	8.004	0.38	0.369
303-3	8.680	35.61	34.14	36.44	6.86	7.22	6.53	6.690	8.897	4.002	35.40	6.87	6.757	0.32	0.331
305-1	8.334	43.96	42.53	43.15	7.97	7.65	8.05	8.866	10.669	4.028	43.21	7.89	11.566	0.56	0.216
305-2	8.310	42.81	42.56	42.77	7.48	7.13	7.49	8.876	10.852	4.005	42.71	7.37	10.550	0.51	0.221
305-3	8.106	43.19	13.05	42.95	7.39	8.05	7.10	8.889	10.828	3.985	33.06	7.51	6.448	0.31	0.338
312-1	7.545	38.10	37.45	37.23	5.49	4.94	5.39	6.664	8.321	3.873	37.59	5.27	5.850	0.28	0.344
312-2	7.931	37.57	36.28	38.30	6.35	5.38	5.83	6.694	8.462	4.016	37.38	5.85	6.421	0.31	0.334
312-3	7.863	35.38	34.27	37.24	6.56	5.52	6.19	6.686	8.419	4.012	35.63	6.09	6.069	0.29	0.349

Table A 7. Contd.

	15 BAR							Post Experiment				Calculations			
Sample	Soil+Ring [g]	D1 [mm]	D2 [mm]	D3 [mm]	H1 [mm]	H2 [mm]	H3 [mm]	Box Weight [g]	Box + Dry Soil [g]	Ring Weight [g]	Average D [mm]	Average H [mm]	Average Volume [cm^3]	VC Ratio	VWC
313-1	7.599	38.40	43.15	40.52	4.25	4.96	5.75	6.544	8.177	3.983	40.69	4.99	6.481	0.31	0.306
313-2	7.844	41.89	42.33	40.48	5.59	5.04	6.09	6.493	8.047	3.997	41.57	5.57	7.559	0.36	0.303
313-3	7.971	49.47	39.31	40.89	6.19	6.55	4.30	6.573	8.086	3.973	43.22	5.68	8.330	0.40	0.298
314-1	7.946	40.21	41.00	39.72	6.64	5.51	6.01	8.938	10.947	4.057	40.31	6.05	7.722	0.37	0.243
314-2	8.005	40.89	41.34	39.86	7.01	6.88	7.88	6.669	8.967	3.891	40.70	7.26	9.435	0.45	0.235
314-3	8.191	40.25	39.96	40.14	8.91	8.02	7.89	8.930	11.263	3.901	40.12	8.27	10.452	0.50	0.253
315-1	8.166	40.45	40.23	39.54	5.88	4.99	5.50	6.640	8.297	4.046	40.07	5.46	6.879	0.33	0.358
315-2	8.005	39.83	41.74	41.48	5.51	5.79	5.04	6.691	8.389	4.035	41.02	5.45	7.193	0.35	0.316
315-3	8.191	40.00	41.68	37.63	6.50	6.72	5.10	6.661	8.432	3.776	39.77	6.11	7.582	0.36	0.349

Table A 8. Readings from the Delta-T PR2 Probe.

		Lysimeter 1				Lysimeter 2				Lysimeter 3			
		Probe Depth 30		Probe Depth 40		Probe Depth 30		Probe Depth 40		Probe Depth 30		Probe Depth 40	
	Time	V	Average V	V	Average V	V	Average V	V	Average V	V	Average V	V	Average V
Date	[PM]	[mV]	[mV]	[mV]	[mV]	[mV]	[mV]	[mV]	[mV]	[mV]	[mV]	[mV]	[mV]
		1049		1056		1051		1041		1052		1044	
		1056		1050		1043		1043		1052		1045	
29-Jan	2:02	1034	1046	1034	1047	1049	1048	1043	1042	1052	1052	1045	1045
		1008		1043		965		1028		999		1034	
		992		1041		965		1028		989		1041	
29-Jan	2:12	994	998	1016	1033	989	973	1034	1030	978	989	1049	1041
		971		1029		993		1028		996		1039	
		970		1030		983		1021		991		1037	
29-Jan	2:22	970	970	1030	1030	1002	993	1029	1026	956	981	1048	1041
		965		1010		957		1022		949		1052	
		969		1046		984		1031		997		1039	
29-Jan	2:32	967	967	1010	1022	949	963	1019	1024	924	957	1038	1043
		939		1038		969		1030		944		1052	
		956		1009		952		1021		987		1043	
29-Jan	2:42	957	951	1044	1030	961	961	1029	1027	904	945	1029	1041
		947		1046		951		1027		970		1040	
		975		1035		934		1019		906		1029	
29-Jan	2:52	954	959	1014	1032	968	951	1029	1025	993	956	1050	1040
		968		1043		953		1028		922		1037	
		954		1008		932		1020		952		1042	
29-Jan	3:02	930	951	1040	1030	961	949	1031	1026	911	928	1033	1037
		974		1037		932		1025		945		1040	
		937		1037		944		1020		920		1034	
29-Jan	3:12	955	955	1011	1028	956	944	1028	1024	951	939	1045	1040

Table A 8. Contd.

		Lysimeter 1				Lysimeter 2				Lysimeter 3			
		Probe Depth 30		Probe Depth 40		Probe Depth 30		Probe Depth 40		Probe Depth 30		Probe Depth 40	
	Time	V	Average V	V	Average V	V	Average V	V	Average V	V	Average V	V	Average V
Date	[PM]	[mV]	[mV]	[mV]	[mV]	[mV]	[mV]	[mV]	[mV]	[mV]	[mV]	[mV]	[mV]
		933		1041		942		1019		895		1030	
		942		1021		940		1026		978		1047	
29-Jan	3:22	970	948	1030	1031	948	943	1025	1023	937	937	1039	1039
		928		1031		935		1018		968		1047	
		953		1011		931		1022		963		1039	
29-Jan	3:32	936	939	1039	1027	944	937	1023	1021	924	952	1028	1038
		934		1042		948		1029		927		1043	
		952		1011		914		1018		980		1048	
29-Jan	3:42	967	951	1042	1032	935	932	1025	1024	921	943	1034	1042
		920		1035		942		1029		917		1031	
		949		1009		923		1024		917		1045	
29-Jan	3:52	931	933	1043	1029	931	932	1026	1026	972	935	1048	1041
		953		1017		936		1027		921		1032	
		922		1034		919		1020		940		1047	
29-Jan	4:02	967	947	1038	1030	956	937	1028	1025	933	931	1038	1039
		923		1019		938		1033		889		1043	
		987		1040		922		1029		917		1044	
30-Jan	2:12	932	947	1011	1023	918	926	1028	1030	904	903	1040	1042
		929		1011		908		1024		910		1034	
		914		1045		927		1034		907		1035	
31-Jan	2:12	928	924	1032	1029	907	914	1027	1028	925	914	1053	1041
		907		1048		892		1027		940		1051	
		938		1042		914		1030		904		1032	
1-Feb	2:12	925	923	1015	1035	887	898	1026	1028	959	934	1047	1043

Table A 8. Contd.

		Lysimeter 1				Lysimeter 2				Lysimeter 3			
		Probe Depth 30		Probe Depth 40		Probe Depth 30		Probe Depth 40		Probe Depth 30		Probe Depth 40	
	Time	V	Average V	V	Average V	V	Average V	V	Average V	V	Average V	V	Average V
Date	[PM]	[mV]	[mV]	[mV]	[mV]	[mV]	[mV]	[mV]	[mV]	[mV]	[mV]	[mV]	[mV]
		936		1035		895		1026		950		1052	
		881		1043		926		1034		944		1050	
2-Feb	2:12	911	909	1015	1031	891	904	1025	1028	899	931	1031	1044
		874		1042		891		1033		931		1049	
		926		1029		923		1035		913		1042	
9-Feb	2:12	881	894	1046	1039	883	899	1026	1031	936	927	1041	1044
		918		1023		886		1028		885		1037	
		893		1049		906		1035		942		1052	
16-Feb	2:12	902	904	1022	1031	900	897	1032	1032	935	921	1041	1043
		868		1045		871		1027		920		1044	
		904		1020		916		1034		923		1048	
23-Feb	2:12	923	898	1046	1037	890	892	1030	1030	899	914	1038	1043
		696		1040		882		1038		896		1051	
		678		1026		877		1035		896		1050	
2-Mar	2:15	859	744	1051	1039	916	892	1043	1039	845	879	1035	1045

APPENDIX B – R Codes

Appendix B provides the R codes developed and run in Eclipse with MRO (Microsoft R Open). The following are presented herewith:

- Script to compile and set up data (Chapter 2)
- Script that performs agglomerative cluster analysis (Chapter 2)
- Script to analyze the results from the agglomerative clustering (Chapter 2)
- Script to plot vGM related graphs (Chapter 2)
- Script using REVC with Whelan et al., 2006 site (Chapter 4)

```
##############################################################################
# TODO: Import Data Files and Create the Dataframe
#
# Author: Anupama John
##############################################################################

#----------------------Import Retention Data--------------------------------

# Retention data is imported from an csv file with average diameter, height,
# volume, VCR, and MC calculated for each triplicate
# sample names are 22-1, 22-2, 22-3 etc.
# this snippet does the following
#      1. Import data from csv and read into dataframe
#      2. Import the list of station names
#      3. Calculate averages of each station
#      4. Calculate standard deviations of each station
#      5. Merge Average and Standard Deviation
#      6. Write outfile with the merged tables of average and std deviation
#      7. Import mean and SD of OC, FC, HC, BD and merge with previous table


#----------------------1. Import data from csv-------------------------------

# Output file name
ver <- 002
outFile <- paste('Average_WaterRet_REMAP_', ver, '.csv', sep='')

# Set root to input data file location
root <- "C:/Users/Anupama/Documents/02_Academic/DISSERTATION/Data"
setwd(root)

# Read from csv and save to datafreame
WaterRet <- read.csv("_WaterRet_Rscript_GEODERMA.csv")
as.data.frame(WaterRet)


#-----------------2. Import the list of station names-----------------------

# Sites sampled
Site_List <- read.csv("Site_List.csv")


#-----3. Calculate averages of each station and store in a new dataframe------

# Create a new data frame with average
Avg_WaterRet<- data.frame(Site_List[ , 1])


for (l in 2:length(WaterRet))
{
       d <- 1
       for (i in seq(1, nrow(WaterRet), 3))
       {
```

```
            Avg_WaterRet[ d, l] <- round(((WaterRet[i,l] + WaterRet[i+1,l]
                  + WaterRet[i+2,l])/3),3)
            d <- d+1
      }
}

# Column names from WaterRet
names(Avg_WaterRet) <-names(WaterRet)


#---4. Calculate stadard deviations of each station, store in new dataframe---
#
Std_WaterRet<- data.frame(Site_List[ , 1])


for (l in 2:length(WaterRet))
{
      d <- 1
      for (i in seq(1, nrow(WaterRet), 3))
      {
            Std_WaterRet[ d, l] <- round(sd(c(WaterRet[i,l], WaterRet[i+1,l],
                  WaterRet[i+2,l])), 3)
            d <- d+1
      }
}

names(Std_WaterRet) <-names(WaterRet)

#--------------5. Merge Average and Standard Deviation Dataframes-------------

Avg_Std_WaterRet_Merge<- merge(Avg_WaterRet, Std_WaterRet, by="Sample")

#----6. Write outfile with the merged tables of average and std deviation-----

write.csv(Avg_Std_WaterRet_Merge,
      file = "_WaterRet_Average_StandardDeviationGEODERMA.csv")


#----7. Import mean and SD of OC, FC, HC, BD and merge with previous table----

# OC, FC, HC, BD are imported with a csv file and the data is merged with the
# data frame Avg_Std_WaterRet_Merge using the site names.
# Sample names are x_022, x_023 etc.
# This snippet does the following:
#                        1. Import data from csv and read into dataframe
#                        2. Merge with dataframe Avg_Std_WaterRet_Merge to
create REMAP1

# Read from csv and save to datafreame
SoilDat <- read.csv("_R_INPUT_OC_FC_HC_VERIF.csv")
as.data.frame(SoilDat)

# Merge with dataframe Avg_Std_WaterRet_Merge to create REMAP1
```

```
REMAP1<- merge(Avg_Std_WaterRet_Merge, SoilDat, by="Sample")

#------------------------8. Calculate the no-shrink VWC-----------------------
REMAP1$MC_10kPa_NoVC <- REMAP1$MC_10kPa.x*REMAP1$VCR_10kPa.x
REMAP1$MC_50kPa_NoVC <- REMAP1$MC_50kPa.x*REMAP1$VCR_50kPa.x
REMAP1$MC_1500kPa_NoVC <- REMAP1$MC_1500kPa.x*REMAP1$VCR_1500kPa.x


write.csv(REMAP1, file = "_REMAP_AllData_GEODERMA.csv")

##############################################################################
```

```
################################################################################
# TODO: Perform Hierarchical Cluster Analysis on Soil Variables
#
# Author: Anupama John
################################################################################

#-------------------------Cluster Analysis-----------------------------------

# VGM data obtained from RETC is imported from a csv file and
# clustering techniques are applied to it
# sample names are x_022, x_023 etc.
# this snippet does the following
#      1. Set root to C:/Users/Anupama/Desktop/02_Academic/DISSERTATION/Data
#      2. Import data from VGM.csv and read into dataframe
#      3. Set variables, create data frame, omit NAs
#      4. Scale Data
#      5. Compute dissimilarity matrix
#      6. Cluster Analysis
#      7. Plot cluster
#      8. Agglomerative coefficient
#      9. Cutting dendrograms
#      10. Add cluster number to dataframe df2
#      11. Plot rectangular borders
#      12. Calculate optimal number of clusters
#      13. Merge REMAP1 to VGM and Clustering Data
#      14. Export Data


library(cluster)    # clustering algorithms
library(factoextra) # clustering visualization
library(dendextend) # for comparing two dendrograms
library(purrr)
library(dplyr)

#----1. Set root to C:/Users/Anupama/Desktop/02_Academic/DISSERTATION/Data----

root <- "C:/Users/Anupama/Documents/02_Academic/DISSERTATION/Data"
setwd(root)

#------------2. Import data from VGM.csv and read into dataframe--------------

#df <-read.csv("VGM5.csv")
#df <-read.csv("WaterRet_Cluster_Input.csv")
inFile <-read.csv("_REMAP_AllData_GEODERMA.csv")
dF <- inFile[,-1]

#dF <- subset(dF, Sample != "x_094" & Sample != "x_023")

#----------------3. Set variables, create data frame, omit NAs---------------

#myvars <- c("Sample", "Theta_S", "Theta_R", "Alpha", "n")
#myvars <- c("Sample", "MC_0kPa.x", "MC_6kPa.x", "MC_10kPa.x", "MC_50kPa.x",
#        "MC_1500kPa.x", "VCR_10kPa.x", "VCR_50kPa.x", "VCR_1500kPa.x")
```

```
myvars <- c("Sample", "V_H2O_6kPa.x", "V_H2O_10kPa.x", "V_H2O_50kPa.x",
             "V_H2O_1500kPa.x","VCR_10kPa.x", "VCR_50kPa.x", "VCR_1500kPa.x",
             "MC_0kPa.x")
df_select <- dF[myvars]

df1 <- df_select[,-1]
rownames(df1) <- dF[,1]

df1 <- na.omit(df1)

#------------------------------4. Scale Data---------------------------------

df1 <- scale(df1)

#--------------------5. Compute dissimilarity matrix-------------------------

d <- dist(df1, method = "euclidean")

#----------------------------6. Cluster Analysis-----------------------------

# Agglomerative clustering using Complete Linkage
hc1 <- hclust(d, method = "ward.D2")

# Plot the obtained dendrogram
chartTitle <- paste("Hierarchical Cluster Analysis")
OPfileName <- paste (root, '/_ClusterWaterRetGEODERMA_MC0.tif', sep ='')
tiff(filename = OPfileName, width = 10, height = 10,
             units = 'in', pointsize = 12,
             compression = c('lzw'), bg = 'white', res = 600,
             restoreConsole = TRUE)
plot(hc1,  hang = -1)
dev.off()

# Compute with agnes
hc2 <- agnes(df1, method = "ward")

#----------------------8. Agglomerative coefficient-------------------------

hc2$ac

#methods to assess
m <- c("average", "single", "complete", "ward")
names(m) <- c( "average", "single", "complete", "ward")

# function to compute coefficient
ac <- function(x) {
       agnes(d, method = x)$ac
}

# compute coefficient for each method
#install.packages('purrr')
#library('purrr')
purrr:::map_dbl(m, ac)
```

```
# visualizing dendrogram using agnes
hc3 <- agnes(d, method = "ward")
x11()
pltree(hc3, cex = 0.6, hang = -1, main = "Dendrogram of agnes")

#-------------------------Cutting dendrograms-------------------------------

hc5 <- hclust(d, method = "ward.D2" )

# Cut tree into 4 groups
sub_grp <- cutree(hc5, k = 3)

# Number of members in each cluster
table(sub_grp)

#--------------------10. Add cluster number to dataframe----------------------

df2 <- dF %>%
             mutate(cluster = sub_grp)

#----------------------11. Plot rectangular borders--------------------------

chartTitle <- paste("Hierarchical Cluster Analysis")
OPfileName <- paste (root, '/_ClusterDendrodWaterRetGEODERMA_MC0.tif', sep
='')
tiff(filename = OPfileName, width = 10, height = 10,
             units = 'in', pointsize = 12,
             compression = c('lzw'), bg = 'white', res = 300,
             restoreConsole = TRUE)
plot(hc5, cex = 0.6, lwd = 1.5)
#colors set up to match cluster plot fviz
rect.hclust(hc5, k=3, border = c("green", "blue", "red"))
dev.off()

# Plot the clusters
chartTitle <- paste("Cluster Plot")
OPfileName <- paste (root, '/_ClusterPlotWaterGEODERMA_MC0.tif', sep ='')
tiff(filename = OPfileName, width = 10, height = 10,
             units = 'in', pointsize = 12,
             compression = c('lzw'), bg = 'white', res = 600,
             restoreConsole = TRUE)
fviz_cluster(list(data = df1, cluster = sub_grp), labelsize = 4)
dev.off()

#----------------12. Calculate optimal number of clusters--------------------

x11()
# Optimal number of clusters - ELBOW method
fviz_nbclust(df1, FUN = hcut, method = "wss")

chartTitle <- paste("Silhouette Method Optimal Cluster Number")
OPfileName <- paste (root, '/ClusterOptWaterRet4.tif', sep ='')
```

```
tiff(filename = OPfileName, width = 10, height = 10,
             units = 'in', pointsize = 12,
             compression = c('lzw'), bg = 'white', res = 600,
             restoreConsole = TRUE)
# Optimal number of clusters - AVERAGE SILHOUETTE method
fviz_nbclust(df1, FUN = hcut, method = "silhouette", labelsize = 14)
dev.off()

x11()
# Optimal number of clusters - GAP STATISTIC method
gap_stat <- clusGap(df1, FUN = hcut, nstart = 25, K.max = 10, B = 50)
fviz_gap_stat(gap_stat)


#----------------------------13. Read vGM data-------------------------------
# read vGM data from csv
vGM <- read.csv("_VGM_Geoderma_fitted_VC_noVC.csv")
REMAP_COMP<- merge(df2, vGM, by="Sample")

#----------------------------14. Export Data---------------------------------

write.csv(REMAP_COMP, file = "_REMAP_COMP_GEODERMA_MC0.csv")

################################################################################
```

```
#############################################################################
# TODO: Analysis of Clustered Data
#
# Author: Anupama John
#############################################################################

#-------------------------Cluster Analysis---------------------------------

# REMAP_COMP output dataframe from the 02_Agglocluster.R all properties
# including the cluster number of each sample
# sample names are x_022, x_023 etc.
# this snippet does the following
#      1. Create boxplot of cluster volumes
#      2. Create boxplot of cluster volumetric water contents
#      3. Create boxplot of vGM parameters with VC and without VC
#      4. Plot VGM curves within the clusters
#      5. Plot unsaturated hydraulic conductivity curves
#      6. Plot relative hydraulic conductivity curves
#      7. Plot capacity function within the clusters
#      8. Plot capacity function with pore size radius
#      9. Plot volume change within the clusters
#      10. Plot diameter change within the clusters
#      11. Plot height change within the clusters
#      12. Plot observed versus measured for all pressure heads
#      13. Plot capacity function with pore size radius
#      14. Plot capacity function with pressure head
#      15. Plot vGM parameters
#      16. Stats and ANOVA

#-----------------------------------------------------------------------------

root <- "C:/Users/Anupama/Documents/02_Academic/DISSERTATION/Data"
setwd(root)

REMAP_COMP <- read.csv("_REMAP_COMP_GEODERMA_MC0.csv") #sites sampled
as.data.frame(REMAP_COMP)


#------1. Create boxplot of cluster volumes
# Volume of water and volume of samples  in a multi panel graph

#Number of rows and columns to be plotted
plotRows <- 2
plotCols <- 4
plotLabel <- c('a','b','c', 'd', 'e', 'f', 'g', 'h')
plotReso <- 600
plotWidth <- 8
plotHeight <- 4
cexStatLab <- 0.7

# Create a file to save the plot of cluster properties
dev.new()
OPfileName <- paste (root, '/_ClusterPropertiesGEODERMA_MC0.tif', sep ='')
```

```
tiff(filename = OPfileName, width = plotWidth, height = plotHeight,
             units = 'in', pointsize = 12,
             compression = c('lzw'), bg = 'white', res = plotReso,
             restoreConsole = TRUE)
# Format plot area
par(mgp = c(0.75,0.1,0.0), tck = -0.02, mfcol = c(plotRows, plotCols),
             mai=c(0.3,0.35,0.2,0.01), lwd=1, omi=c(0.1,0.1,0.1,0.1),
             cex.lab=.9, cex.axis=0.7, cex.main=.9)

# ROW 1 COLUMN 1 - 6 kPa Vw
boxplot(REMAP_COMP$V_H2O_10kPa.x~REMAP_COMP$cluster, xlab = "Cluster",
             ylab = "Vw 6 kPa (cm3)", ylim = c(0,19), cex=.5, main =
                          paste('(', plotLabel[1], ')'))


# ROW 2 COLUMN 1  - OC temporarily
boxplot(REMAP_COMP$V_6kPa.x~REMAP_COMP$cluster, xlab = "Cluster", ylab =
                          "Vs 6 kPa (cm3)", cex=.5, ylim = c(0,20.8), main =
                          paste('(', plotLabel[5],')'))

# ROW 1 COLUMN 2 - 10kPa Vw
boxplot(REMAP_COMP$V_H2O_10kPa.x~REMAP_COMP$cluster, xlab = "Cluster", ylab =
                          "Vw 10 kPa (cm3)", ylim = c(0,19), cex=.5, main =
                          paste('(', plotLabel[2],')'))

# ROW 2 COLUMN 2 - VCR 10kPa
boxplot(REMAP_COMP$V_10kPa.x~REMAP_COMP$cluster, xlab = "Cluster", ylab =
                          "Vs 10 kPa (cm3)", cex=.5, ylim = c(0,20.8), main =
                          paste('(', plotLabel[6], ')'))

# ROW 1 COLUMN 3
boxplot(REMAP_COMP$V_H2O_1500kPa.x~REMAP_COMP$cluster , xlab = "Cluster", ylab
=
                          "Vw 50 kPa (cm3)", ylim = c(0,19), cex=.5, main =
                          paste('(', plotLabel[3], ')'))

# ROW 2 COLUMN 3
boxplot(REMAP_COMP$V_50kPa.x~REMAP_COMP$cluster, xlab = "Cluster", ylab =
                          "Vs 50 kPa (cm3)", cex=.5, ylim = c(0,20.8), main =
                          paste('(', plotLabel[7],')'))

# ROW 1 COLUMN 4
boxplot(REMAP_COMP$V_H2O_1500kPa.x~REMAP_COMP$cluster, xlab = "Cluster", ylab
=
                          "Vw 1500 kPa (cm3)", ylim = c(0,19), cex=.5, main =
                          paste('(', plotLabel[4], ')'))

# ROW 2 COLUMN 4
boxplot(REMAP_COMP$H_10kPa.x~REMAP_COMP$cluster, xlab = "Cluster", ylab =
                          "Vs 1500 kPa (cm3)", cex=.5, ylim = c(0,20.8), main
=
                          paste('(', plotLabel[8], ')'))
```

```
dev.off()



#------2. Create boxplot of cluster volumetric water contents
# Volumetric water contents in a multi panel graph

#Number of rows and columns to be plotted
plotRows <- 2
plotCols <- 4
plotLabel <- c('a','b','c', 'd', 'e', 'f', 'g', 'h')
plotReso <- 600
plotWidth <- 8
plotHeight <- 4
cexStatLab <- 0.7

# Create a file to save the plot of cluster properties
dev.new()
OPfileName <- paste (root, '/_ClusterPropertiesVWC_MC0.tif', sep ='')
tiff(filename = OPfileName, width = plotWidth, height = plotHeight,
             units = 'in', pointsize = 12,
             compression = c('lzw'), bg = 'white', res = plotReso,
             restoreConsole = TRUE)
# Format plot area
par(mgp = c(0.75,0.1,0.0), tck = -0.02, mfcol = c(plotRows, plotCols),
             mai=c(0.3,0.35,0.2,0.01), lwd=1, omi=c(0.1,0.1,0.1,0.1),
             cex.lab=.9, cex.axis=0.7, cex.main=.9)

# ROW 1 COLUMN 1 - 6 kPa Vw
boxplot(REMAP_COMP$MC_6kPa.x~REMAP_COMP$cluster, xlab = "Cluster",
             ylab = "VWC 6 kPa (-)", ylim = c(0,1), cex=.5, main =
                          paste('(', plotLabel[1], ')'))


# ROW 2 COLUMN 1  - OC temporarily
boxplot(REMAP_COMP$MC_6kPa.x~REMAP_COMP$cluster, xlab = "Cluster", ylab =
                          "NonVC VWC 6 kPa (-)", cex=.5, ylim = c(0,1), main =
                          paste('(', plotLabel[5],')'))

# ROW 1 COLUMN 2 - 10kPa Vw
boxplot(REMAP_COMP$MC_10kPa.x~REMAP_COMP$cluster, xlab = "Cluster", ylab =
                          "VWC 10 kPa (-)", ylim = c(0,1), cex=.5, main =
                          paste('(', plotLabel[2], ')'))

# ROW 2 COLUMN 2 - VCR 10kPa
boxplot(REMAP_COMP$MC_10kPa_NoVC~REMAP_COMP$cluster, xlab = "Cluster", ylab =
                          "NonVC VWC 10 kPa (-)", cex=.5, ylim = c(0,1), main
=
                          paste('(', plotLabel[6], ')'))

# ROW 1 COLUMN 3
boxplot(REMAP_COMP$MC_50kPa.x~REMAP_COMP$cluster , xlab = "Cluster", ylab =
```

```
                          "VWC 50 kPa (-)", ylim = c(0,1), cex=.5, main =
paste('(',
                          plotLabel[3], ')'))

# ROW 2 COLUMN 3
boxplot(REMAP_COMP$MC_50kPa_NoVC~REMAP_COMP$cluster, xlab = "Cluster", ylab =
                          "NonVC VWC 50 kPa (-)", cex=.5, ylim = c(0,1), main
=
                          paste('(', plotLabel[7],')'))

# ROW 1 COLUMN 4
boxplot(REMAP_COMP$MC_1500kPa.x~REMAP_COMP$cluster, xlab = "Cluster", ylab =
                          "VWC 1500 kPa (-)", ylim = c(0,1), cex=.5, main =
paste('(',
                          plotLabel[4], ')'))

# ROW 2 COLUMN 4
boxplot(REMAP_COMP$MC_1500kPa_NoVC~REMAP_COMP$cluster, xlab = "Cluster", ylab
=
                          "NonVC VWC 1500 kPa (-)", cex=.5, ylim = c(0,1),
main =
                          paste('(', plotLabel[8], ')'))
dev.off()


#------3. Create boxplot of vGM parameters with VC and without VC---------
# Volumetric water contents in a multi panel graph

Outliers <- c("x_112", "x_155", "x_270", "x_024", "x_038",
              "x_206", "x_213")
vGM <- REMAP_COMP
for (i in 1:length(Outliers)){
       vGM <- subset(vGM, Sample != Outliers[i])
}


#Number of rows and columns to be plotted
plotRows <- 2
plotCols <- 4
plotLabel <- c('a','b','c', 'd', 'e', 'f', 'g', 'h')
plotReso <- 600
plotWidth <- 8
plotHeight <- 4
cexStatLab <- 0.7

# Create a file to save the plot of cluster properties
dev.new()
OPfileName <- paste (root, '/_ClusterPropertiesVGM_MC0.tif', sep ='')
tiff(filename = OPfileName, width = plotWidth, height = plotHeight,
             units = 'in', pointsize = 12,
             compression = c('lzw'), bg = 'white', res = plotReso,
             restoreConsole = TRUE)
# Format plot area
```

```
par(mgp = c(0.75,0.1,0.0), tck = -0.02, mfcol = c(plotRows, plotCols),
             mai=c(0.3,0.35,0.2,0.01), lwd=1, omi=c(0.1,0.1,0.1,0.1),
             cex.lab=.9, cex.axis=0.7, cex.main=.9)

# ROW 1 COLUMN 1 - 6 kPa Vw
boxplot(vGM$Theta_R~vGM$cluster, xlab = "Cluster",
             ylab = "Saturated VWC (-)", ylim = c(0,1), cex=.5, main =
                          paste('(', plotLabel[1], ')'))


# ROW 2 COLUMN 1  - OC temporarily
boxplot(vGM$Theta_S_NoVC~vGM$cluster, xlab = "Cluster", ylab =
                          "NonVC Saturated VWC (-)", cex=.5, ylim = c(0,1),
                          main = paste('(', plotLabel[5],
                          ')'))

# ROW 1 COLUMN 2 - 10kPa Vw
boxplot(vGM$Theta_R~vGM$cluster, xlab = "Cluster", ylab =
                          "Residual VWC (-)", ylim = c(0,1), cex=.5, main =
                          paste('(', plotLabel[2],
                          ')'))

# ROW 2 COLUMN 2 - VCR 10kPa
boxplot(vGM$Theta_R_NoVC~vGM$cluster, xlab = "Cluster", ylab =
                          "NonVC Residual VWC (-)", cex=.5, ylim = c(0,1),
                          main = paste('(', plotLabel[6], ')'))

# ROW 1 COLUMN 3
boxplot(vGM$Alpha~vGM$cluster , xlab = "Cluster", ylab =
                          "Alpha (1/cm)", cex=.5, main = paste('(',
                          plotLabel[3], ')'), ylim = c(0,0.1))

# ROW 2 COLUMN 3
boxplot(vGM$Alpha_NoVC~vGM$cluster, xlab = "Cluster", ylab =
                          "NonVC Alpha (1/cm)", cex=.5, main =
                          paste('(', plotLabel[7],
                          ')'), ylim = c(0,0.1))

# ROW 1 COLUMN 4
boxplot(vGM$n~vGM$cluster, xlab = "Cluster", ylab =
                          "n (-)", cex=.5, main = paste('(',
                          plotLabel[4], ')'), ylim = c(0,2))

# ROW 2 COLUMN 4
boxplot(vGM$n_NoVC~vGM$cluster, xlab = "Cluster", ylab =
                          "NonVC n (-)", cex=.5, main = paste('(',
                          plotLabel[8], ')'), ylim = c(0,2))
dev.off()



#Number of rows and columns to be plotted
```

```
plotRows <- 4
plotCols <- 3
plotLabel <- c('a','b','c', 'd', 'e', 'f', 'g', 'h')
plotReso <- 600
plotWidth <- 5.5
plotHeight <- 6
cexStatLab <- 0.7

# Create a file to save the plot of cluster properties
dev.new()
OPfileName <- paste (root, '/_ClusterVGMGEODERMA.tif', sep ='')
tiff(filename = OPfileName, width = plotWidth, height = plotHeight,
       units = 'in', pointsize = 12,
       compression = c('lzw'), bg = 'white', res = plotReso,
       restoreConsole = TRUE)
# Format plot area
par(mgp = c(0.75,0.1,0.0), tck = -0.02, mfcol = c(plotRows, plotCols),
       mai=c(0.3,0.35,0.2,0.01), lwd=1, omi=c(0.1,0.1,0.1,0.1),
       cex.lab=.9, cex.axis=0.7, cex.main=.9)
# ROW 1 COLUMN 1
boxplot(REMAP_COMP$OC.x~REMAP_COMP$cluster, xlab = "Cluster", ylab =
       "Organic Content (%)", cex=.5#, main = paste('(', plotLabel[1],')')
)

# ROW 2 COLUMN 1
REMAP_COMP$log_HC.x <- log(REMAP_COMP$HC.x) #calculate log of HC
boxplot(REMAP_COMP$log_HC.x~REMAP_COMP$cluster, xlab = "Cluster",
       ylab = "log(Hydraulic Conductivity (cm/d)", cex=.5, main =
       paste('(', plotLabel[4], ')'))

# ROW 3 COLUMN 1
boxplot(REMAP_COMP$Alpha~REMAP_COMP$cluster, xlab = "Cluster", ylab =
       "Alpha (1/cm)", cex=.5, main = paste('(', plotLabel[7],
       ')'))

# ROW 1 COLUMN 2
boxplot(REMAP_COMP$FC~REMAP_COMP$cluster , xlab = "Cluster", ylab =
       "Fiber Content (%)", cex=.5, main = paste('(',
       plotLabel[2], ')'))

# ROW 2 COLUMN 2
boxplot(REMAP_COMP$Theta_R~REMAP_COMP$cluster, xlab = "Cluster", ylab =
       "Saturated Water Content (-)", cex=.5, main = paste('(',
       plotLabel[5], ')'))

# ROW 3 COLUMN 2
boxplot(REMAP_COMP$n~REMAP_COMP$cluster, xlab = "Cluster", ylab = "n",
       cex=.5, main = paste('(', plotLabel[8], ')'))

# ROW 1 COLUMN 3
boxplot(REMAP_COMP$BD.x~REMAP_COMP$cluster, xlab = "Cluster", ylab =
       "Bulk Density (g/cm^3)", cex=.5, main = paste('(', plotLabel[3],
       ')'))
```

```
# ROW 2 COLUMN 3
boxplot(REMAP_COMP$Theta_R~REMAP_COMP$cluster, xlab = "Cluster", ylab =
       "Residual Water Content (-)", cex=.5, main = paste('(',
       plotLabel[6], ')'))

dev.off()


#-------------4. Plot VGM curves within the clusters--------------------------
for (Clust in 1:3)
{
       ClustSub <- subset(REMAP_COMP, cluster == Clust)
       x11()
       for (i in 1:nrow(ClustSub)){
              vGM_Theta_S <- ClustSub$Theta_R[i]
              vGM_Theta_R <- ClustSub$Theta_R[i]
              vGM_Alpha <- ClustSub$Alpha[i]
              vGM_n <- ClustSub$n[i]

              #m is calculated from n
              vGM_m <- 1 - (1/vGM_n)


              #create an R function for vGM
              vGM <- function(x){
                     ((vGM_Theta_S - vGM_Theta_R)/((1+(vGM_Alpha * x)^ vGM_n)^
                     vGM_m)) + vGM_Theta_R
              }

              #plot R function with log transformed x-axis
              curve(vGM, from = 0.1, to = 15296, log = "x", xlab =
                     "Pressure Head (cm)", ylab = "Volumetric Water Content
                     (-)",ylim = c(0,1.2), xlim = c(1,10000), main = paste
                     ('Cluster ', Clust), lwd = 1.5, cex.lab = 1.2,
                     cex.axis = 1.2, cex.main = 1.5)
              par(new=TRUE)
              #points(a~b)

       }

}

#------------5. Plot unsaturated hydraulic conductivity curves----------------
for (Clust in 1:3)
{
       ClustSub <- subset(REMAP_COMP, cluster == Clust & HC.x != 'NA')
       x11()
       for (i in 1:nrow(ClustSub)){
              vGM_Theta_S <- ClustSub$Theta_R[i]
              vGM_Theta_R <- ClustSub$Theta_R[i]
              vGM_Alpha <- ClustSub$Alpha[i]
              vGM_n <- ClustSub$n[i]
```

```
                HC <- ClustSub$HC.x[i]
                #m is calculated from n
                vGM_m <- 1 - (1/vGM_n)
                l <- 0.5

                #create an R function for unsaturated hyd. conductivity
                vGM_unsat_HC <- function(x){
                        HC * ((1/((1 + (vGM_Alpha*x)^vGM_n)^vGM_m)) ^ l) *
                        ((1 - (1 - (1/((1 + (vGM_Alpha*x)^vGM_n)^vGM_m)) ^
                        (1/vGM_m))^vGM_m)^2)
                }

                #plot R function
                curve(vGM_unsat_HC, from = 0.1, to = 15000, log = "x",
                        xlab = "Pressure Head (cm)",
                        ylab = "Hydraulic Conductivity (cm/d)",
                        ylim = c(0,max(ClustSub$HC.x)), xlim = c(0.2,10000.1),
                        main = paste('Cluster ', Clust), lwd = 1.5, cex.lab=1.2,
                        cex.axis=1.2, cex.main=1.5)
                par(new=TRUE)

        }

}

#------------6. Plot relative hydraulic conductivity curves-------------------
for (Clust in 1:3){
        ClustSub <- subset(REMAP_COMP, cluster == Clust & HC.x != 'NA')
        x11()
        for (i in 1:nrow(ClustSub)){
                vGM_Theta_S <- ClustSub$Theta_R[i]
                vGM_Theta_R <- ClustSub$Theta_R[i]
                vGM_Alpha <- ClustSub$Alpha[i]
                vGM_n <- ClustSub$n[i]
                HC <- ClustSub$HC.x[i]
                #m is calculated from n
                vGM_m <- 1 - (1/vGM_n)
                l <- 0.5

                #create an R function for relative unsaturated hyd. conductivity

                vGM_unsat_HC <- function(x){
                        ((1 / ((1 + (vGM_Alpha * x) ^ vGM_n) ^ vGM_m)) ^ l) *
                        ((1 - ( 1 - (1 / (( 1 + (vGM_Alpha * x)^ vGM_n) ^ vGM_m))
                        ^ (1 / vGM_m)) ^ vGM_m) ^ 2)
                }

                #plot R function
                curve(vGM_unsat_HC, from = 0.000001, to = 15000, log = "x",
                        xlab = "Pressure Head (cm)",
                        ylab = "Relative Hydraulic Conductivity (-)",
                        ylim = c(0,1),
                        xlim = c(0.000001,10000.1),
```

```
                  main = paste('Cluster ', Clust), lwd = 1.5, cex.lab=1.2,
                  cex.axis=1.2, cex.main=1.5)
            par(new=TRUE)
      }

}

#-------------7. Plot capacity function within the clusters-------------------
for (Clust in 1:3){
      ClustSub <- subset(REMAP_COMP, cluster == Clust & HC.x != 'NA')
      x11()
      for (i in 1:nrow(ClustSub)){
            vGM_Theta_S <- ClustSub$Theta_R[i]
            vGM_Theta_R <- ClustSub$Theta_R[i]
            vGM_Alpha <- ClustSub$Alpha[i]
            vGM_n <- ClustSub$n[i]
            HC <- ClustSub$HC.x[i]
            #m is calculated from n
            vGM_m <- 1 - (1/vGM_n)
            l <- 0.5

            #create an R function for capacity function
            vGM_unsat_Cw <- function(x){
                  ((vGM_Alpha^vGM_n)*(vGM_Theta_S - vGM_Theta_R)*vGM_m*
                  vGM_n*((x)^(vGM_n-1)))/((1 + (vGM_Alpha*(x))^(vGM_n))
                  ^(vGM_m+1))
            }

            #plot R function
            curve(vGM_unsat_Cw, from = 0.000001, to = 15000, log = "x",
                  xlab = "Pressure Head (cm)", ylab =
                  "Hydraulic Capacity (1/cm)", ylim = c(0,0.011),
                  xlim = c(0.0001,10000), main = paste('Cluster ',
                  Clust), lwd = 1.5, cex.lab=1.2, cex.axis=1.2,
                  cex.main=1.5)
            par(new=TRUE)

      }

}

#----------8. Plot capacity function with pore size radius--------------------

for (Clust in 1:3){
      ClustSub <- subset(REMAP_COMP, cluster == Clust & HC.x != 'NA')
      x11()
      for (i in 1:nrow(ClustSub)){
            vGM_Theta_S <- ClustSub$Theta_R[i]
            vGM_Theta_R <- ClustSub$Theta_R[i]
            vGM_Alpha <- ClustSub$Alpha[i]
            vGM_n <- ClustSub$n[i]
            HC <- ClustSub$HC.x[i]
            #m is calculated from n
```

```
            vGM_m <- 1 - (1/vGM_n)
            l <- 0.5


            vGM_unsat_Cw <- function(x){
                  ((vGM_Alpha^vGM_n)*(vGM_Theta_S - vGM_Theta_R)*
                  vGM_m*vGM_n*((0.104/x)^(vGM_n-1)))/
                  ((1 + (vGM_Alpha*(0.104/x))^
                  (vGM_n))^(vGM_m+1))
            }

            #plot R function
            curve(vGM_unsat_Cw, from = 0.00001, to = 100, log = "x",
                  xlab = "Pore Radius (cm)", ylab =
                  "Hydraulic Capacity (1/cm)", ylim = c(0,0.011),
                  xlim = c(0.0001,50), main = paste('Cluster ', Clust),
                  lwd = 1.5, cex.lab=1.2, cex.axis=1.2, cex.main=1.5)
            par(new=TRUE)

      }

}

#----------------9. Plot volume change within the clusters--------------------

Pressure <- c(1, 61, 102, 510, 15296)
log_Pres <- log(Pressure)
color <- c("red", "blue", "green")
x11()
for (Clust in 1:3)
{
      ClustSub <- subset(REMAP_COMP, cluster == Clust)


      mean_VCR_ClusSub <- c(1, mean(ClustSub$VCR_6kPa.x),
            mean(ClustSub$VCR_10kPa.x), mean(ClustSub$VCR_50kPa.x),
            mean(ClustSub$VCR_1500kPa.x))
      std_VCR_ClusSub <- c(0, sd(ClustSub$VCR_6kPa.x),
            sd(ClustSub$VCR_10kPa.x), sd(ClustSub$VCR_50kPa.x),
            sd(ClustSub$VCR_1500kPa.x))


      smoothingSpline1 <- smooth.spline(log_Pres, mean_VCR_ClusSub, spar = 0)

      plot (log_Pres, mean_VCR_ClusSub, ylim = c(0,1),
            xlim = c(0, max(log_Pres)), xlab = "log(Pressure Head (cm))",
            ylab = "Volume Change Ratio (-)", pch = 1,
            col = color[Clust], cex = 1.2, cex.lab = 1.2)

      arrows(log_Pres, mean_VCR_ClusSub - std_VCR_ClusSub, log_Pres,
            mean_VCR_ClusSub + std_VCR_ClusSub, length=0.05, angle=90,
            code=3, col = color[Clust])
```

```
        lines(smoothingSpline1, col = color[Clust])
        par(xpd = TRUE)
        legend("bottomleft",
               legend=c("Cluster 1","Cluster 2", "Cluster 3"),
               cex = 1,
               pch=c(1,1,1,1),
               col = color,
               horiz = FALSE)

        par(new=TRUE)
}


#----------10. Plot diameter change within the clusters-----------------------

Pressure <- c(1, 61, 102, 510, 15296)
log_Pres <- log(Pressure)
color <- c("red", "blue", "green")

REMAP_COMP$DC_6kPA <- REMAP_COMP$D_6kPa.x/51.5
REMAP_COMP$DC_10kPA <- REMAP_COMP$D_10kPa.x/51.5
REMAP_COMP$DC_50kPA <- REMAP_COMP$D_50kPa.x/51.5
REMAP_COMP$DC_1500kPA <- REMAP_COMP$D_1500kPa.x/51.5


x11()
for (Clust in 1:3){
        ClustSub <- subset(REMAP_COMP, cluster == Clust)


        mean_DC_ClusSub <- c(1, mean(ClustSub$DC_6kPA), mean(ClustSub$DC_10kPA),
               mean(ClustSub$DC_50kPA), mean(ClustSub$DC_1500kPA))
        std_DC_ClusSub <- c(0, sd(ClustSub$DC_6kPA), sd(ClustSub$DC_10kPA),
               sd(ClustSub$DC_50kPA), sd(ClustSub$DC_1500kPA))


        smoothingSpline1 <- smooth.spline(log_Pres, mean_DC_ClusSub, spar = 0)

        plot (log_Pres, mean_DC_ClusSub, ylim = c(0.5,1), xlim = c(0,
               max(log_Pres)), xlab = "log( Pressure Head (cm)) ",
               ylab = "Diameter Change Ratio (-) ", pch = 1, col =
               color[Clust], cex = 1.2, cex.lab = 1.2, main = "(a)")

        arrows(log_Pres, mean_DC_ClusSub - std_DC_ClusSub, log_Pres,
               mean_DC_ClusSub + std_DC_ClusSub, length=0.05, angle=90, code=3,
               col = color[Clust])

        lines(smoothingSpline1, col = color[Clust])
        par(xpd = TRUE)
        legend("bottomleft",
               legend=c("Cluster 1","Cluster 2", "Cluster 3"),
               cex = 1,
               pch=c(1,1,1),
```

```
              col = color,
              horiz = FALSE)

       par(new=TRUE)
}


#--------------11. Plot height change within the clusters --------------------

Pressure <- c(1, 61, 102, 510, 15296)
log_Pres <- log(Pressure)
color <- c("red", "green", "blue")

REMAP_COMP$HC_6kPA <- REMAP_COMP$H_6kPa.x/10
REMAP_COMP$HC_10kPA <- REMAP_COMP$H_10kPa.x/10
REMAP_COMP$HC_50kPA <- REMAP_COMP$H_50kPa.x/10
REMAP_COMP$HC_1500kPA <- REMAP_COMP$H_1500kPa.x/10


x11()
for (Clust in 1:3){
       ClustSub <- subset(REMAP_COMP, cluster == Clust)


       mean_HC_ClusSub <- c(1, mean(ClustSub$HC_6kPA), mean(ClustSub$HC_10kPA),
              mean(ClustSub$HC_50kPA), mean(ClustSub$HC_1500kPA))
       std_HC_ClusSub <- c(0, sd(ClustSub$HC_6kPA), sd(ClustSub$HC_10kPA),
              sd(ClustSub$HC_50kPA), sd(ClustSub$HC_1500kPA))


       smoothingSpline1 <- smooth.spline(log_Pres, mean_HC_ClusSub, spar = 0)

       plot (log_Pres, mean_HC_ClusSub, ylim = c(0.5,1), xlim = c(0,
              max(log_Pres)), xlab = "log( Pressure Head (cm)) ",
              ylab = "Height Change Ratio (-) ", pch = 1,
              col = color[Clust], cex = 1.2, cex.lab = 1.2)

       arrows(log_Pres, mean_HC_ClusSub - std_HC_ClusSub, log_Pres,
              mean_HC_ClusSub + std_HC_ClusSub, length=0.05, angle=90, code=3,
              col = color[Clust])

       lines(log_Pres, mean_HC_ClusSub, ylim = c(0.5,1), xlim = c(0,
              max(log_Pres)), col = color[Clust])

       par(xpd = TRUE)
       legend("bottomleft",
              legend=c("Cluster 1","Cluster 2", "Cluster 3"),
              cex = 1,
              pch=c(1,1,1,1),
              col = c("red","green", "blue"),
              horiz = FALSE)

       par(new=TRUE)
```

```
}

# ANOVA for HCR
anova1 <- aov(REMAP_COMP$HC_6kPA ~ factor(REMAP_COMP$cluster))
summary(anova1)
# ANOVA for HCR
anova2 <- aov(REMAP_COMP$HC_10kPA ~ factor(REMAP_COMP$cluster))
summary(anova2)
# ANOVA for HCR
anova3 <- aov(REMAP_COMP$HC_50kPA ~ factor(REMAP_COMP$cluster))
summary(anova3)
# ANOVA for HCR
anova4 <- aov(REMAP_COMP$HC_1500kPA ~ factor(REMAP_COMP$cluster))
summary(anova4)
TukeyHSD(anova4)


#--------12. Plot observed versus measured for all pressure heads------------

for (i in 1:nrow(REMAP_COMP)){
       vGM_Theta_S <-REMAP_COMP$Theta_R[i]
       vGM_Theta_R <- REMAP_COMP$Theta_R[i]
       vGM_Alpha <- REMAP_COMP$Alpha[i]
       vGM_n <- REMAP_COMP$n[i]

       #m is calculated from n
       vGM_m <- 1 - (1/vGM_n)

       #create an R function for vGM
       vGM <- function(x){
              ((vGM_Theta_S - vGM_Theta_R)/((1+(vGM_Alpha * x)^ vGM_n)^
              vGM_m))+ vGM_Theta_R
       }

       MCmes <- c(REMAP_COMP$MC_0kPa.x[i], REMAP_COMP$MC_6kPa.x[i],
              REMAP_COMP$MC_10kPa.x[i], REMAP_COMP$MC_50kPa.x[i],
              REMAP_COMP$MC_1500kPa.x[i])
       MCcalc <- c(vGM(1), vGM(61), vGM(102), vGM(510), vGM(15296))
       MCRatio <- MCcalc/MCmes
       Pressure <- c(0, 6, 10, 50, 1500)

       DAT <-data.frame(Pressure, MCcalc, MCmes, MCRatio)

       #Check for outliers in data
       for (j in 1:5){
              if (DAT$MCRatio[j] >= 1.5){
                     print(REMAP_COMP$Sample[i])
                     print (Pressure[j])
                     print (MCmes[j])
                     print (MCcalc[j])
                     print (MCRatio[j])

              }
```

```
            if (DAT$MCRatio[j] <= 0.8){
                  print(REMAP_COMP$Sample[i])
                  print (Pressure[j])
                  print (MCmes[j])
                  print (MCcalc[j])
                  print (MCRatio[j])

            }
      }

      plot(DAT$MCcalc~DAT$MCmes, xlim= c(0, 1), ylim = c(0,1), pch =1,
            col = rainbow(5), xlab = "Measured Volumetric Water Content (-)",
            ylab = "vGM Estimated Volumetric Water Content (-)")

      par(new=TRUE)
}

# 45 degree line
abline(0, 1, lty = 2, col = "grey")
par(xpd = FALSE)

#legend
legend("bottomright",
            title = "kPA",
            legend=c("0","6", "10", "50", "1500"),
            cex = 1,
            pch=c(1,1,1,1,1),
            col = rainbow(5),
            horiz = FALSE)


#---------13. Plot capacity function with pore size radius-------------------

Colors <- c("red", "blue", "green")


      x11()
      for (i in 1:nrow(REMAP_COMP)){
            vGM_Theta_S <- REMAP_COMP$Theta_R[i]
            vGM_Theta_R <- REMAP_COMP$Theta_R[i]
            vGM_Alpha <- REMAP_COMP$Alpha[i]
            vGM_n <- REMAP_COMP$n[i]
            HC <- REMAP_COMP$HC.x[i]
            Linecol <- Colors[REMAP_COMP$cluster[i]]

            #m is calculated from n
            vGM_m <- 1 - (1/vGM_n)


            #plot R function with log transformed x-axis
            l <- 0.5
```

```
            vGM_unsat_Cw <- function(x){
                  ((vGM_Alpha^vGM_n)*(vGM_Theta_S - vGM_Theta_R)*vGM_m*
                  vGM_n*((0.104/x)^(vGM_n-1)))/((1 + (vGM_Alpha*
                  (0.104/x))^(vGM_n))^(vGM_m+1))
            }

            curve(vGM_unsat_Cw, from = 0.00001, to = 100, log = "x",
                  xlab = "Pore Radius (cm)", ylab =
                  "Hydraulic Capacity (1/cm)",ylim = c(0,0.011),
                  xlim = c(0.0001,50), lwd = 1.5, cex.lab=1.2,
                  cex.axis=1.2, cex.main=1.5, col = Linecol)
            par(new=TRUE)

      }

#legend
legend("topright",
      title = "Cluster",
      legend=c("1","2","3"),
      cex = 1,
      pch = c("-", "-", "-"),
      col = Colors,
      horiz = FALSE)


#-------------14. Plot capacity function with pressure head------------------

Colors <- c("red", "blue", "green")


x11()
for (i in 1:nrow(REMAP_COMP)){
      vGM_Theta_S <- REMAP_COMP$Theta_R[i]
      vGM_Theta_R <- REMAP_COMP$Theta_R[i]
      vGM_Alpha <- REMAP_COMP$Alpha[i]
      vGM_n <- REMAP_COMP$n[i]
      HC <- REMAP_COMP$HC.x[i]
      Linecol <- Colors[REMAP_COMP$cluster[i]]

      #m is calculated from n
      vGM_m <- 1 - (1/vGM_n)


      #plot R function with log transformed x-axis
      l <- 0.5


      vGM_unsat_Cw <- function(x){
            ((vGM_Alpha^vGM_n)*(vGM_Theta_S - vGM_Theta_R)*vGM_m*vGM_n*((x)^
            (vGM_n-1)))/((1 + (vGM_Alpha*(x))^(vGM_n))^(vGM_m+1))
      }

      curve(vGM_unsat_Cw, from = 0.000001, to = 15000, log = "x", xlab =
```

```
            "Pressure Head (cm)", ylab = "Hydraulic Capacity (1/cm)",
            ylim = c(0,0.011), xlim = c(0.0001,10000), lwd = 1.5,
            cex.lab=1.2, cex.axis=1.2, cex.main=1.5, col = Linecol)
      par(new=TRUE)

}

#legend
legend("topright",
      title = "Cluster",
      legend=c("1","2","3"),
      cex = 1,
      pch = c("-", "-", "-"),
      col = Colors,
      horiz = FALSE)

#--------------15. Plot vGM parameters------------------
#--------ThetaS---------
Count <- 1
symbVC <- c(2,1,5)
symb <- c(24,21,23)

x11()
for (Clust in 1:3){
      ClustSub <- subset(REMAP_COMP, cluster == Clust)
      count_seq <- seq(Count, Count+nrow(ClustSub)-1)
      plot(ClustSub$Theta_R~count_seq, xlim = c(0,53),
                  ylim = c(0.6,1), pch=symb[Clust],
                  col="black", bg="grey")
      par(new=TRUE)
      plot(ClustSub$Theta_S_NoVC~count_seq, xlim = c(0,53),
                  ylim = c(0.6,1), pch=symbVC[Clust])
      Count <- Count+nrow(ClustSub)
      par(new=TRUE)
}

#--------ThetaR---------
Count <- 1
symbVC <- c(2,1,5)
symb <- c(24,21,23)

x11()
for (Clust in 1:3){
      ClustSub <- subset(REMAP_COMP, cluster == Clust)
      count_seq <- seq(Count, Count+nrow(ClustSub)-1)
      plot(ClustSub$Theta_R~count_seq, xlim = c(0,53),
                  ylim = c(0,1), pch=symb[Clust],
                  col="black", bg="grey")
      par(new=TRUE)
      #plot(ClustSub$Theta_R_NoVC~count_seq, xlim = c(0,53),
      #            ylim = c(0,1), pch=symbVC[Clust])
      Count <- Count+nrow(ClustSub)
      #par(new=TRUE)
```

```
}

#--------Alpha---------
Count <- 1
symbVC <- c(2,1,5)
symb <- c(24,21,23)

x11()
for (Clust in 1:3){
      ClustSub <- subset(REMAP_COMP, cluster == Clust)
      count_seq <- seq(Count, Count+nrow(ClustSub)-1)
      plot(ClustSub$Alpha~count_seq, xlim = c(0,53),
                  ylim = c(0,0.2), pch=symb[Clust],
                  col="black", bg="grey")
      par(new=TRUE)
      plot(ClustSub$Alpha_NoVC~count_seq, xlim = c(0,53),
                  ylim = c(0,0.2), pch=symbVC[Clust])
      Count <- Count+nrow(ClustSub)
      par(new=TRUE)
}

#--------n---------
Count <- 1
symbVC <- c(2,1,5)
symb <- c(24,21,23)

x11()
for (Clust in 1:3){
      ClustSub <- subset(REMAP_COMP, cluster == Clust)
      count_seq <- seq(Count, Count+nrow(ClustSub)-1)
      plot(ClustSub$n~count_seq, xlim = c(0,53),
                  ylim = c(0,2), pch=symb[Clust],
                  col="black", bg="grey")
      par(new=TRUE)
      plot(ClustSub$n_NoVC~count_seq, xlim = c(0,53),
                  ylim = c(0,2), pch=symbVC[Clust])
      Count <- Count+nrow(ClustSub)
      par(new=TRUE)
}


#--------------16. Stats and ANOVA-----------------

#-------OC---------
boxplot(REMAP_COMP$OC.x ~ REMAP_COMP$cluster)
anova1 <- aov(sqrt(REMAP_COMP$OC.x) ~factor(REMAP_COMP$cluster))
summary(anova1)
plot(anova1, which=2)
shapiro.test(residuals(anova1))

#-------FC---------
boxplot(REMAP_COMP$FC)
boxplot(REMAP_COMP$FC ~ REMAP_COMP$cluster)
```

```r
#remove outliers
FCsub <- subset(REMAP_COMP, FC != "NA")
g <- quantile(FCsub$FC)
boxplot(FCsub$FC)
FCsub <- subset(FCsub, FCsub$FC <= g[3]+(IQR(FCsub$FC)*1.5) &
                          FCsub$FC >= g[2]-(IQR(FCsub$FC)*1.5))

anova1 <- aov(log(FCsub$FC) ~factor(FCsub$cluster))
summary(anova1)
plot(anova1, which=2)
shapiro.test(residuals(anova1))

#-------BD---------
boxplot(REMAP_COMP$BD.x)
boxplot(REMAP_COMP$BD.x ~ REMAP_COMP$cluster)
anova1 <- aov(log(REMAP_COMP$BD.x) ~factor(REMAP_COMP$cluster))
summary(anova1)
plot(anova1, which=2)
shapiro.test(residuals(anova1))

df <- subset(REMAP_COMP, BD.x != "NA")
g <- quantile(df$BD.x)
boxplot(df$BD.x)
df <- subset(df, df$BD.x <= g[3]+(IQR(df$BD.x)*1.5) &
                          df$BD.x >= g[2]-(IQR(df$BD.x)*1.5))

#------HC----------
boxplot(REMAP_COMP$HC.x)

#remove outliers
df <- subset(REMAP_COMP, HC.x != "NA")
g <- quantile(df$HC.x)
boxplot(df$HC.x)
df <- subset(df, df$HC.x <= g[3]+(IQR(df$HC.x)*1.5) &
                          df$HC.x >= g[2]-(IQR(df$HC.x)*1.5))
boxplot(df$HC.x ~ df$cluster)


anova1 <- aov(log(df$HC.x) ~factor(df$cluster))
summary(anova1)
plot(anova1, which=2)
shapiro.test(residuals(anova1))
TukeyHSD(anova1)

#-----Porosity------
g <- quantile(REMAP_COMP$MC_0kPa.x)
df<- subset(REMAP_COMP,
            REMAP_COMP$MC_0kPa.x <= g[3]+(IQR(REMAP_COMP$MC_0kPa.x)*1.5) &
            REMAP_COMP$MC_0kPa.x >= g[2]-(IQR(REMAP_COMP$MC_0kPa.x)*1.5))
anova1 <- aov(log(df$MC_0kPa.x) ~factor(df$cluster))
summary(anova1)
plot(anova1, which=2)
```

```
shapiro.test(residuals(anova1))
TukeyHSD(anova1)

#-----Vw6kPa------
g <- quantile(REMAP_COMP$V_H2O_6kPa.x)
df<- subset(REMAP_COMP,
            REMAP_COMP$V_H2O_6kPa.x <=
g[3]+(IQR(REMAP_COMP$V_H2O_6kPa.x)*1.5) &
            REMAP_COMP$V_H2O_6kPa.x >= g[2]-
(IQR(REMAP_COMP$V_H2O_6kPa.x)*1.5))
anova1 <- aov(df$V_H2O_6kPa.x ~factor(df$cluster))
summary(anova1)
plot(anova1, which=2)
shapiro.test(residuals(anova1))
TukeyHSD(anova1)

#-----Vw10kPa------
g <- quantile(REMAP_COMP$V_H2O_10kPa.x)
df<- subset(REMAP_COMP,
            REMAP_COMP$V_H2O_10kPa.x <=
g[3]+(IQR(REMAP_COMP$V_H2O_10kPa.x)*1.5) &
            REMAP_COMP$V_H2O_10kPa.x >= g[2]-
(IQR(REMAP_COMP$V_H2O_10kPa.x)*1.5))
anova1 <- aov(df$V_H2O_10kPa.x ~factor(df$cluster))
summary(anova1)
plot(anova1, which=2)
shapiro.test(residuals(anova1))
TukeyHSD(anova1)

#-----Vw50kPa-----
g <- quantile(REMAP_COMP$V_H2O_50kPa.x)
df<- subset(REMAP_COMP,
            REMAP_COMP$V_H2O_50kPa.x <=
g[3]+(IQR(REMAP_COMP$V_H2O_50kPa.x)*1.5) &
            REMAP_COMP$V_H2O_50kPa.x >= g[2]-
(IQR(REMAP_COMP$V_H2O_50kPa.x)*1.5))
anova1 <- aov(df$V_H2O_50kPa.x ~factor(df$cluster))
summary(anova1)
plot(anova1, which=2)
shapiro.test(residuals(anova1))
TukeyHSD(anova1)

#-----Vw1500kPa-----
g <- quantile(REMAP_COMP$V_H2O_1500kPa.x)
df<- subset(REMAP_COMP,
            REMAP_COMP$V_H2O_1500kPa.x <=
g[3]+(IQR(REMAP_COMP$V_H2O_1500kPa.x)*1.5) &
            REMAP_COMP$V_H2O_1500kPa.x >= g[2]-
(IQR(REMAP_COMP$V_H2O_1500kPa.x)*1.5))
anova1 <- aov(df$V_H2O_1500kPa.x ~factor(df$cluster))
summary(anova1)
plot(anova1, which=2)
shapiro.test(residuals(anova1))
```

```
TukeyHSD(anova1)

#-----Vs10kPa-----
g <- quantile(REMAP_COMP$V_10kPa.x)
df<- subset(REMAP_COMP,
            REMAP_COMP$V_10kPa.x <= g[3]+(IQR(REMAP_COMP$V_10kPa.x)*1.5) &
            REMAP_COMP$V_10kPa.x >= g[2]-(IQR(REMAP_COMP$V_10kPa.x)*1.5))
anova1 <- aov(df$V_10kPa.x ~factor(df$cluster))
summary(anova1)
plot(anova1, which=2)
shapiro.test(residuals(anova1))
TukeyHSD(anova1)

#-----Vs50kPa-----
g <- quantile(REMAP_COMP$V_50kPa.x)
df<- subset(REMAP_COMP,
            REMAP_COMP$V_50kPa.x <= g[3]+(IQR(REMAP_COMP$V_50kPa.x)*1.5) &
            REMAP_COMP$V_50kPa.x >= g[2]-(IQR(REMAP_COMP$V_50kPa.x)*1.5))
anova1 <- aov(df$V_50kPa.x ~factor(df$cluster))
summary(anova1)
plot(anova1, which=2)
shapiro.test(residuals(anova1))
TukeyHSD(anova1)

#-----Vs1500kPa-----
g <- quantile(REMAP_COMP$V_1500kPa.x)
df<- subset(REMAP_COMP,
            REMAP_COMP$V_1500kPa.x <= g[3]+(IQR(REMAP_COMP$V_1500kPa.x)*1.5)
&
            REMAP_COMP$V_1500kPa.x >= g[2]-(IQR(REMAP_COMP$V_1500kPa.x)*1.5))
anova1 <- aov(df$V_1500kPa.x ~factor(df$cluster))
summary(anova1)
plot(anova1, which=2)
shapiro.test(residuals(anova1))
TukeyHSD(anova1)

#-----Theta_R-----
df <- subset(REMAP_COMP, Sample != "x_221")
g <- quantile(df$Theta_S)
df<- subset(df, df$Theta_S <= g[3]+(IQR(df$Theta_S)*1.5) &
                          df$Theta_S >= g[2]-(IQR(df$Theta_S)*1.5))
anova1 <- aov(log(df$Theta_S) ~factor(df$cluster))
summary(anova1)
plot(anova1, which=2)
shapiro.test(residuals(anova1))
TukeyHSD(anova1)


#-----Theta_R-----
df <- subset(REMAP_COMP, Sample != "x_221")
g <- quantile(df$Theta_R)
df<- subset(df, df$Theta_R <= g[3]+(IQR(df$Theta_R)*1.5) &
                          df$Theta_R >= g[2]-(IQR(df$Theta_R)*1.5))
```

```r
anova1 <- aov(df$Theta_R ~factor(df$cluster))
summary(anova1)
plot(anova1, which=2)
shapiro.test(residuals(anova1))
TukeyHSD(anova1)

#-----Alpha-----
df <- subset(REMAP_COMP, Sample != "x_221")
g <- quantile(df$Alpha)
df<- subset(df, df$Alpha <= g[3]+(IQR(df$Alpha)*1.5) &
                          df$Alpha >= g[2]-(IQR(df$Alpha)*1.5))
anova1 <- aov(df$Alpha ~factor(df$cluster))
summary(anova1)
plot(anova1, which=2)
shapiro.test(residuals(anova1))
TukeyHSD(anova1)

#-----n-----
df <- subset(REMAP_COMP, Sample != "x_221")
g <- quantile(df$n)
df<- subset(df, df$n <= g[3]+(IQR(df$n)*1.5) &
                          df$n >= g[2]-(IQR(df$n)*1.5))
anova1 <- aov(log(df$n) ~factor(df$cluster))
summary(anova1)
plot(anova1, which=2)
shapiro.test(residuals(anova1))
TukeyHSD(anova1)

#-----Theta_S_NoVC-----
df <- subset(REMAP_COMP, Sample != "x_221")
g <- quantile(df$Theta_S_NoVC)
df<- subset(df, df$Theta_S_NoVC <= g[3]+(IQR(df$Theta_S_NoVC)*1.5) &
                          df$Theta_S_NoVC >= g[2]-(IQR(df$Theta_S_NoVC)*1.5))
anova1 <- aov(log(df$Theta_S_NoVC) ~factor(df$cluster))
summary(anova1)
plot(anova1, which=2)
shapiro.test(residuals(anova1))
TukeyHSD(anova1)

#-----Theta_R_NoVC-----
df <- subset(REMAP_COMP, Sample != "x_221")
g <- quantile(df$Theta_R_NoVC)
df<- subset(df, df$Theta_R_NoVC <= g[3]+(IQR(df$Theta_R_NoVC)*1.5) &
                          df$Theta_R_NoVC >= g[2]-(IQR(df$Theta_R_NoVC)*1.5))
anova1 <- aov(df$Theta_R_NoVC ~factor(df$cluster))
summary(anova1)
plot(anova1, which=2)
shapiro.test(residuals(anova1))
TukeyHSD(anova1)

#-----Alpha_NoVC-----
df <- subset(REMAP_COMP, Sample != "x_221")
g <- quantile(df$Alpha_NoVC)
```

```
df<- subset(df, df$Alpha_NoVC <= g[3]+(IQR(df$Alpha_NoVC)*1.5) &
                           df$Alpha_NoVC >= g[2]-(IQR(df$Alpha_NoVC)*1.5))
anova1 <- aov(df$Alpha_NoVC ~factor(df$cluster))
summary(anova1)
plot(anova1, which=2)
shapiro.test(residuals(anova1))
TukeyHSD(anova1)

#-----n_NoVC-----
df <- subset(REMAP_COMP, Sample != "x_221")
g <- quantile(df$n_NoVC)
df<- subset(df, df$n_NoVC <= g[3]+(IQR(df$n_NoVC)*1.5) &
                           df$n_NoVC >= g[2]-(IQR(df$n_NoVC)*1.5))
anova1 <- aov(df$n_NoVC ~factor(df$cluster))
summary(anova1)
plot(anova1, which=2)
shapiro.test(residuals(anova1))
TukeyHSD(anova1)

#### BETWEEN MODEL TYPES ##########

#-----Theta_S--------
df <- subset(REMAP_COMP, Sample != "x_221")
Theta_S_sub <- c(df$Theta_S, df$Theta_S_NoVC)
Mod <- c(rep("VC",52), rep("NoVC",52))
Theta_S_df <- data.frame(Theta_S_sub, Mod)
g <- quantile(Theta_S_df$Theta_S_sub)
df1<- subset(Theta_S_df ,
             Theta_S_df$Theta_S_sub <= g[3]+(IQR(Theta_S_df$Theta_S_sub)*1.5)
&
             Theta_S_df$Theta_S_sub >= g[2]-(IQR(Theta_S_df$Theta_S_sub)*1.5))

anova1 <- aov(log(df1$Theta_S_sub)~df1$Mod)
summary(anova1)
plot(anova1, which=2)
shapiro.test(residuals(anova1))
TukeyHSD(anova1)

#-----Theta_R--------
df <- subset(REMAP_COMP, Sample != "x_221")
Theta_R_sub <- c(df$Theta_R, df$Theta_R_NoVC)
Mod <- c(rep("VC",52), rep("NoVC",52))
Theta_R_df <- data.frame(Theta_R_sub, Mod)
g <- quantile(Theta_R_df$Theta_R_sub)
df1<- subset(Theta_R_df ,
             Theta_R_df$Theta_R_sub <= g[3]+(IQR(Theta_R_df$Theta_R_sub)*1.5)
&
             Theta_R_df$Theta_R_sub >= g[2]-(IQR(Theta_R_df$Theta_R_sub)*1.5))

anova1 <- aov(df1$Theta_R_sub~df1$Mod)
summary(anova1)
plot(anova1, which=2)
shapiro.test(residuals(anova1))
```

```
TukeyHSD(anova1)



#----Alpha-----------
df <- subset(REMAP_COMP, Sample != "x_221")
Alpha_sub <- c(df$Alpha, df$Alpha_NoVC)
Mod <- c(rep("VC",52), rep("NoVC",52))
Alpha_df <- data.frame(Alpha_sub, Mod)
g <- quantile(Alpha_df$Alpha_sub)
df1<- subset(Alpha_df ,
             Alpha_df$Alpha_sub <= g[3]+(IQR(Alpha_df$Alpha_sub)*1.5) &
             Alpha_df$Alpha_sub >= g[2]-(IQR(Alpha_df$Alpha_sub)*1.5))

anova1 <- aov(df1$Alpha_sub~df1$Mod)
summary(anova1)
plot(anova1, which=2)
shapiro.test(residuals(anova1))
TukeyHSD(anova1)

mean(df1$Alpha_sub[df1$Mod=="VC"])/mean(df1$Alpha_sub[df1$Mod=="NoVC"])


#----n-----------
df <- subset(REMAP_COMP, Sample != "x_221")
n_sub <- c(df$n, df$n_NoVC)
Mod <- c(rep("VC",52), rep("NoVC",52))
n_df <- data.frame(n_sub, Mod)
g <- quantile(n_df$n_sub)
df1<- subset(n_df , n_df$n_sub <= g[3]+(IQR(n_df$n_sub)*1.5) &
                          n_df$n_sub >= g[2]-(IQR(n_df$n_sub)*1.5))

anova1 <- aov(df1$n_sub~df1$Mod)
summary(anova1)
plot(anova1, which=2)
shapiro.test(residuals(anova1))
TukeyHSD(anova1)

#---------------Location Analysis-----------

#-----------FC--------------------
df <- subset(REMAP_COMP, Sample != "x_221")
df <- subset(df, cluster == 3)
df <- subset(df, LOC != "ENP")

FCtest <- subset(df, FC != "NA")
anova1 <- aov(FCtest$FC ~ FCtest$LOC)
summary(anova1)
plot(anova1, which=2)
shapiro.test(residuals(anova1))
TukeyHSD(anova1)

mean(FCtest$FC[FCtest$LOC=="WCA3"])/mean(FCtest$FC[FCtest$LOC=="WCA1"])
```

```r
#-----------BD--------------------
df <- subset(REMAP_COMP, Sample != "x_221")
df <- subset(df, cluster == 3)
df <- subset(df, LOC != "ENP")

BDtest <- df
anova1 <- aov(BDtest$BD.x ~ BDtest$LOC)
summary(anova1)
plot(anova1, which=2)
shapiro.test(residuals(anova1))
TukeyHSD(anova1)

mean(df$BDtest[FCtest$LOC=="WCA3"])/mean(FCtest$FC[FCtest$LOC=="WCA1"])

#-----------n---------------------
df <- subset(REMAP_COMP, Sample != "x_221")
df <- subset(df, cluster == 3)
df <- subset(df, LOC != "ENP")


anova1 <- aov(df$n ~ df$LOC)
summary(anova1)
plot(anova1, which=2)
shapiro.test(residuals(anova1))
TukeyHSD(anova1)

#----------Alpha-----------------
df <- subset(REMAP_COMP, Sample != "x_221")
df <- subset(df, cluster == 3)
df <- subset(df, LOC != "ENP")


anova1 <- aov(log(df$Alpha) ~ df$LOC)
summary(anova1)
plot(anova1, which=2)
shapiro.test(residuals(anova1))
TukeyHSD(anova1)

#----------Theta_S-----------------
df <- subset(REMAP_COMP, Sample != "x_221")
df <- subset(df, cluster == 3)
df <- subset(df, LOC != "ENP")


anova1 <- aov(log(df$Theta_S) ~ df$LOC)
summary(anova1)
plot(anova1, which=2)
shapiro.test(residuals(anova1))
TukeyHSD(anova1)

#-----------Theta_R---------------
df <- subset(REMAP_COMP, Sample != "x_221")
```

```r
df <- subset(df, cluster == 3)
df <- subset(df, LOC != "ENP")


anova1 <- aov(df$Theta_R ~ df$LOC)
summary(anova1)
plot(anova1, which=2)
shapiro.test(residuals(anova1))
TukeyHSD(anova1)

#---------------Summary of stats-----------

df <- subset(REMAP_COMP, Sample != "x_221")

Clust <- 2
round(mean(df$Theta_S[df$cluster == Clust]),3)
round(median(df$Theta_S[df$cluster == Clust]),3)
round(min(df$Theta_S[df$cluster == Clust]),3)
round(max(df$Theta_S[df$cluster == Clust]),3)
length(df$Theta_S[df$cluster == Clust])


round(mean(df$Theta_R[df$cluster == Clust]),3)
round(median(df$Theta_R[df$cluster == Clust]),3)
round(min(df$Theta_R[df$cluster == Clust]),3)
round(max(df$Theta_R[df$cluster == Clust]),3)
length(df$Theta_R[df$cluster == Clust])


round(mean(df$Alpha[df$cluster == Clust]),3)
round(median(df$Alpha[df$cluster == Clust]),3)
round(min(df$Alpha[df$cluster == Clust]),3)
round(max(df$Alpha[df$cluster == Clust]),3)
length(df$Alpha[df$cluster == Clust])

round(mean(df$n[df$cluster == Clust]),3)
round(median(df$n[df$cluster == Clust]),3)
round(min(df$n[df$cluster == Clust]),3)
round(max(df$n[df$cluster == Clust]),3)
length(df$n[df$cluster == Clust])

#--------NoVC------------------------

df <- subset(REMAP_COMP, Sample != "x_221")

Clust <- 1
round(mean(df$Theta_S_NoVC[df$cluster == Clust]),3)
round(median(df$Theta_S_NoVC[df$cluster == Clust]),3)
round(min(df$Theta_S_NoVC[df$cluster == Clust]),3)
round(max(df$Theta_S_NoVC[df$cluster == Clust]),3)
length(df$Theta_S_NoVC[df$cluster == Clust])
```

```
round(mean(df$Theta_R_NoVC[df$cluster == Clust]),3)
round(median(df$Theta_R_NoVC[df$cluster == Clust]),3)
round(min(df$Theta_R_NoVC[df$cluster == Clust]),3)
round(max(df$Theta_R_NoVC[df$cluster == Clust]),3)
length(df$Theta_R_NoVC[df$cluster == Clust])



round(mean(df$Alpha_NoVC[df$cluster == Clust]),3)
round(median(df$Alpha_NoVC[df$cluster == Clust]),3)
round(min(df$Alpha_NoVC[df$cluster == Clust]),3)
round(max(df$Alpha_NoVC[df$cluster == Clust]),3)
length(df$Alpha_NoVC[df$cluster == Clust])


round(mean(df$n_NoVC[df$cluster == Clust]),3)
round(median(df$n_NoVC[df$cluster == Clust]),3)
round(min(df$n_NoVC[df$cluster == Clust]),3)
round(max(df$n_NoVC[df$cluster == Clust]),3)
length(df$n_NoVC[df$cluster == Clust])


#--------WITOUT OUTLIERS

Clust <- 3

df <- subset(REMAP_COMP, Sample != "x_221")
g <- quantile(df$Theta_S)
df<- subset(df, df$Theta_S <= g[3]+(IQR(df$Theta_S)*1.5) &
                          df$Theta_S >= g[2]-(IQR(df$Theta_S)*1.5))


round(mean(df$Theta_S[df$cluster == Clust]),3)
round(median(df$Theta_S[df$cluster == Clust]),3)
round(min(df$Theta_S[df$cluster == Clust]),3)
round(max(df$Theta_S[df$cluster == Clust]),3)
length(df$Theta_S[df$cluster == Clust])


df <- subset(REMAP_COMP, Sample != "x_221")
g <- quantile(df$Theta_R)
df<- subset(df, df$Theta_R <= g[3]+(IQR(df$Theta_R)*1.5) &
                          df$Theta_R >= g[2]-(IQR(df$Theta_R)*1.5))

round(mean(df$Theta_R[df$cluster == Clust]),3)
round(median(df$Theta_R[df$cluster == Clust]),3)
round(min(df$Theta_R[df$cluster == Clust]),3)
round(max(df$Theta_R[df$cluster == Clust]),3)
length(df$Theta_R[df$cluster == Clust])

df <- subset(REMAP_COMP, Sample != "x_221")
g <- quantile(df$Alpha)
```

```
df<- subset(df, df$Alpha <= g[3]+(IQR(df$Alpha)*1.5) &
                          df$Alpha >= g[2]-(IQR(df$Alpha)*1.5))


round(mean(df$Alpha[df$cluster == Clust]),3)
round(median(df$Alpha[df$cluster == Clust]),3)
round(min(df$Alpha[df$cluster == Clust]),3)
round(max(df$Alpha[df$cluster == Clust]),3)
length(df$Alpha[df$cluster == Clust])

df <- subset(REMAP_COMP, Sample != "x_221")
g <- quantile(df$n)
df<- subset(df, df$n <= g[3]+(IQR(df$n)*1.5) &
                          df$n >= g[2]-(IQR(df$n)*1.5))

round(mean(df$n[df$cluster == Clust]),3)
round(median(df$n[df$cluster == Clust]),3)
round(min(df$n[df$cluster == Clust]),3)
round(max(df$n[df$cluster == Clust]),3)
length(df$n[df$cluster == Clust])


####----------NoVC--------------------
Clust <- 3

df <- subset(REMAP_COMP, Sample != "x_221")
g <- quantile(df$Alpha_NoVC)
df<- subset(df, df$Alpha_NoVC <= g[3]+(IQR(df$Alpha_NoVC)*1.5) &
                          df$Alpha_NoVC >= g[2]-(IQR(df$Alpha_NoVC)*1.5))


round(mean(df$Alpha_NoVC[df$cluster == Clust]),3)
round(median(df$Alpha_NoVC[df$cluster == Clust]),3)
round(min(df$Alpha_NoVC[df$cluster == Clust]),3)
round(max(df$Alpha_NoVC[df$cluster == Clust]),3)
length(df$Alpha_NoVC[df$cluster == Clust])

df <- subset(REMAP_COMP, Sample != "x_221")
g <- quantile(df$n_NoVC)
df<- subset(df, df$n_NoVC <= g[3]+(IQR(df$n_NoVC)*1.5) &
                          df$n_NoVC >= g[2]-(IQR(df$n_NoVC)*1.5))

round(mean(df$n_NoVC[df$cluster == Clust]),3)
round(median(df$n_NoVC[df$cluster == Clust]),3)
round(min(df$n_NoVC[df$cluster == Clust]),3)
round(max(df$n_NoVC[df$cluster == Clust]),3)
length(df$n_NoVC[df$cluster == Clust])



#----------------Regression----------------------

df <- subset(REMAP_COMP, cluster == 3 & FC != "NA")
```

```
x11()
plot(df$MC_6kPa.x~df$FC)
mod <- lm(df$MC_6kPa.x~df$FC)
summary(mod)
x11()
par(mfrow = c(2,2))
plot(mod)

x11()
plot(df$MC_10kPa.x~df$FC)
mod <- lm(df$MC_10kPa.x~df$FC)
summary(mod)
x11()
par(mfrow = c(2,2))
plot(mod)

x11()
plot(df$MC_50kPa.x~df$FC)
mod <- lm(df$MC_50kPa.x~df$FC)
summary(mod)
x11()
par(mfrow = c(2,2))
plot(mod)

x11()
plot(df$MC_1500kPa.x~df$FC)
mod <- lm(df$MC_1500kPa.x~df$FC)
summary(mod)
x11()
par(mfrow = c(2,2))
plot(mod)

#--------BD Regression-----

df <- subset(REMAP_COMP, cluster == 3)

x11()
plot(df$MC_0kPa.x~df$BD.x)
mod <- lm(df$MC_0kPa.x~df$BD.x)
mod1 <- lm(df$MC_0kPa.x~df$BD.x+I(df$BD.x^2))
summary(mod)
summary(mod1)
x11()
par(mfrow = c(2,2))
plot(mod)

x11()
plot(df$MC_6kPa.x~df$BD.x)
mod <- lm(df$MC_6kPa.x~df$BD.x)
mod1 <- lm(df$MC_6kPa.x~df$BD.x+I(df$BD.x^2))
summary(mod)
summary(mod1)
```

```
x11()
par(mfrow = c(2,2))
plot(mod)

x11()
plot(df$MC_10kPa.x~df$BD.x)
mod <- lm(df$MC_10kPa.x~df$BD.x)
mod1 <- lm(df$MC_10kPa.x~df$BD.x+I(df$BD.x^2))
summary(mod)
summary(mod1)
x11()
par(mfrow = c(2,2))
plot(mod)

x11()
plot(df$MC_50kPa.x~df$BD.x)
mod <- lm(df$MC_50kPa.x~df$BD.x)
mod1 <- lm(df$MC_50kPa.x~df$BD.x+I(df$BD.x^2))
summary(mod)
summary(mod1)
x11()
par(mfrow = c(2,2))
plot(mod)

x11()
plot(df$MC_1500kPa.x~df$BD.x)
mod <- lm(df$MC_1500kPa.x~df$BD.x)
mod1 <- lm(df$MC_1500kPa.x~df$BD.x+I(df$BD.x^2))
summary(mod)
summary(mod1)
x11()
par(mfrow = c(2,2))
plot(mod)

################################################################################
```

```
################################################################################
# TODO: Plot vGM related graphs
#      1. Import data from csv
#      2. Pick Data Columns for transform
#      3. Script to transform w/ VC
#      4. Script to transform no VC
#      5. Obs vs Mes Plot
#      6. Plot VGM curves within the clusters
#      7. Examples of Deviations from vGM
#      8. Plot the Ksat for each cluster w/ and w/o VC
#      9. Plot the capacity func for each cluster w/ and w/o VC
#
# Author: Anupama
################################################################################


#----------------------1. Import data from csv-------------------------------

# Set root to input data file location
root <- "C:/Users/Anupama/Documents/02_Academic/DISSERTATION/Data"
setwd(root)

# Read from csv and save to datafreame
WaterRet <- read.csv("_WaterRet_Rscript_GEODERMA.csv")
as.data.frame(WaterRet)


#--------------2. Pick Data Columns for transform---------------------------

# Subset with required variables
myvars <- c("MC_0kPa", "MC_6kPa", "MC_10kPa", "MC_50kPa", "MC_1500kPa")
newdata <- WaterRet[myvars]

# Import site list
Site_List <- read.csv("Site_List.csv")


#-------------------------3. Script to transform w/ VC----------------------
-

# create a matrix
vGM_ObsVC <- matrix(data = NA, nrow=15, ncol = 53)

d <- 1


for (i in seq(1,157,by=3)){

      for(j in 1:length(myvars)){
            vGM_ObsVC[((3*j)-2),d] <- newdata[i,j]
            vGM_ObsVC[((3*j)-1),d] <- newdata[i+1,j]
            vGM_ObsVC[((3*j)),d] <- newdata[i+2,j]
      }
```

```
	d <- d+1
}

write.csv(vGM_ObsVC, file = "_vGM_ObsVC.csv")
vGM_ObsVC


#-------------------------4. Script to transform no VC-----------------------
-

# calculate VWC w/ no VC
myvars <- c("MC_0kPa", "MC_6kPa", "MC_10kPa", "MC_50kPa", "MC_1500kPa",
            "VCR_6kPa", "VCR_10kPa", "VCR_50kPa", "VCR_1500kPa")
newdata <- WaterRet[myvars]

newdata$MC_6kPa_noVC <- newdata$MC_6kPa * newdata$VCR_6kPa
newdata$MC_10kPa_noVC <- newdata$MC_10kPa * newdata$VCR_10kPa
newdata$MC_50kPa_noVC <- newdata$MC_50kPa * newdata$VCR_50kPa
newdata$MC_1500kPa_noVC <- newdata$MC_1500kPa * newdata$VCR_1500kPa

# Script to transform the data
sub_vars <- c("MC_0kPa", "MC_6kPa_noVC", "MC_10kPa_noVC", "MC_50kPa_noVC",
            "MC_1500kPa_noVC")
newdata_sub <-  newdata[sub_vars]

# create a matrix
vGM_Obs_noVC <- matrix(data = NA, nrow=15, ncol = 53)

d <- 1


for (i in seq(1,157,by=3)){

	for(j in 1:length(sub_vars)){
		vGM_Obs_noVC[((3*j)-2),d] <- newdata_sub[i,j]
		vGM_Obs_noVC[((3*j)-1),d] <- newdata_sub[i+1,j]
		vGM_Obs_noVC[((3*j)),d] <- newdata_sub[i+2,j]
	}
	d <- d+1
}

write.csv(vGM_Obs_noVC, file = "_vGM_ObsNoVC.csv")

#----------------------5. Obs vs Mes Plot-------------------------

VWC_Obs_VC <- read.csv("_vGM_ObsVC_plotInput.csv")
VWC_Obs_NoVC <- read.csv("_vGM_ObsNoVC_plotInput.csv")

as.data.frame(VWC_Obs_VC)
as.data.frame(VWC_Obs_NoVC)

vGM_Param <- read.csv("_VGM_Geoderma_fitted_VC_noVC.csv")
as.data.frame(vGM_Param)
```

```r
#create an R function for vGM
vGM <- function(x){
       ((vGM_Theta_S - vGM_Theta_R)/((1+(vGM_Alpha * x)^ vGM_n)^
                                    vGM_m))+ vGM_Theta_R
}

MCcalcVC <- matrix(data=NA, nrow=5, ncol=53)
for (i in 1:nrow(vGM_Param)){
       vGM_Theta_S <-vGM_Param$Theta_S[i]
       vGM_Theta_R <- vGM_Param$Theta_R[i]
       vGM_Alpha <- vGM_Param$Alpha[i]
       vGM_n <- vGM_Param$n[i]

       #m is calculated from n
       vGM_m <- 1 - (1/vGM_n)

       MCcalcVC[,i] <- c(vGM(1), vGM(61), vGM(102), vGM(510), vGM(15296))
}

#Create a table of VGM

Pres_seq <- seq(3,12, by=3)
colfunc <- colorRampPalette(c("royalblue", "springgreen", "yellow", "red"))
Colors <- c(colfunc(5))

#drop x_221 record number 39 from MCcalcVC and VWC_Obs_VC
MCcalcVC <- MCcalcVC[,-39]
VWC_Obs_VC <- VWC_Obs_VC[,-39]

x11()
for (i in 2:ncol(VWC_Obs_VC)){
       plot(rep(MCcalcVC[1,i-1],3)~VWC_Obs_VC[1:3,i],
                    xlim = c(0,1), ylim=c(0,1), col = Colors[1],
                    xlab = "Measured Volumetric Water Content (-)",
                    ylab = "vGM Estimated Volumetric Water Content (-)")
       par(new=TRUE)
       plot(rep(MCcalcVC[2,i-1],3)~VWC_Obs_VC[4:6,i],
                    xlim = c(0,1), ylim=c(0,1), col = Colors[2],
                    xlab = "Measured Volumetric Water Content (-)",
                    ylab = "vGM Estimated Volumetric Water Content (-)")
       par(new=TRUE)
       plot(rep(MCcalcVC[3,i-1],3)~VWC_Obs_VC[7:9,i],
                    xlim = c(0,1), ylim=c(0,1), col = Colors[3],
                    xlab = "Measured Volumetric Water Content (-)",
                    ylab = "vGM Estimated Volumetric Water Content (-)")
       par(new=TRUE)
       plot(rep(MCcalcVC[4,i-1],3)~VWC_Obs_VC[10:12,i],
                    xlim = c(0,1), ylim=c(0,1), col = Colors[4],
                    xlab = "Measured Volumetric Water Content (-)",
                    ylab = "vGM Estimated Volumetric Water Content (-)")
       par(new=TRUE)
```

```
      plot(rep(MCcalcVC[5,i-1],3)~VWC_Obs_VC[13:15,i],
                  xlim = c(0,1), ylim=c(0,1), col = Colors[5],
                  xlab = "Measured Volumetric Water Content (-)",
                  ylab = "vGM Estimated Volumetric Water Content (-)",
                  main = "VC vGM")
      par(new=TRUE)
}

abline(0, 1, lty = 2, col = "grey")
par(xpd = FALSE)

legend("bottomright",
            title = "kPA",
            legend=c("0","6", "10", "50", "1500"),
            cex = 1,
            pch=c(1,1,1,1,1),
            col = Colors,
            horiz = FALSE)


MCcalcNoVC <- matrix(data=NA, nrow=5, ncol=53)
for (i in 1:nrow(vGM_Param)){
      vGM_Theta_S <-vGM_Param$Theta_S_NoVC[i]
      vGM_Theta_R <- vGM_Param$Theta_R_NoVC[i]
      vGM_Alpha <- vGM_Param$Alpha_NoVC[i]
      vGM_n <- vGM_Param$n_NoVC[i]

      #m is calculated from n
      vGM_m <- 1 - (1/vGM_n)

      MCcalcNoVC[,i] <- c(vGM(1), vGM(61), vGM(102), vGM(510), vGM(15296))
}


Pres_seq <- seq(3,12, by=3)
colfunc <- colorRampPalette(c("royalblue", "springgreen", "yellow", "red"))
Colors <- c(colfunc(5))

#drop x_221 record number 39 from MCcalcVC and VWC_Obs_VC
MCcalcNoVC <- MCcalcNoVC[,-39]
VWC_Obs_NoVC <- VWC_Obs_NoVC[,-39]

x11()
for (i in 2:ncol(VWC_Obs_NoVC)){
      plot(rep(MCcalcNoVC[1,i-1],3)~VWC_Obs_NoVC[1:3,i],
                  xlim = c(0,1), ylim=c(0,1), col = Colors[1],
                  xlab = "Measured Volumetric Water Content (-)",
                  ylab = "vGM Estimated Volumetric Water Content (-)")
      par(new=TRUE)
      plot(rep(MCcalcNoVC[2,i-1],3)~VWC_Obs_NoVC[4:6,i],
                  xlim = c(0,1), ylim=c(0,1), col = Colors[2],
                  xlab = "Measured Volumetric Water Content (-)",
                  ylab = "vGM Estimated Volumetric Water Content (-)")
```

```
        par(new=TRUE)
        plot(rep(MCcalcNoVC[3,i-1],3)~VWC_Obs_NoVC[7:9,i],
                    xlim = c(0,1), ylim=c(0,1), col = Colors[3],
                    xlab = "Measured Volumetric Water Content (-)",
                    ylab = "vGM Estimated Volumetric Water Content (-)")
        par(new=TRUE)
        plot(rep(MCcalcNoVC[4,i-1],3)~VWC_Obs_NoVC[10:12,i],
                    xlim = c(0,1), ylim=c(0,1), col = Colors[4],
                    xlab = "Measured Volumetric Water Content (-)",
                    ylab = "vGM Estimated Volumetric Water Content (-)")
        par(new=TRUE)
        plot(rep(MCcalcNoVC[5,i-1],3)~VWC_Obs_NoVC[13:15,i],
                    xlim = c(0,1), ylim=c(0,1), col = Colors[5],
                    xlab = "Measured Volumetric Water Content (-)",
                    ylab = "vGM Estimated Volumetric Water Content (-)",
                    main = "NonVC vGM")
        par(new=TRUE)
}

abline(0, 1, lty = 2, col = "grey")
par(xpd = FALSE)

legend("bottomright",
              title = "kPA",
              legend=c("0","6", "10", "50", "1500"),
              cex = 1,
              pch=c(1,1,1,1,1),
              col = Colors,
              horiz = FALSE)


#------------------Create  a table of vGM data--------------------------------


#matrix to store the calculated VWCs from vGM to calculate R-squared
MCcalcVCmat <- matrix(data=NA, nrow=15, ncol=52)
MCcalcNoVCmat <- matrix(data=NA, nrow=15, ncol=52)

for (j in 1:ncol(MCcalcVC)){
        increm <- 1
        for (i in seq(1,13, by=3)){
                MCcalcVCmat[i:(i+2),j] <- rep(MCcalcVC[increm,j],3)
                MCcalcNoVCmat[i:(i+2),j] <- rep(MCcalcNoVC[increm,j],3)
                increm <- increm + 1
        }
}


# Table with observed and calculated points

#Two column matrix to store the observed and calculated for all the sites
vGM_VWC_VC_Table <- matrix(data=NA, nrow = (15*52), ncol = 2)
vGM_VWC_noVC_Table <- matrix(data=NA, nrow = (15*52), ncol = 2)
```

```
append_seq <- seq(1,(15*53), by=15)
for (i in 1:52){

	#calculated VWCS
	vGM_VWC_VC_Table[append_seq[i]:(append_seq[i+1]-1),1]<-MCcalcVCmat[,i]
	vGM_VWC_noVC_Table[append_seq[i]:(append_seq[i+1]-1),1]<-
MCcalcNoVCmat[,i]

	#measured VWCs
	vGM_VWC_VC_Table[append_seq[i]:(append_seq[i+1]-1),2]<-VWC_Obs_VC[,i+1]
	vGM_VWC_noVC_Table[append_seq[i]:(append_seq[i+1]-1),2]<-
VWC_Obs_NoVC[,i+1]
}

modVC <- lm(vGM_VWC_VC_Table[,1]~vGM_VWC_VC_Table[,2])
summary(modVC)

modNoVC <- lm(vGM_VWC_noVC_Table[,1]~vGM_VWC_noVC_Table[,2])
summary(modNoVC)

#-------------6. Plot VGM curves within the clusters--------------------------

#-----------------Marl and Marl Peat Cluster--------------------

REMAP_COMP <- read.csv("_REMAP_COMP_GEODERMA_MC0.csv") #sites sampled
as.data.frame(REMAP_COMP)

chartTitle <- c("vGM Curves Cluster 1 (Marl)",
		"vGM Curves Cluster 2 (Marl-Peat)",
		"vGM Curves Cluster 3 (Peat)")

for (Clust in 1:3)
{
	ClustSub <- subset(REMAP_COMP, cluster == Clust)
	if(Clust == 1){
		ClustSub <- subset(ClustSub, Sample != "x_221")
	}

	if(Clust == 2){
		ClustSub <- subset(ClustSub, Sample != "x_038")
		ClustSub <- subset(ClustSub, Sample != "x_206")
		ClustSub <- subset(ClustSub, Sample != "x_213")
	}

	if(Clust == 3){
		ClustSub <- subset(ClustSub, Sample != "x_112")
		ClustSub <- subset(ClustSub, Sample != "x_155")
		ClustSub <- subset(ClustSub, Sample != "x_270")
	}
	x11()
	for (i in 1:nrow(ClustSub)){
		vGM_Theta_S <- ClustSub$Theta_S[i]
```

```
            vGM_Theta_R <- ClustSub$Theta_R[i]
            vGM_Alpha <- ClustSub$Alpha[i]
            vGM_n <- ClustSub$n[i]

            #m is calculated from n
            vGM_m <- 1 - (1/vGM_n)


            #create an R function for vGM
            vGM <- function(x){
                  ((vGM_Theta_S - vGM_Theta_R)/((1+(vGM_Alpha * x)^ vGM_n)^
                                                vGM_m)) + vGM_Theta_R
            }

            #plot R function with log transformed x-axis
            curve(vGM, from = 0.1, to = 25000, log = "x",
                        xlab = "Pressure Head (cm)",
                        ylab = "Volumetric Water Content (-)",
                        ylim = c(0,1), xlim = c(1,16000),
                        main = chartTitle[Clust], lwd = 1.5,
                        cex.lab = 1.2, cex.axis = 1.2,
                        cex.main = 1.5, col="grey")
            par(new=TRUE)
            #points(a~b)

      }
      #plot the characteristic curve
      #vGM_Theta_S <- mean(ClustSub$Theta_S)
      #vGM_Theta_R <- mean(ClustSub$Theta_R)
      #vGM_Alpha <- mean(ClustSub$Alpha)
      #vGM_n <- mean(ClustSub$n)

      #m is calculated from n
      #vGM_m <- 1 - (1/vGM_n)

      #curve(vGM, from = 0.1, to = 25000, log = "x",
      #            xlab = "Pressure Head (cm)",
      #            ylab = "Volumetric Water Content (-)",
      #            ylim = c(0,1), xlim = c(1,16000),
      #            main = chartTitle[Clust], lwd = 1.5,
      #            cex.lab = 1.2, cex.axis = 1.2,
      #            cex.main = 1.5, col="blue")
      #par(new=TRUE)

}

#----------------------Peat Cluster--------------------
REMAP_COMP <- read.csv("_REMAP_COMP_GEODERMA_MC0.csv") #sites sampled
as.data.frame(REMAP_COMP)

ClustSub <- subset(REMAP_COMP, cluster == 3)
ClustSub <- subset(ClustSub, LOC != "ENP")
vegType <- c("SG", "SR", "WL", "CT", "GM")
```

```
Col  <- c("red", "blue", "green", "yellow", "orange")

Area <- c("WCA1", "WCA2", "WCA3")
for (i_area in 1:(length(Area))){
      AreaSub <- subset(ClustSub, LOC == Area[i_area])
      x11()
      for (i in 1:nrow(AreaSub)){
            vGM_Theta_S <- AreaSub$Theta_S[i]
            vGM_Theta_R <- AreaSub$Theta_R[i]
            vGM_Alpha <- AreaSub$Alpha[i]
            vGM_n <- AreaSub$n[i]

            #m is calculated from n
            vGM_m <- 1 - (1/vGM_n)


            #create an R function for vGM
            vGM <- function(x){
                  ((vGM_Theta_S - vGM_Theta_R)/((1+(vGM_Alpha * x)^ vGM_n)^
                                                vGM_m)) + vGM_Theta_R
            }

            for(icol in 1:length(vegType)){
                  if (AreaSub$VEG[i] == vegType[icol]){
                        linecol <- Col[icol]
                  }
            }

            #plot R function with log transformed x-axis
            curve(vGM, from = 0.1, to = 25000, log = "x",
                        xlab = "Pressure Head (cm)",
                        ylab = "Volumetric Water Content (-)",
                        ylim = c(0,1), xlim = c(1,16000),
                        main = Area[i_area], lwd = 1.5,
                        cex.lab = 1.2, cex.axis = 1.2,
                        cex.main = 1.5, col=linecol)
            par(new=TRUE)
      }
      legend("topright",
                  title = "Vegetation",
                  legend=vegType[1:4],
                  cex = 1,
                  lty=1,
                  col = Col[1:4],
                  horiz = FALSE)

}


#-----------------------Mean Curves per Cluster--------------------
REMAP_COMP <- read.csv("_REMAP_COMP_GEODERMA_MC0.csv") #sites sampled
as.data.frame(REMAP_COMP)
```

```
Color <- c("red", "blue", "green")

x11()
for (Clust in 1:3)
{
	ClustSub <- subset(REMAP_COMP, cluster == Clust)
	if(Clust == 1){
		ClustSub <- subset(ClustSub, Sample != "x_221")
	}

	if(Clust == 2){
		ClustSub <- subset(ClustSub, Sample != "x_038")
		ClustSub <- subset(ClustSub, Sample != "x_206")
		ClustSub <- subset(ClustSub, Sample != "x_213")
	}

	if(Clust == 3){
		ClustSub <- subset(ClustSub, Sample != "x_112")
		ClustSub <- subset(ClustSub, Sample != "x_155")
		ClustSub <- subset(ClustSub, Sample != "x_270")
	}

	#plot the characteristic curve
	vGM_Theta_S <- mean(ClustSub$Theta_S)
	vGM_Theta_R <- mean(ClustSub$Theta_R)
	vGM_Alpha <- mean(ClustSub$Alpha)
	vGM_n <- mean(ClustSub$n)

	#m is calculated from n
	vGM_m <- 1 - (1/vGM_n)

	curve(vGM, from = 0.1, to = 25000, log = "x",
		xlab = "Pressure Head (cm)",
		ylab = "Volumetric Water Content (-)",
		ylim = c(0,1), xlim = c(1,16000),
		main = "Mean vGM VC Curves", lwd = 1.5,
		cex.lab = 1.2, cex.axis = 1.2,
		cex.main = 1.5, col=Color[Clust])
	par(new=TRUE)

	legend("topright",
		title = "Cluster",
		legend=c("1 (Marl)","2 (Marl-Peat)","3 (Peat)"),
		cex = 1,
		lty=1,
		col = Color[1:3],
		horiz = FALSE)
	par(new=TRUE)

}


#-------------7. Examples of Deviations from vGM-------------------------
```

```
root <- "C:/Users/Anupama/Documents/02_Academic/DISSERTATION/Data"
setwd(root)

# Read VWC VC Observations
VWC_Obs_VC <- read.csv("_vGM_ObsVC_plotInput.csv")
as.data.frame(VWC_Obs_VC)

# Read VWC no VC Observations
VWC_Obs_NoVC <- read.csv("_vGM_ObsNoVC_plotInput.csv")
as.data.frame(VWC_Obs_NoVC)

# Read vGM parameters
vGM_Param <- read.csv("_VGM_Geoderma_fitted_VC_noVC.csv")
as.data.frame(vGM_Param)

# Sites to display
SiteList <- vGM_Param$Sample

writeFolder <-
"C:/Users/Anupama/Documents/02_Academic/DISSERTATION/Data/plots_vGM2"



# Script to select site from dataframe and make plots of vGM models with obs

# for loop to run through vGM_Param  and select the site required using subset
for(i in 1:length(SiteList)){

      # Select vGM parameters
      df <- subset(vGM_Param, Sample == SiteList[i])
      vGM_Theta_S <- df$Theta_S
      vGM_Theta_R <- df$Theta_R
      vGM_Alpha <- df$Alpha
      vGM_n <- df$n

      #m is calculated from n
      vGM_m <- 1 - (1/vGM_n)

      # Select column names
      df1 <- VWC_Obs_VC[,i+1]
      df3 <- VWC_Obs_NoVC[,i+1]
      df2 <- c(rep(1,3), rep(61,3), rep(102,3), rep(510,3), rep(15296,3))



      #create an R function for vGM
      vGM <- function(x){
            ((vGM_Theta_S - vGM_Theta_R)/((1+(vGM_Alpha * x)^ vGM_n)^
                                    vGM_m)) + vGM_Theta_R
      }

      OPfileName <- paste (writeFolder, paste("/vGM_", SiteList[i],".tif",
sep=""), sep ='')
```

```
tiff(filename = OPfileName, width = 8, height = 8,
             units = 'in', pointsize = 12,
             compression = c('lzw'), bg = 'white', res = 600,
             restoreConsole = TRUE)

#plot R function with log transformed x-axis
curve(vGM, from = 0.1, to = 25000, log = "x",
             xlab = "Pressure Head (cm)",
             ylab = "Volumetric Water Content (-)",
             ylim = c(0,1), xlim = c(1,16000), lwd = 1.5,
             cex.lab = 1.2, cex.axis = 1.2,
             cex.main = 1.5)
par(new=TRUE)

#plot the data points
plot(df1~df2, log="x",
             xlab = "Pressure Head (cm)",
             ylab = "Volumetric Water Content (-)",
             main = paste(SiteList[i]),
             ylim = c(0,1), xlim = c(1,16000),
             cex.lab = 1.2, cex.axis = 1.2, pch=4,
             cex=1.5)

par(new=TRUE)

#plot vGM no VC
# Select vGM parameters
df <- subset(vGM_Param, Sample == SiteList[i])
vGM_Theta_S <- df$Theta_S_NoVC
vGM_Theta_R <- df$Theta_R_NoVC
vGM_Alpha <- df$Alpha_NoVC
vGM_n <- df$n_NoVC

#m is calculated from n
vGM_m <- 1 - (1/vGM_n)

curve(vGM, from = 0.1, to = 25000, log = "x",
             xlab = "Pressure Head (cm)",
             ylab = "Volumetric Water Content (-)",
             ylim = c(0,1), xlim = c(1,16000), lwd = 1.5,
             cex.lab = 1.2, cex.axis = 1.2,
             cex.main = 1.5, col="blue")
par(new=TRUE)

plot(df3~df2, log="x",
             xlab = "Pressure Head (cm)",
             ylab = "Volumetric Water Content (-)",
             main = paste(SiteList[i]),
             ylim = c(0,1), xlim = c(1,16000),
             cex.lab = 1.2, cex.axis = 1.2, col="blue",
             cex=1.5)
Rlab1 <- expression(paste(R^2))
text(1,0.2, expression(paste(R^2)), pos=4)
```

```
        text(1,0.15, expression(paste(R^2)), pos=4, col="blue")
        text(1.5, 0.2, paste("vGM VC", round(df$R.squared,3)), pos=4)
        text(1.5, 0.15, paste("vGM NoVC", round(df$R.squared_NoVC,3)), pos=4,
                    col="blue")

        par(new=TRUE)
        legend("topright",
                    legend=c("vGM VC model", "vGM NoVC model",
                                "VC Observations", "NoVC Observations"),
                    lty=c(1,1,NA,NA),pch=c(NA,NA,4,1),
                    cex = 1,
                    col = c("black", "blue"),
                    horiz = FALSE)

        dev.off()
}


sub <- subset(allData, cluster == 3)
minR <- subset(sub, R.squared == min(sub$R.squared))

minR

#-------------8. Plot the Ksat for each cluster w/ and w/o VC-----------------
---------

# read data from csv
allData <- read.csv("_REMAP_COMP_GEODERMA_MC0.csv")

# subset for sites with HC
subHC <- subset(allData, HC.x != 'NA')

# writefile location
writeFolder<-
"C:/Users/Anupama/Documents/02_Academic/DISSERTATION/Data/plots_HC"

# Script to make plots for each site
for(i in 1:nrow(subHC)){

        OPfileName <- paste (writeFolder,
                    paste("/HC_", subHC$Sample[i],".tif", sep=""), sep ='')
        tiff(filename = OPfileName, width = 10, height = 10,
                    units = 'in', pointsize = 12,
                    compression = c('lzw'), bg = 'white', res = 600,
                    restoreConsole = TRUE)

        l <- 0.5

        # Select vGM parameters
        vGM_Theta_S <- subHC$Theta_S[i]
        vGM_Theta_R <- subHC$Theta_R[i]
        vGM_Alpha <- subHC$Alpha[i]
        vGM_n <- subHC$n[i]
```

```
        HC <- subHC$HC.x[i]

        #m is calculated from n
        vGM_m <- 1 - (1/vGM_n)


        #create an R function for unsaturated hyd. conductivity
        vGM_unsat_HC <- function(x){
              HC * ((1/((1 + (vGM_Alpha*x)^vGM_n)^vGM_m)) ^ l) *
                          ((1 - (1 - (1/((1 + (vGM_Alpha*x)^vGM_n)^vGM_m)) ^
                                              (1/vGM_m))^vGM_m)^2)
        }

        #plot R function
        curve(vGM_unsat_HC, from = 0.1, to = 25000, log = "x",
                    xlab = "Pressure Head (cm)",
                    ylab = "Hydraulic Conductivity (cm/d)",
                    ylim = c(0,HC), xlim = c(0.2,16000.1),
                    lwd = 1.5, cex.lab=1.2,
                    cex.axis=1.2, cex.main=1.5)
        par(new=TRUE)

        # Select vGM parameters NoVC
        vGM_Theta_S <- subHC$Theta_S_NoVC[i]
        vGM_Theta_R <- subHC$Theta_R_NoVC[i]
        vGM_Alpha <- subHC$Alpha_NoVC[i]
        vGM_n <- subHC$n_NoVC[i]
        HC <- subHC$HC.x[i]

        #m is calculated from n
        vGM_m <- 1 - (1/vGM_n)

        #plot R function
        curve(vGM_unsat_HC, from = 0.1, to = 25000, log = "x",
                    xlab = "Pressure Head (cm)",
                    ylab = "Hydraulic Conductivity (cm/d)",
                    ylim = c(0,HC), xlim = c(0.2,16000.1),
                    lwd = 1.5, cex.lab=1.2,
                    cex.axis=1.2, cex.main=1.5, col="blue",
                    main=paste(subHC$Sample[i]))

        par(new=TRUE)
        legend("topright",
                    legend=c("vGM VC HC model", "vGM NoVC HC model"),
                    lty=c(1,1),
                    cex = 1,
                    col = c("black", "blue"),
                    horiz = FALSE)

        dev.off()
}
```

```
#----------9. Plot the capacity func for each cluster w/ and w/o VC-----------
-------

# read data from csv
allData <- read.csv("_REMAP_COMP_GEODERMA_MC0.csv")

# writefile location
writeFolder <-
"C:/Users/Anupama/Documents/02_Academic/DISSERTATION/Data/plots_Cw"

# Script to make plots for each site
for(i in 1:nrow(allData)){

      OPfileName <- paste (writeFolder, paste("/Cw_",
                  allData$Sample[i],".tif", sep=""), sep ='')
      tiff(filename = OPfileName, width = 10, height = 10,
                  units = 'in', pointsize = 12,
                  compression = c('lzw'), bg = 'white', res = 600,
                  restoreConsole = TRUE)

      l <- 0.5

      # Select vGM parameters NoVC
      vGM_Theta_S <- allData$Theta_S_NoVC[i]
      vGM_Theta_R <- allData$Theta_R_NoVC[i]
      vGM_Alpha <- allData$Alpha_NoVC[i]
      vGM_n <- allData$n_NoVC[i]
      HC <- allData$HC.x[i]

      #m is calculated from n
      vGM_m <- 1 - (1/vGM_n)

      #create an R function for capacity function
      vGM_unsat_Cw <- function(x){
            ((vGM_Alpha^vGM_n)*(vGM_Theta_S - vGM_Theta_R)*vGM_m*
                              vGM_n*((x)^(vGM_n-1)))/((1 +
(vGM_Alpha*(x))^(vGM_n))
                              ^(vGM_m+1))
      }

      #calculate the ymax
      xSeq <- seq(1,10000, by=1)
      Cw_seq <- vGM_unsat_Cw(xSeq)
      ymax <- max(Cw_seq)

      #plot R function
      curve(vGM_unsat_Cw, from = 0.1, to = 25000, log = "x",
                  xlab = "Pressure Head (cm)",
                  ylab = "Hydraulic Capacity (1/cm)",
                  ylim = c(0,ymax), xlim = c(0.2,16000.1),
                  lwd = 1.5, cex.lab=1.2,
                  cex.axis=1.2, cex.main=1.5, col="blue",
                  main=paste(allData$Sample[i]))
```

```
        par(new=TRUE)


        # Select vGM parameters
        vGM_Theta_S <- allData$Theta_S[i]
        vGM_Theta_R <- allData$Theta_R[i]
        vGM_Alpha <- allData$Alpha[i]
        vGM_n <- allData$n[i]
        HC <- allData$HC.x[i]

        #m is calculated from n
        vGM_m <- 1 - (1/vGM_n)



        #plot R function
        curve(vGM_unsat_Cw, from = 0.1, to = 25000, log = "x",
                    xlab = "Pressure Head (cm)",
                    ylab = "Hydraulic Capacity (1/cm)",
                    ylim = c(0,ymax), xlim = c(0.2,16000.1),
                    lwd = 1.5, cex.lab=1.2,
                    cex.axis=1.2, cex.main=1.5)
        par(new=TRUE)


        legend("topright",
                    legend=c("vGM VC HC model", "vGM NoVC HC model"),
                    lty=c(1,1),
                    cex = 1,
                    col = c("black", "blue"),
                    horiz = FALSE)
        par(new=FALSE)
        dev.off()
}

##############################################################################
```

```
################################################################################
# TODO: Use REVC Code to model Whelan et al., 2006 site
#
# Author: Anupama
################################################################################

#----------------------Boundary Conditions-------------------------------
root <- "C:/Users/Anupama/Documents/02_Academic/DISSERTATION/Data"
setwd(root)

BCInfile <- read.csv(file="FieldApplicationBCGAvg.csv")

# Change the date format
BCInfile$Date <- as.Date(BCInfile$Date, format = "%Y-%m-%d")

# Replace flux greater than zero with 0 - rainfall
BCInfile$TopFluxBC_cm[BCInfile$TopFluxBC_cm >= 0] <- 0

#-------------------------------------------------------------------------


# Input Hydraulic Parameters
Theta_S <- 0.92
Theta_R <- 0
Alpha <- 0.030
n <- 1.72
HC <- 19# cm per day
l <- 0.5
hCrit <- -1000

# Input Volume Change Values for LookUp Table
HCR0 <- 1
HCR6 <- 0.96
HCR10 <- 0.85
HCR50 <- 0.2
HCR1500 <- 0.1


# Input Initial Profile - This is the profile at saturation
MaxSoilDep <- 35 # cm
IniDelZ <- 0.1 #cm
NumCells <- MaxSoilDep/IniDelZ # Calculate the number of nodes
NumNodes <- NumCells+1
DelT <- 1 #days - cannot be greater than 1 day - this can affect the input
meteo

#Create LookUp Table
h_cm <- seq(0,15296)
delZ<- rep(IniDelZ,62)
delZ[1:62] <- IniDelZ*seq(from=HCR0, to=HCR6, length.out=(62-1)+1)
delZ[63:103] <- IniDelZ*seq(from=HCR6, to=HCR10, length.out=(103-63+1))
delZ[103:511] <- IniDelZ*seq(from=HCR10, to=HCR50, length.out=(511-103+1))
delZ[511:15297] <- IniDelZ*seq(from=HCR50, to=HCR1500,
```

```
            length.out=(15297-511+1))
delZ <- round(delZ, 3)
LUTableHCR <- data.frame(h_cm, delZ)

# Assign to function parameters
vGM_Theta_S <- Theta_S
vGM_Theta_R <- Theta_R
vGM_Alpha <- Alpha
vGM_n <- n

# Meteo
hLim <- -50000

#m is calculated from n
vGM_m <- 1 - (1/vGM_n)

#vGM model
vGM <- function(x){
      ((vGM_Theta_S - vGM_Theta_R)/((1+(vGM_Alpha * x)^ vGM_n)^ vGM_m) )
      + vGM_Theta_R
}


# Calculate unsaturated HC
vGM_unsat_HC <- function(x){
      HC * ((1 / ((1 + (vGM_Alpha * x) ^ vGM_n) ^ vGM_m)) ^ l) *
                  ((1 - ( 1 - (1 / (( 1 + (vGM_Alpha * x)^ vGM_n) ^ vGM_m))
                                    ^ (1 / vGM_m)) ^ vGM_m) ^ 2)
}

# Calculate capacity function
vGM_unsat_Cw <- function(x){
      ((vGM_Alpha^vGM_n)*(vGM_Theta_S - vGM_Theta_R)*vGM_m*vGM_n*((x)^
                                  (vGM_n-1)))/((1 +
(vGM_Alpha*(x))^(vGM_n))^(vGM_m+1))
}

# Time and Convergence
FinalTime <- 455 #days
FinalStep <- FinalTime/DelT # days
IterConverge <- 100 # Max iterations until convergence
hTol <- 1 # Stop Iterations if tolerace is reached

# Initial Conditions
IniHead <- matrix(data=0, nrow=NumNodes)

# Intialize temporary matrix to store all the pressure heads
hNext <- matrix(data=NA, nrow=NumNodes)

# Initialize matrix to store all pressure heads at all timesteps
# Initialized as a single column matrix - other columns to be added w/ cbind
hTimeAll <- matrix(data=IniHead, nrow=NumNodes)
```

```
# Initialize temporary matrix to store all the node heights
DelZ <- matrix(data=IniDelZ, nrow=NumCells)

# Initialize matrix to store all the node heights and store Initial DelZ
# Initialized as a single column matrix - other columns to be added w/ cbind
DelZAll <- matrix(data=IniDelZ, nrow=NumCells)

Flux <- 1

for (timeStep in 1:FinalStep){
# Check for condition of water level

      # CON 1 - Watertable higher than or at Surface
      # if water table is higher than or equal to the surface
      if (BCInfile$BottomBC_cm[timeStep] >= (MaxSoilDep-1)){

            # Assign zero pressure head to all nodes
            hNext[1:NumNodes] <- 0

            # Assign Max DelZ to all Cells
            DelZ[1:NumCells] <- IniDelZ

            #Assign Flux zero
            qCalc <- 0
      }

      # CON 2 - Watertable below surface
      if (BCInfile$BottomBC_cm[timeStep] < (MaxSoilDep-1)){

            # if water table is below surface but higher than bottom node
            if (BCInfile$BottomBC_cm[timeStep] > 0){

                  # Calcuate the number of nodes to run calculations and
                  # cells
                  CalcNodes <- as.integer(round(1+((MaxSoilDep
                                    -BCInfile$BottomBC_cm[timeStep])
                                    /IniDelZ),0))
                  CalcCells <- CalcNodes-1

                  # Bottom Node
                  BNode <- as.integer(round((BCInfile$BottomBC_cm[timeStep]
                              /IniDelZ), digits=0)+1)

                  # Assign zero pressure head boundary condition
                  BCbot <- 0

                  # Assign zero pressure head to all the nodes below the
                  # bottom node
                  hNext[1:(BNode-1)] <- 0

                  # Assign Max DelZ to all CELLS below the bottom node
                  DelZ[1:(BNode-2)] <- IniDelZ
```

```
}


# if water table is below bottom node
if(BCInfile$BottomBC_cm[timeStep] <= 0){

      # Assign number of nodes as total nodes and cells
      CalcNodes <- NumNodes
      CalcCells <- CalcNodes-1

      # Bottom Node
      BNode <- 1

      # Assign bottom BC as water table depth below bottom node
      BCbot <- BCInfile$BottomBC_cm[timeStep]

}

# Initialize h for calculations
h <- matrix(data=hTimeAll[BNode:NumNodes,timeStep],
            nrow=CalcNodes)

# Initialize t+1 pressure head matrix
hPlus <- matrix (data=-30, nrow=CalcNodes)

# Initialize CalcDelZ matrix
CalcDelZ <- matrix(data=NA, nrow=CalcCells)

# Use LookUp Table to calculate the DelZ
# DelZ is calculated at timeStep
for (i1 in 1:CalcCells){
      CalcDelZ[i1] <- LUTableHCR$delZ[LUTableHCR$h_cm ==
                                round(-((h[i1+1]+ h[i1])/2),0)]
}

# a, b, c, d initialized
a <- matrix(data = NA, nrow = CalcCells-1)
b <- matrix(data = NA, nrow = CalcCells-1)
c <- matrix(data = NA, nrow = CalcCells-1)
d <- matrix(data = NA, nrow = CalcCells-1)

# Initialize the capacity functions and the K functions
CwPlus <- matrix (data = NA, nrow = CalcNodes)
KPlus <- matrix (data = NA, nrow = CalcNodes)
Cw <- matrix (data = NA, nrow = CalcNodes)

##Within CON 2 we can have two situations -
# 1. Infiltration - The Top BC is 0 - infiltration when
# the matrix is negative
# Large changes in pressure head at the top BC can only be
# handled by small timesteps

# 2. Evaporation - The Top BC is negative
```

```
#####---------- RUN VGM CODE INSIDE CON 2 IF STATEMENT

# for each iteration
for (m in 1:IterConverge){
      # Calculate the r
      r <- DelT/CalcDelZ

      # Calculate CwPlus and KPlus with hPlus & Cw with h
      for (i2 in 1:CalcNodes){

            # if forward head is less than zero uses functions
            # to calculate capacity head and unsat HC
            if (hPlus[i2] < 0){
                  CwPlus[i2] <- vGM_unsat_Cw(abs(hPlus[i2]))
                  KPlus[i2] <- vGM_unsat_HC(abs(hPlus[i2]))
            }

            # if forward head is greater than zero then hyd
            # capacity is 0 and unsat HC is max at HC
            if (hPlus[i2] >= 0){
                  CwPlus[i2] <- 0
                  KPlus[i2] <- vGM_unsat_HC(0)
            }

            # if current head is less than zero uses function
            # to calculate capacity head and unsat HC
            if (h[i2] < 0){
                  Cw[i2] <- vGM_unsat_Cw(abs(h[i2]))

            }

            # if current head is greater than zero then hyd
            # capacity is 0
            if (h[i2] >= 0){
                  Cw[i2] <- 0
            }
      }# Parenthesis: for (i2 in 1:CalcNodes)

      # Calculate a,b,c,d
      for (i3 in 2:CalcCells){

            if (CwPlus[i3] == 0 & Cw[i3] == 0){

                  a[i3-1] <- 0
                  c[i3-1] <- 0
            }

            else{

                  a[i3-1] <- -r[i3-1]*(KPlus[i3]+KPlus[i3-1])/
                              (Cw[i3] + CwPlus[i3])
                  c[i3-1] <- -r[i3-1]*(KPlus[i3]+KPlus[i3+1])/
```

```
                        (Cw[i3] + CwPlus[i3])

        }

        b[i3-1] <- 1 - a[i3-1] - c[i3-1]
        d[i3-1] <- h[i3] + (CalcDelZ[i3-1]*
                        (a[i3-1]-c[i3-1]))

}

# Create the coefficient matrix
CoefMat <- matrix(data=0, nrow=CalcNodes, ncol=CalcNodes)
CoefMat[1,1] <- 1
CoefMat[CalcNodes,CalcNodes] <- 1

# Create RHS matrix and Assign BCs
RHS <- matrix(data=0, nrow=CalcNodes)

# Assign Boundary Conditions
RHS[1] <- BCbot
# Calculate Top BC
#BCtop <- -100

# check is q is positive or negative


# if q is positive assign 0 as the h top
if(BCInfile$TopFluxBC_cm[timeStep] >= 0){
        BCtop <- -1
        qCalc <- 0
}else{# else if q is negative

        # Calculate the matric head for BC top
        #if(t != 1){
        BChDiff <- 2
        qN <- -BCInfile$TopFluxBC_cm[timeStep]
        while(BChDiff > 0.001){
                eNminus <- -(vGM_unsat_HC(abs(hPlus
                        [CalcNodes-1]))
                        + vGM_unsat_HC(abs(hPlus
                        [CalcNodes])))/
                        (2*DelZ[CalcNodes-1])

                dN <- (DelZ[CalcNodes-1]*CwPlus
                        [CalcNodes]/
                        (2*DelT))+
                        ((vGM_unsat_HC(abs(hPlus
                        [CalcNodes]))
                        + vGM_unsat_HC(abs(hPlus
                        [CalcNodes-1])))/
                        (2*DelZ[CalcNodes-1]))

                fN <- (DelZ[CalcNodes-1]*CwPlus
```

```
                                [CalcNodes]
                                *hPlus[CalcNodes]
                                /(2*DelT)) - (DelZ[CalcNodes-1]*
                                (vGM(abs(hPlus[CalcNodes]))
                                - vGM(abs(h[CalcNodes])))/
                                (2*DelT)) -
                                ((vGM_unsat_HC(abs(hPlus
                                [CalcNodes]))
                                + vGM_unsat_HC(abs(hPlus
                                [CalcNodes-1])))
                                /2)-(qN)

                        hPred <- (fN - (eNminus*hPlus
                                [CalcNodes-1]))/dN

                        BChDiff <- abs(hPlus[CalcNodes]-hPred)

                        hPlus[CalcNodes] <- hPred

                        if(abs(hPlus[CalcNodes]) > abs(hCrit)){
                                BCtop <- hCrit
                                hPlus[CalcNodes] <- hCrit
                                break
                        } #if
                }

                # Check that matric head is not less than hCrit
                if(abs(hPred) > abs(hCrit)){
                        BCtop <- hCrit
                        hPlus[CalcNodes] <- hCrit
                }else{
                        BCtop <- hPred
                }

        }

        RHS[CalcNodes] <- BCtop

        # Assign Coefficient Matrix
        for (i4 in 2: (CalcNodes-1)){

                CoefMat[i4,i4] <- b[i4-1]
                CoefMat[i4,i4-1] <- a[i4-1]
                CoefMat[i4,i4+1] <- c[i4-1]
                RHS[i4] <- d[i4-1]

        }

        # Calculate Solution
        InverMat <- solve(CoefMat)
        hSol <-  InverMat %*% RHS

        # Check if tolerance is met
```

```
                hDiff <- round(hSol,5)-hPlus
                Diff <- sum(hDiff^2)

                # If tolerance is reached break iteration loop
                if (Diff < hTol){

                        break

                }else{# Else assign current solution to hPlus

                        hPlus <- round(hSol,5)
                }

        } # Parenthesis: for (m in 1:IterConverge)

        # if solution does not converge
        if (m == IterConverge){

                print(c("Solution does not converge", timeStep))
                #break

        }else{

                # Assign the hPlus to the the large matrix hNext
                hNext[BNode:NumNodes] <- hPlus

                # Assign calcDelZ to DelZ from waterlevel to surface
                DelZ[BNode:NumCells] <- CalcDelZ


                if(BCInfile$TopFluxBC_cm[timeStep] != 0){
                        qCalc <- -vGM_unsat_HC(abs(mean(c(hNext[NumNodes],
                                        hNext[NumNodes-1])))) *
                                        (((hNext[NumNodes]-
                                        hNext[NumNodes-1])/DelZ[NumCells])+1) -
                                        ((DelZ[NumCells]/(2*DelT))*
                                        (vGM(abs(hNext[NumNodes]))-
                                        vGM(abs(h[CalcNodes]))))


                }else{
                        qCalc <- 0
                }

        }

    }# Parenthesis: if (BCInfile$BottomBC_cm[timeStep] < MaxSoilDep)

    hTimeAll <- cbind(hTimeAll, hNext)
    DelZAll <- cbind(DelZAll, DelZ)
    Flux <- cbind(Flux,qCalc)

} # for loop with time
```

```
#Remove NA from Flux
Flux <- Flux[2:456]

# Save the change in column heights for each day
colHeights_cm <- colSums(DelZAll)
colHeights_cm <- colHeights_cm[2:456]

colHeightsDiff_cm <- colSums(DelZAll)-35
colHeightsDiff_cm <- colHeightsDiff_cm[2:456]

BCInfile <- cbind(BCInfile, colHeights_cm)
BCInfile <- cbind(BCInfile, colHeightsDiff_cm)

BCInfile$Months <- months(BCInfile$Date)
BCInfile$Year <- format(BCInfile$Date, format="%y")

output <- aggregate((BCInfile$colHeightsDiff_cm*10),
             list(format(BCInfile$Date, "%Y-%m")), mean)
output1 <- aggregate((BCInfile$colHeightsDiff_cm*10),
             list(format(BCInfile$Date, "%Y-%m")), min)
output2 <- aggregate((BCInfile$colHeightsDiff_cm*10),
             list(format(BCInfile$Date, "%Y-%m")), max)
output3 <- aggregate((BCInfile$colHeightsDiff_cm*10),
             list(format(BCInfile$Date, "%Y-%m")), sd)

Heights_Monthly <- aggregate((BCInfile$colHeights_cm),
             list(format(BCInfile$Date, "%Y-%m")), mean)

#Input RSETdata
RSET <- read.csv(file="ShallowZoneThickness.csv")

# Factor
Factor <- output$x[3]

OP <- cbind(output$x-Factor, output1$x-Factor, output2$x-Factor)


x11()
plot((output$x-Factor), type="l", ylim=c(-10,15), axes=FALSE,
             xlab="", ylab="", xlim = c(1,15))
polygon(c(seq(1:15),rev(seq(1:15))), c((output1$x-Factor),
             rev(output2$x-Factor)),
             col="lightgrey",
             border=NA)
par(new=TRUE)
plot((output$x-Factor), type="l", ylim=c(-10,15), axes=FALSE,
             xlab="", ylab="", xlim = c(1,15))
par(new=TRUE)
plot((output$x-Factor), ylim=c(-10,15), axes=FALSE,pch=15,
             xlab="", ylab="", xlim = c(1,15))
arrows(seq(1:15), ((output$x-output3$x)-Factor), seq(1:15),
             ((output$x+output3$x)-Factor), length=0.05, angle=90,
```

```
             code=3, col="black")

par(new=TRUE)
plot(RSET$x, RSET$avg, type='l', col="red", xlab="", ylab="",
             axes=FALSE, xlim = c(1,15), ylim=c(-10,15))
par(new=TRUE)
plot(RSET$x, RSET$avg, col="red", pch=15, xlab="",
             ylab=paste("Change in Thickness (mm",
             label="\u00B1", "1SD)"), xaxt = 'n',
             xlim = c(1,15), ylim=c(-10,15), main =
             paste("HCR 6kPa=",HCR6,"; HCR 10kPa=",
             HCR10, sep=''))
arrows(seq(4,15), RSET$min, seq(4,15), RSET$max, length=0.05,
             angle=90, code=3, col="red")
axis(side=1, at=c(seq(1,15)),
             labels= c("J","F","M","A","M","J","J","A","S","O",
                       "N","D","J","F","M"),
             tck=-0.025)
mtext('2002', side=1, line=2.5, at=7.5)
mtext('2003', side=1, line=2.5, at=14)
legend("topright",
             legend =c('Observed - Whelan et al., 2006',
                       'Modeled - Monthly Mean','Modeled - Monthly Range'),
                       col=c("red","black", "lightgrey"), lty = c(1, 1,NA),
                       pch = c(15, 15, 15), pt.cex=c(1,1,1.5))

RMSE <- ((sum(((output$x[4:15]-Factor)-(RSET$avg))^2))
                   /length(RSET$avg))^1/2

RMSEN <- 100 * RMSE/((max(RSET$avg))-min(RSET$avg))

#------------------WaterTable and Column Height-------------
x11(width=10, height=6)
par(mar=c(5,5,0,5))
plot(colHeights_cm~seq(1:455), type = 'l', col = "black", xaxs= "i",
             ylab="Soil Profile Height (cm)", xlab="Time (Days)",
             ylim=c(34.5,35.05))
par(new = TRUE)
plot(BCInfile$BottomBC_cm, type = "l", axes = FALSE, bty = "n",
             xaxs= "i", col= "blue",xlab = "", ylab = "")
axis(side=4, at = pretty(range(BCInfile$BottomBC_cm)), col.axis="blue",
             col="blue")
mtext("Water Table Height (cm)",side=4,line=3, col="blue")



x11(width=10, height=4)
par(mar=c(0,5,5,5))
barplot(-BCInfile$TopFluxBC_cm, col= "black", beside=TRUE, xaxs= "i",
             ylab = "Flux (cm/d)", ylim=c(0,1))
par(new=TRUE)
barplot(round(Flux,1), col= "red", beside=TRUE, xaxs= "i",
             ylab = "Flux (cm/d)", border="red", density=0, ylim=c(0,1))
```

```
legend("topright", legend =c("Potential ET",
             "Actual ET - Calculated"), pch=c(15,0),
             col=c("black", "red"),
             bty='n')



#--------------------Volumetric Water Content [-] ---------------------
b <- abs(hTimeAll[,2:456])
b <- vGM(b)*100/92

pal <- colorRampPalette(c("white", "blue"))
palnum <- 5
x11(width=10, height=6)
par(xpd=TRUE)
image(1:ncol(b), 1:nrow(b), t(b),
             xlab = "Time (Days)", ylab = "Nodes", ylim = c(1,351),
             col = pal(palnum),
             main="Degree of Saturation with Time at SH3"
)
legend("bottomright", inset=c(0,-0.25),
             bty='n', lty=1, lwd=1.5, legend="Phreatic Surface")
par(new=TRUE)
par(xpd=FALSE)
plot(BCInfile$BottomBC_cm*10, type = "l", lwd=1.5, axes = FALSE,
             bty = "n", xaxs= "i",
             col= "black",xlab = "", ylab = "", ylim=c(0,350))

x11(width=2, height=4)
par(mar=c(0,0,1,0))
legend_image <- as.raster(rev(matrix(pal(palnum), ncol=1)))
plot(c(0,2),c(0,1),type = 'n', axes = F,xlab = '', ylab = '',
             main = 'DoS [-]')
text(x=1.5, y = seq(0,1,l=5), labels = round(seq(round(min(b),2),
             round(max(b),2), l=5),2))

rasterImage(legend_image, 0, 0, 1,1)
#-------------------------------------------------------------


#-----------------Cell Heights---------------------------------
d <- abs(DelZAll[,2:456])

pal <- colorRampPalette(c("red", "yellow"))
palnum <- 5
x11(width=10, height=6)
par(xpd=TRUE)
image(1:ncol(d), 1:nrow(d), t(d),
             xlab = "Time (Days)", ylab = "Cells", ylim = c(1,350),
             col = pal(palnum),
             main="Cell Height with Time at SH3"
)
```

```
x11(width=2, height=4)
par(mar=c(0,0,1,0))
legend_image <- as.raster(rev(matrix(pal(palnum), ncol=1)))
plot(c(0,2),c(0,1),type = 'n', axes = F,xlab = '', ylab = '',
             main = 'Delta Z [cm]')
text(x=1.5, y = seq(0,1,l=5), labels = round(seq(round(min(d),3),
             round(max(d),3), l=5),4))
rasterImage(legend_image, 0, 0, 1,1)

################################################################################
```

VITA

ANUPAMA JOHN

Born, Kerala, India

2008-2012	B.S., Civil Engineering Embry-Riddle Aeronautical University Daytona Beach, Florida
2012-2013	M.S., Civil Engineering Florida International University Miami, Florida
2014-2015	Research Assistant Florida International University Miami, Florida
2015-2018	Graduate Teaching Assistant Florida International University Miami, Florida
2018	Research Assistant - GIS & RS Florida International University Miami, Florida
2016-2020	Doctoral Candidate Florida International University Miami, Florida

PUBLICATIONS AND PRESENTATIONS

John, A., Fuentes, H. R., and George, F. (2020). *Characterization of Unsaturated Hydraulic Properties of Everglades Wetland Soils*. Submitted to Geoderma.

John, A., Fuentes, H. R., (2019). *Vadose Zone Hydrology and Subsidence in the Everglades – A Coupled Numerical Model Approach.* Poster presented at the centennial meeting of the American Geophysical Union, San Francisco, California.

John, A., Fuentes, H. R., (2017). *Laboratory Assessment of Hydraulic Properties of Heterogeneous Organic Soils in the Everglades*. Poster Presented at the Greater Everglades Ecosystem Restoration. Coral Springs, Florida.

John, A., Fuentes, H. R., and Gann, D. (2016). *Application of Single Polarimetric RADARSAT-2 Images in Estimating Water Stage in the Everglades*. Proceedings of the

World Environmental and Water Resources Congress. https://doi.org/10.1061/9780784479841.006

John, A., Fuentes, H. R., and Gann, D. (2016). *Application of Single Polarimetric RADARSAT-2 Images in Estimating Water Stage in the Everglades*. Poster Presented at the Greater Everglades Ecosystem Restoration. Coral Springs, Florida.

John, A., Fuentes, H. R., and Gann, D. (2016). *Application of Single Polarimetric RADARSAT-2 Images in Estimating Water Stage in the Everglades*. Poster Presented at the NASA-NISAR Workshop. Mountainview, California.

John, A., Fuentes, H. R., and Gann, D. (2015). *Monitoring Water Stage and Vegetation in the Everglades using Single-Polarimetric RADARSAT-2 Imagery.* Poster Presented at the Greater Everglades Ecosystem Restoration. Coral Springs, Florida.